THE STRUCTURE, COLOR, AND RHEOLOGY OF CONCENTRATED DIBLOCK BOTTLEBRUSH POLYMER SOLUTIONS

BY

MATTHEW A. WADE

DISSERTATION

Submitted in partial fulfillment of the requirements
for the degree of Doctor of Philosophy in Chemical Engineering
in the Graduate College of the
University of Illinois Urbana-Champaign, 2022

Urbana, Illinois

Doctoral Committee:

Associate Professor Simon A. Rogers, Chair
Associate Professor Christopher M. Evans
Professor Brendan A. Harley
Assistant Professor Antonia Statt

Abstract

Bottlebrush polymers are a class of highly branched polymers consisting of a single linear backbone with side chain polymers densely grafted along its length. The steric repulsion between the side chains forces the backbone bottlebrush polymer to elongate resulting in the inhibition of entanglements and the polymer exhibiting a much faster relaxation time then linear polymers of equivalent molecular weight. Due to the wide range of properties that can be accessed simply by changing the architecture and chemistry of a bottlebrush polymer, extensive studies have been conducted describing the rapid dynamics of this material, the assembly of this material into larger structures, and the use of this material in application requiring super soft, highly elastic materials. Of note are the photonic properties exhibited by diblock bottlebrush polymers as they rapidly assembly into highly uniform structures with characteristics on the order of the wavelength of light. **This work seeks to explore these properties and develop these materials for applications in direct-ink-writing by developing structure-property-process relations between the microstructure, bulk color, and processing conditions.**

We first explore the fundamental structure and shape of bottlebrush polymers to lay the foundation that can be used to eventually characterize the structure-property-process relations exhibited by this material. We probe the fundamental shape through intrinsic viscosity and dynamic light scattering measurements. Upon characterizing the intrinsic viscosity and hydrodynamic radius as a function of molecular weight, we note that the scaling factors are lower than their linear counterparts suggesting that the bottlebrush molecule itself is more collapsed than the linear polymer. We also observe the transition from a star-like structure to a short-cylinder and eventually flexible cylinder with increasing backbone length. We explore the sensitivity of the bottlebrush polymer to slight changes in architecture noting how two bottlebrushes with equivalent molecular weight but different side chain dispersities exhibit different bulk rheological properties. This result highlights the weaknesses of size exclusion chromatography techniques when characterizing complex molecules while highlighting the sensitivity of rheology at identifying differences in the relaxation modes.

Having established a basic understanding of how this material behaves in a single molecule environment, we begin to develop the structure-property-process relation for this material through a combination of rheology, neutron scattering, and imaging techniques. In this study, we focus on diblock bottlebrush polymers with poly-lactic acid side chains in one block and polystyrene side chains in the other block. These polymers were dispersed in toluene with a concentration of 175 mg/ml. By combining imaging, neutron scattering, and rheology, we are able to observe how the color of the sample changes under flow and related that back to the self-assembled microstructure. Through these studies we note that the sample appears green at quiescence and low shear rates,cyan at moderate shear rates, and indigo at high shear rates. These colors were found to correspond to a highly uniform lamellea, a compressed lamellae with a reduced characteristic length scale, and an incoherent lamellae with notable variation in the characteristic lengthscale. The initial decrease in lamellae spacing was found to correspond to the green to cyan color transition. While the lamellae continued

to compress with increasing rate, the change in length scale is not sufficient to account for the change in reflect wavelength. Instead the development of incoherence's and thus local smaller length scales is attributed to the cyan to indigo transition. Throughout these tests, the intramolecular spacing was found to remain consistent. As part of these studies we are also able to identify the orientation of the lamellae which we find remains relatively consistent until the highest tested shear rates where it rotates to align along the vorticity direction, resulting in the sample appearing colorless. The combination of this structural study with the imaging and rheological measurements thus allows us to define a structure-property-relation between the microstructure, structural color, and applied flow conditions.

Having identified the ability to control the self-assembled microstructure and thus color of the sample with flow, we turn to investigating this material in the context of printing processes. Specifically we investigate the material's shear memory and retention of color. By carrying out relaxation studies, we note that the material reverts to its quiescent state on the order of less than a second. As such, we begin to explore possible avenues to increase the relaxation time of the polymer solution and thus retain any shear induced color. We first explore the use of a UV activated crosslinking mechanism achieved by functionalizing the PLA block of the bottlebrush with -allyl groups. Proof of concept tests were carried out by curing this material while applying steady stress from 0 Pa to 62.9 Pa. Macroscopic images were captured under zero stress conditions after the sample had cured clearly demonstrate a color change from green to cyan, highlighting our ability to lock-in the shear induced microstructure. Measurements were also carried out to describe the time scale over which the UV-curable bottlebrush transitioned from a sol to a gel. Due to key assumptions in the Winter-Chambon criterion not applying to this material, we were unable to define an exact gel point. That said, estimates based on the G', G" crossover indicate the material solidifies on a similar time scale to the color relaxation time. SPP analysis was applied to this system in an attempt to expand the range of frequencies that could be measured during gelation. Analysis of these results is still ongoing but should allow us to carry out gelation studies without having to worry about the mutation number.

A secondary approach to increasing the relaxation time of the bottlebrush polymer solution was explored by doubling the concentration from 175 mg/ml to 350 mg/ml. With this concentrated bottlebrush solution, we observe features in the flow curve and amplitude sweep that are typically associated with yield-like behavior. We predicted that yield-like behavior would allow us to lock in the microstructure simply by imposing a shear-induced structure while the material was flowing and then releasing the material such that it reverts to a solid state with a theoretically infinite relaxation time. Proof of concept studies demonstrated that this was not the case as the color of the concentrated polymer solution reverted back to its quiescent state on the order of 5 s, highlighting how yielding is not an instantaneous process. To further explore this idea, we carried out rheological studies to decompose the strain into recoverable and unrecoverable components and calculate the fluid and solid components of the loss moduli. The resulting moduli demonstrated that the bottlebrush polymer was exhibiting fluid-like behavior at low strains, further reinforcing the idea that yielding in this material does not occur instantly at the yield stress. We investigate the structural changes and processes that occur during yielding by calculating the transient Deborah number for a number of steady oscillatory deformations with amplitudes from 5.62% to 1000%. From this dimensionless group, we were able to identify points within an oscillation where the bottlebrush polymer undergoes yielding and recovery. Future experiments are planned to investigate the structural changes that occur at these points in time.

Overall, this thesis combines a number of different techniques and measurements in order to explore the structure-property-process relations exhibited by a bottlebrush polymer system. This work then explores avenues that can be taken to adjust the material and begin optimizing it for applications in direct-ink-writing.

On a broader sense, this work describes the steps and studies that need to be performed in order to develop a material for applications in on-the-fly property control in which the microstructure of a material is adjusted by changing the processing conditions in order to get a specific bulk property.

To my parents. Without their love and support, I would have never have gotten to where I am today. They tried to give me every opportunity to ask questions and learn about the world around me. As I finish up my doctorate, I'm happy to say they succeeded in instilling in me a love for learning and science and that the questions I now ask have only become more obtuse.

Acknowledgments

I would like to thank the following individuals for their contributions to this work:

My advisor, Prof. Simon Rogers for supporting me throughout my Ph.D. Through his efforts, I have learned so much and grown both as a researcher and as a person. From helping me understand the broader impacts of my research to helping me drag my head out of the weeds as I continuously question the accuracy and validity of my work. Through his efforts, Simon has helped me build my confidence both in my own work and in how I present my work to others. His push towards developing a holistic understanding has helped me expand my knowledge base and has encouraged me to dig deeper to better understand the techniques I incorporate into my studies. For all of these things, I am truly thankful.

My collaborators from the bottlebrush research group, Prof. Ying Diao, Prof. Damien Guironnet, Prof. Charles Sing and their students and post-docs, Dr. Bijal Patel, Dr. Dylan Walsh, Dr. Saritt Dutta, and Yash Kamble, for their help in understanding the physics that govern bottlebrush polymer behavior and architecture, the potential applications for these materials in printing processes, and the complex synthetic process required to manufacture these materials. Their help and intellectual contributions ensured that I was able to develop a complete understanding of this material. I would also like to thank Dr. Dylan Walsh and Yash Kamble for synthesizing the materials used in this thesis and for putting up with me when came to them and asked for more than 10 grams of bottlebrush polymer when their starting synthesis methods only produced 0.5 to 1 gram of polymer.

My collaborators from the NCNR, Dr. Katie Weigandt and Dr. Elizabeth Kelley, for their help conducting neutron scattering measurements on the 30 m SANS and VSANS beamlines. Through their help, I was able to develop an understanding of neutron scattering and how it can be used to capture the structural behavior of a material during deformation. As a result of their efforts, I was able to identify my own interests in neutron scattering as a future career path.

The current and former members of the Rogers Research Group, Prof. JD Park, Dr. Johnny Lee, Dr. Jiho Choi, Dr. Gavin Donley, Dr. Piyush Singh, Dr. Yuhui Shim, Jiachun Shi, Eric Burgeson, Krutarth Kamani, Jimmy Griebler, Destiny Gray, and Eden Li, for all of their help and support over the years. From being willing to talk about all things science to sharing our frustrations after another overnight experiment failing due to a rheometer shut down or random Windows update, their intellectual and emotional support has been extremely helpful over the years.

My committee members, Prof. Christopher M. Evans, Prof. Brendan A. Harley, and Prof. Antonia Statt for their contributions and assessment of my work throughout my Ph.D.

I would like to thank my housemates and fellow graduate students, Carl Schultz, Ben Hulbert, Alex Deptula, and Michael Tuttle for their support as we all tried to figure out what to do with ourselves when the world temporarily shutdown as a result of a global pandemic. The Friday movie nights, random board games, and trips out to the local beer garden make the last few years of quarantining and social distancing

far easier to manage.

Finally I would like to thank my family and friends for all their love and support over these incredible five and a half years. Their help as gotten me through the numerous challenges presented by graduate school. I would particularly like to thank my parents Mike and Julie for their words of encouragement and wisdom whenever I found myself questioning my choice to attend graduate school, as well as my little brother Nathan for helping me find random things to do outside of my research and for pushing me to start hiking. Without their help, I would have never grown into the person I am today.

Financially support for this project was provided by the National Science Foundation under the DMREF Award Number DMR-1727605.

Instrumentation was provided by the Anton-Paar academic VIP program for providing the Rogers lab with an MCR 702 rheometer along with the rheo-microscope and UV curing accessories, which played a key role in a number of measurements described in this thesis.

Access to VSANS and the 30 m SANS was provided by the Center for High Resolution Neutron Scattering, a partnership between the National Institute of Standards and Technology and the National Science Foundation under Agreement No. DMR-1508249. M. A. W, J. C.-W. L and S. A. R. Any mention of commercial products in this manuscript are for information only and does not imply endorsement by NIST.

Table of contents

Chapter 1

Introduction[1]

1.1 Bottlebrush Architecture

Bottlebrush polymers are a class of high molecular weight polymers consisting of a single linear backbone with a series of side chains densely grafted along the length of a linear backbone. These materials have garnered significant attention due to the wide range of physical properties that are accessed by adjusting the polymer's chemistry, backbone length, ($N_b b$), side chain length ($N_s c$), and graft density (f) [4]–[9]. Bottlebrush polymers are characterized by the steric repulsions between side chains forcing the linear backbone to elongate, thus inhibiting the formation of entanglements along the length of the polymer at molecular weights where entanglements are observed in linear chains of the same chemistry [2], [5], [10]–[15]. The extent of this steric repulsive effect is dependent on the length of the arms relative to their spacing along the backbone [4], [6], [16], [17].

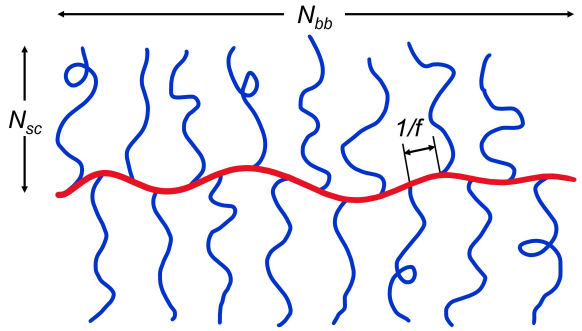

Figure 1.1: Schematic of a bottlebrush polymer with the key variables used to describe the architecture of the molecule labeled.

The branched topology of a bottlebrush polymer as depicted in Figure 1.1 allows for a wide range of polymer properties to be accessed simply by modifying the polymer's topology. This extensive range of properties can be further augmented by adjusting the composition and architecture of the side groups grafted onto the linear backbone. In two cases, bulky wedge and dendrimer side groups grafted onto a linear backbone lead to an increase in the polymer's persistence length, thus resulting in a stiffer molecule [18]–[27]. The

[1] This chapter has been adapted from the following publications with permission: [1]–[3]

space occupied by dendrimer and wedge polymers is significantly larger than that occupied by a liner polymer of equivalent length [26]. As a result, dendrimer graft polymers differentiate themselves from bottlebrush polymers by adopting an intrinsic shape that is retained when the material is deposited on a surface [25], [28]. On the other hand, lowering the graft density of bottlebrush polymers leads to what are known as low density bottlebrush polymers and comb polymers [29]. These materials are significantly more flexible than bottlebrush polymers [4], [29], [30]. With such a broad range of properties accessible simply through modifications to the topology of the material, a number of potential applications for these polymers have been identified, such as super soft elastomers [29], drug delivery mechanisms [31], [32], stimuli responsive polymers [33], [34], liquid crystals [19], and photonic materials [22], [35]–[37].

1.2 The Role of Branching in Polymer Engineering

Bottlebrush polymers represent the culmination of over 60 years of research in polymer physics that explores the impact of branching on the bulk strength, strain-hardening behavior, and relaxation dynamics. Historically, research into the dynamics and behavior of branched polymers has been motivated by applications in industry, with early investigations into branched polymers focused on the impact of long-chain branching in low density polyethylene (LDPE) and the effects it has on the dynamics and structure of the polymer [38]–[40]. Sperati et al. [40] demonstrated that the degree of branching in LDPE leads to a decrease in the overall strength and melt extensibility of the material under tensile conditions. In his paper from 1975, Meissner further demonstrated that branching in LDPE can also lead to vastly different melt fracture points, swelling ratios, and stress responses during nonequilibrium processing conditions [38]. This was despite similarities in the measured shear modulus and viscosity in the linear regime as well as the intrinsic viscosity and molecular weight [38]. This work also demonstrated that long chain polymer branching results in a reduction of the bulk moduli and an increase in melt strength and strain hardening [38], two properties that are integral to manufacturing techniques such as thermoforming, blow molding, and foaming [41]. On the other hand, the presence of short-chain branching can lead to a slight increase in the tensile strength of the polymer when compared to a linear polymer of equivalent molecular weight [42]. This type of branching does not exhibit the same level of strain hardening and melt strength observed in long-chain branching systems [43].

The ability to suppress and control the moduli, viscosities, and relaxation times by adjusting branching has led to widespread interest in characterizing and modeling the size and shape of polymers [44]–[49] and comb polymers [49]–[51]; all of these architectures provide insights important for bottlebrush polymers [12], [52]. The combination of theoretical work, scattering, and intrinsic viscosity measurements to determine the structure of these complex molecules with rheological techniques such as small amplitude oscillatory shear, steady shear, and time temperature superposition to determine the frequency-dependent shear moduli, zero shear viscosity, steady shear viscosity, and relaxation spectrum has allowed for propertyprocess relations to be established between the architecture of a polymer and its physical properties [12], [44]–[54]. This concept of branching and its impact on physical properties such as elasticity and extensibility has been taken to what could be considered an extreme limit in the form of highly functionalized star polymers and dendritic polymers [55], [56]. The architecture of these polymers results in coreshell structures and dynamics reminiscent of micelles and soft particles and gives rise to bulk polymers that have poor mechanical strength and a Newtonian-like response during flow [56]. As a result, this has prompted a discussion on the distinction between branched polymers and particles [57].

To better understand how branching and polymer topology affects the dynamics and physical properties

of a material, several groups have worked to understand the relaxation mechanisms of branched polymer systems that capture their rheological behavior. Early studies applied modified versions of the Doi-Edwards tube model that accounted for the retraction and movement of branches in a confining tube to explain the relaxation dynamics of simple branched polymers [46], [48], [53], [54]. In work from 1988 on modeling H-polymers, McLeish notes that the points where the polymer branches constrain the motion of the polymer and require the branch to retrace its contour back toward the branching point in order for the molecule to fully relax [53]. This phenomenon results in a slowing down of the dynamics, with larger deformations appearing to accelerate this process and thus the relaxation of the polymer [53]. The relaxation of more complicated architectures such as star polymers involves arms undergoing a breathing motion as they retract toward a central branching point, resulting in a broader relaxation spectrum than observed in equivalent linear polymers [46]. More recently, Lentzakis et al. presented a modified version of the pom-pom model in which they incorporate equations to describe the stretching of interbranch backbone segments and side arm retraction to capture the different contributions of each segment to dynamics of comb polymers as shown in Figure 1.2 [51]. Upon arm retraction, the backbone is able to move with greater freedom, which in turn can lead to a cascade effect as an arm's outer segments relax first, followed by inner segments [51]. This work is corroborated by van Ruymbeke et al.'s proposal of a hierarchical relaxation scheme for branched polymers in which the polymer segments furthest away from the center or backbone of a complex branched polymer are the first to relax [58]. As external segments relax, constraints on the internal segments are released, allowing those portions of the molecule to move and relax and eventually resulting in the relaxation of the entire molecule [58]. A schematic of this hierarchical relaxation mechanism is shown in Figure 1.2 with the relaxation times t_1, t_2, and t_3 corresponding to increasing relaxation times [58]. This proposed mechanism of hierarchical relaxation gives rise to the broad spectrum of relaxation times observed in early studies of branched polymer systems.

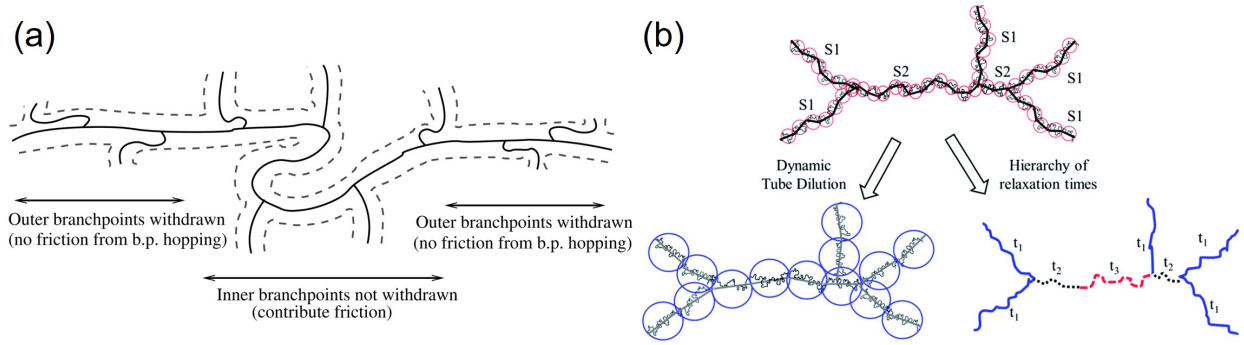

Figure 1.2: (a) A diagram depicting the withdrawing of outer branches during flow, leading to sections of the molecule not contributing to the overall friction and viscosity of the material [51]. (b) A schematic representing the hierarchical relaxation of a branched polymer. The outer branches will relax first at time t_1, followed by the shorter inner segments at time t_2, followed by the longer inner segment at time t_3 [58]. Reprinted with permission from [51] and [58]. Copyright 2014, The Society of Rheology, and The Royal Society of Chemistry, respectively.

In general, branching in polymers allows for the design and control over the relaxation time and moduli simply by changing the topology of the material. In the case of long-chain branching, this can lead to a softening of the material while also increasing the melt strength of the system [38], [41]. To overcome the strength limitations that arise from long-chain branching, these polymers are often mixed with linear or

short-chain branched polymers, resulting in an increase in the moduli while retaining the high melt strength and strain hardening characteristics of long-chain branched polymers [43], [59], thus making these blends ideal for the manufacturing of blown films. Higher degrees of repeated, dense branching can also lead to brittle systems with low elasticity, physical characteristics typically not associated with linear polymers, as the branches inhibit the formation of entanglements [55], [56], [60]. Bottlebrush polymers represent a natural extension of these studies carried out on branched polymer systems; these materials similarly exhibit the softening effect that results from branches inhibiting backbone interactions while simultaneously exhibiting a broad spectrum of relaxation dynamics due to the hierarchical arm-backbone structure [52].

1.3 Bottlebrush Architecture and its Impact on Rheology and Dynamics

In the bottlebrush architecture, the steric repulsions between side chains along the backbone have been known to affect the dynamics and rheology of bottlebrush polymers and, in turn, inhibit the formation of topological entanglements along the backbone contour. Thus in bottlebrush melts and solutions, entangled dynamics only emerge at molecular weights well beyond where entanglements are observed in linear chains of the same chemistry [2], [5], [10]–[15]. The extent of this steric repulsive effect is highly dependent on the length of the arms relative to their spacing [4], [6], [16], [30]. As a result, rheological properties of a bottlebrush polymers can be adjusted and manipulated simply by varying key architectural parameters, such as the length of the side chains, length of the polymer backbone, and grafting density of side chains along the backbone.

Extensive work has been carried out to classify the impact of these molecular parameters on shear moduli determined through small amplitude oscillatory measurements. Hu et al. demonstrated the impact of both backbone length and side chain length on the dynamic moduli master curves as a function of frequency for a series of polylactic acid-g-norbornene polymers [15]. In their work, segmental, arm, and terminal regimes were identified in the master curves of the dynamic moduli [15]. These features can be seen in the G', G" master curve constructed through time temperature superposition studies carried out on a PLA bottlebrush polymer in Figure 1.3. Plateaus in the dynamic moduli as a function of frequency were observed in the segmental and arm regime for bottlebrushes with 4.4 and 8.7 kDa side chains [15]. The separation of these plateaus in frequency corresponds to a hierarchical relaxation of the arms at short time scales followed by the polymer backbone at longer time scales. Iwawaki et al. corroborated these results with a series of rheo-optical studies that were carried out on polystyrene polymacromonomers with varying backbone and arm lengths [61], [62]. This hierarchical relaxation is similar to the phenomenon observed in other branched architectures in which outer branches of the molecule relax first, followed by inner portions of the molecule [51], [58].

The impact of longer side chains on dynamic moduli has been studied by Dalsin et al. in which a series of atactic polypropylene (aPP) and poly(ethylene-alt-propylene) (PEP) bottlebrush polymers were rheologically characterized [5]. The molecular weight of the side chains for the aPP bottlebrushes was approximately half the linear entanglement molecular weight, while the molecular weight of the side chains for the PEP bottlebrush was 3.5 times the linear entanglement molecular weight. In the arm regime of the dynamic moduli master curve, a plateau in the dynamic moduli was observed for the PEP bottlebrushes while no plateau was observed for the aPP bottlebrushes [5]. The presence of a rubbery plateau indicated an entanglement of the side chains for the PEP bottlebrushes [5]. At lower frequencies, neither aPP nor PEP bottlebrushes exhibited a rubbery plateau, indicating a lack of entanglements between backbones despite the very high molecular weights of the polymers [5]. On the opposite end of the spectrum, Lopez-Barron et al. characterized the

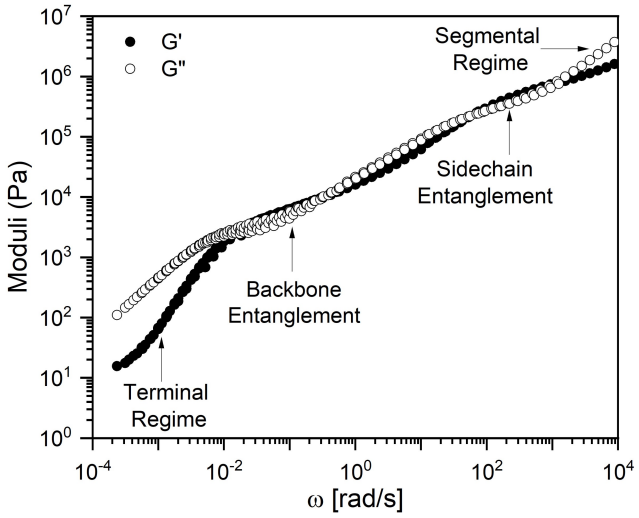

Figure 1.3: G' and G" as a function of oscillation frequency for a polylactic acid-g-polynorbornene bottlebrush polymer. For this polymer, $N_{bb} = 500$, $N_{sc} = 70$, and $T_{ref} = 90$ °C.

linear rheology of a series of bottlebrush polymers with very short side chains ranging from 4 to 16 carbons in length [6]. The dynamic moduli master curves for these α-olefin bottlebrush polymers exhibited well-defined rubbery plateaus at low frequency [6]. These plateaus were attributed to the entanglement of the bottlebrush backbone as the side chains were far too short to entangle themselves. The entanglement molecular weight for each of these polymers was determined based on the observed plateau modulus. This calculation allowed for scaling parameters to be determined, relating the entanglement molecular weight to the length of the side chains for short arm bottlebrushes [6].

The density of the bottlebrush polymer arms along the backbone has been shown to play a key role in the dynamics of the polymer. Liang et al. characterized the scaling of the entanglement modulus as a function of both the graft polymer composition parameter $\phi = N_g/(N_g + N_{sc})$, where N_g is the length between grafts along the backbone and N_{sc} is the length of a side chain, and ϕ is the crowding parameter, which is defined as the ratio between the volume fraction of monomers of the graft polymer in the pervaded volume of the side chains along the backbone [63]. The resulting structural parameter provided insight into how the rubbery plateau modulus can be affected by the relative crowding of the side chains along the backbone and thus helped define the key difference between comb and bottlebrush polymers [63]. Haugan et al. carried out an extensive linear rheological characterization of a series of poly-(norbornene)-graft-poly(lactide) bottlebrush polymers with varying backbone length, side chain length, and density [4]. The resulting dynamic moduli master curves demonstrated the impact of all three of these physical parameters on the linear rheological properties of the polymer. By comparing the side chain grafting density to the normalized plateau modulus, key scaling regimes are identified, highlighting key differences between comb and brush-like polymers [4]. A loose brush regime is not observed in the work carried out by Haugan et al [4]. This is attributed to the transition between barely overlapping and densely overlapping arms occurring over a very narrow range of grafting densities, resulting in the loose brushes not appearing in the experimental results [4]. Haugan et al. also considered the impact of these molecular parameters on additional rheological parameters such as

the zero-shear viscosity. Bottlebrush polymers that exceed the entanglement molecular weight exhibited zero-shear viscosity scaling as a function of molecular weight with a power-law scaling $\eta_0 \approx N_{bb}^3$. Unentangled bottlebrush polymers had a Rouse-like scaling for the zero-shear viscosity with molecular weight exhibiting a power-law scaling of $\eta_0 \approx N_{bb}$. Departure from Rouse scaling for dense bottlebrush polymers is interpreted as entanglement of these polymers [4].

1.4 Bottlebrushes as Photonic Crystals

Diblock bottlebrush polymers have been shown to self-assemble into lamellae, which act as one-dimensional photonic crystals, also known as Bragg stacks [22], [35], [36], [64]–[67]. These structures are composted of alternating layers of material with two different indicies of refraction with periodic spacing on the order of the wavelength of light, which results in a photonic band gap within the material [68]–[71]. This photonic band gap prevents select wavelengths of light from propagating through the material, and instead constructively reflects these wavelengths giving rise to the material appearing to have a specific color as shown in Figure 1.4 [35], [68]–[70]. For one-dimensional photonic crystal, the wavelength of light reflected by the materials microstructure can be approximated based on the layer spacing, d, the refractive indicies of each layer, η, using

$$\lambda_{calc} = 2(\eta_1 d_1 + \eta_2 d_2), \tag{1.1}$$

where λ_{calc} is the calculated reflected wavelength of light, and the subscripts for d and η correspond to two different layers within the structure [35], [72].

While it is possible produce photonic crystals with domain spacing on the order of 100 nm using ultrahigh molecular weight linear diblock copolymers [73], [74], challenges arise with regards to the processability of these polymers due to significant entanglement between chains and a corresponding slowing of dynamics [35], [36]. This issue limits the practicality of ultrahigh molecular wight linear polymers. Diblock bottlebrush copolymers circumvent these challenges. The semi-flexible behavior, as well as the increased effective radius of these polymers, allow for the rapid self-assembly of microstructures with large domain sizes that are typically difficult or impossible to access with linear polymers of equivalent molecular weight [66]. Recent studies have focused on the self-assembly of uniform diblock bottlebrush copolymers into regular lamellar structures with domain spacings upward of 100 nm to form one-dimensional photonic crystals [22], [35], [64]–[67].

A number of recent studies have focused on the impact of various molecular parameters on the self-assembly of diblock bottlebrush copolymers into uniform lamellae that act as one dimensional photonic crystals [22], [35], [64], [66], [67], [75]. Most of these studies consider self-assembled diblock bottlebrush copolymers in dried thin films. For example, Miyake et al. characterized the effects of molecular weight on the reflected color and concluded that increasing the backbone length without changing the arm length caused an increase in the lamellar spacing, resulting in the peak reflected wavelength shifting toward longer wavelengths /citeMiyake2012. The impact of additives on the self-assembly of a single bottlebrush copolymer has been characterized by Macfarlane et al. and Miyake et al [65], [66]. The addition of linear polymers and higher molecular weight diblock bottlebrush copolymers both resulted in an increase in lamellar domain spacing and a red-shift in the reflected wavelength, thus allowing access to a broad range of wavelengths in the visible spectrum as shown in Figure 1.4 [65], [66]. These observations demonstrate the ability to adjust the photonic behavior of the self-assembled photonic crystals simply by varying the molecular parameters of the bottlebrush block copolymer as well as the composition of the solution used to make the polymer thin

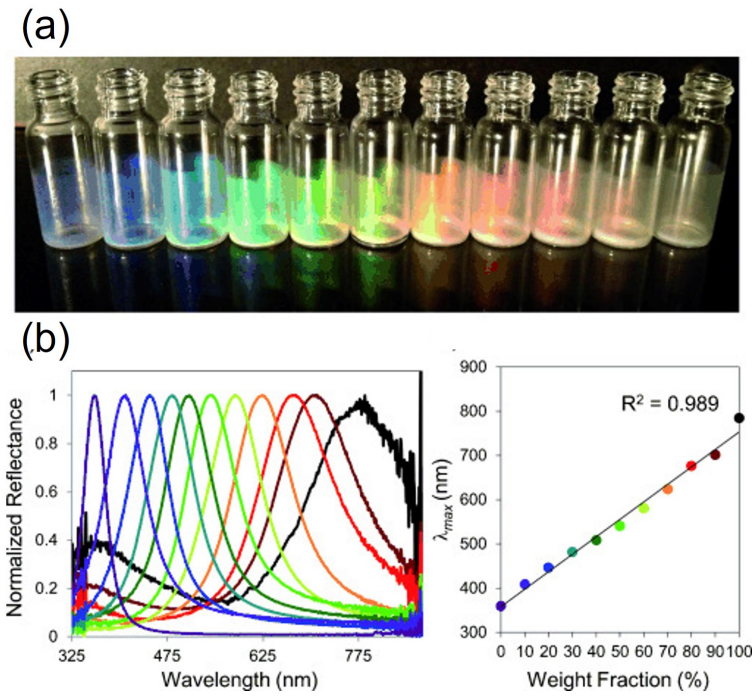

Figure 1.4: (A) Photographs and (B) UV-vis reflection spectra for a series of lamellar bottlebrush block copolymer photonic crystal films prepared by blending of low and high molecular weight polymers at different weight fractions [65]. Reprinted with permission from [65]. Copyright 2012, Wiley Online Library

film.

In addition to polymer architecture and sample composition, processing conditions have also been shown to have a significant impact on the photonic properties of diblock bottlebrush polymers. In the case of thin films, studies have demonstrated that solvent casting techniques can result in the polymer getting trapped in a non-equilibrium state due to the rate of solvent evaporation [22], [67], [76]–[78]. Thermally annealing these films can result in significant color change as the material is allowed to explore a larger potential energy landscape and progress towards a lower energy state [22], [67], [76], [77]. Patel et al., utilized the kinetic trapping of bottlebrush microstrutures during thin film formation to obtain multiple colors from a single diblock bottlebrush copolymer [78]. Utilizing a custom direct ink writing setup, Patel et al. varied both print speed and substrate temperature to control the rate of evaporation of the solvent and, in turn, the photonic properties of the printed bottlebrush polymer [78]. The resulting thin films reflected wavelengths of light spanning across a significant portion of the visible spectrum [78].

1.5 Development and Properties of Bottlebrush Elastomers

Advances in bottlebrush synthesis and the theory of bottlebrush elasticity and entanglement have motivated the development of elastomers-one way in which the community has begun to bridge the previous gap between fundamental study and practical materials. Cross-linked bottlebrush polymer elastomers have received significant attention due to the elastomer's low modulus (G $\approx$ 1 to 10 kPa) and ability to undergo large deformations relative to linear polymers of equivalent molecular weight [29], [52], [79]–[81]. These

unique characteristics, along with the ability to tune the physical properties by adjusting the molecular parameters such as side chain length, side chain density, and backbone length between cross-links, has prompted consideration of bottlebrush networks in a wide range of applications such as mimicking biological systems [52], [80], [82]–[85], supersoft actuators [52], [82], self-healing polymers [86]–[89], and 3D printing [90], [91]. The suppression entanglements by side chains is the central feature of these networks, with the side chains conceptualized as a "solvent" that dilutes the backbone of the bottlebrush [29]. The ability to artificially swell a network by increasing the side chain length in addition to the inhibition of entanglements allows for the physical properties of bottlebrush elastomers to be tuned over a broader range than their linear counterparts [29].

Various polymer architectures have been explored as an avenue to tune the bulk properties of bottlebrush polymer elastomers. Specifically, linear-brush-linear triblock copolymers with linear segments that cross-link to one another have garnered significant interest due to the relative elongation of the bottlebrush polymer between the densely cross-linked linear polymers [83]–[85], [92]. The inherent elongation of the bottlebrush leads to unique stressstrain behavior that has been taken advantage of by Keith et al. and Vatankhah-Varnosfaderani et al. to replicate the characteristics of various biological materials, such as with structural color or biomechanical properties [83], [84]. The unique hierarchical structure that results from these bottlebrush elastomers leads to an initial unfolding of the bottlebrush at very small strains, followed by a stretching of the backbone at larger strains [83]. As a result, these bottlebrush elastomers exhibited a low modulus at small deformation, followed by a rapid strain stiffening with increasing strain [83]. The impact of changing molecular parameters on the physical properties of these bottlebrush elastomers was explored by Daniel et al [92]. In their study, the ratio of side chain length to block length was varied to identify the impact of the aspect ratio on the assembly, and the resulting bulk characteristics of these linear-brush-linear copolymer elastomers [92]. When the side chain lengths were well below the backbone length, percolated crystals form from the linear blocks. Increasing the backbone length inhibited the formation of these crystalline structures, resulting in supersoft elastomeric properties. Increasing the side chain length such that it is comparable to the backbone length prevented the cross-linking of linear blocks, resulting in a bottlebrush melt [92].

Bottlebrush polymers have also been identified for applications in self-healing networks . By selecting specific cross-linkers, bottlebrush polymers have been crosslinked to form covalent adaptable networks (CANs), self-healing networks that can reform form after mechanical failure [88]. These bottlebrush networks broadened the spectrum of physical properties exhibited by CANS to include supersoft elastomers. Self et al. demonstrated the ability to synthesize these cross-linked bottlebrush networks and the impact backbone and side chain length have on the elastic properties of the elastomer [88]. Upon failure, the material was reconstructed and reprocessed by heating and hot pressing it at 180 °C for 5 h. The resulting recycled sample exhibited nearly identical stressstrain behavior during tensile testing [88].299 Choi et al. demonstrated similar reprocessability with PDMS-α-lipoic acid and bis-PDMS-α-lipoic acid macromonomers [89]. When exposed to UV light, these macromonomers reacted to form a bottlebrush network. Upon mechanical failure, the sample was once again exposed to UV-light, resulting in the macromonomers re-cross-linking and forming a network with near identical elastic properties [89]. Non-covalent systems have also been investigated for self-healing bottlebrush elastomers by Chen and Guan [86]. In their work, they synthesized bottlebrushes with a PMMA backbone and polyacrylate-amide (PAamide) side chains that formed temporary cross-links through hydrogen bonding interactions between the side chains [86]. The stressstrain behavior was measured through tensile testing for both pristine samples and samples that were cut and allowed to heal for varying

lengths of time at room temperature. As the healing time increased, the stressstrain behavior approached the initial tensile response of the pristine material, demonstrating self-healing behavior [86].

1.6 Impact of Processing on Polymer Microstructure

Processing conditions, specifically those that take the material into an out-of-equilibrium state, have been shown to have a significant impact on the self-assembled microstructure and resulting macroscopic properties of gels and linear polymeric systems [93]–[102]. In the case of linear copolymers assembled into lamellae, extensive experimental and computational work has shown that shear can lead to a reorientation and complete reconfiguration of the microstructure depending on the strength of the deformation and composition of the polymer system [94]–[98], [103]. In Diet et al. and Wunenburger et al., utilized structural characterization techniques and theoretical analysis, respectively, to characterize how the lamellae microsctructure of a surfactant system changed as a function of shear [97], [98]. Through these studies, they were able to identify how the orientation of the lamellae changed as a function of both shear rate and concentration, as well as identify the intermediate phases that the layers adopted between orientations [97], [98]. At low shear rates, the lamellae was observed to assemble "face-on" with the walls along the velocity gradient direction of the couette cell [97], [98]. The application of higher resulted in these lamellae "rolling up" to form layered cylinders oriented along the vorticity direction [97], [98]. At the highest rates tested, the cylinders appear to break down, and result in the reorientation of the lamellae in an "edge-on" configuration with layers stacked along the vorticity direction.

In the case of bottlebrush polymers, we expect similar phenomena to be observed as a function of shear. It has already been discussed that processing conditions can have a significant impact on the microstructure of the material, with kinetic trapping playing a key role in the final microstructures and thus photonic properties exhibited by bottlebrush polymers when probing these materials under quiescent conditions [22], [67], [76]–[78]. This opens the possibility for developing a material with a wide range of physical properties, in this case structural color, that can be adjusted on the fly based on the applied processing conditions.

1.7 Bottlebrush Synthesis

The materials synthesized for the work presented in this thesis were prepared as part of the collaboration with the Guironnet Group. Dr. Dylan Walsh and Yash Kamble prepared these materials by ring opening polymerization of rac-lactide utilizing a 1,8-diazabicyclo[5.4.0]undec-7-ene (DBU) catalyst, followed by the ring opening metathesis polymerization (ROMP) of norbornene terminated macromonomer with a thir generation Grubbs catalyst [104]–[106]. A schematic of this reaction can be found in Figure 1.5. Boric acid was used as a quenching agent for the ROP catalyst to perform the graft-through process without isolating the macromonomers [107]. Molecular weight of the bottlebrush polymers were determined based on the macromonomer to initiator ratio and macronomomer conversion as determined by gel permeation chromatography [107].

Note that the reaction scheme discussed in this section serves as a general synthetic method for producing the bottlebrushes studied throughout this thesis. Slight variations were made in order to synthesize diblock PLA-PS bottlebrush copolymers and bottlebrush polymers functionalized with allyl groups. Further discussion of these variations will be provided in Chapter 3 and 5.

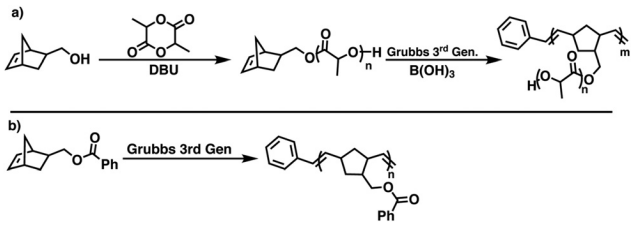

Figure 1.5: (a) Synthetic scheme for the one pot synthesis of PLA bottlebrush polymers. (b) Synthetic scheme for the synthesis of linear poly(5-norbornene-2-(methylbenzoate)).

1.8 Motivation and Thesis Overview

We have discussed the state of the bottlebrush literature prior to the work carried out in this thesis. We have addressed the development of these materials from a historical perspective, noting the impact of polymer architecture on a materials macroscopic properties [38]–[41], [43], [46], [48], [53], [54], [58], [59] . These studies demonstrate the importance of polymer architecture and how slight changes to the polymer can give rise to vastly different macroscopic properties. We also noted the recent efforts from a rheological perspective that have sought to understand the key features and properties that distinguish bottlebrush polymers from linear and comb polymers [2], [4]–[6], [10]–[16], [30], [63] . These studies highlight the hierarchical structure of bottlebrush polymers as well as the rapid dynamics that arise due to the bottlebrush architecture inherently inhibiting the formation of entanglements. We also addressed the development of bottlebrush polymer for applications in photonic crystals [22], [35], [36], [64]–[67], [75], [76], [78] and elastomers [29], [52], [79]–[81], [83]–[85], [92] , two applications that take advantage of the bottlebrush architecture and its rapid dynamics. In the case of bottlebrush studies focused on photonic crystals, we identify works that has demonstrated the importance of processing conditions and how these processing conditions can directly impact the photonic properties of the bottlebrush polymer [22], [67], [76]–[78]. Finally we present studies that are focused the impact that shear and deformation can have on the self-assembled microsctructure of a polymeric system [93]–[102]. These works demonstrate the importance of processing conditions prior to a sample drying and undergoing kinetic trapping and the range of microstructures that can be accessed through controlled deformation. Based on these studies, we identify the possibility of developing bottlebrush polymers with microstructures and corresponding photonic properties that can be controlled through careful application of deformation.

In this thesis, we seek to characterize the structure-property-process relations exhibited by bottlebrush polymers that give rise to a wide range of macroscopic properties based on both the molecular architecture and the self-assembled microstructure, with specific focus on the photonic properties of these materials. These structure-property-process relations would allow us to develop control schemes that relate the processing conditions experienced by a set of bottlebrush polymers to the material's microstructure, and thus control its photonic properties on the fly. To achieve this, we discuss the following topics in this thesis:

- Chapter 2 - The shape and size adopted by bottlebrush polymers and their sensitivity to changes in polymer architecture.
- Chapter 3 - The structure-property-process relations exhibited by bottlebrush polymer solutions under steady shear conditions between the applied shear rate, microstructure, and bulk color of the sample.

- Chapter 4 [1] - The timescales over which structural and color change occur and the use of UV-activated chemical crosslinking to gel bottlebrush polymers under shear to "lock-in" shear induced microstructures.
- Chapter 5 [1] - The use of yield-like behavior found in concentrated bottlebrush solutions to "lock-in" shear induced microstructures.
- Chapter 6 - A summary of the work presented in this thesis and an outlook on the development of structure-property-process relations for this bottlebrush polymers with applications in direct ink writing.

The data discussed in the second chapter serves to provide a fundamental understanding of how these materials behave. This information is built upon in the third chapter in which we utilize rheology, scattering, and microscopy to relate shear, microstructure, and color. For considerations in practical applications, we explore the timescales and dynamics of this structure-property-process relation in chapter five. Chapters five and six explore two avenues to increase the relaxation time of a bottlebrush polymer system and thus retain any shear induced color.

It should be noted that the work described in this thesis was carried out as part of a larger collaboration with the Guironnet, Diao, and Sing groups in order to develop bottlebrush polymer materials for applications in direct ink writing processes as an ink with on-the-fly tunable color based on the processing conditions experienced during printing. The collaboration with all three of these groups allows for a holistic understanding of the architecture and self-assembled structure of bottlebrush polymers on a molecular scale and the impact these fundamental properties can have on the material's macroscopic behavior.

1.9 References

[1] M. A. Wade, D. Walsh, J. C. W. Lee, *et al.*, "Color, Structure, and Rheology of a Diblock Bottlebrush Copolymer Solution," *Soft Matter*, vol. 16, no. 21, pp. 4919–4931, Jun. 2020, ISSN: 17446848. DOI: 10.1039/d0sm00397b. [Online]. Available: https://pubs.rsc.org/en/content/articlehtml/2020/sm/d0sm00397b%20https://pubs.rsc.org/en/content/articlelanding/2020/sm/d0sm00397b.

[2] S. Dutta, M. A. Wade, D. J. Walsh, D. Guironnet, S. A. Rogers, and C. E. Sing, "Dilute solution structure of bottlebrush polymers," *Soft Matter*, vol. 15, no. 14, pp. 2928–2941, 2019, ISSN: 17446848. DOI: 10.1039/c9sm00033j.

[3] T. Pan, S. Dutta, Y. Kamble, *et al.*, *Materials Design of Highly Branched Bottlebrush Polymers at the Intersection of Modeling, Synthesis, Processing, and Characterization*, 2022. DOI: 10.1021/acs.chemmater.1c04030. [Online]. Available: https://doi.org/10.1021/acs.chemmater.1c04030.

[4] I. N. Haugan, M. J. Maher, A. B. Chang, *et al.*, "Consequences of Grafting Density on the Linear Viscoelastic Behavior of Graft Polymers," *ACS Macro Letters*, vol. 7, no. 5, pp. 525–530, 2018, ISSN: 21611653. DOI: 10.1021/acsmacrolett.8b00116. [Online]. Available: http://pubs.acs.org/doi/10.1021/acsmacrolett.8b00116%20https://pubs.acs.org/sharingguidelines.

[5] S. J. Dalsin, M. A. Hillmyer, and F. S. Bates, "Linear Rheology of Polyolefin-Based Bottlebrush Polymers," *Macromolecules*, vol. 48, no. 13, pp. 4680–4691, 2015, ISSN: 15205835. DOI: 10.1021/acs.macromol.5b01153. [Online]. Available: https://pubs.acs.org/sharingguidelines%20http://pubs.acs.org/doi/pdf/10.1021/acs.macromol.5b01153.

[1] Ongoing research to be published in the near future.

[6] C. R. López-Barrón, A. H. Tsou, J. R. Hagadorn, and J. A. Throckmorton, "Highly Entangled α-Olefin Molecular Bottlebrushes: Melt Structure, Linear Rheology, and Interchain Friction Mechanism," *Macromolecules*, vol. 51, no. 17, pp. 6958–6966, 2018, ISSN: 0024-9297. DOI: 10.1021/acs.macromol.8b01431. [Online]. Available: http://pubs.acs.org/doi/10.1021/acs.macromol.8b01431.

[7] J. Rzayev, "Molecular bottlebrushes: New opportunities in nanomaterials fabrication," *ACS Macro Letters*, vol. 1, no. 9, pp. 1146–1149, 2012, ISSN: 21611653. DOI: 10.1021/mz300402x. [Online]. Available: https://pubs.acs.org/sharingguidelines.

[8] S. Lecommandoux, F. Chécot, R. Borsali, *et al.*, "Effect of dense grafting on the backbone conformation of bottlebrush polymers: Determination of the persistence length in solution," *Macromolecules*, vol. 35, no. 23, pp. 8878–8881, Nov. 2002, ISSN: 00249297. DOI: 10.1021/ma0203344. [Online]. Available: https://pubs.acs.org/sharingguidelines.

[9] S. Desvergne, V. Héroguez, Y. Gnanou, and R. Borsali, "Polymacromonomers: Dynamics of dilute and nondilute solutions," *Macromolecules*, vol. 38, no. 6, pp. 2400–2409, Mar. 2005, ISSN: 00249297. DOI: 10.1021/ma0487958.

[10] S. J. Dalsin, M. A. Hillmyer, and F. S. Bates, "Molecular weight dependence of zero-shear viscosity in atactic polypropylene bottlebrush polymers," *ACS Macro Letters*, vol. 3, no. 5, pp. 423–427, 2014, ISSN: 21611653. DOI: 10.1021/mz500082h. [Online]. Available: https://pubs.acs.org/sharingguidelines.

[11] S. L. Pesek, Q. Xiang, B. Hammouda, and R. Verduzco, "Small-angle neutron scattering analysis of bottlebrush backbone and side chain flexibility," *Journal of Polymer Science, Part B: Polymer Physics*, vol. 55, no. 1, pp. 104–111, 2017, ISSN: 10990488. DOI: 10.1002/polb.24251.

[12] S. Rathgeber, T. Pakula, A. Wilk, K. Matyjaszewski, H. i. Lee, and K. L. Beers, "Bottle-brush macromolecules in solution: Comparison between results obtained from scattering experiments and computer simulations," *Polymer*, vol. 47, no. 20, pp. 7318–7327, Sep. 2006, ISSN: 00323861. DOI: 10.1016/j.polymer.2006.06.010. [Online]. Available: https://www.sciencedirect.com/science/article/pii/S0032386106006872.

[13] H. Liang, G. S. Grest, and A. V. Dobrynin, "Brush-Like Polymers and Entanglements: From Linear Chains to Filaments," *ACS Macro Letters*, vol. 8, no. 10, pp. 1328–1333, 2019, ISSN: 2161-1653. DOI: 10.1021/acsmacrolett.9b00519.

[14] H. Liang, Z. Wang, S. S. Sheiko, and A. V. Dobrynin, "Comb and Bottlebrush Graft Copolymers in a Melt," *Macromolecules*, vol. 52, no. 10, pp. 3942–3950, 2019, ISSN: 15205835. DOI: 10.1021/acs.macromol.9b00611. [Online]. Available: https://pubs.acs.org/sharingguidelines.

[15] M. Hu, Y. Xia, G. B. McKenna, J. A. Kornfield, and R. H. Grubbs, "Linear Rheological Response of a Series of Densely Branched Brush Polymers," *Macromolecules*, vol. 44, no. 17, pp. 6935–6943, Sep. 2011, ISSN: 0024-9297. DOI: 10.1021/ma2009673. [Online]. Available: https://pubs.acs.org/sharingguidelines%20https://pubs.acs.org/doi/10.1021/ma2009673.

[16] C. R. López-Barrón, M. E. Shivokhin, and J. R. Hagadorn, "Extensional rheology of highly-entangled α-olefin molecular bottlebrushes," *Journal of Rheology*, vol. 63, no. 6, pp. 917–926, 2019, ISSN: 0148-6055. DOI: 10.1122/1.5110557.

[17] K. Terao, Y. Takeo, M. Tazaki, Y. Nakamura, and T. Norisuye, "Polymacromonomer Consisting of Polystyrene. Light Scattering Characterization in Cyclohexane," *Polymer Journal*, vol. 31, no. 2, pp. 193–198, Feb. 1999, ISSN: 0032-3896. DOI: 10.1295/polymj.31.193. [Online]. Available: http://www.nature.com/doifinder/10.1295/polymj.31.193.

[18] S. Jahromi, J. H. Palmen, and P. A. Steeman, "Rheology of side chain dendritic polymers," *Macromolecules*, vol. 33, no. 2, pp. 577–581, 2000, ISSN: 00249297. DOI: 10.1021/ma9905977.

[19] O. V. Borisov, E. B. Zhulina, and T. M. Birshtein, "Persistence length of dendritic molecular brushes," *ACS Macro Letters*, vol. 1, no. 10, pp. 1166–1169, Oct. 2012, ISSN: 21611653. DOI: 10.1021/mz3003903.

[20] Z. Qian, Y. P. Koh, M. R. Pallaka, *et al.*, "Linear Rheology of a Series of Second-Generation Dendronized Wedge Polymers," *Macromolecules*, vol. 52, no. 5, pp. 2063–2074, Mar. 2019, ISSN: 0024-9297. DOI: 10.1021/acs.macromol.8b02122. [Online]. Available: https://pubs.acs.org/sharingguidelines%20http://pubs.acs.org/doi/10.1021/acs.macromol.8b02122.

[21] A. Aluculesei, A. Pipertzis, V. A. Piunova, *et al.*, "Thermomechanical Behavior and Local Dynamics of Dendronized Block Copolymers and Constituent Homopolymers," *Macromolecules*, vol. 48, no. 12, pp. 4142–4150, Jun. 2015, ISSN: 15205835. DOI: 10.1021/acs.macromol.5b00779.

[22] B. M. Boyle, T. A. French, R. M. Pearson, B. G. McCarthy, and G. M. Miyake, "Structural Color for Additive Manufacturing: 3D-Printed Photonic Crystals from Block Copolymers," *ACS Nano*, vol. 11, no. 3, pp. 3052–3058, Mar. 2017, ISSN: 1936-0851. DOI: 10.1021/acsnano.7b00032. [Online]. Available: http://pubs.acs.org/doi/10.1021/acsnano.7b00032.

[23] H. Frauenrath, *Dendronized polymers - Building a new bridge from molecules to nanoscopic objects*, Mar. 2005. DOI: 10.1016/j.progpolymsci.2005.01.011.

[24] S. Costanzo, L. F. Scherz, T. Schweizer, *et al.*, "Rheology and Packing of Dendronized Polymers," *Macromolecules*, vol. 49, no. 18, pp. 7054–7068, 2016, ISSN: 15205835. DOI: 10.1021/acs.macromol.6b01311. [Online]. Available: https://pubs.acs.org/sharingguidelines.

[25] S. Costanzo, L. Scherz, G. Floudas, *et al.*, "Hybrid Dendronized Polymers as Molecular Objects: Viscoelastic Properties in the Melt," *Macromolecules*, vol. 52, no. 19, pp. 7331–7342, Oct. 2019, ISSN: 15205835. DOI: 10.1021/acs.macromol.9b01412.

[26] I. V. Mikhailov, A. A. Darinskii, E. B. Zhulina, O. V. Borisov, and F. A. Leermakers, "Persistence length of dendronized polymers: The self-consistent field theory," *Soft Matter*, vol. 11, no. 48, pp. 9367–9378, Dec. 2015, ISSN: 17446848. DOI: 10.1039/c5sm01620g.

[27] M. Hu, Y. Xia, C. S. Daeffler, *et al.*, "The linear rheological responses of wedge-type polymers," *Journal of Polymer Science Part B: Polymer Physics*, vol. 53, no. 13, pp. 899–906, Jul. 2015, ISSN: 08876266. DOI: 10.1002/polb.23716. [Online]. Available: http://doi.wiley.com/10.1002/polb.23716.

[28] A. D. Schlüter, A. Halperin, M. Kröger, D. Vlassopoulos, G. Wegner, and B. Zhang, "Dendronized polymers: Molecular objects between conventional linear polymers and colloidal particles," *ACS Macro Letters*, vol. 3, no. 10, pp. 991–998, Oct. 2014, ISSN: 21611653. DOI: 10.1021/mz500376e.

[29] W. F. Daniel, J. Burdyńska, M. Vatankhah-Varnoosfaderani, *et al.*, "Solvent-free, supersoft and superelastic bottlebrush melts and networks," *Nature Materials*, vol. 15, no. 2, pp. 183–189, 2016, ISSN: 14764660. DOI: 10.1038/nmat4508. [Online]. Available: http://www.nature.com/doifinder/10.1038/nmat4508%20www.nature.com/naturematerials.

[30] M. Abbasi, L. Faust, and M. Wilhelm, "Comb and Bottlebrush Polymers with Superior Rheological and Mechanical Properties," *Advanced Materials*, vol. 31, no. 26, p. 1 806 484, Feb. 2019, ISSN: 15214095. DOI: 10.1002/adma.201806484. [Online]. Available: http://doi.wiley.com/10.1002/adma.201806484.

[31] J. A. Johnson, Y. Y. Lu, A. O. Burts, *et al.*, "Drug-loaded, bivalent-bottle-brush polymers by graft-through ROMP," *Macromolecules*, vol. 43, no. 24, pp. 10 326–10 335, 2010, ISSN: 00249297. DOI: 10.1021/ma1021506.

[32] H. Unsal, S. Onbulak, F. Calik, *et al.*, "Interplay between Molecular Packing, Drug Loading, and Core Cross-Linking in Bottlebrush Copolymer Micelles," *Macromolecules*, vol. 50, no. 4, pp. 1342–1352, 2017, ISSN: 15205835. DOI: 10.1021/acs.macromol.6b02182. [Online]. Available: https://pubs.acs.org/sharingguidelines.

[33] H. i. Lee, J. Pietrasik, S. S. Sheiko, and K. Matyjaszewski, "Stimuli-responsive molecular brushes," *Progress in Polymer Science (Oxford)*, vol. 35, no. 1-2, pp. 24–44, Jan. 2010, ISSN: 00796700. DOI: 10.1016/j.progpolymsci.2009.11.002.

[34] X. Li, S. L. Prukop, S. L. Biswal, and R. Verduzco, "Surface properties of bottlebrush polymer thin films," *Macromolecules*, vol. 45, no. 17, pp. 7118–7127, 2012, ISSN: 00249297. DOI: 10.1021/ma301046n.

[35] A. L. Liberman-Martin, C. K. Chu, and R. H. Grubbs, "Application of Bottlebrush Block Copolymers as Photonic Crystals," *Macromolecular Rapid Communications*, vol. 38, no. 13, p. 1 700 058, Jul. 2017, ISSN: 10221336. DOI: 10.1002/marc.201700058. [Online]. Available: http://doi.wiley.com/10.1002/marc.201700058%20www.advancedsciencenews.com.

[36] C. M. Bates and F. S. Bates, "50th Anniversary Perspective : Block Polymers—Pure Potential," *Macromolecules*, vol. 50, no. 1, pp. 3–22, Jan. 2017, ISSN: 0024-9297. DOI: 10.1021/acs.macromol.6b02355. [Online]. Available: https://pubs.acs.org/doi/10.1021/acs.macromol.6b02355.

[37] Y. Fan, Y. Q. Cai, X. B. Fu, Y. Yao, and Y. Chen, "Core-shell type hyperbranched grafting copolymers: Preparation, characterization and investigation on their intrinsic fluorescence properties," *Polymer*, vol. 107, pp. 154–162, Dec. 2016, ISSN: 00323861. DOI: 10.1016/j.polymer.2016.11.018.

[38] J. Meissner, "Basic Parameters, Melt Rheology, Processing and End-use Properties of Three Similar Low density Polyethylene Samples," *Pure and Applied Chemistry*, vol. 4, pp. 551–574, 1975.

[39] F. W. Billmeyer, "The Molecular Structure of Polyethylene. III. Determination of Long Chain Branching 1," *Journal of the American Chemical Society*, vol. 75, no. 24, pp. 6118–6122, Dec. 1953, ISSN: 0002-7863. DOI: 10.1021/ja01120a007. [Online]. Available: https://pubs.acs.org/doi/abs/10.1021/ja01120a007.

[40] C. A. Sperati, W. A. Franta, and H. W. Starkweather, "The Molecular Structure of Polyethylene. V. The Effect of Chain Branching and Molecular Weight on Physical Properties," *Journal of the American Chemical Society*, vol. 75, no. 24, pp. 6127–6133, Dec. 1953, ISSN: 0002-7863. DOI: 10.1021/ja01120a009. [Online]. Available: https://pubs.acs.org/doi/abs/10.1021/ja01120a009.

[41] J. Tian, W. Yu, and C. Zhou, "The preparation and rheology characterization of long chain branching polypropylene," *Polymer*, vol. 47, no. 23, pp. 7962–7969, Oct. 2006, ISSN: 00323861. DOI: 10.1016/j.polymer.2006.09.042. [Online]. Available: https://linkinghub.elsevier.com/retrieve/pii/S0032386106011074.

[42] D. Yan, W.-J. Wang, and S. Zhu, "Effect of long chain branching on rheological properties of metallocene polyethylene," *Polymer*, vol. 40, no. 7, pp. 1737–1744, Mar. 1999, ISSN: 00323861. DOI: 10.1016/S0032-3861(98)00318-8. [Online]. Available: https://linkinghub.elsevier.com/retrieve/pii/S0032386198003188.

[43] M. H. Wagner, S. Kheirandish, and M. Yamaguchi, "Quantitative analysis of melt elongational behavior of LLDPE/LDPE blends," *Rheologica Acta*, vol. 44, no. 2, pp. 198–218, Dec. 2004, ISSN: 00354511. DOI: 10.1007/s00397-004-0400-9. [Online]. Available: https://link.springer.com/article/10.1007/s00397-004-0400-9.

[44] M. Daoud and J. Cotton, "Star shaped polymers : a model for the conformation and its concentration dependence," *Journal de Physique*, vol. 43, no. 3, pp. 531–538, 1982, ISSN: 0302-0738. DOI: 10.1051/jphys:01982004303053100. [Online]. Available: http://www.edpsciences.org/10.1051/jphys:01982004303053100.

[45] D. Vlassopoulos, G. Fytas, T. Pakula, and J. Roovers, "Multiarm star polymers dynamics," *Journal of Physics: Condensed Matter*, vol. 13, no. 41, R855–R876, Oct. 2001, ISSN: 0953-8984. DOI: 10.1088/0953-8984/13/41/202. [Online]. Available: https://iopscience.iop.org/article/10.1088/0953-8984/13/41/202.

[46] L. J. Fetters, A. D. Kiss, D. S. Pearson, M. Ag, D. Frankfurt, and F. J. Vitus, "Rheological Behavior of Star-Shaped Polymers," pp. 647–654, 1993.

[47] K. Yasuda, R. C. Armstrong, and R. E. Cohen, "Shear flow properties of concentrated solutions of linear and star branched polystyrenes," *Rheologica Acta*, vol. 20, no. 2, pp. 163–178, Mar. 1981, ISSN: 0035-4511. DOI: 10.1007/BF01513059. [Online]. Available: http://link.springer.com/10.1007/BF01513059.

[48] M. Doi and N. Y. Kuzuu, "Rheology of star polymers in concentrated solutions and melts," *Journal of Polymer Science: Polymer Letters Edition*, vol. 18, no. 12, pp. 775–780, Dec. 1980, ISSN: 03606384. DOI: 10.1002/pol.1980.130181205. [Online]. Available: https://onlinelibrary.wiley.com/doi/full/10.1002/pol.1980.130181205%20https://onlinelibrary.wiley.com/doi/abs/10.1002/pol.1980.130181205%20https://onlinelibrary.wiley.com/doi/10.1002/pol.1980.130181205.

[49] J. Roovers and P. M. Toporowski, "Hydrodynamic studies on model branched polystyrenes," *Journal of Polymer Science Part A-2: Polymer Physics*, vol. 18, no. 9, pp. 1907–1917, 1980. DOI: 10.1002/pol.1980.180180904. [Online]. Available: https://doi.org/10.1002/pol.1980.180180904.

[50] M. Kapnistos, K. M. Kirkwood, J. Ramirez, D. Vlassopoulos, and L. G. Leal, "Nonlinear rheology of model comb polymers," *Journal of Rheology*, vol. 53, no. 5, pp. 1133–1153, Sep. 2009, ISSN: 0148-6055. DOI: 10.1122/1.3191781. [Online]. Available: http://sor.scitation.org/doi/10.1122/1.3191781.

[51] H. Lentzakis, C. Das, D. Vlassopoulos, and D. J. Read, "Pom-pom-like constitutive equations for comb polymers," *Journal of Rheology*, vol. 58, no. 6, pp. 1855–1875, Nov. 2014, ISSN: 0148-6055. DOI: 10.1122/1.4895606. [Online]. Available: http://sor.scitation.org/doi/10.1122/1.4895606.

[52] M. Vatankhah-Varnosfaderani, W. F. Daniel, A. P. Zhushma, *et al.*, "Bottlebrush Elastomers: A New Platform for Freestanding Electroactuation," *Advanced Materials*, vol. 29, no. 2, 2017, ISSN: 15214095. DOI: 10.1002/adma.201604209.

[53] T. C. B. McLeish, "Molecular rheology of H-polymers," *Macromolecules*, vol. 21, no. 4, pp. 1062–1070, Apr. 1988, ISSN: 0024-9297. DOI: 10.1021/ma00182a037. [Online]. Available: https://pubs.acs.org/doi/abs/10.1021/ma00182a037.

[54] T. C. McLeish, "Polymer architecture influence on rheology," *Current Opinion in Solid State and Materials Science*, vol. 2, no. 6, pp. 678–682, Dec. 1997, ISSN: 13590286. DOI: 10.1016/S1359-0286(97)80009-5. [Online]. Available: https://linkinghub.elsevier.com/retrieve/pii/S1359028697800095.

[55] S. E. Seo and C. J. Hawker, *The Beauty of Branching in Polymer Science*, May 2020. DOI: 10.1021/acs.macromol.0c00286. [Online]. Available: https://pubs.acs.org/doi/full/10.1021/acs.macromol.0c00286%20https://dx.doi.org/10.1021/acs.macromol.0c00286.

[56] A. Hult, M. Johansson, and E. Malmström, "Hyperbranched Polymers," *Branched Polymers II*, pp. 1–34, 1999. DOI: 10.1007/3-540-49780-3{_}1. [Online]. Available: https://link.springer.com/chapter/10.1007/3-540-49780-3_1.

[57] A. Chremos and J. F. Douglas, "Communication: When does a branched polymer become a particle?" *Journal of Chemical Physics*, vol. 143, no. 11, pp. 111 104–111 106, Sep. 2015, ISSN: 00219606. DOI: 10.1063/1.4931483. [Online]. Available: http://dx.doi.org/10.1063/1.4931483]%20https://aip.scitation.org/doi/abs/10.1063/1.4931483.

[58] E. van Ruymbeke, H. Lee, T. Chang, *et al.*, "Molecular rheology of branched polymers: decoding and exploring the role of architectural dispersity through a synergy of anionic synthesis, interaction chromatography, rheometry and modeling," *Soft Matter*, vol. 10, no. 27, p. 4762, 2014, ISSN: 1744-683X. DOI: 10.1039/c4sm00105b. [Online]. Available: http://xlink.rsc.org/?DOI=c4sm00105b.

[59] F. La Mantia, A. Valenza, and D. Acierno, "Influence of the structure of linear density polyethylene on the rheological and mechanical properties of blends with low density polyethylene," *European Polymer Journal*, vol. 22, no. 8, pp. 647–652, Jan. 1986, ISSN: 00143057. DOI: 10.1016/0014-3057(86)90163-1. [Online]. Available: https://linkinghub.elsevier.com/retrieve/pii/0014305786901631.

[60] D. A. Tomalia, H. Baker, M. Hall, *et al.*, "Dendritic Macromolecules: Synthesis of Starburst Dendrimers," *Macromolecules*, vol. 19, no. 9, pp. 2466–2468, 1986, ISSN: 15205835. DOI: 10.1021/ma00163a029. [Online]. Available: https://pubs.acs.org/doi/abs/10.1021/ma00163a029.

[61] H. Iwawaki, T. Inoue, and Y. Nakamura, "Rheo-optical study on dynamics of bottlebrush-like polymacromonomer consisting of polystyrene," *Macromolecules*, vol. 44, no. 13, pp. 5414–5419, 2011, ISSN: 00249297. DOI: 10.1021/ma2008332. [Online]. Available: https://pubs.acs.org/sharingguidelines.

[62] H. Iwawaki, O. Urakawa, T. Inoue, and Y. Nakamura, "Rheo-optical study on dynamics of bottlebrush-like polymacromonomer consisting of polystyrene. II. side chain length dependence on dynamical stiffness of main chain," *Macromolecules*, vol. 45, no. 11, pp. 4801–4808, 2012, ISSN: 00249297. DOI: 10.1021/ma300269b. [Online]. Available: https://pubs.acs.org/sharingguidelines.

[63] H. Liang, B. J. Morgan, G. Xie, *et al.*, "Universality of the Entanglement Plateau Modulus of Comb and Bottlebrush Polymer Melts," *Macromolecules*, vol. 51, no. 23, pp. 10 028–10 039, Dec. 2018, ISSN: 0024-9297. DOI: 10.1021/acs.macromol.8b01761. [Online]. Available: https://pubs.acs.org/sharingguidelines%20https://pubs.acs.org/doi/10.1021/acs.macromol.8b01761.

[64] G. M. Miyake, R. A. Weitekamp, V. A. Piunova, and R. H. Grubbs, "Synthesis of isocyanate-based brush block copolymers and their rapid self-assembly to infrared-reflecting photonic crystals," *Journal of the American Chemical Society*, vol. 134, no. 34, pp. 14 249–14 254, 2012, ISSN: 00027863. DOI: 10.1021/ja306430k. [Online]. Available: https://pubs.acs.org/sharingguidelines.

[65] G. M. Miyake, V. A. Piunova, R. A. Weitekamp, and R. H. Grubbs, "Precisely tunable photonic crystals from rapidly self-assembling brush block copolymer blends," *Angewandte Chemie - International Edition*, vol. 51, no. 45, pp. 11 246–11 248, Nov. 2012, ISSN: 14337851. DOI: 10.1002/anie.201205743. [Online]. Available: http://doi.wiley.com/10.1002/anie.201205743.

[66] R. J. Macfarlane, B. Kim, B. Lee, *et al.*, "Improving brush polymer infrared one-dimensional photonic crystals via linear polymer additives," *Journal of the American Chemical Society*, vol. 136, no. 50, pp. 17 374–17 377, Dec. 2014, ISSN: 15205126. DOI: 10.1021/ja5093562. [Online]. Available: https://pubs.acs.org/sharingguidelines%20https://pubs.acs.org/doi/10.1021/ja5093562.

[67] C. G. Chae, Y. G. Yu, H. B. Seo, M. J. Kim, R. H. Grubbs, and J. S. Lee, "Experimental Formulation of Photonic Crystal Properties for Hierarchically Self-Assembled POSS-Bottlebrush Block Copolymers," *Macromolecules*, vol. 51, no. 9, pp. 3458–3466, 2018, ISSN: 15205835. DOI: 10.1021/acs.macromol.8b00298.

[68] J. D. Joannopoulos, S. G. Johnson, J. N. Winn, and R. D. Meade, *Photonic Crystals: Molding the Flow of Light*. Princeton, NJ: Princeton University Press, 2008, ISBN: 9780691124568.

[69] A. C. Edrington, A. M. Urbas, P. DeRege, *et al.*, "Polymer-based photonic crystals," *Advanced Materials*, vol. 6, no. 12, pp. 421–425, 2001, ISSN: 21622701.

[70] Y. Fink, J. N. Winn, S. Fan, *et al.*, "A dielectric omnidirectional reflector," *Science*, vol. 282, no. 5394, pp. 1679–1682, Nov. 1998, ISSN: 00368075. DOI: 10.1126/science.282.5394.1679. [Online]. Available: http://www.sciencemag.org/cgi/doi/10.1126/science.282.5394.1679.

[71] B. M. Boyle, J. L. Collins, T. E. Mensch, M. D. Ryan, B. S. Newell, and G. M. Miyake, "Impact of backbone composition on homopolymer dynamics and brush block copolymer self-assembly," *Polymer Chemistry*, vol. 11, no. 45, pp. 7147–7158, 2020, ISSN: 17599962. DOI: 10.1039/d0py01007c.

[72] T. Alfrey, E. F. Gurnee, and W. J. Schrenk, "Physical optics of iridescent multilayered plastic films," *Polymer Engineering & Science*, vol. 9, no. 6, pp. 400–404, 1969, ISSN: 15482634. DOI: 10.1002/pen.760090605.

[73] P. D. Hustad, G. R. Marchand, E. I. Garcia-Meitin, P. L. Roberts, and J. D. Weinhold, "Photonic polyethylene from self-assembled mesophases of polydisperse olefin block copolymers," *Macromolecules*, vol. 42, no. 11, pp. 3788–3794, 2009, ISSN: 00249297. DOI: 10.1021/ma9002819.

[74] J. K. D. Mapas, T. Thomay, A. N. Cartwright, J. Ilavsky, and J. Rzayev, "Ultrahigh molecular weight linear block copolymers: Rapid access by reversible-deactivation radical polymerization and self-assembly into large domain nanostructures," *Macromolecules*, vol. 49, no. 10, pp. 3733–3738, 2016, ISSN: 15205835. DOI: 10.1021/acs.macromol.6b00863. [Online]. Available: https://pubs.acs.org/sharingguidelines.

[75] M. B. Runge and N. B. Bowden, "Synthesis of High Molecular Weight Comb Block Copolymers and Their Assembly into Ordered Morphologies in the Solid State," 2007. DOI: 10.1021/ja072929q. [Online]. Available: https://pubs.acs.org/sharingguidelines.

[76] B. R. Sveinbjörnsson, R. A. Weitekamp, G. M. Miyake, *et al.*, "Rapid self-assembly of brush block copolymers to photonic crystals," *Proceedings of the National Academy of Sciences of the United States of America*, vol. 109, no. 36, pp. 14 332–14 336, 2012, ISSN: 00278424. DOI: 10.1073/pnas.1213055109. [Online]. Available: www.pnas.org/lookup/suppl/.

[77] T. Guo, Y. Wang, Y. Qiao, X. Yuan, Y. Zhao, and L. Ren, "Thermal property of photonic crystals (PCs) prepared by solvent annealing self-assembly of bottlebrush PS-b-PtBA," *Polymer*, vol. 194, p. 122 389, Apr. 2020, ISSN: 0032-3861. DOI: 10.1016/J.POLYMER.2020.122389.

[78] B. B. Patel, D. J. Walsh, D. H. Kim, *et al.*, "Tunable structural color of bottlebrush block copolymers through direct-write 3D printing from solution," *Science Advances*, vol. 6, no. 24, In Press, Jun. 2020, ISSN: 2375-2548. DOI: 10.1126/sciadv.aaz7202. [Online]. Available: http://advances.sciencemag.org/%20https://www.science.org/doi/10.1126/sciadv.aaz7202.

[79] V. G. Reynolds, S. Mukherjee, R. Xie, *et al.*, "Super-soft solvent-free bottlebrush elastomers for touch sensing," *Materials Horizons*, vol. 7, no. 1, pp. 181–187, 2020, ISSN: 20516355. DOI: 10.1039/c9mh00951e.

[80] M. Vatankhah-Varnosfaderani, W. F. Daniel, M. H. Everhart, *et al.*, "Mimicking biological stress–strain behaviour with synthetic elastomers," *Nature*, vol. 549, no. 7673, pp. 497–501, Sep. 2017, ISSN: 14764687. DOI: 10.1038/nature23673. [Online]. Available: https://www.nature.com/articles/nature23673.

[81] T. Pakula, Y. Zhang, K. Matyjaszewski, *et al.*, "Molecular brushes as super-soft elastomers," *Polymer*, vol. 47, no. 20, pp. 7198–7206, Sep. 2006, ISSN: 00323861. DOI: 10.1016/j.polymer.2006.05.064.

[82] V. Karimkhani, M. Vatankhah-Varnosfaderani, A. N. Keith, *et al.*, "Tissue-Mimetic Dielectric Actuators: Free-Standing, Stable, and Solvent-Free," *ACS Applied Polymer Materials*, vol. 2, no. 5, pp. 1741–1745, 2020, ISSN: 2637-6105. DOI: 10.1021/acsapm.0c00141. [Online]. Available: https://dx.doi.org/10.1021/acsapm.0c00141.

[83] A. N. Keith, M. Vatankhah-Varnosfaderani, C. Clair, *et al.*, "Bottlebrush Bridge between Soft Gels and Firm Tissues," *ACS Central Science*, vol. 6, no. 3, pp. 413–419, 2020, ISSN: 23747951. DOI: 10.1021/acscentsci.9b01216. [Online]. Available: https://dx.doi.org/10.1021/acscentsci.9b01216.

[84] M. Vatankhah-Varnosfaderani, A. N. Keith, Y. Cong, *et al.*, "Chameleon-like elastomers with molecularly encoded strain-adaptive stiffening and coloration," *Science*, vol. 359, no. 6383, pp. 1509–1513, Mar. 2018, ISSN: 10959203. DOI: 10.1126/science.aar5308. [Online]. Available: http://science.sciencemag.org/.

[85] S. S. Sheiko and A. V. Dobrynin, "Architectural Code for Rubber Elasticity: From Supersoft to Superfirm Materials," *Macromolecules*, vol. 52, no. 20, pp. 7531–7546, 2019, ISSN: 15205835. DOI: 10.1021/acs.macromol.9b01127. [Online]. Available: https://pubs.acs.org/sharingguidelines.

[86] Y. Chen and Z. Guan, "Self-healing thermoplastic elastomer brush copolymers having a glassy polymethylmethacrylate backbone and rubbery polyacrylate-amide brushes," *Polymer*, vol. 69, pp. 249–254, Jul. 2015, ISSN: 00323861. DOI: 10.1016/j.polymer.2015.03.023.

[87] M. Tang, P. Zheng, K. Wang, *et al.*, "Autonomous self-healing, self-adhesive, highly conductive composites based on a silver-filled polyborosiloxane/polydimethylsiloxane double-network elastomer," *Journal of Materials Chemistry A*, vol. 7, no. 48, pp. 27 278–27 288, 2019, ISSN: 20507496. DOI: 10.1039/c9ta09158k.

[88] J. L. Self, C. S. Sample, A. E. Levi, *et al.*, "Dynamic Bottlebrush Polymer Networks: Self-Healing in Super-Soft Materials," *Journal of the American Chemical Society*, vol. 142, no. 16, pp. 7567–7573, Apr. 2020, ISSN: 15205126. DOI: 10.1021/jacs.0c01467. [Online]. Available: https://pubs.acs.org/doi/full/10.1021/jacs.0c01467%20https://dx.doi.org/10.1021/jacs.0c01467.

[89] C. Choi, J. L. Self, Y. Okayama, *et al.*, "Light-Mediated Synthesis and Reprocessing of Dynamic Bottlebrush Elastomers under Ambient Conditions," *Journal of the American Chemical Society*, vol. 143, no. 26, pp. 9866–9871, 2021, ISSN: 15205126. DOI: 10.1021/jacs.1c03686. [Online]. Available: https://doi.org/10.1021/jacs.1c03686.

[90] R. Xie, S. Mukherjee, A. E. Levi, *et al.*, "Room temperature 3D printing of super-soft and solvent-free elastomers," *Science Advances*, vol. 6, no. 46, eabc6900, Nov. 2020, ISSN: 23752548. DOI: 10.1126/sciadv.abc6900. [Online]. Available: https://advances.sciencemag.org/lookup/doi/10.1126/sciadv.abc6900%20https://www.science.org.

[91] R. Xie, S. Mukherjee, A. E. Levi, *et al.*, "Yielding Behavior of Bottlebrush and Linear Block Copolymers," *Macromolecules*, vol. 54, no. 12, pp. 5636–5647, Jun. 2021, ISSN: 15205835. DOI: 10.1021/acs.macromol.1c00557. [Online]. Available: https://pubs.acs.org/doi/10.1021/acs.macromol.1c00557%20https://doi.org/10.1021/acs.macromol.1c00557.

[92] W. F. Daniel, G. Xie, M. Vatankhah Varnoosfaderani, *et al.*, "Bottlebrush-Guided Polymer Crystallization Resulting in Supersoft and Reversibly Moldable Physical Networks," *Macromolecules*, vol. 50, no. 5, pp. 2103–2111, 2017, ISSN: 15205835. DOI: 10.1021/acs.macromol.7b00030. [Online]. Available: https://pubs.acs.org/sharingguidelines.

[93] D. E. Angelescu, J. H. Waller, R. A. Register, and P. M. Chaikin, "Shear-Induced Alignment in Thin Films of Spherical Nanodomains," *Advanced Materials*, vol. 17, no. 15, pp. 1878–1881, Aug. 2005, ISSN: 1521-4095. DOI: 10.1002/ADMA.200401994. [Online]. Available: https://onlinelibrary.wiley.com/doi/full/10.1002/adma.200401994%20https://onlinelibrary.wiley.com/doi/abs/10.1002/adma.200401994%20https://onlinelibrary.wiley.com/doi/10.1002/adma.200401994.

[94] K. I. Winey, S. S. Patel, R. G. Larson, and H. Watanabe, "Interdependence of Shear Deformations and Block Copolymer Morphology," *Macromolecules*, vol. 26, no. 10, pp. 2542–2549, 1993, ISSN: 15205835. DOI: 10.1021/ma00062a024.

[95] A. Nikoubashman, R. A. Register, and A. Z. Panagiotopoulos, "Sequential Domain Realignment Driven by Conformational Asymmetry in Block Copolymer Thin Films," *Macromolecules*, vol. 47, no. 3, pp. 1193–1198, Feb. 2014, ISSN: 0024-9297. DOI: 10.1021/ma402526q. [Online]. Available: https://pubs.acs.org/doi/10.1021/ma402526q.

[96] A. P. Marencic and R. A. Register, "Controlling Order in Block Copolymer Thin Films for Nanopatterning Applications," *Annual Review of Chemical and Biomolecular Engineering*, vol. 1, no. 1, pp. 277–297, Jun. 2010, ISSN: 1947-5438. DOI: 10.1146/annurev-chembioeng-073009-101007. [Online]. Available: https://www.annualreviews.org/doi/10.1146/annurev-chembioeng-073009-101007.

[97] A. S. Wunenburger, A. Colin, T. Colin, and D. Roux, "Undulation instability under shear: A model to explain the different orientations of a lamellar phase under shear?" *European Physical Journal E*, vol. 2, no. 3, pp. 277–283, 2000, ISSN: 12928941. DOI: 10.1007/PL00013669. [Online]. Available: https://link.springer.com/content/pdf/10.1007%2FPL00013669.pdf.

[98] O. Diat, D. Roux, and F. Nallet, "Effect of shear on a lyotropic lamellar phase," *Journal de Physique II*, vol. 3, no. 9, pp. 1427–1452, 1993, ISSN: 1427-1452. DOI: 10.1051/jp2:1993211{\"{i}}. [Online]. Available: https://hal.archives-ouvertes.fr/jpa-00247917.

[99] J. Raeburn, A. Z. Cardoso, and D. J. Adams, "The importance of the self-assembly process to control mechanical properties of low molecular weight hydrogels," *Chemical Society Reviews*, vol. 42, no. 12, pp. 5143–5156, 2013, ISSN: 14604744. DOI: 10.1039/c3cs60030k.

[100] G. Qu, J. J. Kwok, and Y. Diao, "Flow-Directed Crystallization for Printed Electronics," *Accounts of Chemical Research*, vol. 49, no. 12, pp. 2756–2764, 2016, ISSN: 15204898. DOI: 10.1021/acs.accounts.6b00445.

[101] Y. Diao, L. Shaw, Z. Bao, and S. C. B. Mannsfeld, "Morphology control strategies for solution-processed organic semiconductor thin films," *Energy and Environmental Science*, vol. 7, no. 7, pp. 2145–2159, 2014, ISSN: 17545706. DOI: 10.1039/c4ee00688g.

[102] R. C. Hayward and D. J. Pochan, "Tailored assemblies of block copolymers in solution: It is all about the process," *Macromolecules*, vol. 43, no. 8, pp. 3577–3584, 2010, ISSN: 00249297. DOI: 10.1021/ma9026806.

[103] D. E. Angelescu, J. H. Waller, D. H. Adamson, *et al.*, "Macroscopic Orientation of Block Copolymer Cylinders in Single-Layer Films by Shearing," *Advanced Materials*, vol. 16, no. 19, pp. 1736–1740, Oct. 2004, ISSN: 0935-9648. DOI: 10.1002/adma.200400643. [Online]. Available: https://onlinelibrary.wiley.com/doi/10.1002/adma.200400643.

[104] T. L. Choi and R. H. Grubbs, "Controlled living ring-opening-metathesis polymerization by a fast-initiating ruthenium catalyst," *Angewandte Chemie - International Edition*, vol. 42, no. 15, pp. 1743–1746, 2003, ISSN: 14337851. DOI: 10.1002/anie.200250632. [Online]. Available: www.angewandte.org.

[105] B. G. G. Lohmeijer, R. C. Pratt, F. Leibfarth, *et al.*, "Guanidine and Amidine Organocatalysts for Ring-Opening Polymerization of Cyclic Esters," *Macromolecules*, vol. 39, no. 25, pp. 8574–8583, Dec. 2006, ISSN: 0024-9297. DOI: 10.1021/ma0619381. [Online]. Available: https://pubs.acs.org/doi/10.1021/ma0619381.

[106] C. W. Bielawski and R. H. Grubbs, "Living ring-opening metathesis polymerization," *Progress in Polymer Science*, vol. 32, no. 1, pp. 1–29, Jan. 2007, ISSN: 0079-6700. DOI: 10.1016/J.PROGPOLYMSCI.2006.08.006.

[107] D. J. Walsh and D. Guironnet, "Macromolecules with programmable shape, size, and chemistry," *Proceedings of the National Academy of Sciences of the United States of America*, vol. 116, no. 5, pp. 1538–1542, Jan. 2019, ISSN: 10916490. DOI: 10.1073/pnas.1817745116.

Chapter 2

Control Over Architecture and its Impact on Physical Properties[1]

2.1 Chapter Overview

In this chapter, the fundamental structure and architecture of bottlebrush polymers are explored in order to lay the foundation towards developing structure-property relations between bottlebrush polymers and their self-assembled microstructure in later chapters. Two studies are discussed that address the impact of polymer architecture on shape and size of these molecules as well as the polymer's macroscopic properties. In one study, three series of polylactic acid bottlebrushes were synthesized with varying backbone and side chain lengths, n_{bb} and n_{sc}, respectively. Two of these sets had a constant side chain lengths of $n_{sc} = 30$ and 70 repeat units with varying backbone length, while the third set had a constant backbone length of $n_{bb} = 200$ repeat units with varying side chain length. This set of samples captured a representative range of possible length scales for these polymers. These bottlebrushes were dispersed in dilute solution and their intrinsic viscosity and hydrodynamic radius were determined through viscometry and dynamic light scattering. From these values, we identify transitions from a star-like structure to a short cylinder to a flexible cylinder with increasing n_{bb}. We also observe a small increase in scaling factors with n_{sc}, corresponding to a stiffening of the polymer with side chain length. In the second study, two polystryene bottlebrush polymers were synthesized, one with mono-disperse side chains and another with tri-disperse side chains. These two bottlebrushes were used to probe the importance of side chain dispersity on the bulk properties of a bottlebrush system. Utilizing oscillatory melt rheology, the storage and loss moduli master curves are measured. We plot the master curves in the van-Gurp and Palmen presentation and observe a shift in the relaxation mode and in the phase angle, indicating that the mono-disperse bottlebrush is more flexible than the tri-disperse bottlebrush. Through these studies, we are able to relate bottlebrush dimensions and architecture to their size and conformation while also demonstrating the impact these dimensions can have on a bottlebrush's physical properties.

[1] This chapter has been adapted from the following publications with permission: [1], [2]

2.2 Introduction

Prior to exploring the structure-property relations that govern the photonic properties of bottlebrush polymer systems and applying these systems to various printing processes, it is first necessary to understand how bottlebrush architecture and chemistry affects the the polymer's fundamental behavior and shape. Developing this understanding allows for the selection of specific dimensions and compositions to achieve desired material properties. Such a goal presents a daunting challenge due to the extensive sample space made available simply by modifying the bottlebrush's backbone length, n_{bb}, the side chain length, n_{sc}, grafting density, ρ_{graft}, and the backbone dispersity, $Đ_{bb}$, and side chain dispersity, $Đ_{sc}$. As would be expected, the the shear size of this sample space has generated a significant amount of interest throughout the macromolecular community [3]–[18].

Extensive theoretical and simulation studies of bottlebrush polymers have focused on developing scaling relations between the polymer's architectural parameters (n_{bb}, n_{sc}, ρ_{graft}, etc) and conformational measures, such as the persistence length, ℓ_p, intrinsic viscosity, $[\eta]$, hydrodynamic radius, R_h, and radius of gyration, R_g [5], [19]–[25]. Early works such as Fredrickson et al., identified 3 distinct regimes relating polymer shape and flexibility to the graft density and side chain length, noting an stiffening of the molecule with increased graft density and side chain length, essentially delineating between linear, comb, and bottlebrush polymers [5]. When exploring the relation between n_{bb} and conformational parameters, several theoretical studies have predicted that the overall size of a bottlebrush polymer scales with an exponent in the range of 0.6 to 0.7 [22], [23], [25].

While there are comparatively fewer pieces of literature on the experimental front due to challenges with the synthesis of these complex molecules, there are a number of experimental studies that demonstrate similar scaling trends between the size and persistence length and the side chain and graft density [16], [26]–[30]. Specifically, small angle neutron scattering (SANS) studies carried out by Pesek et al and Pesek et al, demonstrate conformational changes from spherical to rod-like to flexible cylinders with increaseing n_{bb} [16], [28]. The impact of side chain and graft density was explored by Lecommandoux et al., and Filippov et al., utilizing small angle neutron scattering and viscosity and light scattering measurments, respectively [29], [30]. Their studies demonstrate that ℓ_p increases by orders of magnitude as n_{sc} increases.

The challenges of characterizing the broad architectural parameter space is further complicated when considering the fact that different branch chemistry and architecture can play a significant role in the overall conformation and macroscopic behavior of the polymer. For example, replacing the linear side chains with dendrimers has been shown to have a significant impact on ℓ_p by Dutertre et al., and Grebikova et al., [31], [32]. Increasing the generation of the dendrimer from third to sixth generation has been shown to further increase the persitance length, resulting the polymer appearing as a semi-rigid chain [33].

Recent developments to the synthetic method have led to the synthesis of bottlebrushes with longer arms and backbones then have been previously characterized in the literature [34]–[36]. To build upon the experimental literature that explores the impact of architectural parameters on conformational measures, we characterized the shape and conformations adopted by a series of bottlebrush polymers through viscometric and dynamic light scattering studies. This study captured a representative range of architectures and length scales to provide as further insight into the dependence of bottlebrush's conformation on both backbone length and side chain length. We also looked into the impact of side chain architecture on macroscopic properties and the sensitivity of the bottlebrushes to changes in this architecture. To explore this sensitivity, we considerd two bottlebrushes, one with uniform side chains and one with disperse side chains and performed rheological measurements to see how the macroscopic properties of these materials were affected by small

variations in side chain composition.

It should be noted that the data discussed in this in this chapter were used to verify and tune simulation and synthesis studies carried out by Dr. Sarit Dutta and Dr. Dylan Walsh, respectively. In the case of the simulation studies, the intrinsic viscosity and hydrodynamic radius measures were used to adjust a series of course grained simulations carried out by Dutta et al., [1] thus ensuring the simulations accurately represented physical systems. These simulations allowed us to supplement our understanding of the shape and size of bottlebrush polymers under dilute conditions with the conformation of the molecule, while simultaneously exploring a broader sample space than was practical with experimental methods. As for the synthesis studies, the SEC studies carried out by Walsh et al., [2] on bottlebrushes with mono-disperse and tridisperse arms verified the rheological similarities observed between the two polymers at long length scales. The synthetic analysis, when combined with rheological measurements allows for broader conclusions to be made about the ability of SEC to clearly distinguish between complex molecules of similar molecular weights. Due to the scope of this chapter, the details of the simulations and synthetic characterization from Dutta et al., and Walsh et al., [1], [2] will not be discussed in full.

2.3 Experimental Methods

2.3.1 Material Synthesis and Preparation

For the studies discussed in this chapter, PLA-g-poly(norbornene) and PS-g-poly(norbornene) bottlebrush polymers were synthesized by our collaborators Dr. Dylan Walsh and Prof. Guironnet through ring opening metathesis polymerization according to the methods discussed in Section 1.7. To explore the impact of polymer architecture on the bottlebrush's overall shape and size, 3 different series of bottlebrush polymers were synthesized, spanning a range of backbone and side chain lengths. Two additional bottlebrushes were synthesized with mono-disperse and tri-disperse side chain lengths to identify the importance and impact of side chain dispersity on the macroscopic properties of these bottlebrush polymers.

2.3.1.1 Preparation of Backbone and Side Chain Sweeps

Three series of bottlebrushes were prepared: (i) backbone sweep with long side chains, spanning backbone DP (n_{bb}) from 10 to 1000 at side chain DP (n_{sc}) of 70 polylactic acid (PLA) repeat units (see Table 2.1); (ii) backbone sweep with short side chains, spanning n_{bb} from 10 to 2000 at n_{sc} = 30 PLA repeat units (see Table 2.2); and (iii) side chain sweep, spanning n_{sc} from 5 to 100 at nbb = 200 (see Table 2.3). The spacings between the samples were increased exponentially for each of the above sweeps. Linear poly-(5-norbornene-2-(methylbenzoate)) samples with DP ranging from 10 to 1000 were also synthesized via ROMP (see Table 2.4) to serve as a comparison to linear polymer behavior. GPC traces are provided in Appendix A. The increased dispersity with n_{bb} is likely caused by the slow decomposition of the ruthenium complex.

Dilute solutions of these bottlebrush polymers were prepared by dissolving the bottlebrushes in filtered chlorobenzene to form bulk solutions with concentrations ranging from 12 mg mL^{-1} to 15 mg mL^{-1}. The solutions were mixed on a shaker table for approximately 12 h at 200 rpm to ensure even dispersal of bottlebrushes in the solution. Chlorobenzene (CB) was chosen as the solvent for two reasons: (i) PLA bottlebrushes could be readily dissolved in CB, and (ii) CB has a relatively high boiling point compared to other organic solvents, which reduces the effects of solvent evaporation.

Table 2.1: Bottlebrush polymers used in backbone sweep with long side chains.

Theory		Macromonomer			Bottlebrush		
n_{sc}	n_{bb}	$M_n(gmol^{-1})$	n_{sc}	Đ	$M_n \times 10^3(gmol^{-1})$	$M_n \times 10^3(gmol^{-1})$	Đ
70	10	5200	70.4	1.06	52	44.9	1.06
70	19	5200	70.4	1.06	100	63.3	1.06
70	37	5200	70.4	1.06	194	94.7	1.04
70	72	5200	70.4	1.06	375	152	1.04
70	139	5200	70.4	1.06	724	254	1.05
70	268	5200	70.4	1.06	1400	496	1.04
70	518	5200	70.4	1.06	2700	918	1.13
70	1000	5200	70.4	1.06	5200	1300	1.13

Table 2.2: Bottlebrush polymers used in backbone sweep with short side chains.

Theory		Macromonomer			Bottlebrush		
n_{sc}	n_{bb}	$M_n(gmol^{-1})$	n_{sc}	Đ	$M_n \times 10^3(gmol^{-1})$	$M_n \times 10^3(gmol^{-1})$	Đ
30	10	2300	30.4	1.09	23.2	23.2	1.06
30	19	2300	30.4	1.09	44.8	34.8	1.05
30	37	2300	30.4	1.09	86.4	52.3	1.04
30	72	2300	30.4	1.09	167	84.7	1.04
30	139	2300	30.4	1.09	322	151	1.04
30	268	2300	30.4	1.09	622	281	1.09
30	518	2300	30.4	1.09	1200	539	1.09
30	1000	2300	30.4	1.09	2320	928	1.18
30	2000	2300	30.4	1.09	4640	1360	1.29

2.3.1.2 Preparation of Bottlebrushes with Mixed Side-Chain Dispersity

To capture the significance of arm dispersity on the macroscopic properties of a bottlebrush polymer, two bottlebrush polymers were prepared with the same molecular weight, but different arm dispersites. The arms were synthesized via an anionic polymerization of styrene initiated by secBuLi, and the reaction was quenched with ethylene oxide followed by the addition of norbornene-2-acid chloride [37]–[40]. The anionic polymerization of styrene produces very narrowly dispersed polymers; thus, to get a broader arm distribution, three different degrees of polymerization arms were mixed with equimolar ratio (M_n: 2500; 4300; 6000 g/mol). Ring-opening metathesis polymerization (ROMP) was used to synthesize the bottlebrushes, with $BB-narrow$ referring to the bottlebrush made with $M_n = 4300$ g/mol arms and $BB-mix$ referring to the bottlebrush made from the mixture of arm degree of polymerization [34], [41], [42].As illustrated in Figure 2.1, both bottlebrushes produce essentially identical SEC traces.

2.3.2 Viscometry

The viscosity of each bottlebrush solution in the two backbone sweeps and the side chain sweep described in Tables 2.1, 2.2 and 2.3 was measured at 30 °C using two Cannon–Fenske capillary viscometers with different conversion constants. The viscometers were suspended in a heated ethylene glycol bath to prevent temperature variation. The viscosity was measured for bottlebrush solutions with concentrations between 2 mg mL^{-1} and 15 mg mL^{-1}. Changes in concentration were achieved by removing the small amounts of

Table 2.3: Bottlebrush polymers used in side chain sweep.

Theory		Macromonomer			Bottlebrush		
n_{sc}	n_{bb}	$M_n(gmol^{-1})$	n_{sc}	Đ	$M_n \times 10^3(gmol^{-1})$	$M_n \times 10^3(gmol^{-1})$	Đ
18	200	1500	19	1.11	297	158	1.04
25	200	2000	27	1.09	411	186	1.03
36	200	2900	38	1.08	578	220	1.03
51	200	3900	53	1.07	785	270	1.04
72	200	5200	71	1.06	1050	327	1.04
103	200	7400	101	1.05	1477	399	1.04

Table 2.4: Samples used for linear poly(5-norbornene-2-(methylbenzoate)) sweep.

n_{bb}	$M_n \times 10^3(theory)(gmol^{-1})$	$M_n \times 10^3(GPC)(gmol^{-1})$	Đ
10	2.28	2.26	1.16
19	4.41	4.50	1.21
37	8.51	8.97	1.05
72	16.4	17.1	1.06
139	31.7	31.7	1.04
268	61.2	60.4	1.06
518	118	117	1.09
1000	228	222	1.17

bottlebrush solution from the viscometer and adding the solvent to the viscometer. The intrinsic viscosity, $[\eta]$, was determined by fitting these concentration sweeps to the Kraemer [43] and Huggins [44] models,

$$\eta_{sp}/C = [\eta] + k_h[\eta]^2 C \tag{2.1}$$

and

$$ln(\eta_{rel})/C = [\eta] + k_k[\eta]^2 C, \tag{2.2}$$

respectively. In these two equations, $[\eta]$, η_{sp}, and η_{rel} are the intrinsic, specific, and relative viscosities of the sample, respectively; k_h and k_k are the fitting parameters for the Huggins and Kraemer equations, respectively; C is the concentration of the sample. Fits calculated using these two equations were extrapolated to zero concentration to determine the intrinsic viscosity as shown in Appendix A Figure A.2 for a set of representative bottlebrushes.

2.3.3 Dynamic Light Scattering

Dynamic light scattering was performed using a Malvern Zetasizer Nano S90 to determine the center-of-mass diffusion coefficient and hydrodynamic radius of bottlebrush polymer solutions from the two backbone sweeps and arm sweeps. The setup consisted of a 4 mW HeNe laser with a wavelength of 633 nm and an Avalanche photodiode located at a fixed scattering angle of 90° relative to the incident laser beam [45]–[47]. We note that performing scattering at this relatively large wave-vector may introduce some wave-vector dependence on the hydrodynamic radius. As will be shown, measurements carried out with this setup are consistent with the intrinsic viscosity and thus we do not pursue studying this wave-vector dependence. Bottlebrush samples were diluted in chlorobenzene to concentrations ranging from 4 mg mL^{-1} to 12 mg mL^{-1} and loaded into glass cuvettes. Prior to testing, the samples were heated to a temperature of 30 °C at which point they were

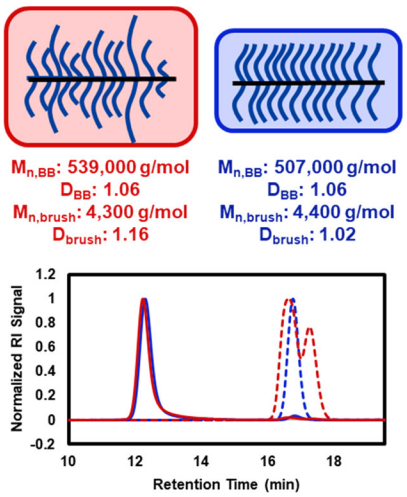

Figure 2.1: SEC Traces for graft-through polymerization with different arm dispersities. (SEC data is from conventional calibration with respect to PS standards). Figure assembled by Dr. Walsh for [2]. Reprinted with permission.

allowed to reach thermal equilibrium over a period of 5 min.

During each test, the intensity of light as a function of time was recorded and compared with itself to generate an autocorrelation function (Equation 2.3). Using the Zetasizer software package provided by Malvern, a set of exponential decay functions were fit to the autocorrelation function according to the cumulant method (Equation 2.4). The center-of-mass diffusivity was determined from the exponential decay coefficient, which was in turn used to calculate the hydrodynamic radius according to the Stokes–Einstein equation (Equations 2.5 and 2.6, respectively).

The autocorrelation function is given by

$$g^{(2)}(\tau) =< I(t)I(t+\tau) > / < I(t) >^2, \tag{2.3}$$

where $g^{(2)}$ is the correlation coefficient, I is the intensity of the scattered light, t is the time, and τ is the time offset. The Zetasizer software fit this data to a set of exponential decay functions according to the method of cumulants. While it is difficult to replicate this process manually, it is possible to check the results generated by the program by fitting the autocorrelation function to a single exponential decay function

$$g^{(2)}(\tau) = Ae^{\Gamma\tau} + b, \tag{2.4}$$

where A and b are fitting parameters and Γ is the decay coefficient. Representative fits using eq 2.4 are shown in Appendix A, Figure A.4. The decay coefficient is directly related to the diffusivity D and the scattering wave vector q via the equation

$$\Gamma = q^2 D. \tag{2.5}$$

Based on the conditions under which this measurement is performed, q is calculated to be 0.0303 nm^{-1}. The hydrodynamic radius is then calculated from the resulting diffusivity constant through the application of the Stokes-Einstein relation

$$D = (k_B T)/(6\pi\eta_s R_h), \tag{2.6}$$

where k_B is the Boltzmann constant, T is the temperature of the sample during the measurement, and η_s is the viscosity of the solvent.

Both D and R_h are known to vary as a function of the concentration of the sample. As such, it is necessary to remove any concentration dependence from these values by extrapolating D and R_h to the limit of infinite dilution. The relation between R_h and concentration is assumed to be a power series of the form

$$R_h = R_0 + aC + bC^2 + ..., \tag{2.7}$$

where R_0 is the hydrodynamic radius in the limit of infinite dilution, and a and b are series coefficients. Fitting the experimentally determined hydrodynamic radii to equation 2.7 (truncated after the quadratic term) provides a direct determination of the R_h at zero concentration. Representative fits using this scheme are shown in Appendix A, Figure A.5.

To verify the accuracy of the diffusivities and hydrodynamic radii calculated by the Zetasizer software, manual calculations were carried out on several samples and compared with the values reported by the software.

2.3.4 Rheology

Rheological time temperature super position studies were carried out on the two bottlebrushes with monodisperse and tridisperse arms. Prior to testing, samples were first formed into uniform pucks using a hot press heated to 130 °C by placing powdered bottlebrush polymer into a 1mm thick × 10 mm diameter circular mold. This mold was placed between two sheets of kapton to ensure that any excess sample did not stick to or damage the platens in the hot press. During hot pressing, two metric ton were applied to the polymer samples for 5 minutes to remove all air bubbles from the sample. If bubbles were observed upon removal from the hot press, additional bottlebrush sample was added to the mold and the hot pressing was hot pressed again. This procedure was repeated until no voids were observed within the formed sample. After hot pressing, samples were left in the mold and were allowed to cool to room temperature. The polymer samples were then removed from the mold by uniformly pressing on the material near the edge of the mold. The uniform pressure minimized the chances of the sample fracturing during mold extraction.

Linear-regime frequency sweeps were carried out on the prepared puck samples using a TA Instruments ARES G2 rheometer equipped with a forced convection oven for temperature control and a 10 mm parallel plate geometry. Frequency sweeps were measured from 0.1 to 100 rad/s with strain amplitudes of 1% for temperatures from 140 to 180 °C, 0.1% for temperatures from 120 to 130 °C, and 0.01% for temperatures from 115 to 120 °C. Strain amplitudes were selected based on a series of strain amplitude sweeps carried out prior to preforming the frequency sweeps. These amplitudes were selected to maximize signal-to-noise while remaining rheologically linear at each temperature. All measurements were performed in a dry nitrogen environment to prevent sample degradation due to oxidation.

2.4 Results and Discussion

2.4.1 Fundamental Bottlebrush Structure and Shape

2.4.1.1 Intrinsic Viscosity

Intrinsic viscosity measurements were performed on a the three series of bottlebrush polymers as described in Section 2.3.1.1. We plot these experimental results as a function of molecular weight M in Figure 2.2.a for bottlebrush molecules with M_{sc} = 2237 and 5220 Da, and linear polynorbornene (PNB). The experimental data for linear PNB fit a power-law behavior $[\eta] \sim M^{0.67}$. The corresponding data for the two backbone sweeps yields scaling parameters of 0.57 and 0.62 for the short and long arm bottlebrushes, respectively at high degrees of backbone polymerization. At n_{bb}, intrinsic viscosity of these bottlebrushes appears independent of molecular weight. The two distinct scaling regimes suggests a transition in the conformation of the bottlebrush as n_{bb} increases. Figure 2.2.b depicts the intrinsic viscosity for bottlebrush molecules with a M_{sc} = 1.88 $\times 10^4$ Da which exhibits a scaling relation of $[\eta] \sim M^{0.19}$. This result suggests that increasing n_{sc} for moderately large bottlebrushes leads to an increase in the size of the molecule, likely due to a "stiffening" of the molecule.

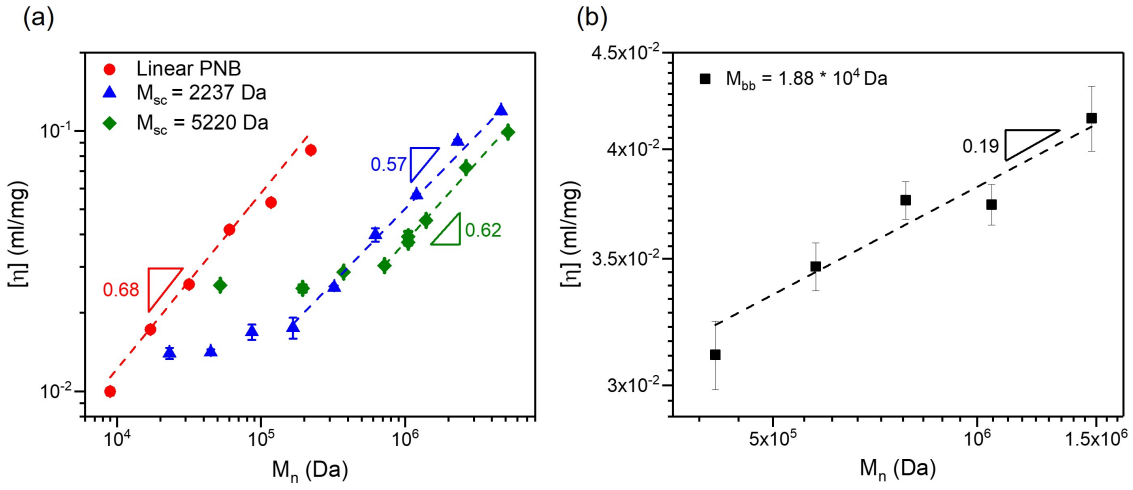

Figure 2.2: Intrinsic viscosity $[\eta]$ as a function of bottlebrush molecular weight for a) the two backbone sweeps and b) the side chain sweep. Data were captured at a temperature of 30 °C. The dashed lines are linear fits to the higher molecular weight data with the resulting scaling factors labeled next to each line.

These experimental results are compared with the simulations conducted by our collaborator in Appendix A Figure A.3, demonstrating qualitative agreement with the experimental measures. The simulation results determined by Dr. Dutta yield $[\eta] \sim M^{0.73}$, which is slightly higher than the experimental result. This differences is to be expected, as the simulations assume an athermal solvent [1]. Despite the slight differences between the experimental results and the simulation, the resulting power law scalings of these studies are in close agreement with the Flory–Fox relationship, consistent with the expectation for a coil in a good solvent. Furthermore, the bottlebrush measurements are consistent with the previous literature [6], [48], [49], showing significant deviations from the Flory–Fox result at low M, with very little initial change in $[\eta]$ with increasing M. We attribute this deviation from the Flory-Fox result to the bottlebrush adopting a star-like conformation at low-$n_b b$, with additional backbone monomers increasing the local density of the branches rather than the

overall aspect ratio of the molecule. This result is supported by simulation snapshots captured in the low-n_{bb} limit by Dr. Dutta and shown in Figure 2.3 [1]. At high M, however, there is once again an increase in the intrinsic viscosity as added n_{bb} reflects an increase in the molecular structure. Interestingly, this system exhibits significant differences in $[\eta]$ values as the molecular structure is changed by either adding to the backbone or branches for a given molecular weight, and thus allows us to distinguish the architecture of the synthesized molecule via experimental characterization. However, many of the differences in $[\eta]$ versus M become less pronounced upon plotting instead versus M_{bb} in the limit of high M_{bb} (Figure A.3). This reflects the increased importance of the backbone length in this limit, which is the primary quantity establishing the molecular size as captured by $[\eta]$.

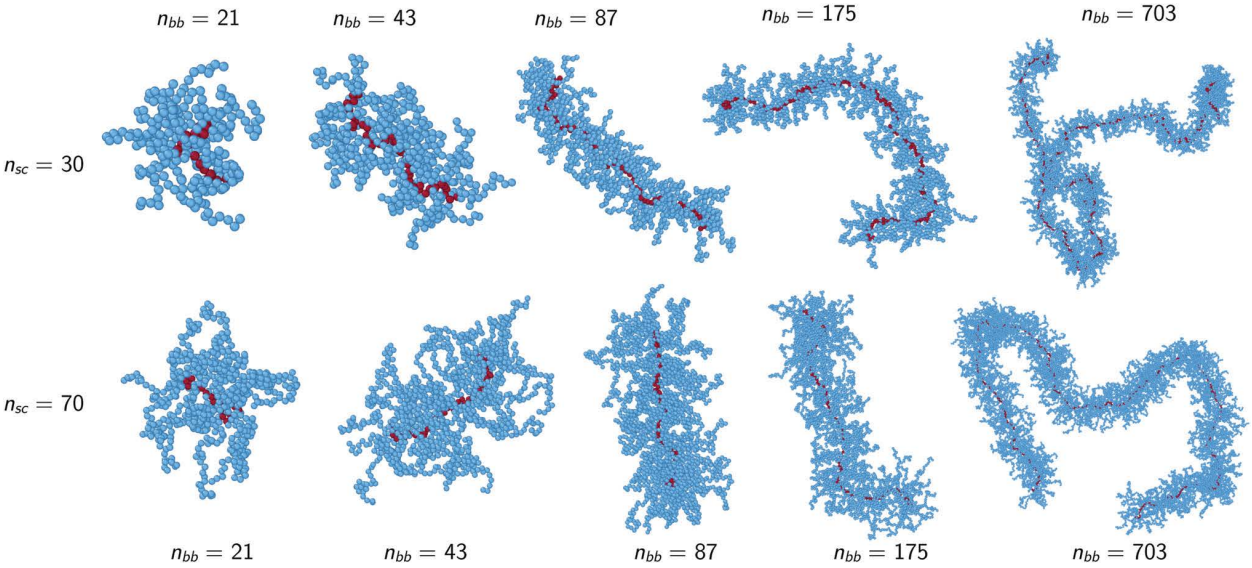

Figure 2.3: Simulation snapshots of a bottlebrush with varying backbone lengths for side chain DP 30 and 70. Figure assembled by Dr. Dutta for [1]. Reprinted with permission.

Given the agreement between experimental and simulation calculations of the intrinsic viscosity, $[\eta]$, we are able to utilize these simulations to provide snapshots of the bottlebrush structures across a range of side chain and backbone lengths, as shown in figure 2.3 [1]. These snapshots were generated using the molecular visualization package Ovito [50]. We note that, for a bottlebrush architecture, the increase in the length of the backbone results in a transition from a roughly starlike polymer, to an elongated structure (around $n_{bb} = 87$ for both n_{sc} shown), and then finally to a coil-like shape. These transitions are subtly different for each different value of n_{sc}, which is especially apparent around $n_{bb} = 87$ and 175, which show that the longer branches lead to a marginally "stiffer"-appearing structure.

2.4.1.2 Hydrodynamic Radius

To further explore the impact of side chain and backbone length on the size and shape of bottlebrush polymers, we characterize the hydrodynamic radius, R_h via the methods described in Section 2.3.3. This value provides an additional measure of the molecular size and supplements the previously discussed intrinsic viscosity measurements by capturing the Stokes drag radius of an equivalent sphere undergoing the same center-of-mass as the bottlebrush. We plot the calculated hydrodynamic radius in Figure 2.4 for large M_n. Lower M_n data

was not considered as part of this discussion due to challenges getting reliable measurements for the smaller sized molecules. From Figure 2.4, we see that both backbone sweeps exhibit power-law scaling factors below that of an ideal coil (0.5), suggesting that the bottlebrushes are adopting a more collapsed conformation than captured by intrinsic viscosity measures. However, given that bottlebrushes are inherently more densely packed than linear polymers, we attributed this lower scaling to the packing of the side chains along the backbone.

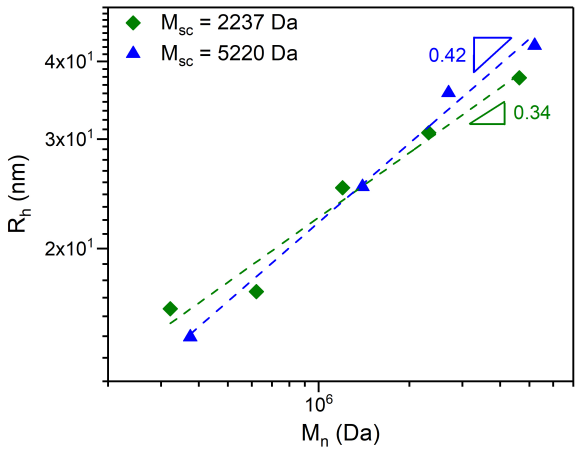

Figure 2.4: Hydrodynamic radius as a function of bottlebrush molecular weight for the two backbone sweeps. Dashed lines represent the linear fits to each data set.

The measured hydrodynamic radius is compared to values generated through simulation in Appendix A Figure A.6 which shows nearly quantitative agreement between the experiment and the simulations. In contrast to the intrinsic viscosity, however, both the simulation predictions and the measured values are less sensitive to the molecular changes (i.e. M_{sc}) and thus provide less insight into dilute solution bottlebrush conformations.

We also use R_h to show that there are only small differences in geometric parameters due to changes in temperature, which we plot for a few characteristic values of M_{sc} as a function of T in Figure 2.5.a. Indeed, relatively small changes in R_h are observed even over a large range of temperatures (0 °C < T < 90 °C). Comparison between experiments and simulations suggests that this means we remain well above the θ-temperature and are in the good solvent regime. We plot in Figure 2.5.b the hydrodynamic radius, R_h, as calculated from simulation as a function of temperature (in units of ϵ/k_B). We note large changes in the bottlebrush size as we transition from a θ-temperature ($T = 1.5\epsilon/k_B$) to the athermal limit (point shown,$T \to \infty$). These changes in the bottlebrush size, however, occur relatively close to the θ-temperature, whereas in the athermal limit, we see only small deviations in terms of size [1]. Furthermore, these athermal limit sizes are more consistent with the measured R_h in experiment.

We verified the results being reported by the Zetasizer software are valid by manually calculating the diffusivity for a select set of bottlebrush. As can be seen from Table 2.5, the diffusivity calculated from the single exponential fit is very close to that of the method of cumulants. Minor differences in the calculated diffusivity are attributed to the differences in fitting technique as the method of cumulants used by the Zetasizer software also calculates the relative dispersity of the sample. Based on this comparison, it is reasonable to

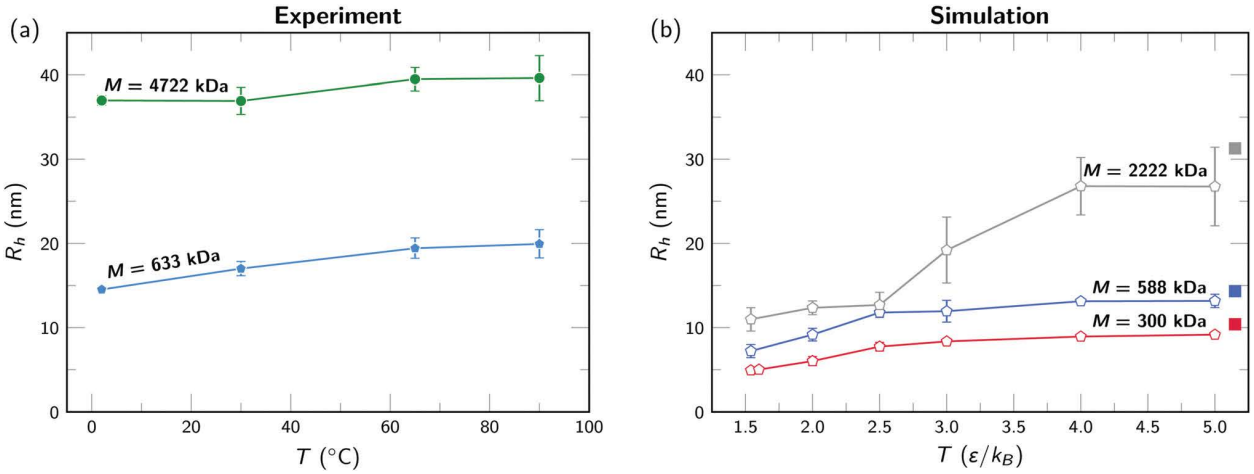

Figure 2.5: Hydrodynamic radius R_h as a function of temperature for bottlebrushes: (a) experiment and (b) simulation. The side chain molecular weight is 2237 Da for all cases. In (b), the filled squares indicate Rh in the athermal limit. Solid lines are intended to guide the eye. Figure assembled by Dr. Dutta for [1]. Reprinted with permission.

conclude that the results generated by the Zetasizer software package are an accurate representation of the data and can be used to calculate the relative size and dispersity of the bottlebrush polymer.

Table 2.5: Diffusivity calculated by applying a single exponential fit to the autocorrelation function and the diffusivity calculated by the Zetasizer software using the method of cumulants.

n_{bb}	n_{sc}	$q(nm^{-1})$	$D_{fit}(\mu m^2/s)$	$D_{DLS}(\mu m^2/s)$
268	30	0.0303	14.5	15.5
512	30	0.0303	17.7	18.1
1000	30	0.0303	22.1	22.6

2.4.2 Impact of Architecture on Physical Properties

We explore the sensitivity of bottlebrush polymers to slight variations in architecture and the impact these changes in architecture can have on physical properties through the comparison of two equivalent molecular weight bottlebrushes, one with uniform arms and one with tridisperse arms. To carry out this investigation, we characterized the linear viscoelastic (LVE) behavior of both polymers. We plot the linear moduli as a function of frequency for both $BB-mix$ and $BB-narrow$ in Figure 2.6.a. As can be seen, these two plots are very similar, overlaying in the segmental (high frequency) and terminal (low frequency) regimes. Between these two regimes, the two curves are subtly different, though the exact differences are difficult to identify. We therefore employ the van Gurp – Palmen presentation, seen in figure 2.6.b. The phase angle difference between the stress and strain, δ, has been identified as being highly sensitive to the molecular weight, polydispersity, and molecular architecture for a given polymer chemistry [51]–[53]. This sensitivity results in the van Gurp – Palmen representation being well-suited to resolving differences in the relaxation processes [54].

When plotting the LVE master curve in the van Gurp-Palmen presentation, in which the phase angle difference, δ, is plotted against the magnitude of the complex modulus,$|G^*|$, several key differences between

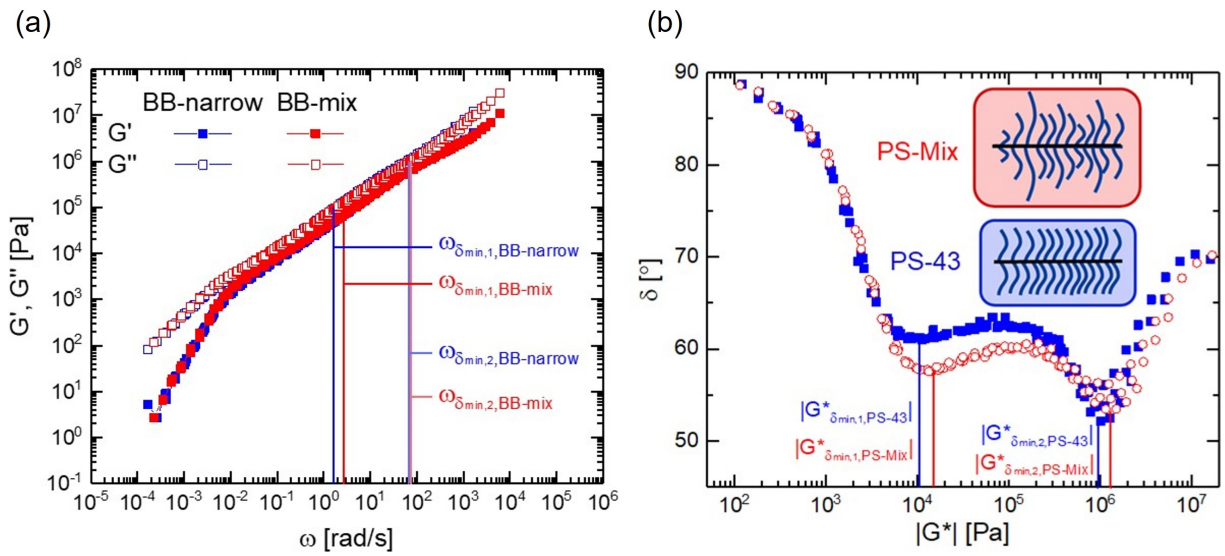

Figure 2.6: Dynamic moduli master curve in the (a) G', G" presentation and (b) van GurpPalmen for $BB-narrow$ (blue symbols) and $BB-Mix$ (red symbols). In the vGP presentation, the locations of local minima in δ for $BB-narrow$ ($G^*_{\delta_{min,1},BB\text{-}narrow}$ and $G^*_{\delta_{min,2},BB\text{-}narrow}$) are denoted with blue lines, while the locations of local minima for $BB-mix$ ($G^*_{\delta_{min,1},BB\text{-}mix}$ and $G^*_{\delta_{min,2},BB\text{-}mix}$) are denoted with red lines. In the G', G" presentation, the frequencies that correspond to the local minima identified in the vGP presentation are denoted with blue and red lines corresponding to $BB-narrow$ and $BB-mix$, respectively. The two G' and G" were plotted at a T_{ref} of 130 °C.

the rheological responses of $BB-narrow$ and $BB-mix$ reflect the distinct relaxation spectra, and therefore the architectures of the polymers. At low moduli, the LVE responses of the two polymers are identical, indicating similar distributions of longest relaxation times, which in turn reflects the similarity of the polymers at their largest length scales. With respect to the total hydrodynamic volume, the rheology is therefore consistent with the SEC results shown in Figure 2.1. At intermediate values of modulus, the differences in architecture manifest as rheological differences from 104 to 106 Pa. $BB-narrow$ has a consistently higher phase angle than $BB-mix$, indicating a more liquid like response that is typical of flexible polymers. Overall, these results indicate that the macroscopic properties are quite sensitive to small variations in side chain architecture which can lead to stiffer or softer materials depending on the degree of polymierization.

In the broader context of the synthetic work discussed by Walsh et al., [2] the observed rheological differences between these two materials have ramifications on the considerations that need to be made when characterizing molecular weight through SEC. Specifically, the SEC traces in Figure 2.1, demonstrates an inability to distinguish between bottlebrushes of equivalent molecular weights but different side chain architectures [2]. This in turn implies that bottlebrush dispersites calculated through SEC are more representative of backbone dispersities, not arm dispersities. Ultimately, the results captured through rheology, demonstrate the shortcomings of traditional SEC characterization methods and the advantages of pairing SEC analysis with additional characterization methods that are more sensitive to structural differences.

2.5 Conclusions

In this chapter, we showed how the conformation and shape of a bottlebrush polymer in dilute conditions can be controlled by adjusting both its backbone length and side chain length. Through a combination of viscosity measures and dynamic light scattering, we were able to characterize the intrinsic viscosity and hydrodynamic radius. Plotting these the intrinsic viscosity as a function of molecular weight allowed us to identify distinct scaling regimes, corresponding to star-like, short cylinder, and flexible cylinder conformations. The long arm bottlebrushes exhibited a higher scaling factor, suggesting a more elongated structure than the short arm bottlebrushes. Both bottlebrush series exhibited lower scaling factors than the linear polymer that was measured as a control, suggesting that the bottlebrushes are more collapsed than a linear polymer in the same solvent. Using these measurements as a basis, simulations were performed and allowed us to verify our results while simultaneously providing snapshots of the shape and conformation adopted by these polymers under dilute conditions.

We also demonstrated the sensitivity of a bottlebrush polymer to slight changes in side chain architecture by comparing a bottlebrush with uniform side chains to a bottlebrush with tri-disperse side chains. Through time temperature superposition measurements presented using the VGP presentation, we were able to identify differences in the backbone relaxation modes that resulted from the dispersity of the side chains, with the $BB-narrow$ being more susceptible to strain than the $BB-mix$. In addition to a shift in the backbone relaxation mode, $BB-narrow$ exhibited a higher phase angle across the entirety of the frequencies measures. This corresponds to more liquid like behavior, and, in conjunction with the higher susceptibility, indicates that $BB-narrow$ is a softer material than $BB-mix$. When considering these results in the context of synthetic characterization methods, we were able to show some of the limitations of SEC. Carrying out additional measures to supplement the molecular weights obtained through SEC allows us to identify architectural differences in polymers that are not immediately obvious from the molecular weight and dispersity.

2.6 References

[1] S. Dutta, M. A. Wade, D. J. Walsh, D. Guironnet, S. A. Rogers, and C. E. Sing, "Dilute solution structure of bottlebrush polymers," *Soft Matter*, vol. 15, no. 14, pp. 2928–2941, 2019, ISSN: 17446848. DOI: 10.1039/c9sm00033j.

[2] D. J. Walsh, M. A. Wade, S. A. Rogers, and D. Guironnet, "Challenges of Size-Exclusion Chromatography for the Analysis of Bottlebrush Polymers," *Macromolecules*, vol. 53, no. 19, pp. 8610–8620, 2020, ISSN: 15205835. DOI: 10.1021/acs.macromol.0c01357.

[3] S. S. Sheiko, B. S. Sumerlin, and K. Matyjaszewski, "Cylindrical molecular brushes: Synthesis, characterization, and properties," *Progress in Polymer Science (Oxford)*, vol. 33, no. 7, pp. 759–785, Jul. 2008, ISSN: 00796700. DOI: 10.1016/j.progpolymsci.2008.05.001.

[4] T. M. Birshtein and E. B. Zhulina, "Conformations of star-branched macromolecules," *Polymer*, vol. 25, no. 10, pp. 1453–1461, 1984. DOI: 10.1016/0032-3861(84)90109-5.

[5] G. H. Fredrickson, "Surfactant-Induced Lyotropic Behavior of Flexible Polymer Solutions," *Macromolecules*, vol. 26, pp. 2825–2831, 1993. [Online]. Available: https://pubs.acs.org/sharingguidelines.

[6] Y. Tsukahara, S. Kohjiya, K. Tsutsumi, and Y. Okamoto, "On the Intrinsic Viscosity of Poly(macromonomer)s," *Macromolecules*, vol. 27, no. 6, pp. 1662–1664, 1994, ISSN: 15205835. DOI: 10.1021/ma00084a061. [Online]. Available: https://pubs.acs.org/sharingguidelines.

[7] M. Wintermantel, K. Fischer, M. Gerle, *et al.*, "Lyotropic Phases Formed by "Molecular Bottlebrushes"," *Angewandte Chemie International Edition in English*, vol. 34, no. 13-14, pp. 1472–1474, Jul. 1995, ISSN: 15213773. DOI: 10.1002/ANIE.199514721.

[8] M. Wintermantel, M. Gerle, K. Fischer, *et al.*, "Molecular bottlebrushes," *Macromolecules*, vol. 29, no. 3, pp. 978–983, 1996, ISSN: 00249297. DOI: 10.1021/ma950227s. [Online]. Available: https://pubs.acs.org/sharingguidelines.

[9] S. Kawaguchi, K. Akaike, Z. M. Zhang, H. Matsumoto, and K. Ito, "Water Soluble Bottlebrushes," *Polymer Journal 1998 30:12*, vol. 30, no. 12, pp. 1004–1007, 1998, ISSN: 1349-0540. DOI: 10.1295/polymj.30.1004. [Online]. Available: https://www.nature.com/articles/pj1998188.

[10] D. Vlassopoulos, G. Fytas, B. Loppinet, F. Isel, P. Lutz, and H. Benoit, "Polymacromonomers: structure and dynamics in nondilute solutions, melts, and mixtures," *Macromolecules*, vol. 33, no. 16, pp. 5960–5969, Aug. 2000, ISSN: 00249297. DOI: 10.1021/ma000634q. [Online]. Available: https://pubs.acs.org/sharingguidelines.

[11] Y. Nakamura, Y. Wan, J. W. Mays, H. Iatrou, and N. Hadjichristidis, "Radius of Gyration of Polystyrene Combs and Centipedes in Solution," 2000. DOI: 10.1021/ma0007076. [Online]. Available: https://pubs.acs.org/sharingguidelines.

[12] S. Rathgeber, T. Pakula, A. Wilk, K. Matyjaszewski, and K. L. Beers, "On the shape of bottle-brush macromolecules: Systematic variation of architectural parameters," *Journal of Chemical Physics*, vol. 122, no. 12, pp. 1–13, Mar. 2005, ISSN: 00219606. DOI: 10.1063/1.1860531. [Online]. Available: https://doi.org/10.1063/1.1860531.

[13] M. Zhang and A. H. Müller, "Cylindrical polymer brushes," *Journal of Polymer Science, Part A: Polymer Chemistry*, vol. 43, no. 16, pp. 3461–3481, 2005, ISSN: 0887624X. DOI: 10.1002/pola.20900.

[14] P. E. Theodorakis, W. Paul, and K. Binder, "Microphase separation in bottlebrush polymers under poor-solvent conditions," *EPL*, vol. 88, no. 6, 2009, ISSN: 02955075. DOI: 10.1209/0295-5075/88/63002. [Online]. Available: www.epljournal.org.

[15] ——, "Pearl-necklace structures of molecular brushes with rigid backbone under poor solvent conditions: A simulation study," *Journal of Chemical Physics*, vol. 133, no. 10, p. 124 904, 2010, ISSN: 00219606. DOI: 10.1063/1.3477981. [Online]. Available: https://doi.org/10.1063/1.3477981.

[16] S. L. Pesek, X. Li, B. Hammouda, K. Hong, and R. Verduzco, "Small-angle neutron scattering analysis of bottlebrush polymers prepared via grafting-through polymerization," *Macromolecules*, vol. 46, no. 17, pp. 6998–7005, 2013, ISSN: 00249297. DOI: 10.1021/ma401246b. [Online]. Available: https://pubs.acs.org/sharingguidelines.

[17] S. C. Radzinski, J. C. Foster, R. C. Chapleski, D. Troya, and J. B. Matson, "Bottlebrush Polymer Synthesis by Ring-Opening Metathesis Polymerization: The Significance of the Anchor Group," *Journal of the American Chemical Society*, vol. 138, no. 22, pp. 6998–7004, Jun. 2016, ISSN: 15205126. DOI: 10.1021/jacs.5b13317. [Online]. Available: https://pubs.acs.org/doi/10.1021/jacs.5b13317%20https://pubs.acs.org/sharingguidelines.

[18] C. R. López-Barrón, A. H. Tsou, J. R. Hagadorn, and J. A. Throckmorton, "Highly Entangled α-Olefin Molecular Bottlebrushes: Melt Structure, Linear Rheology, and Interchain Friction Mechanism," *Macromolecules*, vol. 51, no. 17, pp. 6958–6966, 2018, ISSN: 0024-9297. DOI: 10.1021/acs.macromol.8b01431. [Online]. Available: http://pubs.acs.org/doi/10.1021/acs.macromol.8b01431.

[19] T. M. Birshtein, O. V. Borisov, Y. B. Zhulina, A. R. Khokhlov, and T. A. Yurasova, "Conformations of comb-like macromolecules," *Polymer Science U.S.S.R.*, vol. 29, no. 6, pp. 1293–1300, 1987, ISSN: 00323950. DOI: 10.1016/0032-3950(87)90374-1.

[20] E. B. Zhulina and T. A. Vilgis, "Scaling Theory of Planar Brushes Formed by Branched Polymers," *Macromolecules*, vol. 28, pp. 1008–1015, 1995. [Online]. Available: https://pubs.acs.org/sharingguidelines.

[21] Y. Rouault and O. V. Borisov, "Comb-Branched Polymers: Monte Carlo Simulation and Scaling," Tech. Rep., 1996. [Online]. Available: https://pubs.acs.org/sharingguidelines.

[22] M. Saariaho, A. Subbotin, I. Szleifer, O. Ikkala, and G. Ten Brinke, "Effect of Side Chain Rigidity on the Elasticity of Comb Copolymer Cylindrical Brushes: A Monte Carlo Simulation Study," 1999. DOI: 10.1021/ma990307m. [Online]. Available: https://pubs.acs.org/sharingguidelines.

[23] A. Yethiraj, "A Monte Carlo simulation study of branched polymers," *Journal of Chemical Physics*, vol. 125, no. 20, p. 124 904, 2006, ISSN: 00219606. DOI: 10.1063/1.2374884. [Online]. Available: https://doi.org/10.1063/1.3656072.

[24] J. Paturej and T. Kreer, "Hierarchical excluded volume screening in solutions of bottlebrush polymers," *Soft Matter*, vol. 13, no. 45, pp. 8534–8541, 2017, ISSN: 1744-683X. DOI: 10.1039/C7SM01968H. [Online]. Available: http://xlink.rsc.org/?DOI=C7SM01968H.

[25] S. Elli, F. Ganazzoli, E. G. Timoshenko, Y. A. Kuznetsov, and R. Connolly, "Size and persistence length of molecular bottle-brushes by Monte Carlo simulations," *Journal of Chemical Physics*, vol. 120, no. 13, pp. 6257–6267, 2004, ISSN: 00219606. DOI: 10.1063/1.1651052. [Online]. Available: https://doi.org/10.1063/1.1651052.

[26] H. i. Lee, J. R. Boyce, A. Nese, S. S. Sheiko, and K. Matyjaszewski, "pH-induced conformational changes of loosely grafted molecular brushes containing poly(acrylic acid) side chains," *Polymer*, vol. 49, no. 25, pp. 5490–5496, Nov. 2008, ISSN: 00323861. DOI: 10.1016/J.POLYMER.2008.10.001.

[27] B. Zhang, F. Gro, J. S. Pedersen, *et al.*, "Conformation of cylindrical brushes in solution: Effect of side chain length," *Macromolecules*, vol. 39, no. 24, pp. 8440–8450, 2006, ISSN: 00249297. DOI: 10.1021/ma0613178. [Online]. Available: https://pubs.acs.org/sharingguidelines.

[28] S. L. Pesek, Q. Xiang, B. Hammouda, and R. Verduzco, "Small-angle neutron scattering analysis of bottlebrush backbone and side chain flexibility," *Journal of Polymer Science, Part B: Polymer Physics*, vol. 55, no. 1, pp. 104–111, 2017, ISSN: 10990488. DOI: 10.1002/polb.24251.

[29] S. Lecommandoux, F. Chécot, R. Borsali, *et al.*, "Effect of dense grafting on the backbone conformation of bottlebrush polymers: Determination of the persistence length in solution," *Macromolecules*, vol. 35, no. 23, pp. 8878–8881, Nov. 2002, ISSN: 00249297. DOI: 10.1021/ma0203344. [Online]. Available: https://pubs.acs.org/sharingguidelines.

[30] A. P. Filippov, A. S. Krasova, E. B. Tarabukina, A. V. Kashina, T. K. Meleshko, and A. V. Yakimansky, "The effect of side chain length on hydrodynamic and conformational characteristics of polyimide-graft-polymethylmethacrylate copolymers in thermodynamically good solutions," *Journal of Polymer Research*, vol. 23, no. 10, 2016, ISSN: 15728935. DOI: 10.1007/s10965-016-1111-5.

[31] F. Dutertre, K.-T. Bang, B. Loppinet, I. Choi, T.-L. Choi, and G. Fytas, "Structure and Dynamics of Dendronized Polymer Solutions: Gaussian Coil or Macromolecular Rod?," 2016. DOI: 10.1021/acs.macromol.6b00420. [Online]. Available: https://pubs.acs.org/sharingguidelines.

[32] L. Grebikova, S. Kozhuharov, P. Maroni, *et al.*, "The persistence length of adsorbed dendronized polymers †," vol. 8, p. 13 498, 2016. DOI: 10.1039/c6nr02665f. [Online]. Available: www.rsc.org/nanoscale.

[33] F. Dutertre, K.-T. Bang, E. Vereroudakis, *et al.*, "Conformation of Tunable Nanocylinders: Up to Sixth-Generation Dendronized Polymers via Graft-Through Approach by ROMP," 2019. DOI: 10.1021/acs.macromol.9b00457. [Online]. Available: https://pubs.acs.org/sharingguidelines.

[34] D. J. Walsh, S. H. Lau, M. G. Hyatt, and D. Guironnet, "Kinetic study of living ring-opening metathesis polymerization with third-generation grubbs catalysts," *Journal of the American Chemical Society*, vol. 139, no. 39, pp. 13 644–13 647, 2017, ISSN: 15205126. DOI: 10.1021/jacs.7b08010. [Online]. Available: https://pubs.acs.org/sharingguidelines.

[35] D. J. Walsh and D. Guironnet, "Macromolecules with programmable shape, size, and chemistry," *Proceedings of the National Academy of Sciences of the United States of America*, vol. 116, no. 5, pp. 1538–1542, Jan. 2019, ISSN: 10916490. DOI: 10.1073/pnas.1817745116.

[36] D. J. Walsh, S. Dutta, C. E. Sing, and D. Guironnet, "Engineering of Molecular Geometry in Bottlebrush Polymers," *Macromolecules*, vol. 52, no. 13, pp. 4847–4857, Jul. 2019, ISSN: 0024-9297. DOI: 10.1021/acs.macromol.9b00845.

[37] M. A. Wade, D. Walsh, J. C. W. Lee, *et al.*, "Color, Structure, and Rheology of a Diblock Bottlebrush Copolymer Solution," *Soft Matter*, vol. 16, no. 21, pp. 4919–4931, Jun. 2020, ISSN: 17446848. DOI: 10.1039/d0sm00397b. [Online]. Available: https://pubs.rsc.org/en/content/articlehtml/2020/sm/d0sm00397b%20https://pubs.rsc.org/en/content/articlelanding/2020/sm/d0sm00397b.

[38] D. J. Worsfold and S. Bywater, "ANIONIC POLYMERIZATION OF STYRENE," *Canadian Journal of Chemistry*, vol. 38, no. 10, pp. 1891–1900, Oct. 1960, ISSN: 0008-4042. DOI: 10.1139/v60-254. [Online]. Available: http://www.nrcresearchpress.com/doi/10.1139/v60-254.

[39] R. Waack, A. Rembaum, J. D. Coombes, and M. Szwarc, "MOLECULAR WEIGHTS OF "LIVING" POLYMERS *," *Journal of the American Chemical Society*, vol. 79, no. 8, pp. 2026–2027, Apr. 1957, ISSN: 0002-7863. DOI: 10.1021/ja01565a077. [Online]. Available: https://pubs.acs.org/doi/abs/10.1021/ja01565a077.

[40] S. Breunig, V. Héroguez, Y. Gnanou, and M. Fontanille, "Ring-opening metathesis polymerization of ω-norbornenyl polystyrene macromonomers and characterization of the corresponding structures," *Macromolecular Symposia*, vol. 95, no. 1, pp. 151–166, Jun. 1995, ISSN: 10221360. DOI: 10.1002/masy.19950950114. [Online]. Available: http://doi.wiley.com/10.1002/masy.19950950114.

[41] A. L. Liberman-Martin, C. K. Chu, and R. H. Grubbs, "Application of Bottlebrush Block Copolymers as Photonic Crystals," *Macromolecular Rapid Communications*, vol. 38, no. 13, p. 1 700 058, Jul. 2017, ISSN: 10221336. DOI: 10.1002/marc.201700058. [Online]. Available: http://doi.wiley.com/10.1002/marc.201700058%20www.advancedsciencenews.com.

[42] T. L. Choi and R. H. Grubbs, "Controlled living ring-opening-metathesis polymerization by a fast-initiating ruthenium catalyst," *Angewandte Chemie - International Edition*, vol. 42, no. 15, pp. 1743–1746, 2003, ISSN: 14337851. DOI: 10.1002/anie.200250632. [Online]. Available: www.angewandte.org.

[43] E. O. Kraemer, "Molecular Weights of Celluloses," *Industrial and Engineering Chemistry*, vol. 30, no. 10, pp. 1200–1203, 1983. [Online]. Available: https://pubs.acs.org/doi/pdf/10.1021/ie50346a023.

[44] M. L. Huggins, "The Viscosity of Dilute Solutions of Long-Chain Molecules. IV. Dependence on Concentration," Tech. Rep. 11, 1942, pp. 2716–2718. DOI: ja01263a056. [Online]. Available: https://pubs.acs.org/doi/pdf/10.1021/ja01263a056.

[45] L. M. Polgar, H. Lentzakis, D. Collias, *et al.*, "Synthesis and Linear Viscoelasticity of Polystyrene Stars with a Polyketone Core," *Macromolecules*, vol. 48, no. 18, pp. 6662–6671, 2015, ISSN: 15205835. DOI: 10.1021/acs.macromol.5b01434. [Online]. Available: https://pubs.acs.org/sharingguidelines.

[46] K. Nishi, S. Tochioka, T. Hiroi, *et al.*, "Structural Analysis of Lipophilic Polyelectrolyte Solutions and Gels in Low-Polar Solvents," *Macromolecules*, vol. 48, no. 11, pp. 3613–3621, 2015, ISSN: 15205835. DOI: 10.1021/acs.macromol.5b00753. [Online]. Available: https://pubs.acs.org/sharingguidelines.

[47] H. Unsal, S. Onbulak, F. Calik, *et al.*, "Interplay between Molecular Packing, Drug Loading, and Core Cross-Linking in Bottlebrush Copolymer Micelles," *Macromolecules*, vol. 50, no. 4, pp. 1342–1352, 2017, ISSN: 15205835. DOI: 10.1021/acs.macromol.6b02182. [Online]. Available: https://pubs.acs.org/sharingguidelines.

[48] M. Wintermantel, M. Schmidt, Y. Tsukahara, K. Kajiwara, and S. Kohjiya, "Rodlike combs," *Macromolecular Rapid Communications*, vol. 15, no. 3, pp. 279–284, 1994, ISSN: 15213927. DOI: 10.1002/marc.1994.030150315.

[49] K. Terao, T. Hokajo, Y. Nakamura, and T. Norisuye, "Solution properties of polymacromonomers consisting of polystyrene. 3. Viscosity behavior in cyclohexane and toluene," *Macromolecules*, vol. 32, no. 11, pp. 3690–3694, Jun. 1999, ISSN: 00249297. DOI: 10.1021/ma990091o. [Online]. Available: https://pubs.acs.org/sharingguidelines.

[50] A. Stukowski, "Visualization and analysis of atomistic simulation data with OVITO-the Open Visualization Tool," *Modelling and Simulation in Materials Science and Engineering*, vol. 18, no. 1, p. 7, 2010, ISSN: 09650393. DOI: 10.1088/0965-0393/18/1/015012. [Online]. Available: http://ovito.sourceforge.net/..

[51] S. Trinkle and C. Freidrich, "Van Gurp-Palmen-plot: A way to characterize polydispersity of linear polymers," *Rheologica Acta*, vol. 40, no. 4, pp. 322–328, 2001, ISSN: 00354511. DOI: 10.1007/s003970000137. [Online]. Available: https://link.springer.com/article/10.1007/s003970000137.

[52] S. Trinkle, P. Walter, and C. Friedrich, "Van Gurp-Palmen plot II - Classification of long chain branched polymers by their topology," *Rheologica Acta*, vol. 41, no. 1, pp. 103–113, 2002, ISSN: 00354511. DOI: 10.1007/s003970200010. [Online]. Available: https://link.springer.com/article/10.1007/s003970200010.

[53] Z. Qian and G. B. Mckenna, "Expanding the application of the van Gurp-Palmen plot : New insights into polymer melt rheology," *Polymer*, vol. 155, no. September, pp. 208–217, 2018, ISSN: 00323861. DOI: 10.1016/j.polymer.2018.09.036. [Online]. Available: https://doi.org/10.1016/j.polymer.2018.09.036.

[54] M. Kapnistos, D. Vlassopoulos, J. Roovers, and L. G. Leal, "Linear rheology of architecturally complex macromolecules: Comb polymers with linear backbones," *Macromolecules*, vol. 38, no. 18, pp. 7852–7862, Sep. 2005, ISSN: 00249297. DOI: 10.1021/ma050644x.

Chapter 3

Structure and Color Under Steady Shear Conditions[1]

3.1 Chapter Overview

In this chapter, a structure-property-process relation is established for a diblock bottlebrush copolymer solution, through a combination of neutron scattering, imaging, and rheological measurements. Polylactic acid-b-polystyrene diblock bottlebrush copolymers were dispersed in toluene with a concentration of 175 mg ml^{-1}, where they self-assembled into a lamellar phase. All measurements were carried out at 5 °C. The solution color, as observed in reflection, is shown to be a function of the applied shear rate. Under equilibrium and near-equilibrium conditions, the solution has a green color. At low shear rates the solution remains green, while at intermediate rates it is cyan, and at the highest rates applied the solution is indigo. The lamellar spacing is also shown to be a decreasing function of shear rate, partially accounting for the color change. The lamellae are oriented 'face-on' with the wall under quiescence and low shear rates, while a switch to 'edge-on' is observed at the highest shear rates, where the reflected color disappears. The intramolecular distance between bottlebrush polymers does not change with shear rate, although at high shear rates, the bottlebrush polymers are preferentially aligned in the vorticity direction within the lamellae. Through these observations, we form a consistent relation between structure and function, spanning a wide range of length scales and shear rates.

3.2 Introduction

Investigations into the self-assembly of diblock bottlebrush copolymers into photonic crystals in prior literature have primarily focused on the impact of sample composition and chemistry on the self-assembly of the polymer under quiescent conditions, typically after allowing the bottlebrushes to dry and form a thin film. Miyake et al. characterized the effects of molecular weight on the reflected color, concluding that increasing the backbone length without changing the arm length caused an increase in the lamellar spacing, which resulted in the peak reflected wavelength shifting to longer wavelengths [2]. Two studies, one from Macfarlane et al. and another from Miyake et al., have demonstrated how the domain spacing of the lamellar microstructure

[1] This chapter has been adapted from the following publication with permission: [1]

observed in a diblock bottlebrush thin film could also be increased through the addition of linear polymers or higher molecular weight diblock bottlebrush copolymers, respectively [3], [4].

When characterizing diblock bottlebrush photonic crystals, it is common that the polymer thin film is formed through solvent-casting on either the inside of a vial or on a pre-treated substrate. This process results in a uniform structure formed under no-shear conditions. However, the films formed may not be at equilibrium because of the rate at which the solvent evaporates, leaving the assembly in a kinetically trapped state. Annealing of the thin films at an elevated temperature provides additional thermal energy that can be used to more effectively explore the potential energy landscape, allowing the material to progress toward thermodynamic equilibrium [5], [6]. Considering the microstructure of the bottlebrush polymer under quiescent conditions, therefore, only provides insight into equilibrium and near-equilibrium structures.

Prior studies characterizing the microstructure of gels and polymeric systems have demonstrated the significance of the out-of-equilibrium processing conditions of a soft material can have on its microstructure and thus macroscopic properties [7]–[10]. Extensive experimental and computational work on diblock copolymers has demonstrated how the application of shear can lead to a reorientation [11]–[13] and in certain cases, a complete reconfiguration [14]–[16] of the self-assembled microstructure depending on the applied shear rate and chemistry of the polymer. The well-established relation between self-assembled microstructure and applied shear rate allows for on-the-fly tuning of material properties simply by adjusting the processing conditions. In the case of additive manufacturing processes such as melt extrusion and direct ink writing, this property–process relation implies that the self-assembled microstructure, and thus the color, of the diblock bottlebrush copolymer can be actively adjusted during the printing process. Control over the sample color by adjusting printing conditions has the potential to replace existing color printing technology that relies on the addition of dyes containing toxic material to the bulk filament [17]. Use of this material would also allow for multiple colors to be printed from a single source material, something only achieved with current printing technology using complex and time-consuming setups that require the use of multiple pre-dyed materials to print in more than one color.

In melt extrusion and direct-ink-writing, the deposited polymer undergoes a wide range of deformation processes, leaving it with a complex shear history [18]. Understanding how the self-assembled microstructure of diblock bottlebrush block copolymers will be affected by this process requires a series of studies that examine how printing conditions such as nozzle speed and temperature affect the microstructure during and after the printing process. In the case of melt extrusion, Boyle et al. successfully observed the rapid development of microphases within an extruded diblock bottlebrush polymer filament [5]. While this work demonstrates the possibility of achieving color with diblock bottlebrush copolymers in additive manufacturing, the work of Boyle et al. primarily focuses on the effect of molecular composition rather than the impact of processing conditions. A recent study carried out by Patel et al., has begun to explore the effects of printing conditions on the final self-assembled microstructure of diblock bottlebrush compolymers [19]. The microstructure and corresponding color of the deposited diblock bottlebrush copolymer film was observed to vary systematically with both print speed and substrate temperature.

This variation in structure with printing conditions is reminiscent of the behavior of a baroplastic. Baroplastics are block copolymer melts and thin films that exhibit a shift in the order–disorder transition temperatures as a function of pressure [20]–[24]. Recent work carried out by Lee et al. identify that increasing the pressure leads to a reduction in lamellae spacing and a loss of long range order [25]. It is suggested that the decreased lamellar spacing corresponds to the compressibility of the diblock polymers in melt [25]. A similar process could potentially explain the decrease in lamellar spacing observed in diblock bottlebrush thin

films after undergoing a complex printing process [19].

To understand how the microstructure develops during the printing process, we study the non-equilibrium behavior of a lamellar phase made of diblock bottlebrush copolymer via constant shearing across a wide range of shear rates. The effects of the steady flow conditions on the self-assembled microstructure are elucidated using microscopy, bulk rheology, and rheo-SANS. By considering the structure of the bottlebrush polymers within the solution in tandem with the rheological response, we develop a structure–property–process relation that connects the applied shear rate to the self-assembled microstructure, which dictates the macroscopic color of the sample. This relation can be applied to printing processes to help us better understand how the shear rates experienced by the bottlebrush polymer during a solution printing process affect the final microstructure of the deposited thin film.

3.3 Experimental Methods and Materials

3.3.1 Bottlebrush Synthesis and Sample Preparation

Well-defined poly(styrene)-b-poly(lactic acid) (PS-b-PLA) di-block bottlebrushes were synthesized by our collaborators in the Guironnet group through graft-through polymerization of macromonomers as seen in Figure 3.1. Polystyrene and polylactic acid were chosen since they are synthetically accessible through controlled polymerizations and have a significant refractive index difference, which results in a high reflected light intensity when organized into a photonic crystal.

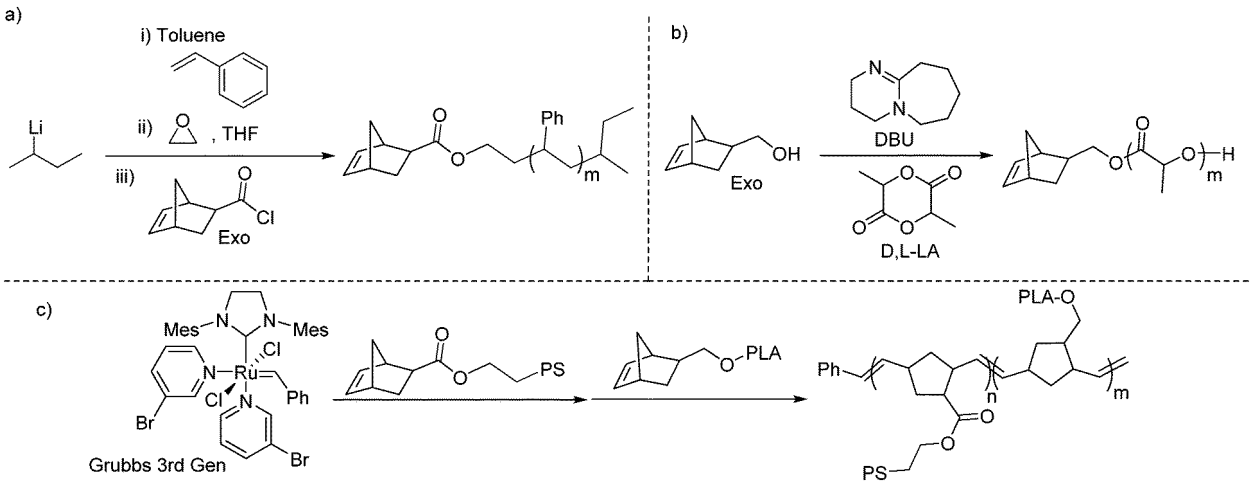

Figure 3.1: Synthesis of PS-b-PLA bottlebrushes. (a) Anionic polymerization of styrene to produce PS macromonomers. (b) DBU catalyzed ROP of lactide to produce PLA macromonomers. (c) Sequential addition ROMP of PS and PLA macromonomers.

The PS macromonomers ($M_{n,GPC} = 4500$ g mol^{-1}; Đ= 1.03) were synthesized via an anionic polymerization of styrene initiated by secBuLi, and the reaction was quenched with ethylene oxide followed by the addition of norobornene-2-acid chloride [26]–[28]. The PLA macromonomers ($M_{n,GPC} = 4200$ g mol^{-1}; Đ= 1.05) were synthesized in situ by an organocatalyzed DBU ring opening polymerization of lactide initiated by norobornene-2-methanol [29], [30]. Sequential addition ring-opening metathesis polymerization (ROMP) was used to synthesize a di-block bottlebrush (targeting 50% by weight of PS; backbone length 400 repeating

units; $M_{n,GPC}$ = 610 kg mol^{-1}; Đ= 1.03) with the polymerization of PS macromonomers first and PLA macromonomers second [30]–[33]. GPC chromatograms were collected and analyzed at each stage of the synthesis (see Appendix B for GPC data). The very narrow distribution of the molecular weight of the bottlebrush enabled us to identify and quantify the percentage of leftover brushes and first block bottlebrushes (homo-polystyrene bottlebrush). By comparing the GPC after block 1 (PS) synthesis with the final di-block synthesis, we can conclude that the leftover brushes are solely polystyrene. 1H NMR of the sample showed no residual double bond signals (characteristic of the norbornene end-group), suggesting that the leftover PS brushes are caused by an incomplete functionalization during the quenching anionic polymerization. Some homopolystyrene bottlebrushes were also detected and are presumably caused by some impurities deactivating part of metathesis catalyst upon addition of PLA macromonomers. Upon fitting normal distributions to the GPC chromatogram, we determine that the sample contains 94% di-block bottlebrush by mass, 4% homopolystyrene bottlebrush by mass, and 2% PS brushes by mass. With the formation of homopolystyrene, the final diblock will have slightly asymmetric blocks. Calculations reveal that the block length of PS is 196 and the block of PLA is 210. This level of homoblock bottlebrush polymer is difficult to prevent and precisely quantify. The very narrow dispersities of the ROMP polymer eased our ability to quantify this, as a broader distribution could ultimately prevent the differentiation between the homopolymer and the diblock polymer. This precision in composition characterization is important when studying material properties, as it is known that the addition of homopolymer to di-block bottlebrushes can result in the swelling of the domain size, which ultimately alters the photonic properties of the material [3].

The PS-PLA diblock bottlebrush polymers were dissolved in toluene to form a solution with a concentration of 175 mg ml_1. To enhance the contrast between the polymer and the solvent neutron scattering experiments were carried out on a solution dispersed in deuterated toluene. The solutions were gently mixed for at least 12 hours using either a shaker table or roller mixer to ensure the polymer solution was homogenous. Samples were maintained at 5 °C throughout all tests to reduce evaporation effects.

3.3.2 Rheometry

The linear rheology and flow properties were characterized using two stress-controlled Anton-Paar rheometers. *In situ* imaging measurements were carried out on an MCR 702 in a 43 mm glass parallel plate geometry that allowed for a microscope and digital camera to be setup beneath the geometry as shown in Fig. 2. *In situ* scattering measurements were carried out on an MCR 501 in a concentric-cylinder Couette cell with a 50 mm quartz cup and a hollow 48 mm titanium bob. Solvent traps were employed on both rheometers to limit the effects of solvent evaporation. Frequency sweeps were measured from 0.1 to 10 rad s^{-1} at a strain amplitude of 1% strain. Flow curves were measured over shear rates from 0.01 to 562 s^{-1} with each shear rate being applied for an equilibration time of 60 s followed by an averaging time of 30 s. In the parallel plate geometry, shear rates greater than 562 s^{-1} resulted in sample ejection. Higher shear rate measurements were collected using the concentric-cylinder Couette cell.

During each run of tests, the linear rheology was regularly characterized and compared against previous measurements to ensure that the properties of the material had not changed due to evaporation or sample degradation. Once the sample's linear rheological response differed from initial measurements by 10%, the sample concentration was corrected by adding a small volume of solvent to dissolve any sample that had dried to form a thin film. The sample was steadily sheared at a rate of 100 s^{-1} for five minutes to dissolve the polymer and incorporate the solvent into the sample.

3.3.3 Microscopy and Imaging

Images of the sample depicting the reflected color at 90° on the microscopic scale were obtained using the microscope attachment for the Anton-Paar MCR 702. Images were captured using a Lumenera LM165C camera. A 20× microscope lens was attached to the camera to narrow the field of view and focus on a region in which the shear rate was nearly constant. The camera was positioned beneath the rheometer such that the outer edge of the image was 0.5 mm away from the edge of the geometry, as shown schematically in Figure 3.2. In this configuration, the camera is positioned far enough away from the edge of the geometry to avoid capturing any color variation due to solvent evaporation along the edge of the geometry. Positioning the camera 0.5 mm from the edge of the geometry also ensured that the shear rate captured within the frame of the geometry was only 2% less than the shear rate reported by the rheometer. The sample was illuminated using a SugarCUBE Ultra White LED light source situated in line with the camera beneath the geometry. A solvent trap isolated the system from ambient light such that images collected by the camera were illuminated by light from the SugarCUBE light source reflecting off the sample. Prior to collecting images, the white balance of the camera was calibrated using white and gray reference cards. This step ensured that images collected as part of this study were reproducible.

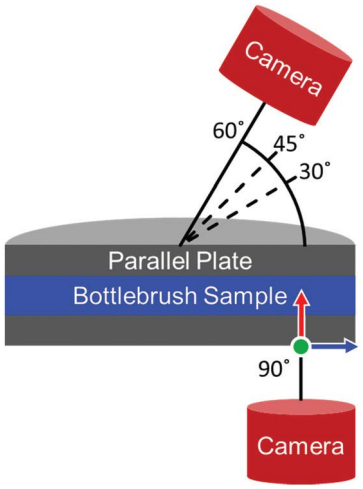

Figure 3.2: A schematic depicting the position of the microscope and camera setup relative to the sample during measurements. All images captured at 90° correspond to the 1–3 shear plane. The light source originates from the camera at each angle. The green, red, and blue arrows correspond to the flow, gradient, and vorticity directions, respectively.

Macroscopic images were obtained using a Nikon D3400 positioned 15 cm away from the center of the glass parallel plate geometry. The camera was positioned to collect images at approximately 60°, 45°, and 30° relative to the bottom plate. Images were captured in a dark room. The sample was illuminated by the camera's flash. At 45° and 30°, a diffuser was placed between the flash and the sample to reduce glare from the geometry. A diffuser was not needed at 60° due to the top of the rheometer partially blocking the flash.

3.3.4 VSANS

Neutron scattering experiments were carried out at the NIST Center for Neutron Research (NCNR) in Gaithersburg, MD on the Very Small Angle Neutron Scattering (VSANS) beamline. Shear rates from 0.01 s^{-1}

to 1770 s^{-1} were applied using a stress-controlled Anton-Paar MCR 501. To capture multiple projections of the three-dimensional self-assembled structure, scattering data was collected with the beam passing through the center of the concentric cylinder (radial configuration) to measure the structure in the 1–3 plane and through the side of the concentric cylinder (tangential configuration) to measure the structure in the 2–3 plane. A diagram depicting these two configurations is shown in Figure 3.3.

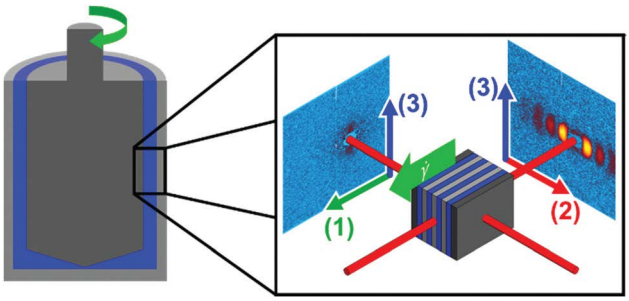

Figure 3.3: A schematic depicting the scattering planes that can be accessed in a concentric cylinder geometry. Scattering with the beam perpendicular to the geometry allows for the 1–3 scattering plane to be accessed, while aligning the beam such that it passes tangentially through the geometry results in scattering in the 2–3 scattering pane. These two images are combined to provide a complete 3-dimensional representation of the microstructure.

Data were collected simultaneously at both low and high scattering vector, q, using the unique detector setup available on the VSANS beamline. An depiction of the detector setup is presented in Figure 3.4. A front set of 4 detectors was situated 4.2 m from the sample. The detectors were spaced around the beam center such that they collected scattered neutrons at scattering vectors with magnitudes from 0.027 $Å^{-1}$ to 0.048 $Å^{-1}$. A second set of detectors was positioned 19.4 m from the sample to collect scattered neutrons across a q range from 0.0027 $Å^{-1}$ to 0.027 $Å^{-1}$. Low-q detectors were positioned such that the right detector captured the beam center while the left detector captured slightly higher q. This setup ensured that as large a q range as possible could be covered without missing any key features due to gaps between detectors. All data were collected using a neutron wavelength (λ) of 5 Åwith a distribution of $\Delta\lambda/\lambda = 0.12$. Corrections for the background, empty cell and sample transmission were carried out using protocols provided by NIST [34].

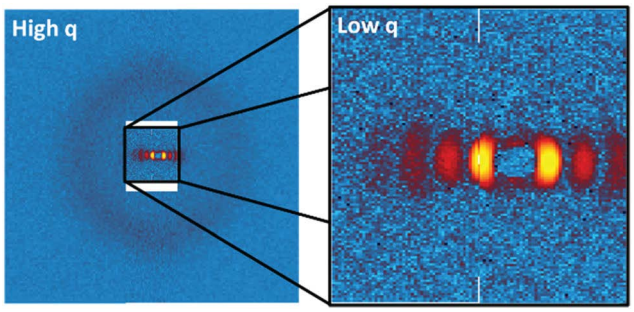

Figure 3.4: A diagram demonstrating how the detectors were setup within the VSANS beamline to capture high q and low q simultaneously. Detectors at high q were positioned such that a portion of the beam could pass through and fall on the detectors at low q. The intensity at high q was rescaled to provide the readers a better sense of how intense the beam is at each point.

3.4 Results

3.4.1 Imaging and Sample Color

The color of the sample, as determined by rheo-microscopy in reflection at 90°, is observed to vary significantly as a function of shear rate. Images collected through rheo-microscopy and standard imaging techniques can be seen in Figure 3.5. At quiescence and very low shear rates, the sample appears green when viewed at 90°. Above a critical shear rate, $\dot{\gamma}_{c,1} = 0.62\ s^{-1}$, which also marks a transition in the rheology, the color begins to transition from green to cyan. At higher shear rates exceeding a second critical shear rates, $\dot{\gamma}_{c,2} = 100\ s^{-1}$, the sample transitions from cyan to indigo. Though shear rates above 562 s^{-1} could not be tested on the MCR 702 without the sample ejecting from the parallel plate geometry, the sample was observed to become colorless when viewed in the 1–3 direction at shear rates of 1000 s^{-1} and greater in the quartz Couette geometry on the MCR 501.

On the macroscopic scale, the colors reflected by the sample were observed to vary with both viewing angle and shear rate (Figure 3.5). The region at the front of the geometry transitions from blue to green with increasing shear rate. The intensity of this band varies significantly with viewing angle. Along the sides of the geometry, the sample is observed to transition from light to dark blue at 60° and dark blue to purple at 30° and 45°. Under quiescent conditions, the color of the sample changes from light blue to green with viewing angle. Similar effects are observed at all subsequent shear rates. This change of color with viewing angle is consistent with the presence of a photonic crystal in which the reflected wavelength increases as with increasing path length through the structure. Radial variation in the sample color is not observed at the macroscopic scale due to the color change occurring at different orders of magnitude of shear rate while the shear rate only varies linearly along the radius of the geometry. In addition, the metal portion of the geometry is approximately half the radius of the geometry, thus limiting the visible portion to a minimum observable shear rate of 0.5× the shear rate at the edge.

3.4.2 Rheometry

The steady shear response of the material taken on the two different rheometers on samples with protonated and deuterated solvent were in reasonable agreement with one another. The viscosities determined for the deuterated sample were approximately 30% larger than those calculated for the protonated solvent. This shift is comparable to observations made in the existing literature[35], [36]. Protonated and deuterated solvents can have additional effects on the self-assembly of a material as shown in the work done by Lopez-Barron et al. on wormlike micelles [35]. However, we do not expect significant differences in the structure and polarity for protonated and deuterated toluene. For the sake of clarity, only the rheological results collected during the rheo-microscopy measurements are shown in Figure 3.6 with the exception the two points at 1000 and 1770 s^{-1} which were collected during the rheo-SANS measurements. A complete flow curve from the rheo-SANS measurements can be found in Appendix B (Figure B.4). No plateau in the viscosity, indicating the presence of a zero-shear viscosity, is observed at low shear rates, as the data are always dependent on the shear rate with a power law slope of -0.42 for shear rates up to $\dot{\gamma}_{c,1} = 0.62\ s^{-1}$. Above $\dot{\gamma}_{c,1}$ the data exhibit a different power law slope of -0.20. Above a second critical shear rate, $\dot{\gamma}_{c,2} = 100\ s^{-1}$, the apparent viscosity transitions to a third regime, where the data follow a lower power-law exponent. The highest shear rate data could only be collected with the concentric-cylinder Couette geometry as the material was ejected from the plate– plate geometry prior to reaching these shear rates.

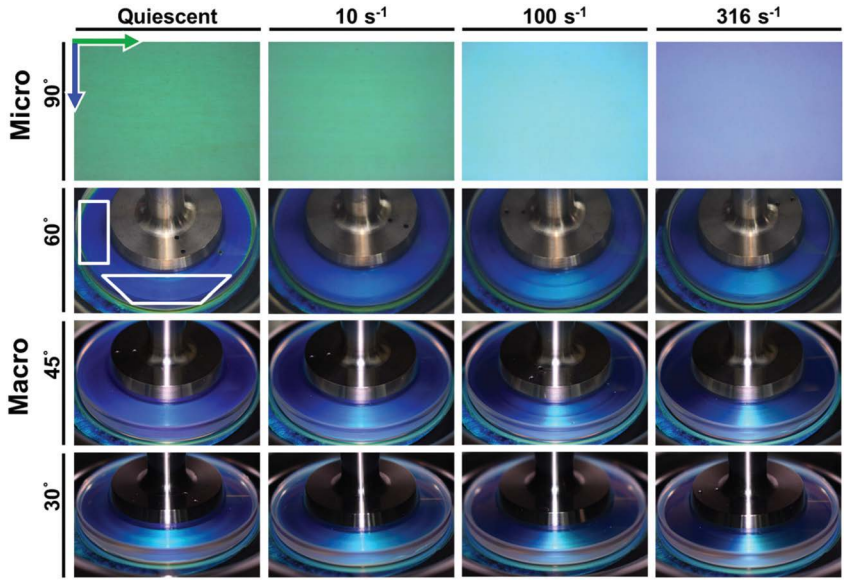

Figure 3.5: Representative microscopy and imaging data collected across a range of angles. Two boxes are drawn on the image taken under quiescence at 60° to serve as guides to the eye, highlighting regions where the color change is most noticeable. Green and blue arrows represent the flow (circumferential) and vorticity (radial) directions relative to the orientation of the microscopy image, respectively.

3.4.3 Neutron Scattering

The 1–3 and 2–3 two-dimensional SANS patterns are reassembled into an isometric view to make it easier to interpret the three-dimensional structure. The scattering data are separated into two regimes due to the configuration of the neutron detectors as laid out in Fig. 4. High q refers to the scattering data collected on the front set of detectors, while low q refers to data collected by the back set of detectors. In the high q regime, an interaction peak is observed in both the 1–3 and 2–3 scattering planes at $q* = 0.048$ Å^{-1}. This peak is understood to be representative of the inter-backbone spacing between the bottlebrush polymers and does not vary in location or intensity across the range of shear rates tested, as seen in 3.7.

At low q, four distinct peaks can be observed in the 2–3 scattering plane under quiescent conditions. This feature is coupled with a lack of identifiable peaks in the 1–3 scattering plane. These peaks are spaced at integer multiples of the lowest observable peak, indicative of a lamellae structure. This structure is in agreement with prior studies that have shown that diblock bottlebrush polymers with blocks of approximately equal size will self-assemble into lamellar structures with a layer spacing determined by the backbone contour length[2]–[6], [37]. Verification of this microstructure can be found in Section 3.4.3.2.

As can be seen in Figure 3.7, these lamellar peaks smear azimuthally as the steady shear rate increases, and they completely reorient along the vorticity direction at 1000 s^{-1} in the 2–3 plane. The peaks also appear to broaden with increasing shear rate. At the same time, increasing the shear rate results in the appearance of peaks in the vorticity direction starting at $\dot{\gamma}_{c,1}$ in the 1–3 plane. To further analyze the features observed in the 1–3 and 2–3 scattering patterns at both low and high q, a series of azimuthal sweeps and sector averages are conducted. Demonstrative figures depicting how the annular sweeps and sector averages were calculated are included in Appendix B (Figure B.5).

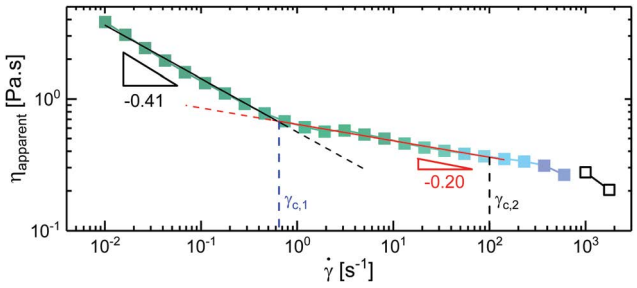

Figure 3.6: The steady flow response of the diblock bottlebrush solution. The color of each point represents the color captured by the microscope at the given shear rate, with open symbols corresponding to a lack of observable color.

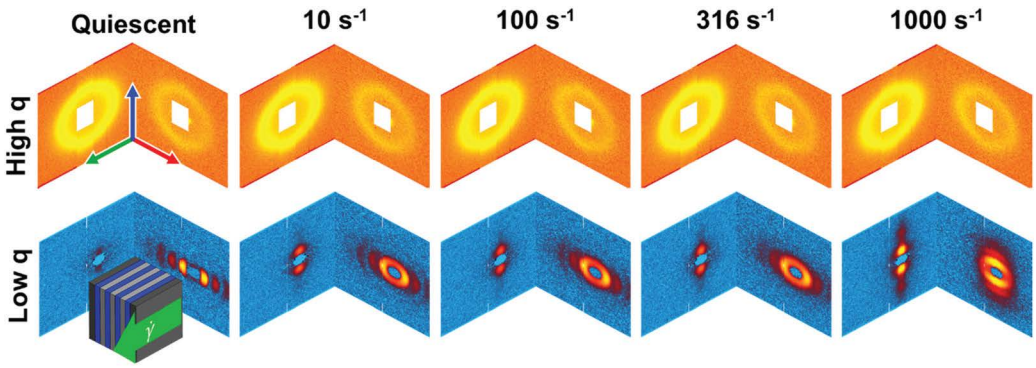

Figure 3.7: Representative scattering data mapped onto an isometric view. The green, red, and blue arrows represent the flow, velocity gradient, and vorticity directions, respectively.

3.4.3.1 Scattering at High q

At high q, a uniform interaction peak is observed at $q* = 0.048$ Å^{-1} (Figure 3.7). The length scale corresponding to $q*$, $l = 2\pi/q$, is approximately 14 nm. This length is on the same order of magnitude as the contour length of the bottlebrush's side chains, thus indicating that this peak is representative of the inter-backbone spacing between the bottlebrush polymers.

The azimuthal variation of scattered intensity at $q*$ indicates the preferential alignment of the bottlebrushes within the lamellae. We show in Figure 3.8 the azimuthal intensity for each shear rate, using an annular average centered at q* with a width of 0.01 Å^{-1}. Under quiescent conditions, any observed variation in the intensity as a function of f in the 1–3 scattering plane is within the noise of our data. As higher shear rates are applied, the intensity of the peak follows a cosinusoidal trend, thus indicating that the bottlebrushes are aligning along the vorticity direction.

The azimuthal variation of scattered intensity at q* indicates the preferential alignment of the bottlebrushes within the lamellae. We show in Fig. 8 the azimuthal intensity for each shear rate, using an annular average centered at q* with a width of 0.01 Å^{-1}. Under quiescent conditions, any observed variation in the intensity as a function of f in the 1–3 scattering plane is within the noise of our data. As higher shear rates are applied, the intensity of the peak follows a cosinusoidal trend, thus indicating that the bottlebrushes are aligning along the vorticity direction.

The extent of this alignment is quantified using the alignment factor (A_f). This term represents the

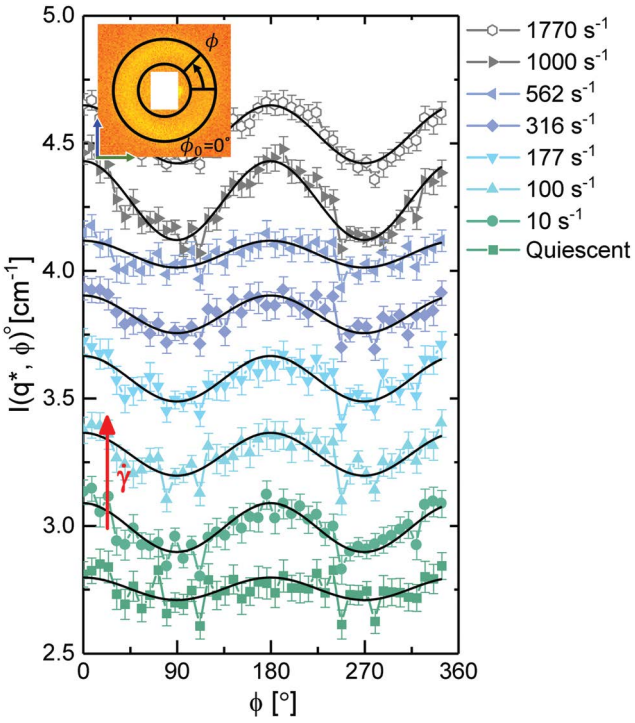

Figure 3.8: The azimuthal variation at $q* = 0.048$ Å^{-1} for a representative set of shear rates. Cosinusoidal fits for each data set have been shown as black lines to highlight the extent of alignment. Error bars represent the standard deviation of scattering intensities over the averaged area. Data have been offset for the sake of comparing intensity variation with ϕ.

degree of alignment relative to a given angle [38] and is determined as the cosinusoidal component of the azimuthal scattering intensity,

$$A_f = \frac{\int_0^{2\pi} I(q,\phi) cos(2(\phi - \phi_0)) d\phi}{\int_0^{2\pi} I(q,\phi) d\phi}, \tag{3.1}$$

where $I(q,\phi)$ is the intensity at a fixed q for a given azimuthal angle ϕ. The term f_0 represents a reference angle, which in this case corresponds to either 0 or 90° depending on the relative location of maximum intensity. For a perfectly isotropic system, A_f is expected to have a value of zero. For a strongly aligned feature, A_f is expected to approach a value of one. The alignment factor assumes that the scattering intensity for a well-aligned system exhibits a $cos(2\phi)$ functional form. Should the intensity exhibit a different dependence, then A_f may not fully capture the extent of alignment within the system [38]. We show in Figure 3.9 the value of the alignment factor for the high-q peak as a function of shear rate.

In the 1–3 scattering plane, the polymers exhibit no preferential alignment for the two lowest shear rates tested, with an alignment factor on the order of 0.003. Prior to $\dot{\gamma}_{c,1}$ at a shear rate of $\dot{\gamma} = 0.1$ s^{-1} the value of the alignment factor jumps to approximately 0.02 where it remains constant up until a shear rate of $\dot{\gamma}_{c,2}$ = 100 s^{-1}. In this regime, the bottlebrush polymers are therefore weakly aligned perpendicular to the flow direction, along the vorticity direction. This alignment occurs at a shear rate prior to any significant changes in the rheology. Once the shear rate exceeds $\dot{\gamma}_{c,2}$, the polymers revert to an isotropic state as indicated by the drop in the alignment factor. At shear rates of 1000 s^{-1} and 1770 s^{-}1 the polymers realign along the

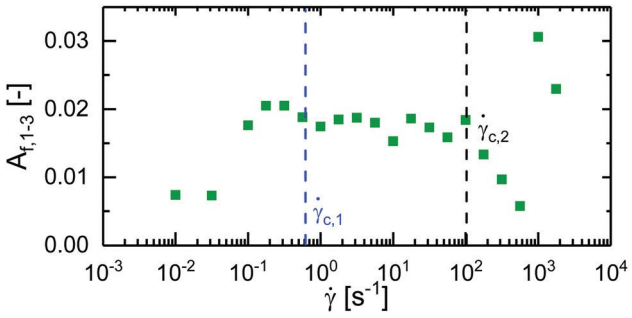

Figure 3.9: Alignment factor along the flow direction calculated from azimuthal sweeps performed at $q = 0.048$ Å^{-1} in the 1–3 scattering plane plotted against shear rate. Critical shear rates $\dot{\gamma}_{c,1}$ and $\dot{\gamma}_{c,2}$ have been highlighted with vertical dotted lines.

vorticity direction as indicated by a jump in the alignment factor up to 0.031.

3.4.3.2 Scattering at Low q

To determine the location and dispersity of each peak observed in the two-dimensional scattering patterns, sector averages were taken along the gradient and vorticity directions for the tangential and radial configurations, respectively. Sector widths of 15° were used to capture the maxima of these peaks. In Figure 3.10, a select set of sector averages are plotted. We highlight the location of each peak under quiescent conditions with dashed lines.

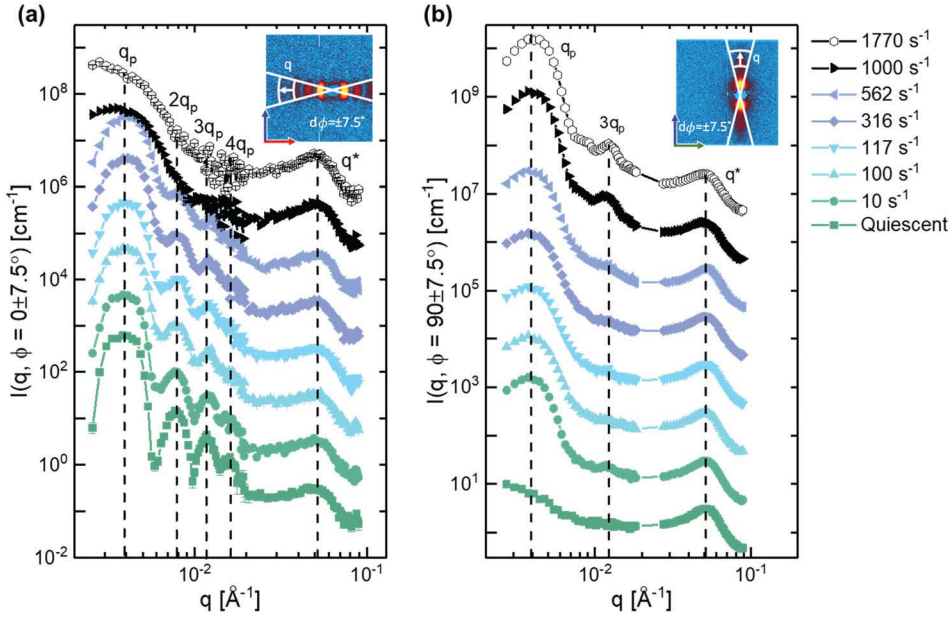

Figure 3.10: (a) Sector averages for select shear rates taken at 0° in the 2–3 scattering plane. Dotted lines serve as guides to the eye, highlighting the initial peak positions under quiescence. (b) Sector averages for select shear rates taken at 90° in the 1–3 scattering plane. Error bars represent the standard deviation of scattering intensities over the averaged area. Data have been offset to aid in the comparison of peak position and width.

From these sector averages, four distinct peaks can be identified in the 2–3 scattering plane during quiescence at q values of 0.0039 $Å^{-1}$, 0.0078 $Å^{-1}$, 0.0117 $Å^{-1}$ and 0.0156 $Å^{-1}$. The fifth peak observed at $q*$, corresponds to the inter-backbone interactions of the bottlebrush polymer and has been discussed in detail in Section 3.4.3.1. The four peaks are all located at integer multiples of the primary peak, q_p = 0.0039 $Å^{-1}$, suggesting that the bottlebrush has self-assembled into a lamellar microstructure with a layer spacing of 161 nm. At quiescence and very low shear rates, features associated with this lamellar structure are only observed along the velocity gradient direction in the 2–3 scattering plane, indicating that the lamellae formed by the bottlebrush polymers is oriented such that the faces of the lamellae are parallel to the walls of the geometry in the so-called 'face-on' configuration. The length scale associated with the lamellae is approximately $3/5^{th}$ the contour length of the bottlebrush, suggesting that the polymer is not adopting a completely rigid conformation within the lamellae. Such an observation is consistent with recent studies carried out on homo and diblock bottlebrush polymer systems [31], [39].

With increasing shear rate, the 3^{rd} and 4^{th} order peaks in the 2–3 plane are observed to widen and lose definition, indicating a loss of long-range order. At shear rates of 1000 s^{-1} and greater, all higher-order peaks in the 2–3 plane become indistinguishable from the primary peak. In the 1–3 scattering plane, higher shear rates lead to the appearance of a primary peak at q_p along the vorticity direction. A tertiary peak is observed to appear for shear rates greater than 1000 s^{-1}, indicating the presence of long-range order. The appearance of regularly spaced peaks along the vorticity direction in both the 1–3 and 2–3 scattering planes indicates that the lamellae have been reoriented and are arranged in the 'edge-on' configuration with the walls of the geometry.

To quantify how shear rate affects the lamellar microstructure, the location of the primary peak (q_p) and full width at half max (FWHM) of each peak was determined by fitting a series of Gaussian curves to the data. A lamellar model fit to this data set was attempted, but the hierarchical microstructure does not lend itself to a simple description provided by lamellar models. The features from the Gaussian fits can be seen in Figure 3.11. A diagram depicting this fitting process can be found in Appendix B (Figure B.6).

In the 2–3 plane, the location of the primary lamellar peak was observed to shift to higher q in the gradient direction as a function of shear rate, as seen in Figure 3.11.a. Between shear rates from $\dot{\gamma}_{c,1}$ to $\dot{\gamma}_{c,2}$, the position of the peak is observed to monotonically increase in magnitude of the scattering vector from 3.89×10^{-3} $Å^{-1}$ to 3.99×10^{-3} $Å^{-1}$. This shift in q_p corresponds to a decreased lamellar spacing of 4 nm, which results in the expected reflected wavelength, lcalc, dropping from 493 nm to 480 nm as shown in Figure 3.11.b. This 13 nm change in λ_{calc} corresponds to a visible color shift from light green to cyan as seen in Figures 3.5 and 3.6. For shear rates from $\dot{\gamma}_{c,2}$ to 562 s^{-1}, the peak location increases from 3.99×10^{-3} $Å^{-1}$ to 4.09×10^{-3} $Å^{-1}$, resulting in a change in lamellar spacing from 157 nm to 153 nm and a decrease in λ_{calc} from 479 nm to 467 nm. This change in scatter wavelength partially accounts for the cyan to indigo transition we observe for shear rates between $\dot{\gamma}_{c,2}$ to 1000 s^{-1} as shown in Figures 3.5 and 3.6. These trends demonstrate that the major cause of the color change observed in the microscopy is the shear-rate-dependent lamellar spacing.

In addition to the peak location, the peak width was also observed to change with shear rate. There are several instrumental factors that can contribute to the width of the observed peaks. To limit these contributions, the instrument setup and experimental conditions were kept constant across all measured shear rates. As such, we interpret the monotonic increase in peak width with shear rate as an indication of increased structural variation. The widening of the peaks is characterized by the full width half max (FWHM), which we show in Figure 3.11.c. For the primary peak along the gradient direction in the 2–3

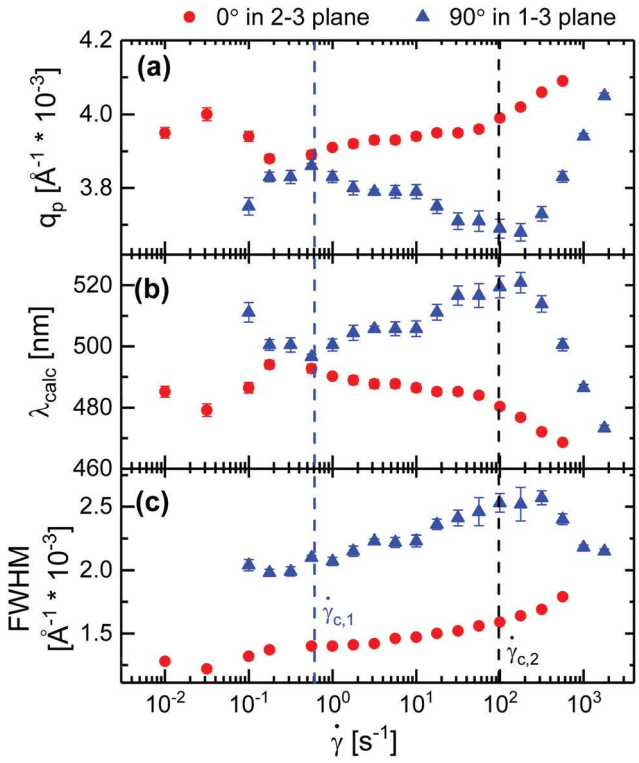

Figure 3.11: (a) The location of the primary peak, q_p, (b) expected reflected wavelength, λ_{calc}, as calculated by equation 1.1, and (c) the full width half max of the primary peak. Values calculated along the gradient direction in the 2–3 plane and vorticity direction in the 1–3 scattering plane. Error bars represent the standard error reported by OriginPro for the fitted Gaussian peaks.

plane, the FWHM is observed to increase as a function of shear rate. This increased dispersity in the primary peak indicates the existence of many scatterers with smaller length scales than suggested by the primary peak position alone. The increased number of smaller spacings therefore also contributes the cyan to indigo color transition observed for shear rates from $\dot{\gamma}_{c,2}$ to 1000 s^{-1} as shown in Figures 3.5 and 3.6.

In contrast, the location of the primary lamellae peak was observed to decrease in the vorticity direction as a function of shear rate in the 1–3 scattering plane as shown in Fig. 11a. Between $\dot{\gamma}_{c,1}$ and $\dot{\gamma}_{c,2}$, q_p decreases from 3.78×10^{-3} Å^{-1} to 3.73×10^{-3} Å^{-1} which results in an increased lamellae spacing of 2.5 nm and an increased reflected wavelength from 507 nm to 514 nm. This 7 nm increase in λ_{calc} corresponds to the green hue observed at low angles on a macroscopic scale as shown in Figure 3.5. For shear rates exceeding $\dot{\gamma}_{c,2}$, the primary lamellae peak is observed to increase up to 4.06×10^{-3} Å^{-1} at 1770 s^{-1}, which leads to decrease in the lamellae spacing from 169 nm to 154 nm and reflected wavelength from 514 nm to 472 nm. This reduction in reflected wavelength contributes to the narrowing of the green region when viewing the sample at low angles as shown in Figure 3.5.

The FWHM of the primary peak observed in the 1–3 plane along the vorticity direction exhibits a non-monotonic trend with increasing shear rate. For shear rates between $\dot{\gamma}_{c,1}$ and $\dot{\gamma}_{c,2}$, the width of the primary peak increases with increasing shear rate. Once $\dot{\gamma}_{c,2}$ is exceeded, the FWHM is observed to decrease with increasing shear rate. The increased definition in the peaks suggests that the lamellae transition from an incoherent state to an ordered state along the vorticity direction. This increased coherence between lamellae,

coupled with the reduced lamellar spacing, results in the reduction of the green band at shear rates above $\dot{\gamma}_{c,2}$.

At quiescence, no features are observed in the 1–3 scattering plane or along the vorticity direction in the 2–3 scattering plane. Similarly, the higher shear rates result in the primary peak being completely smeared out along the velocity gradient direction. As such, peak widths and centers are not included for these two shear rates in 3.11.

To more accurately quantify the overall orientation of the self-assembled microstructure, azimuthal sweeps were taken in both the 1–3 and 2–3 scattering planes at low q. The sweeps were centered at q_p with a width of 0.001 Å^{-1}. In Figure 3.12 , select shear rates are shown to highlight the key changes to the microstructure with increasing shear rate. From the azimuthal sweeps, the alignment factors were calculated according to 3.1 and are shown in Figure 3.13.

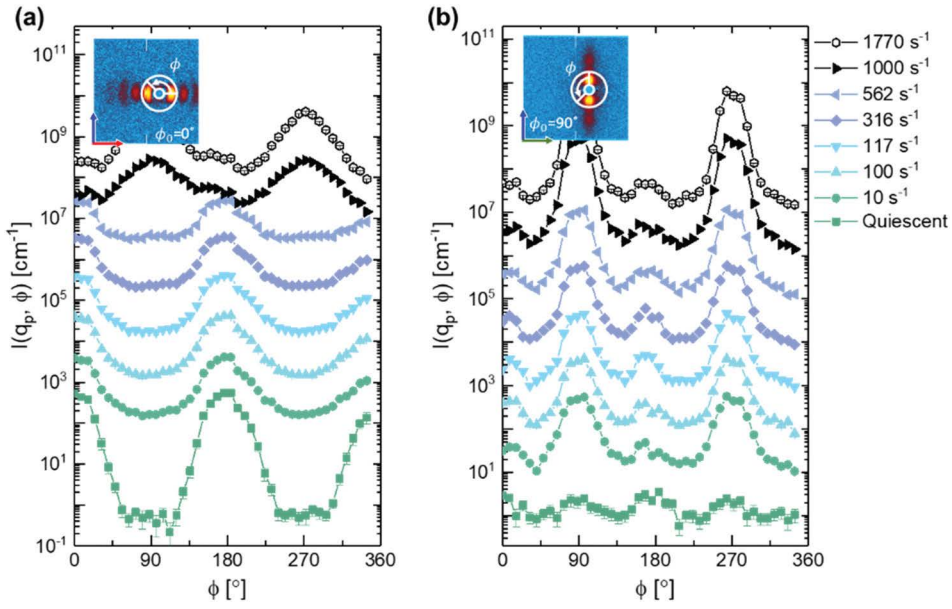

Figure 3.12: The azimuthal variation in the structure peak observed at q = 0.0039 Å^{-1} for a representative set of shear rates in the (a) 2–3 scattering plane and (b) 1–3 scattering plane. Data have been offset for the sake of comparing intensity variation with ϕ.

In the 2–3 plane, the lamellae appear nearly perfectly aligned along the gradient direction under quiescent conditions. At a (low) shear rate of 0.1 s^{-1}, a drop in the alignment of the lamellae along the gradient direction is observed, as can be seen in Figure 3.13.a. This feature is mirrored in Figure 3.13.b, where we observe a jump in alignment along the vorticity direction in the 1–3 plane at 0.1 s^{-1}. This structural change occurs at the same shear rate when the bottlebrush polymers begin to weakly align along the vorticity direction (Figure 3.9). From $\dot{\gamma}_{c,1}$ to $\dot{\gamma}_{c,2}$, the orientation of the lamellae remains constant in both the 1–3 and 2–3 scattering planes. As a result of this distortion, the path length through the lamellae is increased, thus extending the region in which we observe a green color out to 10 s^{-1} despite a reduction in lamellar spacing from green to cyan as shown in Figures 3.6 and 3.11.b.

At shear rates exceeding $\dot{\gamma}_{c,2}$, the extent of alignment exhibited by the lamellae drops in the 2–3 plane until it reaches a shear rate of 1000 s^{-1} at which point the alignment factor increases, albeit along the vorticity direction (see Figure 3.13.a). In the 1–3 plane, the alignment of the lamellae monotonically increases along

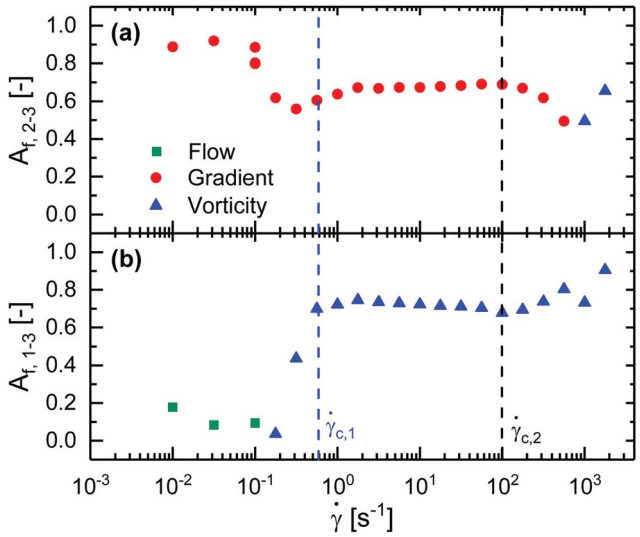

Figure 3.13: Alignment factors calculated from the azimuthal sweeps at 0.0039 $Å^{-1}$ in the (a) 2–3 scattering plane and (b) 1–3 scattering plane. Colors indicate the direction of strongest alignment. Green corresponds to the flow direction in which $\phi_0 = 0°$ in the 1–3 plane. Red corresponds to the gradient direction where $\phi_0 = 0°$ in the 1–3 plane. Blue corresponds to the vorticity direction where $\phi_0 = 90°$ in both the 1–3 and 2–3 plane.

the vorticity direction for shear rates above $\dot{\gamma}_{c,2}$, as shown in Figure 3.13.b. These features correspond to the reorientation of the lamellae from a face-on configuration to an edge-on configuration. This reorientation results in an effectively infinite path length through the material when viewed in the 1–3 plane, thus leaving the sample colorless (Figure 3.6).

3.5 Discussion and Conclusions

We bring together the rheology, microscopy, and neutron scattering at high and low scattering angles to propose a comprehensive structure–property–processing relation, represented visually in Figure 3.14. Under quiescent conditions the bottlebrush polymers self-assemble into well-ordered, flat lamellae that are parallel to the walls of the geometry, as indicated by the well-defined narrow peaks in the 2–3 plane only as shown in Figures 3.7 and 3.10. Within the lamellae, the bottlebrush polymers are isotropically arranged under quiescent conditions in the 1–3 plane, indicated by the weak azimuthal dependence in the scattered intensity of the high q peak shown in Figure 3.8. When shear rates exceeding 0.1 s^{-1} are applied, the individual polymers weakly align within the lamellae along the vorticity direction. The rearrangement at the inter-backbone length scale leads to a reduced modulus in the vorticity direction. This alignment of individual polymers is correlated with the appearance of slight distortions in the lamellar in the (now softer) vorticity direction, in addition to a slight reduction in domain spacing, as seen by the loss of alignment at low shear rates and the increase in q_p with shear rate depicted in Figures 3.12 and 3.11.a, respectively. Our data do not allow us to tell whether the arrangement of bottlebrushes within the lamellae causes the anisotropic modulus of the lamellae, or if the hydrodynamic forces induce undulations in the lamellae which then results in the rearrangement of the individual polymers. However, we can say that the degree of preferential alignment of individual polymers within the lamellae is correlated with the appearance and size of the lamellar undulations: the more aligned the polymers are, the more the larger-scale lamellae undulate.

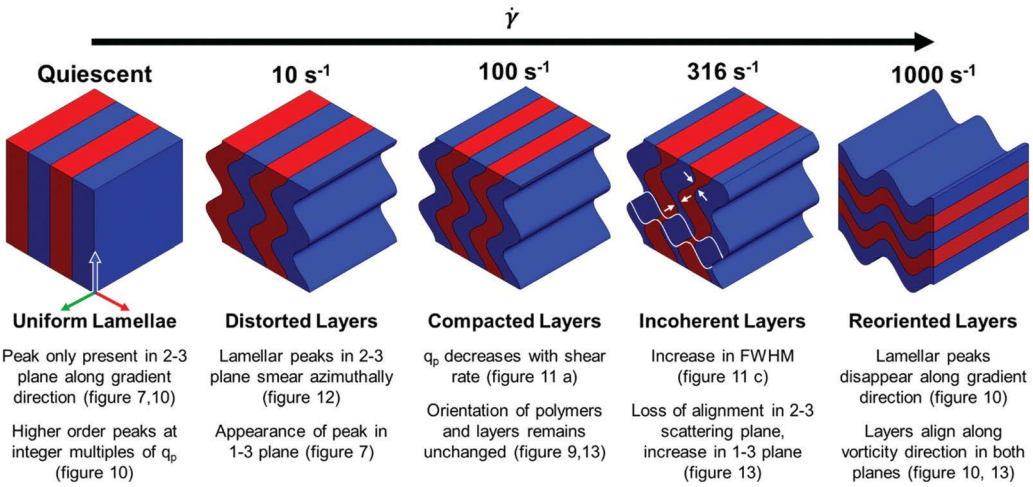

Figure 3.14: A schematic representation of the structural transitions undergone at different shear rates, supported by the data shown elsewhere in this paper. Arrows at $\dot{\gamma} = 316$ s^{-1} serve as guides to the eye, highlighting pinch points that develop between the incoherent layers. White lines at the same shear rate indicate layers that could develop due to these pinch points.

As higher shear rates are applied to the polymer solution, moving from left to right in Figure 3.14, the lamellar spacing is reduced while the orientation remains unchanged, indicated by the decrease in q_p with increasing shear and the alignment factor remaining constant up to $\dot{\gamma}_{c,2}$ as shown in Figures 3.11.a and 3.13, respectively. This structural change results in the sample color transitioning from green to indigo (Figures 3.5 and 3.6). That these changes in color are not observed at rates below $\dot{\gamma}_{c,1}$ suggest that this shear rate acts as some sort of initiation shear rate, or minimum input energy for reducing the lamellae spacing.

At $\dot{\gamma}_{c,2}$, the system is observed to transition to a new shear thinning regime characterized by a power law exponent greater than -0.12. Above this shear rate, the widening of the lamellar peaks indicates a greater dispersity in the lamellar spacing, while the azimuthal smearing indicates a wider range of orientations within the system, as seen by an increase in the FWHM and decrease in A_f in the gradient direction with increasing shear shown in Figures 3.11.c and 3.13, respectively. The system therefore exhibits an average decrease in lamellar spacing, but an increase in the dispersity of those spacings. These trends are consistent with a loss of coherence of the undulations, depicted in Figure 3.13 at 100 s^{-1}. The loss of the fourth-order lamellar peak due to the widening of the peaks, seen in Fig. 10a, indicates an overall reduction in the long-range order of the structure. As higher shear rates are applied the incoherent undulations lead to a pinching and joining of adjacent lamellae highlighted in Figure 3.14 at 316 s^{-1}. At higher rates, the incoherence increases until adjacent undulating blocks of the same chemistry kiss and join, resulting in an apparent rotation that leaves the lamellae oriented perpendicular to the vorticity direction at 1000 s^{-1}. This is depicted in Figure 3.14 by the white lines that indicate regions of different undulating layers that eventually join into a single rotated layer at high shear rates. Above 316 s^{-1} we observe a narrowing of the lamellae peaks in the vorticity direction as shown in Figure 3.11.c, suggesting that 316 s^{-1} not only acts as transition point from face-on to edge-on lamellae, but also from incoherently undulating lamellae to more coherently undulating lamellae. This apparent rotation of the lamellae results in a complete loss of sample color due to the increased path length as seen in Figure 3.6. At these high rates we observed the sample climbing up the walls of the geometry, indicating strong normal forces that are not possible to measure in the concentric cylinder geometry, but lend

support to the dramatic realignment of the lamellar structure.

In conclusion, we have characterized the microstructure and photonic properties of a diblock bottlebrush solution across a broad range of steady shear rates. From this information we have identified features in the rheology, scattering, and microscopy that establish a comprehensive structure–property–processing relation. This relation highlights how the complex flow environment in printing processes such as additive manufacturing and solution printing can impact the self-assembled microstructure and can therefore impact the wide range of photonic properties accessible with diblock bottlebrush polymers.

3.6 References

[1] M. A. Wade, D. Walsh, J. C. W. Lee, *et al.*, "Color, Structure, and Rheology of a Diblock Bottlebrush Copolymer Solution," *Soft Matter*, vol. 16, no. 21, pp. 4919–4931, Jun. 2020, ISSN: 17446848. DOI: 10.1039/d0sm00397b. [Online]. Available: https://pubs.rsc.org/en/content/articlehtml/2020/sm/d0sm00397b%20https://pubs.rsc.org/en/content/articlelanding/2020/sm/d0sm00397b.

[2] G. M. Miyake, R. A. Weitekamp, V. A. Piunova, and R. H. Grubbs, "Synthesis of isocyanate-based brush block copolymers and their rapid self-assembly to infrared-reflecting photonic crystals," *Journal of the American Chemical Society*, vol. 134, no. 34, pp. 14 249–14 254, 2012, ISSN: 00027863. DOI: 10.1021/ja306430k. [Online]. Available: https://pubs.acs.org/sharingguidelines.

[3] R. J. Macfarlane, B. Kim, B. Lee, *et al.*, "Improving brush polymer infrared one-dimensional photonic crystals via linear polymer additives," *Journal of the American Chemical Society*, vol. 136, no. 50, pp. 17 374–17 377, Dec. 2014, ISSN: 15205126. DOI: 10.1021/ja5093562. [Online]. Available: https://pubs.acs.org/sharingguidelines%20https://pubs.acs.org/doi/10.1021/ja5093562.

[4] G. M. Miyake, V. A. Piunova, R. A. Weitekamp, and R. H. Grubbs, "Precisely tunable photonic crystals from rapidly self-assembling brush block copolymer blends," *Angewandte Chemie - International Edition*, vol. 51, no. 45, pp. 11 246–11 248, Nov. 2012, ISSN: 14337851. DOI: 10.1002/anie.201205743. [Online]. Available: http://doi.wiley.com/10.1002/anie.201205743.

[5] B. M. Boyle, T. A. French, R. M. Pearson, B. G. McCarthy, and G. M. Miyake, "Structural Color for Additive Manufacturing: 3D-Printed Photonic Crystals from Block Copolymers," *ACS Nano*, vol. 11, no. 3, pp. 3052–3058, Mar. 2017, ISSN: 1936-0851. DOI: 10.1021/acsnano.7b00032. [Online]. Available: http://pubs.acs.org/doi/10.1021/acsnano.7b00032.

[6] C. G. Chae, Y. G. Yu, H. B. Seo, M. J. Kim, R. H. Grubbs, and J. S. Lee, "Experimental Formulation of Photonic Crystal Properties for Hierarchically Self-Assembled POSS-Bottlebrush Block Copolymers," *Macromolecules*, vol. 51, no. 9, pp. 3458–3466, 2018, ISSN: 15205835. DOI: 10.1021/acs.macromol.8b00298.

[7] J. Raeburn, A. Z. Cardoso, and D. J. Adams, "The importance of the self-assembly process to control mechanical properties of low molecular weight hydrogels," *Chemical Society Reviews*, vol. 42, no. 12, pp. 5143–5156, 2013, ISSN: 14604744. DOI: 10.1039/c3cs60030k.

[8] G. Qu, J. J. Kwok, and Y. Diao, "Flow-Directed Crystallization for Printed Electronics," *Accounts of Chemical Research*, vol. 49, no. 12, pp. 2756–2764, 2016, ISSN: 15204898. DOI: 10.1021/acs.accounts.6b00445.

[9] Y. Diao, L. Shaw, Z. Bao, and S. C. B. Mannsfeld, "Morphology control strategies for solution-processed organic semiconductor thin films," *Energy and Environmental Science*, vol. 7, no. 7, pp. 2145–2159, 2014, ISSN: 17545706. DOI: 10.1039/c4ee00688g.

[10] R. C. Hayward and D. J. Pochan, "Tailored assemblies of block copolymers in solution: It is all about the process," *Macromolecules*, vol. 43, no. 8, pp. 3577–3584, 2010, ISSN: 00249297. DOI: 10.1021/ma9026806.

[11] D. E. Angelescu, J. H. Waller, D. H. Adamson, *et al.*, "Macroscopic Orientation of Block Copolymer Cylinders in Single-Layer Films by Shearing," *Advanced Materials*, vol. 16, no. 19, pp. 1736–1740, Oct. 2004, ISSN: 0935-9648. DOI: 10.1002/adma.200400643. [Online]. Available: https://onlinelibrary.wiley.com/doi/10.1002/adma.200400643.

[12] K. I. Winey, S. S. Patel, R. G. Larson, and H. Watanabe, "Interdependence of Shear Deformations and Block Copolymer Morphology," *Macromolecules*, vol. 26, no. 10, pp. 2542–2549, 1993, ISSN: 15205835. DOI: 10.1021/ma00062a024.

[13] A. Nikoubashman, R. A. Register, and A. Z. Panagiotopoulos, "Sequential Domain Realignment Driven by Conformational Asymmetry in Block Copolymer Thin Films," *Macromolecules*, vol. 47, no. 3, pp. 1193–1198, Feb. 2014, ISSN: 0024-9297. DOI: 10.1021/ma402526q. [Online]. Available: https://pubs.acs.org/doi/10.1021/ma402526q.

[14] A. P. Marencic and R. A. Register, "Controlling Order in Block Copolymer Thin Films for Nanopatterning Applications," *Annual Review of Chemical and Biomolecular Engineering*, vol. 1, no. 1, pp. 277–297, Jun. 2010, ISSN: 1947-5438. DOI: 10.1146/annurev-chembioeng-073009-101007. [Online]. Available: https://www.annualreviews.org/doi/10.1146/annurev-chembioeng-073009-101007.

[15] A. S. Wunenburger, A. Colin, T. Colin, and D. Roux, "Undulation instability under shear: A model to explain the different orientations of a lamellar phase under shear?" *European Physical Journal E*, vol. 2, no. 3, pp. 277–283, 2000, ISSN: 12928941. DOI: 10.1007/PL00013669. [Online]. Available: https://link.springer.com/content/pdf/10.1007%2FPL00013669.pdf.

[16] O. Diat, D. Roux, and F. Nallet, "Effect of shear on a lyotropic lamellar phase," *Journal de Physique II*, vol. 3, no. 9, pp. 1427–1452, 1993, ISSN: 1427-1452. DOI: 10.1051/jp2:1993211{\"{i}}. [Online]. Available: https://hal.archives-ouvertes.fr/jpa-00247917.

[17] M. Braungart, W. McDonough, and P. B. Clinton, *The upcycle : beyond sustainability–designing for abundance*. Farrar, Straus and Giroux, 2014, ISBN: 1429969059.

[18] M. E. Mackay, "The importance of rheological behavior in the additive manufacturing technique material extrusion," *Journal of Rheology*, vol. 62, no. 6, pp. 1549–1561, Nov. 2018, ISSN: 0148-6055. DOI: 10.1122/1.5037687. [Online]. Available: http://sor.scitation.org/doi/10.1122/1.5037687%20https://doi.org/10.1122/1.5037687.

[19] B. B. Patel, D. J. Walsh, D. H. Kim, *et al.*, "Tunable structural color of bottlebrush block copolymers through direct-write 3D printing from solution," *Science Advances*, vol. 6, no. 24, In Press, Jun. 2020, ISSN: 2375-2548. DOI: 10.1126/sciadv.aaz7202. [Online]. Available: http://advances.sciencemag.org/%20https://www.science.org/doi/10.1126/sciadv.aaz7202.

[20] M. Pollard, T. P. Russell, A. V. Ruzette, A. M. Mayes, and Y. Gallot, "The effect of hydrostatic pressure on the lower critical ordering transition in diblock copolymers," *Macromolecules*, vol. 31, no. 19, pp. 6493–6498, Sep. 1998, ISSN: 00249297. DOI: 10.1021/ma980316f.

[21] A. V. Ruzette, A. M. Mayes, M. Pollard, T. P. Russell, and B. Hammouda, "Pressure effects on the phase behavior of styrene/n-alkyl methacrylate block copolymers," *Macromolecules*, vol. 36, no. 9, pp. 3351–3356, May 2003, ISSN: 00249297. DOI: 10.1021/ma021394c.

[22] Y. Lee, H. Lee, S. W. Kim, *et al.*, "Baroplastic behavior of miscible block copolymer blends," *Polymer*, vol. 55, no. 26, pp. 6967–6972, Dec. 2014, ISSN: 00323861. DOI: 10.1016/j.polymer.2014.11.011.

[23] D. Y. Ryu, D. J. Lee, J. K. Kim, *et al.*, "Effect of Hydrostatic Pressure on Closed-Loop Phase Behavior of Block Copolymers," *Physical Review Letters*, vol. 90, no. 23, p. 235 501, Jun. 2003, ISSN: 10797114. DOI: 10.1103/PhysRevLett.90.235501. [Online]. Available: https://link.aps.org/doi/10.1103/PhysRevLett.90.235501.

[24] H. Hasegawa, N. Sakamoto, H. Takeno, *et al.*, "Small-angle neutron scattering studies on phase behavior of block copolymers," *Journal of Physics and Chemistry of Solids*, vol. 60, no. 8, pp. 1307–1312, Sep. 1999, ISSN: 00223697. DOI: 10.1016/S0022-3697(99)00109-2.

[25] J. Lee, T. Wang, K. Shin, and J. Cho, "High-pressure neutron scattering and random-phase approximation analysis of a molten Baroplastic diblock copolymer," *Polymer*, vol. 175, pp. 265–271, Jun. 2019, ISSN: 00323861. DOI: 10.1016/j.polymer.2019.05.013.

[26] D. J. Worsfold and S. Bywater, "ANIONIC POLYMERIZATION OF STYRENE," *Canadian Journal of Chemistry*, vol. 38, no. 10, pp. 1891–1900, Oct. 1960, ISSN: 0008-4042. DOI: 10.1139/v60-254. [Online]. Available: http://www.nrcresearchpress.com/doi/10.1139/v60-254.

[27] R. Waack, A. Rembaum, J. D. Coombes, and M. Szwarc, "MOLECULAR WEIGHTS OF "LIVING" POLYMERS *," *Journal of the American Chemical Society*, vol. 79, no. 8, pp. 2026–2027, Apr. 1957, ISSN: 0002-7863. DOI: 10.1021/ja01565a077. [Online]. Available: https://pubs.acs.org/doi/abs/10.1021/ja01565a077.

[28] S. Breunig, V. Héroguez, Y. Gnanou, and M. Fontanille, "Ring-opening metathesis polymerization of ω-norbornenyl polystyrene macromonomers and characterization of the corresponding structures," *Macromolecular Symposia*, vol. 95, no. 1, pp. 151–166, Jun. 1995, ISSN: 10221360. DOI: 10.1002/masy.19950950114. [Online]. Available: http://doi.wiley.com/10.1002/masy.19950950114.

[29] B. G. G. Lohmeijer, R. C. Pratt, F. Leibfarth, *et al.*, "Guanidine and Amidine Organocatalysts for Ring-Opening Polymerization of Cyclic Esters," *Macromolecules*, vol. 39, no. 25, pp. 8574–8583, Dec. 2006, ISSN: 0024-9297. DOI: 10.1021/ma0619381. [Online]. Available: https://pubs.acs.org/doi/10.1021/ma0619381.

[30] D. J. Walsh and D. Guironnet, "Macromolecules with programmable shape, size, and chemistry," *Proceedings of the National Academy of Sciences of the United States of America*, vol. 116, no. 5, pp. 1538–1542, Jan. 2019, ISSN: 10916490. DOI: 10.1073/pnas.1817745116.

[31] S. Dutta, M. A. Wade, D. J. Walsh, D. Guironnet, S. A. Rogers, and C. E. Sing, "Dilute solution structure of bottlebrush polymers," *Soft Matter*, vol. 15, no. 14, pp. 2928–2941, 2019, ISSN: 17446848. DOI: 10.1039/c9sm00033j.

[32] J. A. Love, J. P. Morgan, T. M. Trnka, and R. H. Grubbs, "A Practical and Highly Active Ruthenium-Based Catalyst that Effects the Cross Metathesis of Acrylonitrile," *Angewandte Chemie International Edition*, vol. 41, no. 21, pp. 4035–4037, Nov. 2002, ISSN: 1433-7851. DOI: https://doi.org/10.1002/1521-3773(20021104)41:21<4035::AID-ANIE4035>3.0.CO;2-I. [Online]. Available: https://doi.org/10.1002/1521-3773(20021104)41:21%3C4035::AID-ANIE4035%3E3.0.CO%202-I.

[33] S. C. Radzinski, J. C. Foster, R. C. Chapleski, D. Troya, and J. B. Matson, "Bottlebrush Polymer Synthesis by Ring-Opening Metathesis Polymerization: The Significance of the Anchor Group," *Journal of the American Chemical Society*, vol. 138, no. 22, pp. 6998–7004, Jun. 2016, ISSN: 15205126. DOI: 10.1021/jacs.5b13317. [Online]. Available: https://pubs.acs.org/doi/10.1021/jacs.5b13317%20https://pubs.acs.org/sharingguidelines.

[34] S. R. Kline, "Reduction and analysis of SANS and USANS data using IGOR Pro," *Journal of Applied Crystallography*, vol. 39, no. 6, pp. 895–900, Dec. 2006, ISSN: 00218898. DOI: 10.1107/S0021889806035059.

[35] C. R. López-Barrón and N. J. Wagner, "Solvent isotope effect on the microstructure and rheology of cationic worm-like micelles near the isotropic-nematic transition," *Soft Matter*, vol. 7, no. 22, pp. 10 856–10 863, 2011, ISSN: 1744-683X. DOI: 10.1039/c1sm05878a. [Online]. Available: http://xlink.rsc.org/?DOI=c1sm05878a.

[36] P. Mukerjee, P. Kapauan, and H. G. Meyer, "Micelle formation and hydrophobic bonding in deuterium oxide," *Journal of Physical Chemistry*, vol. 70, no. 3, pp. 783–786, 1966, ISSN: 00223654. DOI: 10.1021/j100875a029.

[37] B. R. Sveinbjörnsson, R. A. Weitekamp, G. M. Miyake, *et al.*, "Rapid self-assembly of brush block copolymers to photonic crystals," *Proceedings of the National Academy of Sciences of the United States of America*, vol. 109, no. 36, pp. 14 332–14 336, 2012, ISSN: 00278424. DOI: 10.1073/pnas.1213055109. [Online]. Available: www.pnas.org/lookup/suppl/.

[38] L. M. Walker and N. J. Wagner, "SANS analysis of the molecular order in poly(γ-benzyl L-glutamate)/deuterated dimethylformamide (PBLG/d-DMF) under shear and during relaxation," *Macromolecules*, vol. 29, no. 6, pp. 2298–2301, 1996, ISSN: 00249297. DOI: 10.1021/ma951127p.

[39] S. J. Dalsin, T. G. Rions-Maehren, M. D. Beam, F. S. Bates, M. A. Hillmyer, and M. W. Matsen, "Bottlebrush Block Polymers: Quantitative Theory and Experiments," *ACS Nano*, vol. 9, no. 12, pp. 12 233–12 245, Dec. 2015, ISSN: 1936086X. DOI: 10.1021/acsnano.5b05473. [Online]. Available: http://pubs.acs.org/doi/10.1021/acsnano.5b05473%20www.acsnano.org12233.

Chapter 4

Locking in Microstructure Via Chemical Means

4.1 Chapter Overview

In this chapter, we identify the rapid relaxation of the diblock bottlebrush polymer microstructure from its cyan, sheared state, to its green, quiescent state, in less than a second and explore one of two avenues to increase this relaxation time and thus the shear memory of the material. We focus on the ultra violet activated curing properties and dynamics of a diblock bottlebrush polymer solution. These studies are carried out with the goal of locking in shear induced microstructures by increasing the relaxation time of the polymer material to effectively infinite via a sol-gel transition. Polylactic acid-b-polystyrene diblock bottlebrush polymers were functionalized with -allyl groups on each side chain by our collaborators in the Guironnet group. These polymers were dispersed in a toluene solution with Pentaerylthritol tetrakis(3-meracaptorpropionate), which acted as a crosslinking molecule, binding to the -allyl groups on the bottlebrush polymer via a thiol-ene reaction and 2,2-Dimethoxy-2-phenylacetophenone which acted as a photo-initiator, generating free radicals when exposed to UV light. Rheo-microscopy and sample imaging were employed to assess out ability to lock-in microstructures induced through steady shear. During these tests, steady stress was applied to mimic direct ink writing processes while also avoiding issues with sample fracture after the sample had undergone gelation. Macroscopic images captured under zero stress after steady stress gelation clearly demonstrate a color change from green to green-blue to cyan, serving as a proof of concept. To characterize the dynamics of the system, steady oscillatory shear was applied to the sample as it underwent gelation at several different frequencies to identify the gel point, where G' and G" were congruent to one another across a range of frequencies. Challenges resulting from high mutation number limited the range of frequencies that could be considered. The Winter-Chambon criteria appeared to fail for this system due to the complex chemistry and non-uniform gelation thus resulting in an inability to accurately characterize the gel point described by the Winter-Chambon criteria. A rough estimate of the gelation kinetics was obtained by measuring the G', G" crossover in the limit of zero frequency. SPP analysis was applied to this system in an effort to overcome limitations with the large mutation number. Due to the differential nature of this analysis method, smoothing techniques were applied to reduce noise in the recorded strain, strain rate, and stress. Through this process, transient moduli could be calculated, though the exact interpretation of these values is still forthcoming.

4.2 Introduction

Having demonstrated the ability to control the self-assembled microstructure, and in turn, sample color, through the application of steady deformation in Chapter 3, we begin to explore the rates at which this structure reverts to its quiescent state and mechanisms by which we can control the material's memory of its shear history. In this chapter we take a chemical approach, utilizing a sol-gel transition to increase the relaxation time to effectively infinity. In Chapter 5, we explore the viability of increasing the relaxation time through physical means, utilizing the liquid to solid transition observed in yield-stress fluids to increase the relaxation time. In the context of direct-ink-writing processes, controlling the relaxation time of the material through either of these approaches is appealing as it allows us to control how structures induced through the printing process are "locked-in" after the material has been deposited onto a substrate.

Chemical crosslinking and rapid gelation processes have been shown to kinetically trap a material in a metastable state, thus resulting in an effectively infinite relaxation time through the formation of permanent chemical bonds [1]–[6]. Specifically, recent studies carried out by Wang et al., highlight the importance of gelation kinetics when compared to self-assembly and relaxation dynamics, noting how control over the reaction kinetics can lead to different microstructures within a gel that have potential applications in molecule transport and drug delivery [4]. Taken in tandem with the work done by Rumer et al., which demonstrates the impact of crosslinking on the ability to retain precise microstructures and prevent phase separation with time [1], crosslinking provides a unique opportunity to control and retain select meta-stable microstructures that are induced into a polymer system.

In the case of bottlebrush polymers, the chemical crosslinking of these materials under quiescent conditions to form super soft elastomers has been explored quite thoroughly by Daniel et al., Pakula et al., and Nian et al., [7]–[9]. These studies focused on the unique super-soft properties exhibited by these polymers that originate from the side chains sterically elongating the backbones of these polymers while simultaneously acting as a solvent and preventing the molecules from entangling with one another [7], [9] However, processing conditions are known to have a significant impact on the final microstructure of a bottlebrush polymer sample which can in turn, be preserved through kinetic trapping mechanisms, as shown in Chapter 3 and by Patel et al., [10], respectively.

Based on the understanding that rapid polymer crosslinking reactions can kinetically trap materials before they are able to reach equilibrium and our previous work developing structure-property-process relations between microstructure, color, and flow conditions, we expect to be able to lock shear induced microstructures by crosslinking the material such that it goes through a sol-gel transition without relaxing to its quiescent state. To achieve this, we utilize a UV initiated thiol-ene reaction that allows us to gel -allyl functionalized bottlebrush polymer while the material undergoes shear stress. We will first demonstrate a proof of concept, showing that different colors, and thus, different microstructures can be obtained when crosslinking under steady stress. We will then explore the gelation kinetics of these reactions to capture the time at which these materials transition from a sol to a gel and compare it to the relaxation time of the polymer. Due to the rapid gelation time that will be necessary to lock in the induced microstructure prior to the bottlebrush polymer relaxing, we employ the sequence of physical processes analysis method in an effort to access shorter time scales.

4.2.1 The Winter-Chambon Criteria

When characterizing the time it takes for a polymer to undergo the sol-gel transition, literature typically reports a critical gel point as described by Winter and Chambon [11]. The gel point is defined as the point where $G'(\omega)$ and $G"(\omega)$ scale with the same power law exponent n, and are thus congruent, for all frequencies. During early studies investigating the gelation time, the reaction being studied reaction was quenched at intermediate points during gelation. At these points frequency sweep were performed to assess the congruency of G' and G" [11], [12]. While this experimental design was viable for reactions that could be readily stopped and provided early insight into gelation process, it is not practical for most systems. More recent studies instead opt to measure the change in G' and G" during gelation, performing multiple tests at different frequencies [13]–[18]. The resulting moduli can be used to calculate the phase angle which is then plotted against time. The intersection of all these phase angles as a function of time corresponds to the point where G' and G" are congruent over multiple frequencies and can thus be used as a measure of the critical gel point [13]–[18]. In cases with limited sample or where multiple tests are impractical, several groups have applied multiple frequencies overlaid on top of one another as the sample was allowed to cure [19]–[22]. The material response data are then deconvoluted and the moduli are calculated for each superimposed frequency, thus allowing for multiple phase angles to be calculated from one study.

When performing any of these types of studies, in which a material undergoes rapid changes over a period of time, it is imperative to take into account the mutation number, N_{Mu}, as defined by Mours and Winter [23], where

$$N_{Mu} = t_{exp}\frac{1}{g}\frac{\partial g}{\partial t}. \tag{4.1}$$

In this equation, N_{Mu} is the mutation number, t_{exp} is the timescale of the experiment and g represents the measured quantity [23]. The mutation number compares the rate at which the measured quantity changes to the time it takes to measure said quantity with a N_{Mu} of 0.1 representing a measured quantity that changes by 10% over the course of a single measurement. Mutation numbers greater than 0.1 to 0.2 generally indicate that the measured quantity is changing too quickly relative to the time of the experiment to be accurately measured. In the case of oscillation averaged shear rheology in which the moduli are it to the stress and strain as sine and cosine components, t_exp can be treated as the time it takes to complete a half an oscillation. As a result, there is a lower limit on the frequencies that can be reasonably tested using oscillation averaged shear rheology.

Due to the rapid response time and short relaxation time observed in bottlebrush polymer solutions as described in Chapter 1 and as will be discussed in more detail in this chapter, we will need to probe a gelation reaction that can occur on a very short timescale. As such, accurately characterizing the gelation time will prove quite difficult as any measurements taken at a reasonable frequency will have a relatively large mutation number due to rapid changes in G' and G". To avoid the issue of large mutation numbers all together, we turn towards time resolved analytical methods that do not rely on oscillation averaged values.

4.2.2 The Sequence of Physical Processes Analytical Framework

The sequence of physical processes (SPP) formalism, first proposed in 2011 [24], [25] and later refined in 2017 [26], describes a material's rheological response as a trajectory in deformation space by

$$\mathbf{A} = [A_\gamma \; A_{\dot{\gamma}/\omega} \; A_\sigma] = [\gamma(t) \; \dot{\gamma}(t)/\omega \; \sigma(t)]. \tag{4.2}$$

In the case of oscillatory deformation, the γ and $\dot{\gamma}$ can be described as

$$\gamma(t) = \gamma_0 sin(\omega t), \tag{4.3}$$

and

$$\dot{\gamma} = \gamma_0 \omega cos(\omega t). \tag{4.4}$$

The corresponding σ can be decomposed into energy storage and energy loss components of the form

$$\sigma(t) = \gamma_0[G^{'}(\omega)sin(\omega t) + G^{"}(\omega)cos(\omega t)], \tag{4.5}$$

where $G'(\omega)$ represents the extend of energy stored and $G"(\omega)$ represents the extend of energy dissipated.

Using the Frenet-Serret apparatus [27], [28], the trajectory $\mathbf{A}$ can be described by a set of orthonormal vectors called the tangent, $\mathbf{T}$, principle normal, $\mathbf{N}$, and the binormal, $\mathbf{B}$. The tangent vector points in the direction of instantaneous motion,

$$\mathbf{T} = \frac{\dot{\mathbf{A}}}{\|\mathbf{A}\|}. \tag{4.6}$$

The principle normal vector points in the direction of the derivative of the tangent vector,

$$\mathbf{N} = \frac{\dot{\mathbf{T}}}{\|\mathbf{T}\|} \tag{4.7}$$

The binormal is the cross product of normal and tangent vectors,

$$\mathbf{B} = \mathbf{T} \times \mathbf{N}. \tag{4.8}$$

The binormal vector describes the orientation of the osculating plane that passes through trajectory $\mathbf{A}$ and is spanned by the tangent and normal vector. The point normal form of this plane is

$$B_x[x - A_x] + B_y[y - A_y] + B_z[z - A_z] = 0. \tag{4.9}$$

The SPP framework defines two transient moduli, $G_t^{'}$ and $G_t^{"}$, two differential parameters that represent the orientation of osculating plane at every point along the trajectory. A displacement term, σ_d is introduced to describe the position of the osculating plane through deformation space [26]. The general form of the osculating plane is thus given by

$$\sigma(t) = G_t^{'}(t)\gamma + G_t^{"}(t)\gamma + \sigma_d. \tag{4.10}$$

To determine the form of the displacement stress, we take the point-normal form of the osculating plane from Eq. 4.9, set the x and y components to zero, and solve for displacement along the stress axis,

$$\sigma_d = \frac{B_\gamma}{B_\sigma} A_\gamma + \frac{B_{\gamma(\dot{t})/\omega}}{B_\sigma} A_{\gamma(\dot{t})/\omega} + \sigma(t) \tag{4.11}$$

Substituting the form for the displacement stress in Eq. 4.11 into Eq. 4.10 gives the following

$$[G_t^{'}(t) + \frac{B_\gamma}{B_\sigma}]\gamma + [G_t^{"}(t) + \frac{B_{\dot{\gamma}/\omega}}{B_\sigma}]\frac{\dot{\gamma}}{\omega} = 0. \tag{4.12}$$

Solutions to Eq. 4.12 can be found by setting the terms inside each bracket to zero, giving definitions for the transient moduli:

$$G_t^{'}(t) = -\frac{B_{\gamma}(t)}{B_{\sigma}(t)} \tag{4.13}$$

$$G_t^{"}(t) = -\frac{B_{\dot{\gamma}/\omega}(t)}{B_{\sigma}(t)}. \tag{4.14}$$

The SPP framework was derived as a mechanism to investigate large deformations and describe the observed rheological phenomena as a series of time resolved parameters that describe the state of a material and track the evolution of its response [24]–[26]. This approach has been successfully implemented to describe several complex flow and yielding processes [29], [30]. That being said, this approach is not limited to non-linear studies, with the definitions given in Eqs. 4.13 and 4.14 simplifying down to their linear counterparts, G' and G" under linear deformation conditions [26]. This allows for characterization of the linear moduli a material based on the strain, strain rate, stress trajectory without relying on oscillation averaged measurements. This is particularly appealing from a gelation perspective as measuring the transient waveform and then calculating the time-resolved moduli results in a N_{Mu} that is based on the time resolution of the data rather than the frequency applied during testing. By removing the mutation number as a limiting factor, SPP analysis of gelation data allows for a broader range of frequencies to be tested while simultaneously providing a more accurate measure of the exact point where the material becomes a percolated network.

4.3 Methods and Materials

4.3.1 Bottlebrush Functionalization and Sample Preparation

Details regarding the synthetic preparation and molecular weight characterization carried out by Yash Kamble, our collaborator from the Guironnet group, to functionalize diblock bottlebrush polymers for the purpose of UV-curing can be found in Appendix C Section C.1.

For the UV-curing studies in the rheometer, samples were prepared by dissolving the functionalized diblock bottlebrush polymers in toluene to form a 175 mg/ml solution. Pentaerylthritol tetrakis(3-meracaptorpropionate) was then added to the solution to get a concentration of 25 mg/ml to serve as a crosslinker between the bottlebrush polymers once they were exposed to UV light. 2,2-Dimethoxy-2-phenylacetophenone was also added to the solution with a concentration of 14 mg/ml to act as a photo-initator. Once the photo-iniator was added to the sample, the vial was wrapped in tinfoil to prevent exposure to ambient UV radiation. Samples were mixed for at least 24 hrs on a SciLogex tube roller.

For transient microscopy studies, solutions of non-functionalized diblock bottlebrush polymers were dissolved in toluene to form a 175 mg/ml solution. The bottlebrush polymers were synthesized by collaborators according to the methods described in 3.3.1. Solutions were mixed for at least 12 hrs using a shaker or a roller table to ensure uniform dispersion of the polymers within the solution.

4.3.2 Characterization of Microstructure Kinetics

The time scale over which the color and, in turn, the microstructure, of the dissolved PS-PLA bottlebrush relaxed from its sheared state to its quiescent state was captured using the rheo-microscope setup for the Anton-Paar MCR 702 as described in 3.3.3. Tests consisted of applying steady shear to the bottlebrush

polymer solution while recording a video using the rheo-microscope camera. Steady shear was applied to the bottlebrush polymers for at least 30 s to ensure that the structure and reflected color of the polymer had reached a steady state. At 30 s (t_{stop}), the shear rate was set to zero and the rate of the color change was observed. The sample was held at a shear rate of zero while the camera continued to record for an additional 70s to identify how quickly the color reverted back to its quiescent state. It should be noted that the camera was started slightly before steady shear was applied to the sample in order to capture a reference state that could be compared to the sheared and final, quiescent state.

4.3.3 Characterization of Gelation Kinetics

The rheological properties of these materials were characterized during gelation using the UV-curing attachment for the Anton-Paar MCR 702. This setup consisted of a quartz bottom plate mounted above a UV light guide and a 25 mm stainless steel parallel plate top geometry. The light guide beneath the quartz plate was connected to a UV light source consisting of a Omnicure Series 2000 lamp equipped with a Excelitas Technologies 200 watt mercury arc bulb. The shutter of the lamp was controlled using a aux cable connected the uv lamp to the MCR 702. This configuration allowed us to open and close the shutter by adjusting a variable in Anton-Paar's Rheocompass software and program in the exact UV exposure time. A 25 mm aperture was installed just beneath the quartz bottom plate to ensure that only the area covered by the sample was exposed to UV light. A diagram depicting the UV curing setup can be seen in Figure 4.1. To isolate the sample from ambient UV radiation as well as limit our own exposure to UV light, the MCR evaporation blocker was installed over the top geometry.

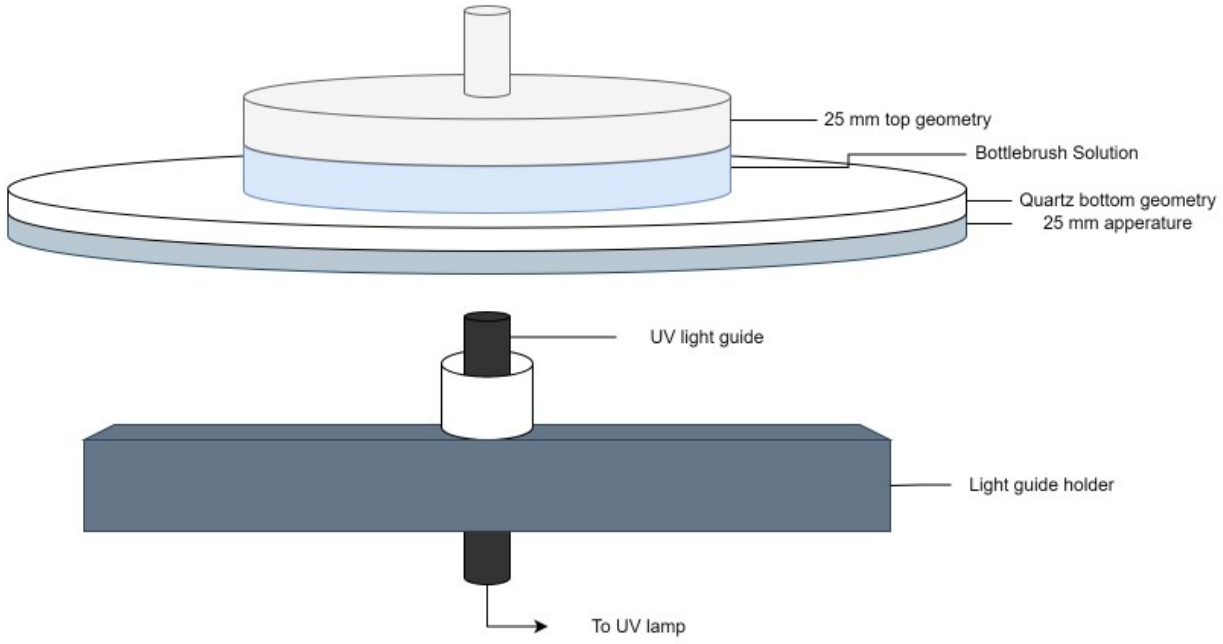

Figure 4.1: A schematic depicting the UV curing setup used to perform gelation studies on the Anton-Paar MCR 702. Schematic not drawn to scale.

Prior to testing, the intensity of the UV light was checked using a Thorlabs power meter equipped with a S401C sensor. The sensor was positioned approximately 2 mm away from the bottom geometry to minimize

the risk of the sensor coming in contact with the bottom plate and scratching it. After recording the UV intensity, the sample was loaded onto the bottom geometry and the top was lowered to a gap height of 0.25-0.5 mm. A preshear at a rate of 25 $s^{-}1$ was applied to the sample for 300 s to remove any bias within the sample that may have been due to loading. Frequency sweeps were then carried out from 1 to 10 rad/s at 1% strain amplitude and compared with a previous linear characterization from 0.1 t0 10 rad/s at 1% strain amplitude. This comparison allowed us to check the material and identify any variation between loadings.

The gelation kinetics of the bottlebrush polymer were characterized by applying steady oscillatory shear to the polymer and calculating the storage and elastic moduli as a function of time. Tests were carried out with frequencies from 3.16 to 56.2 rad/s with a strain amplitude of 1%. Oscillatory shear was applied to the sample for 60 s prior to turning the lamp on to ensure the material was at steady state. The sample was found to reach steady state in this time while also allowing us to minimize the effects of solvent evaporation. At 60 s, the lamp was turned on and the change in moduli was recorded. The sample was exposed for 1800 s to observe how long term exposure to UV light affected the bottlebrush gelation. After 1800 s, the lamp was turned off and the sample was observed for another 500 s to characterize the effect of evaporation. By performing these tests multiple times at different frequencies, we were able to reconstruct a frequency sweep and identify a time frame in which the moduli are congruent. This point is represented as a time at which all of the phase angles as determined from the calculated G' and G", intersect with one another as described by [23], [31], [32].

To capture data for analysis by sequence of physical properties, the procedure to characterize the gelation kinetics was slightly modified by including transient stress measurements during the first few minutes of gelation. Similar to the gelation kinetics studies, steady oscillatory strain was applied for approximately 60 s prior to gelation to ensure the sample was at steady state before turning on the UV lamp. The exact time of this step was adjusted based on the frequency applied, thus ensuring that the sample was at 0 % strain prior gelation. Once the lamp was turned on at 60 s, we measured the transient stress under oscillatory strain with a constant dt of 0.05 s. This transient stress data was recorded for the first 3 to 4 minutes of the sample undergoing gelation. These tests were carried out at frequencies of 0.1, 0.316, 1, and 3.16 rad/s. Under traditional oscillatory methods, these frequencies would have had too high of a mutation number due to the time it would take to complete half an oscillation as compared to the rate at which the moduli changes. As such, the resulting reported values measured at these lower frequencies would not accurately represent the rheological properties of the material. Higher frequencies were not tested due to limitations with the number of points that could be applied in a single measurement step in Rheocompass as well as concerns regarding the introduction of noise at very low dts. Frequencies lower than 0.1 were not tested due to the torque approaching the MCR 702's lower measurable limit.

4.3.4 Characterization of Gelation Under Steady Stress

To characterize the possibility of locking in select microstructures and thus colors through UV curing process, we use the UV setup described in Section 4.3.3 and apply steady stress to the material while simultaneously exposing it to UV light. This study allows us to mimic the conditions considered in various printing studies [33]–[35] in which constant pressure is applied to a material to force it out of a nozzle. Testing this material under constant stress also has the added benefit of preventing the destruction of the bottlebrush sample as it solidified during gelation. Tests were carried out using an aluminum disposable 25 mm parallel plate geometry to allow us to remove the geometry and sample from the rheometer without damaging the newly crosslinked gel. Prior to gelation, steady stress was applied to the sample for 300 s to ensure the material was undergoing

steady deformation. After 300 s, the shutter for the UV lamp was opened and the sample was exposed to 10 mW/cm^2 of UV light for 500 s. This exposure time ensured that the sample was completely gelled without running into significant changes in material properties due to evaporation and secondary reactions. After 500 s, the shutter for the UV lamp was removed and the sample was allowed to reach room temperature.

After approximately 3 minutes or when the rheometer read 25 °C for at least 60 s, the sample was removed from the rheomter by first unscrewing the top disposable geometry and disconnecting it from the shaft connected to the rheometer. The bottom quartz plate was unscrewed from the rheometer thus preventing the sample from being disturbed and possibly fractured due to removal from either geometry. The entire quartz plate, sample, disposable geometry configuration was inverted and placed in a sample holder that supported the quartz plate while allowing the top geometry to hang freely. This ensured that the sample was not compressed or twisted when capturing images. The setup was positioned beneath a camera and illuminated with a single point light source. Images were captured of the sample and labeled based on the stress applied during the gelation process. Stresses from 0 Pa to 63 Pa to capture points along the flow curve that had previously demonstrated color change as described in Chapter 3. Stresses higher then 63 Pa could not be recorded due to the sample fracturing after it had undergone crosslinking.

4.4 Results and Discussion

4.4.1 Structural Kinetics

The time it takes for the color, and thus the microstructure of a uniform diblock bottlebrush polymer suspended in solution to revert back to its quiescent state after undergoing steady shear deformation was found to be on the order of 1 s. This rapid change in color can be seen in Figure 4.2 in which the color of the sample, represented by measured hue rapidly reverts from cyan during steady shear to green shortly after the shear rate is set to zero. For the purposes of this discussion we will focus on the shear rates shown in Figure 4.2 as these rates span the range where the most significant color change is visually observed. A complete set of shear rates that span from 0.1 to 100 s^{-1} can be found in Appendix C and were found to revert back to their quiescent colors on a similar time scale as those shown in Figure 4.2. The complete videos used to generate Figure 4.2 can be found as supplementary material and are labeled according to the applied shear rate. Note that the videos start approximately 15 s before steady shear is applied to the sample. The point at which the color relaxes can be found at approximately the 45 s timestamp. Images shown in Figure 4.2.b prior to and immediately after t_{stop} demonstrate how significant and rapid this color change can be. Given the timescale observed during this study and the work described in Chapter 3, we attribute this rapid change to the microstructure reverting from a compressed and distorted state under high shear to a more uniform structure shortly after flow is stopped. This rapid change indicates that the bottlebrush polymer solution has a very short memory of its shear history and thus does not retain an of the shear induced microstrutures after t_{stop}.

At longer time scales, the measured hue is observed to asymptotically approach the same hue observed prior to deforming the polymer solution. This change in color is relatively small compared to the difference between the color during steady shear and after t_{stop} (Figure 4.2.b). Given that we expect the lamellae to have reverted to approximately the same spacing and orientation as its quiescent state after approximately 1 s, we attribute this gradual change over longer time scales to the gradual assembly and ordering of the bottlebrush polymer lamellae into a larger more uniform structure, thus resulting in the sample appearing

more more green as a function of time.

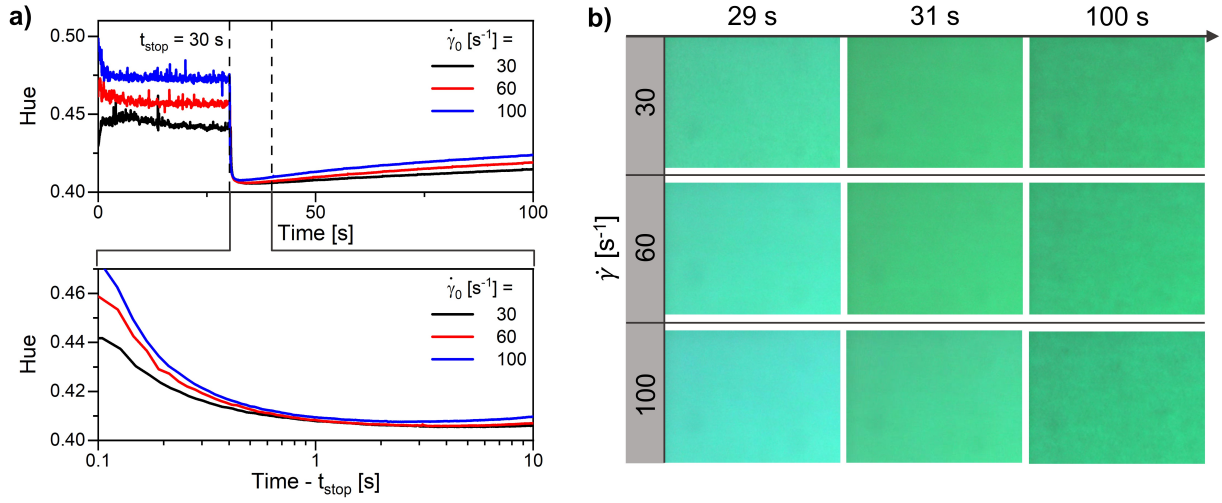

Figure 4.2: (a) The average color of the sample as captured by the rheo-microscope as a function of time during steady shear and shear cessation for a set of shear rates in which significant color change is observed. The color immediately after the shear rate is set to zero is shown on a logarithmic time scale, highlighting how quickly this material reverts to its quiescent state. (b) Representative frames pulled from the recorded videos showing the color shortly before cessation (29 s), shortly after (31 s) and at longer times (100 s).

It should be noted that the color of the sample is represented using the hue from the Hue-Saturation-Value color model in which the digitized color is described as a perceived color (hue), intensity (saturation), and lightness (value). This model is implemented due to an inability to directly convert between the red, green, and blue values measured by the digital microscope camera and the wavelength of the light reflected by the bottlebrush polymer solution. Despite this disconnect, the recorded hue serves as a reasonable measure of the color change as demonstrated by the clear distinctions in sample color seen in frames taken at 29 s and 31 s in Figure 4.2.b mirroring the sudden drop in hue around t_{stop} in Figure 4.2.

The short shear memory of this bottlebrush solution presents a challenge when considering this material for applications in direct-ink-writing processes. In the case of solution printing, the drying process that finalizes the microstructure of the bottlebrush polymer has been shown to take on the order of a couple of seconds [10]. While Patel et al., effectively demonstrated that kinetic trapping can occur based on the rate of evaporation [10], the final microstructure cannot be effectively controlled by adjusting the flow conditions experienced by the bottlebrush polymer during printing. As such, increasing the relaxation time of the bottlebrush solution, and thus its shear memory should nominally allow for the retention of shear induced structures. In the remainder of this chapter, we explore the use of chemical crosslinking and UV-curing processes to physically lock the material in place, increasing its relaxation time to effectively infinity and thus giving us a mechanism by which the shear-induced microstructure can be retained.

4.4.2 Locking in Microstructure

To demonstrate the ability to lock in different microstructures and as a result different colors the diblock bottlebrush polymer solution was cured under steady stress from 1 Pa to 63 Pa with an additional test taken at 0 Pa to compare with the color of the bottlebrush polymer under quiescent conditions. The flow curve

shown in Figure 4.3.a, depicts the color of the bottlebrush material captured using the rheo-microscope under steady flow conditions, labeled "Color Prior to Gelation". Despite the material having the same composition and concentration as the bottlebrush polymer solution studied in Chapter 3, the color change goes from green-yellow to green-blue instead of the previously observed green to cyan. We attribute this difference in color range to slight variations in the molecular weight of polymers as the materials were synthesized as two separate batches. Additional factors such as image exposure time could have also led to this difference in color.

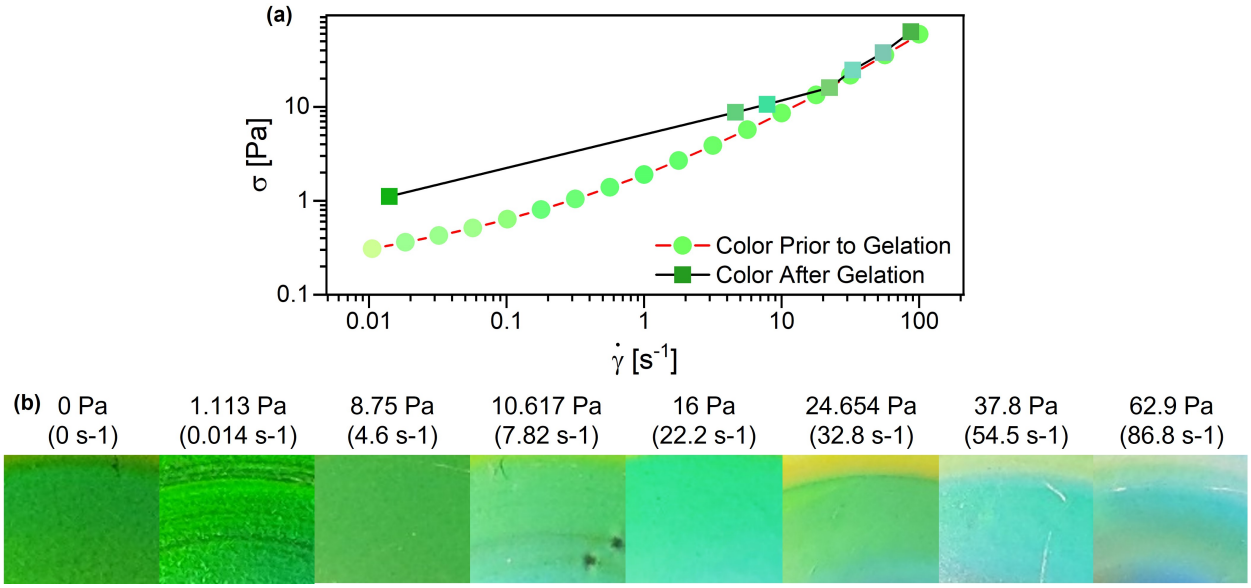

Figure 4.3: (a) A flow curve (red) and the applied stress and shear rate captured immediately before the UV lamp is turned on (black) for the diblock bottlebrush solution described in Section 4.3.1. The colors of individual points are based on the average color of the image captured during steady steady shear (red) and after the gel had been removed from the rheometer (black), using the rheo-microscope and a digital camera, respectively. (b) Images depicting the color of the bottlebrush samples gelled under steady stress conditions. Images were captured after the samples were under zero stress

Based off of the flow curve, stresses from 1 Pa to 63 Pa were selected to capture the region of the flow curve where we would expect the most color change. The resulting flow conditions prior to gelation are plotted in black in Figure 4.3.a. Macroscopic images of the sample after it had been exposed to UV light and removed from the rheometer according to the procedure discussed in Section 4.3.4. are shown in Figure 4.3.b. These images were cropped spanning from 6.25 mm to 9.4 mm to remove edge effects and focus on the region of the sample that experienced a shear rate close to what the rheometer reported. We observe that the gelled materials exhibit a color dependence on steady stress with the quiescent, 0 Pa, sample exhibiting a green color. With increasing stress, the color of the material transitions to blue-green and eventually cyan at 37.8 Pa and 63 Pa. The fact that these images were captured under zero stress conditions after the materials had been gelled demonstrates our ability to lock in the various microstructures induced in bottlebrushes via deformation through the chemical crosslinking of the molecules to form a solid network.

4.4.3 Gelation Kinetics

The gelation kinetics of a diblock bottlebrush bottlebrush with -allyl functionalized side chains in a toluene solution as described in Section 4.3.1 were characterized at 4 logarithmically spaced frequencies from 3.16 rad/s to 31.6 rad/s. Prior to loading the samples, the intensity of the UV lamp at the surface of the bottom geometry was found to be 10 mw/cm^2. We plot these experimental results in Figure 4.4 for times from 50 s to 150 s, thus depicting the rapid change in the moduli and approach toward steady state after the shutter for the UV lamp was opened at 60 s. A complete map of the phase angle as a function of time during gelation can be found in Appendix C, Figure C.5. The sudden jump and discontinuity in the 3.16 rad/s curve is attributed to noise in the calculated G' and G" due to the low torque observed during these measurements.

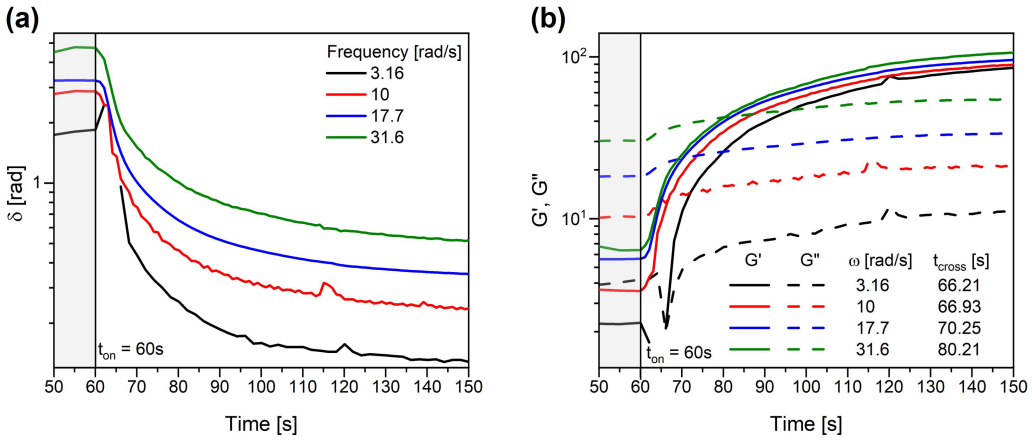

Figure 4.4: (a) The calculated phase angle and (b) the corresponding storage and loss moduli as a function of time during gelatiom tests carried out at different frequencies. The shutter for the UV lamp was opened at 60 s, as denoted by t_{on}. The gray box marks the time prior to exposing the sample.

The phase angles shown in Figure 4.4.a do not intersect with one another, thus making it difficult to determine the exact point in time where a percolated network forms as described by the Winter-Chambon criteria. This lack of an intersection could potentially be due to several factors, one of which being that the material is too quickly to accurately determine the moduli based on the mutation number. For the the test taken at 3.16 rad/s, lowest frequency presented in figure 4.4, the maximum mutation number was found to be 1.3 shortly after the shutter for the UV lamp was opened, thus indicating that the moduli was changing by 130% within half an oscillation. The mutation number for 10 rad/s was found to be 0.22 while the mutation number for the 17.7 and 31.6 rad/s were well below 0.1. As such, lower frequency tests were not able to be reliably carried out due to the rapid change in the material's properties.

There is also the possibility that the several assumptions made to get the Winter-Chambon criterion do not hold for the bottlebrush system studied in this work. Specifically, the Winter-Chambon criterion assumes that the crosslinking reaction occurs at the end of a polymer chain and propagates uniformly through sample, resulting in mechanical self-similarity [13], [31], [36], [37]. Due to each side chain within the bottlebrush being functionalized with the -allyl group it is quite possible that a bottlebrush could be bonded to another bottlebrush at multiple points along its length, thus resulting in a structure that does not exhibit self-similarity. From an experimental setup perspective, the MCR 702's UV curing setup introduces complications in the form of intensity variation and uneven exposure of the sample. In the UV curing setup, the sample is only

exposed to the UV light from the bottom surface. This arrangement can potentially result in the bottom portion of the sample reacting faster than the top portion. Similarly, the fiber optic light guide acts as a light point source instead of a uniform beam of UV radiation, leading to a significant drop in UV intensity when moving away from the center of the geometry. Measurements using the UV power meter, indicated that the intensity could drop between 40 to 60% between the center and the edge of the 25 mm geometry. Such variation has the potential can lead to non-uniform gelation rates across the 25 mm sample. Both of these effects can give rise to phase separation effects similar to those observed Chiou et al., [15] and in turn, result in a lack of self-similar structures throughout the gel.

Despite the inability to apply the Winter-Chambon criterion, an additional set of gelation studies were carried out to estimate the rate at which the polymer undergoes a sol-gel transition. Given that it was not possible to determine the exact gelation point, rough time scales for the sol-gel transition can be determined based on the G', G" crossover point. This approximation of the gelation time has been widely used in literature for systems where the Winter-Chambon criteria does not apply or cannot be applied due to experimental limitations [13], [20], [38]–[42]. We also consider the G', G" crossover point taken in the limit of zero frequency which was shown by Kim et al., to remove the frequency dependence fom the estimate [20]. Before considering the data and the G', G" crossover, it is important to note, that the crossover point and the gelation point are not the same. The crossover point only coincides with the gelation point when the sample is a linear chain and has perfect stoichiometry [12], [32], [40]. The bottlebrush polymer system addressed in this work does not meet either of these criteria.

Tests were carried out at five frequencies from 5.62 to 56.2 rad/s at four different intensities, 6.5, 28, 105, and 288 mW/cm^2. The results of these experiments are shown in figure 4.5 with the corresponding phase angle plots in Appendix C Figure C.5. The plots are shown from 50 to 100 s to highlight the crossover points and the dynamics of the bottlebrush polymers immediately after the lamp was turned on. Plots depicting the full 1800 s exposure can be found in Appendix C Figure C.6. From the data shown in Figure 4.5, we see that increasing the intensity results in the crossover points decreasing from 5 to 10 s down to 1 to 4 s. The relatively fast crossover times are beneficial to applications in 3D and solution printing where the microstructure of the bottlebrush polymer needs to be locked in prior to the material completely relaxing. However, from a rheological characterization perspective, these rapid gelation times prove a problem due to resulting high mutation number. Specifically for the 5.62 rad/s test carried out at 288 mW/cm^2, the mutation number reached a maximum value of 0.3. The maximum mutation number for all other testing conditions were near or below 0.2.

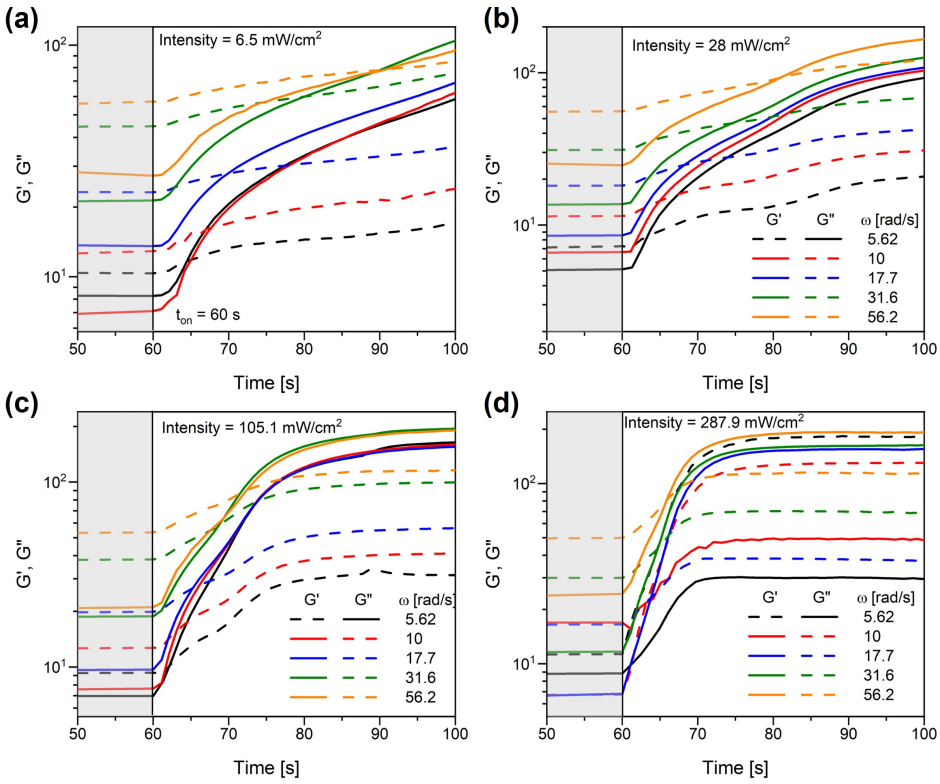

Figure 4.5: The calculated moduli for gelation studies carried out a frequencies from 5.62 rad/s to 56.2 rad/s while being exposed to an UV intensity of (a) 6.5 mW/cm^2, (b) 28 mW/cm^2, (c) 105.1 mW/cm^2, and (d) 287.9 mW/cm^2. The UV lamp shutter was opened at 60 s as denoted by t_{on}.

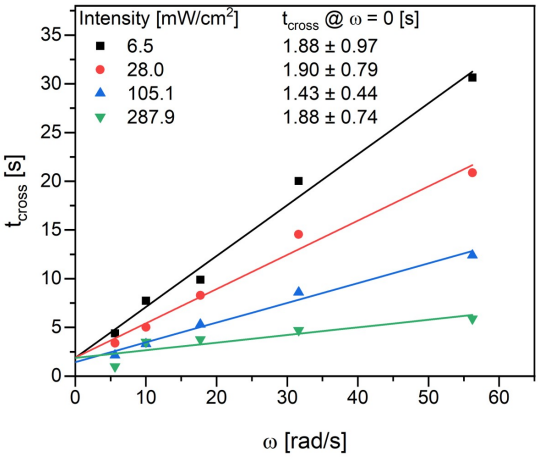

Figure 4.6: The observed G', G" crossover point plotted as a function of frequency applied during the gelation test. Linear fits were applied to each measured intensity and are shown as solid lines. These fits were extrapolated to zero frequency, with the points at zero frequency listed next to the legend.

To very roughly approximate the gelation time at low frequency and thus when considering larger structures, the crossover points were extrapolated down to zero frequency using a linear fit results shown as solid lines in Figure 4.6. Note, that the extrapolation to low frequencies serves to capture longer length scales, thus serving as a very rough approximation of the formation of large structures within the polymer solution. Interestingly enough, the resulting calculated G' and G" crossover all intersected at approximately the same time of 1.9 s with relatively large errors. These results are counter-intuitive as we would expect the crosslinking reaction rate to scale with UV intensity. This unexpected result is possibly due to the relatively high mutation numbers observed during the 5.62 rad/s measurements as the inability to accurately capture the rapidly changing material properties could have skewed the linear fits towards an average value. Despite this issue, the short calculated crossover times suggests that the material is very sensitive to UV radiation and will rapidly crosslink when exposed to UV light. For applications in 3D and solution printing, this property is particularly appealing as it provides a mechanism by which any shear induced microstructure can be locked in after the bottlebrush solution is deposited onto a substrate.

4.4.4 Use of SPP Analysis to Capture Rapid Gelation

In an effort reduce the high mutation numbers observed when characterizing the gelation time and as such accurately characterize the rapid crosslinking kinetics discussed in Section 4.4.3, we turn to SPP analysis to calculate the time resolved moduli based on the strain, strain rate, and stress. For this study, we apply a sinusoidal strain to the sample and record the bottlebrush polymers stress response as it undergoes gelation. The resulting stress responses are shown in Figure 4.7 where we observe an increase in both stress amplitude and stress offset. We attribute the stress amplitude increase to the formation of bonds between bottlebrush polymers, thus forming a network and stiffening the material. The appearance of a stress offset is due to the bottlebrushes crosslinking while in a deformed state, thus resulting in non-equilibrium configurations getting locked in as the reaction progresses. The formation of these structures leads to an accumulation of stress within the newly formed gel, thus exhibiting a stress offset that increases with time.

Both the stress offset and increasing stress amplitude make it difficult to perform SPP analysis on the captured data as the signal is no-longer periodic and as such, cannot be represented as a closed periodic loop as depicted in Equation 4.5. As such, it is necessary to carry out this analysis via differential calculation methods as described by Rogers et al., in [26]. In order for these methods be accurately applied, the data are smoothed to eliminate any noise due to the MCR 702, a stress controlled rheometer, operating under strain control. We achieve this by passing the applied strain, calculated strain rate based on the applied strain, and measured stress through a low pass filter that removes all signals with a frequencies above the frequency applied during the test. The resulting smoothed curves are show in Figure 4.7 as red lines. The strain and strain rate curves were further smoothed by fitting a simple sine function to the data. The raw data compared to these fits can be found in Appendix C Figure C.7. Note that a simple sine function could not be fit to the smoothed stress due to the increasing stress amplitude and stress offset with time. Further signal processing was not performed on the data to avoid distorting the data and reducing the amplitude of the measured stress at higher frequencies.

After the data were smoothed, differential SPP was carried out on the strain, strain rate, and stress. The analysis was carried out over 5 point boxcar in an effort to further limit the impact of noise on the calculated $G'_t(t)$ and $G''_t(t)$. Though the resulting transient moduli, shown in Figure 4.8, are still quite noisy, the higher frequencies demonstrate a clear increase in the transient G' and G" as the sample undergoes gelation. Sudden jumps in the transient moduli are observed at regular intervals in all of the data presented in

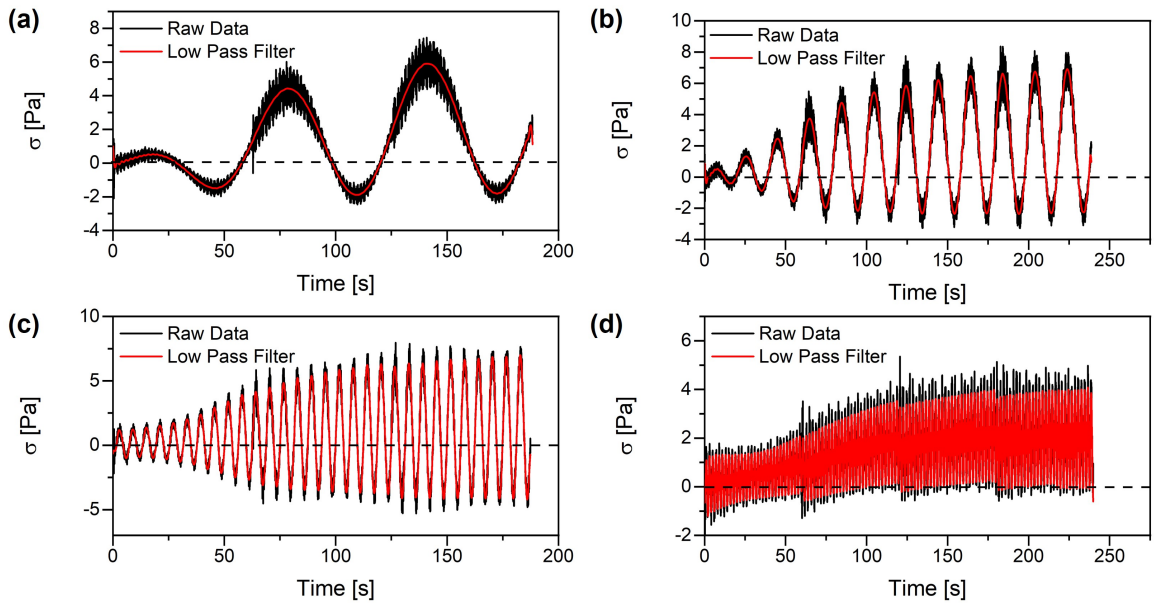

Figure 4.7: The raw (black) and processed (red) stress response to oscillatory strain at frequencies of (a) 0.1, (b) 0.316, (c) 1, and (d) 3.16 rad/s. Zero stress is highlighted with a dotted line to aid in identifying the increasing stress offset with time. The intensity of the UV lamp was 10 mW/cm^2. A strain amplitude of 3.16% was applied during testing.

Figure 4.8 with the exception of the data collected at 0.1 rad/s. The timing of these discontinuities coincides with the individual measurement step that were setup in Rheocompass to control the MCR 702, leading us to believe that they are artifacts resulting from the instrument loading the next measurement step. We are currently working with Anton-Paar to identify improvements that can be made to the MCR 702 and Rheocompass software to avoid artifacts such as these when measuring transient data. We are also working with Anton-Paar to implement premade measuring steps that should make it easier to access the recorded stress and strain waveforms.

Upon taking a closer look at the calculated loss moduli for the transient gelation studies carried out at 1 and 3.16 rad/s, Figure 4.8.c and d, we observe that the transient loss moduli is negative for the entirety of the test. Taken at face value, this result suggests that the material is generating energy through flow processes, a phenomenon which has been interpreted as non-physical when observed in oscillation averaged measurements and has been attributed to experimental error [43], [44]. In the context of SPP analysis, negative moduli have been observed when the signal to noise ratio is low. We are also looking into other factors that could have resulted in this unexpected result such as the stress offset and the complications it leads to when calculating the transient moduli as well as the impact of the gelation reaction on the total energy within the bottlebrush system. As such, additional studies are needed to identify the potential cause of this negative moduli and determine if this result is an accurate representation of the physical properties of the bottlebrush during gelation.

Despite the challenges presented by the data discussed in this section, the use of SPP analysis during sample gelation studies presents a unique opportunity to augment and improve upon the Winter-Chambon criterion for identifying the gel point. The SPP analysis method allows for the mutation number of a gelation study to be based on the *dt* used to carry out the measurement instead of the frequency and the corresponding

time it takes the rheometer to complete a an oscillation. This essentially eliminates one of the key challenges with applying the Winter-Chambon criterion where only a certain window of frequencies could be accurately studied based on the reaction time of the material. In order to properly apply the SPP method and identify the gelation point using transient phase angles, work needs to be carried out to address some of the technical challenges that have been discussed in this section. Namely the reduction of noise in the measured stress or strain will be explored in more detail. Unfortunately differential analysis of the data is required as the properties of the material irreversibly change as it undergoes gelation. Further noise reduction that does not warp the signal should allow us to reduce the large spikes observed in the calculated moduli at lower frequencies and thus extend the frequency range over which the SPP analysis can be applied. Additionally, we plan to look into how the stress offset develops during the gelation process and the impact it has on both the oscillation averaged moduli as well as the transient moduli. Such an understanding should allow us to better understand the significance of accumulated stress and the impact it can have on the observed gelation time. Finally, interpretation of the calculated transient moduli is currently ongoing. Experiments are planned to verify the negative transient loss moduli presented in Figure 4.8 and the possible factors that could be contributing to this unexpected result.

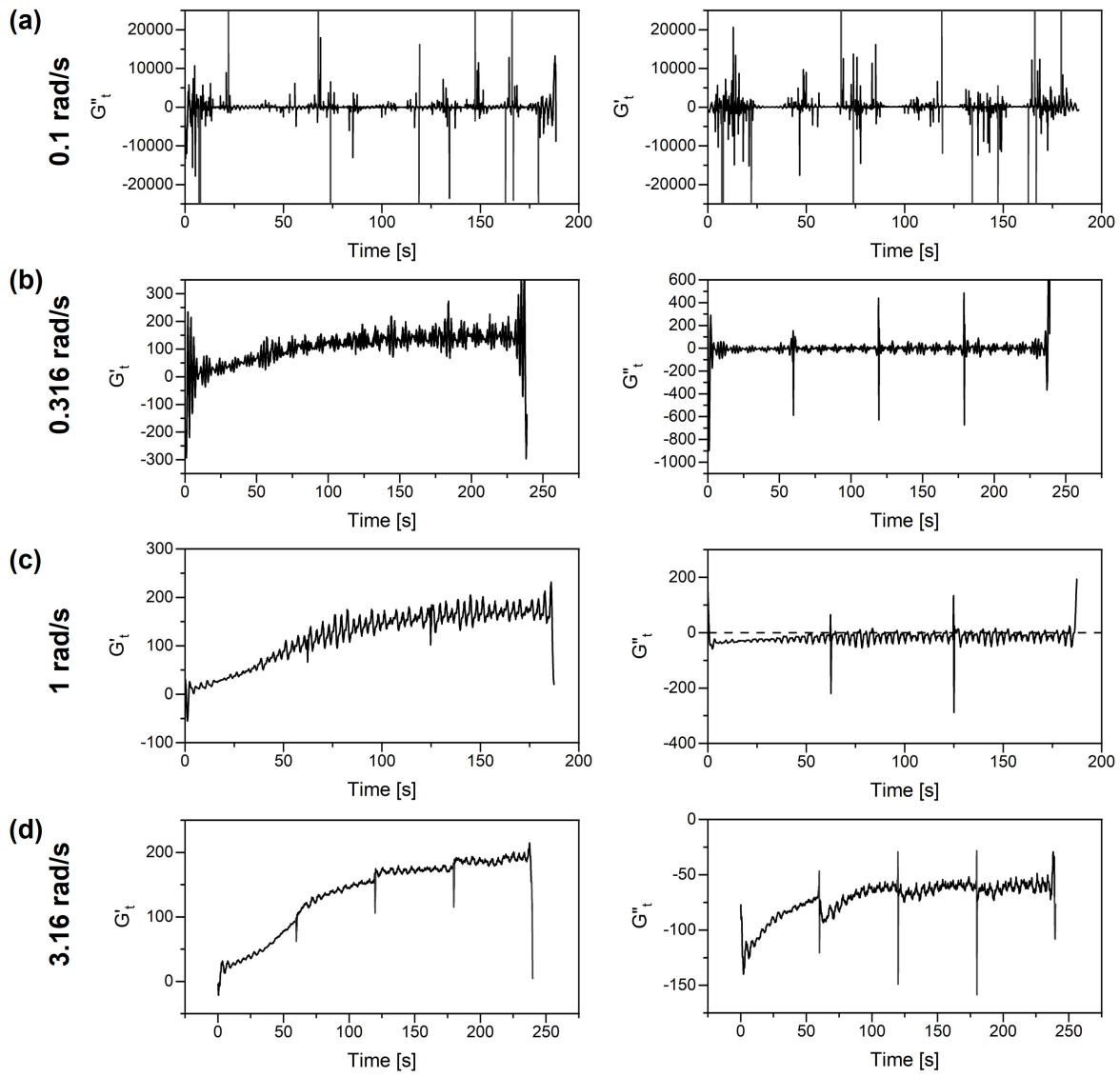

Figure 4.8: The transient storage moduli (left column) and loss moduli (right column) calculated with the SPP framework for diblock bottlebrush solutions undergoing gelation. An oscillatory strain with an amplitude of 3.16% and a frequency of (a) 0.1, (b) 0.316, (c) 1, and (d) 3.16 rad/s were applied to the samples during gelation. The intensity of the UV lamp was set to 10 mw/cm^2.

4.5 Outlook and Remaining Challenges

In this work, we investigate the use of a UV activated crosslinking mechanism to lock in shear induced microstructures in a diblock bottlebrush solution. We demonstrate clear proof of concept by curing the bottlebrush sample under steady stress conditions. After removing the samples from the rheometer and allowing them to sit at zero stress while images were taken, we show that we are able to retain a range of microstructures that in turn give rise to distinct colors as we increase the applied stress from 0 to 63 Pa. After establishing proof of concept, we worked towards characterizing the critical gel point and the reaction rate of these bottlebrush polymers by applying oscillatory shear at different frequencies while the sample was exposed to UV light. Though we were unable to apply the Winter-Chambon criterion and identify an intersection between the phase angles, we were able to provide a rough estimate of the gelation time based on the G', G" crossover point. We predict that the Winter-Chambon criterion was not applicable due to the bottlebrush architecture and uneven exposure to UV radiation leading to non-uniform gelation and thus a breakdown of the self-similar assumption. Despite these challenges, the estimates for the gelation time indicate that at the intensities tested, the bottlebrush polymer solution was undergoing sol-gel transition within a few seconds of being exposed to UV radiation. This timeframe is on the same scale the relaxation time, thus indicating that we can chemically crosslink these materials and thus lock the microstructure faster than the material can relax after undergoing deformation or a printing process.

The rapid gelation kinetics observed in this chapter presented a challenge in the form of a high mutation number for several of the gelation studies. For frequencies lower than 10 rad/s the linear moduli were often changing too fast than could be accurately captured by oscillation averaged rheological methods. In an effort to get around this limitation and explore a broader range of frequencies, we implement the SPP analysis framework to calculate the transient moduli based on the measured strain, strain rate, and stress waveforms. This approach allowed us to reduce the mutation number until it was effectively negligible by changing the timescale of time measurement from the time it takes to complete at least one half an oscillation to the time it takes the rheometer to measure a single point. As such, we could probe frequencies down to 0.1 rad/s without running into issues of the oscillation averaged moduli changing too quickly. Actually implementing this analysis framework required some work to be done to properly smooth out the applied strain and strain rate and the measured stress response. Specifically low pass filters were applied to account for the MCR 702 strain controller. Despite these efforts, the resulting time resolved moduli were still quite noisy, with the data taken at 0.1 being too noisy to observe any trends. Higher frequencies demonstrate clear trends in $G_t^{'}$ with time. Frequencies of 1 and 3.16 also demonstrate clear trends in $G_t^{"}$ with both the transient storage and loss modulus increasing as the sample crosslinked to form a gel. The transient loss moduli was also observed to be below zero or the extent of the test. The exact interpretation is still being explored, though it could possibly be attributed to the observed stress offset complicating the SPP calculations.

Overall the SPP framework provides a unique opportunity to eliminate the mutation number as a factor when considering testing conditions or a gelation study. This change in mentality allows us to assess a broader range of testing conditions in order to provide the best representation of the rheology of a material. Challenges still need to be overcome with this approach, with a focus being placed on how to best process the stress, strain, and strain rate data in order to boost signal to noise and ensure lower frequencies can be properly tested. Interpretation of the negative transient moduli also poses a unique challenge as such results that suggest the material is producing energy during flow are typically considered non-physical. Despite these challenges, the SPP framework allows us to approach the characterization of a critical gel time without many of the common challenges that limit the experiments that can be carried out. Removing these limitations

will allow or better characterization of the gelation dynamics both in terms of testable frequency range and accuracy of the reported gelatin time.

4.6 References

[1] J. W. Rumer and I. McCulloch, "Organic photovoltaics: Crosslinking for optimal morphology and stability," *Materials Today*, vol. 18, no. 8, pp. 425–435, Oct. 2015, ISSN: 18734103. DOI: 10.1016/J.MATTOD.2015.04.001.

[2] S. Panja, A. M. Fuentes-Caparrós, E. R. Cross, L. Cavalcanti, and D. J. Adams, "Annealing Supramolecular Gels by a Reaction Relay," *Chemistry of Materials*, vol. 32, no. 12, pp. 5264–5271, Jun. 2020, ISSN: 15205002. DOI: 10.1021/ACS.CHEMMATER.0C01483/ASSET/IMAGES/LARGE/CM0C01483{_}0006.JPEG. [Online]. Available: https://pubs.acs.org/doi/full/10.1021/acs.chemmater.0c01483.

[3] K. Liu, A. Levy, C. Liu, and J. H. Olivier, "Tuning Structure-Function Properties of π-Conjugated Superstructures by Redox-Assisted Self-Assembly," *Chemistry of Materials*, vol. 30, no. 6, pp. 2143–2150, Mar. 2018, ISSN: 15205002. DOI: 10.1021/ACS.CHEMMATER.8B00518/ASSET/IMAGES/MEDIUM/CM-2018-00518N{_}M001.GIF. [Online]. Available: https://pubs.acs.org/doi/full/10.1021/acs.chemmater.8b00518.

[4] H. Wang, A. Paul, D. Nguyen, A. Enejder, and S. C. Heilshorn, "Tunable Control of Hydrogel Microstructure by Kinetic Competition between Self-Assembly and Crosslinking of Elastin-like Proteins," 2018. DOI: 10.1021/acsami.8b02461. [Online]. Available: www.acsami.org.

[5] S. Braun, S. Rappoport, R. Zusman, D. Avnir, and M. Ottolenghi, "Biochemically active sol-gel glasses: the trapping of enzymes," *Materials Letters*, vol. 10, no. 1-2, pp. 1–5, Sep. 1990, ISSN: 0167-577X. DOI: 10.1016/0167-577X(90)90002-4.

[6] N. Lorén and A. M. Hermansson, "Phase separation and gel formation in kinetically trapped gelatin/maltodextrin gels," *International Journal of Biological Macromolecules*, vol. 27, no. 4, pp. 249–262, Jul. 2000, ISSN: 01418130. DOI: 10.1016/S0141-8130(00)00127-6.

[7] S. Nian, H. Lian, Z. Gong, M. Zhernenkov, J. Qin, and L. H. Cai, "Molecular Architecture Directs Linear-Bottlebrush-Linear Triblock Copolymers to Self-Assemble to Soft Reprocessable Elastomers," *ACS Macro Letters*, vol. 8, no. 11, pp. 1528–1534, 2019, ISSN: 21611653. DOI: 10.1021/acsmacrolett.9b00721. [Online]. Available: https://pubs.acs.org/sharingguidelines.

[8] T. Pakula, Y. Zhang, K. Matyjaszewski, *et al.*, "Molecular brushes as super-soft elastomers," *Polymer*, vol. 47, no. 20, pp. 7198–7206, Sep. 2006, ISSN: 00323861. DOI: 10.1016/j.polymer.2006.05.064.

[9] W. F. Daniel, J. Burdyńska, M. Vatankhah-Varnoosfaderani, *et al.*, "Solvent-free, supersoft and superelastic bottlebrush melts and networks," *Nature Materials*, vol. 15, no. 2, pp. 183–189, 2016, ISSN: 14764660. DOI: 10.1038/nmat4508. [Online]. Available: http://www.nature.com/doifinder/10.1038/nmat4508%20www.nature.com/naturematerials.

[10] B. B. Patel, D. J. Walsh, D. H. Kim, *et al.*, "Tunable structural color of bottlebrush block copolymers through direct-write 3D printing from solution," *Science Advances*, vol. 6, no. 24, In Press, Jun. 2020, ISSN: 2375-2548. DOI: 10.1126/sciadv.aaz7202. [Online]. Available: http://advances.sciencemag.org/%20https://www.science.org/doi/10.1126/sciadv.aaz7202.

[11] H. H. Winter and F. Chambon, "Analysis of Linear Viscoelasticity of a Crosslinking Polymer at the Gel Point," *Journal of Rheology*, vol. 30, no. 2, pp. 367–382, Apr. 1986, ISSN: 0148-6055. DOI: 10.1122/1.549853. [Online]. Available: http://sor.scitation.org/doi/10.1122/1.549853.

[12] F. Chambon and H. H. Winter, "Linear Viscoelasticity at the Gel Point of a Crosslinking PDMS with Imbalanced Stoichiometry," *Journal of Rheology*, vol. 31, no. 8, pp. 683–697, 1987, ISSN: 0148-6055. DOI: 10.1122/1.549955.

[13] B.-S. Chiou, S. R. Raghavan, and S. A. Khan, "Effect of Colloidal Fillers on the Cross-Linking of a UV-Curable Polymer: Gel Point Rheology and the WinterChambon Criterion," *Macromolecules*, vol. 34, no. 13, pp. 4526–4533, Jun. 2001, ISSN: 0024-9297. DOI: 10.1021/ma010281a. [Online]. Available: https://pubs.acs.org/doi/10.1021/ma010281a%20https://pubs.acs.org/sharingguidelines.

[14] M. E. De Rosa and H. H. Winter, "The effect of entanglements on the rheological behavior of polybutadiene critical gels," Tech. Rep., 1994, pp. 220–237.

[15] B.-S. Chiou, R. J. English, and S. A. Khan, "Rheology and Photo-Cross-Linking of ThiolEne Polymers," *Macromolecules*, vol. 29, no. 16, pp. 5368–5374, Jan. 1996, ISSN: 0024-9297. DOI: 10.1021/ma960383e. [Online]. Available: https://pubs.acs.org/sharingguidelines%20https://pubs.acs.org/doi/10.1021/ma960383e.

[16] C. A. Bonino, J. E. Samorezov, O. Jeon, E. Alsberg, and S. A. Khan, "Real-time in situ rheology of alginate hydrogel photocrosslinking," *Soft Matter*, vol. 7, no. 24, p. 11 510, Dec. 2011, ISSN: 1744-683X. DOI: 10.1039/c1sm06109g. [Online]. Available: www.rsc.org/softmatter%20http://xlink.rsc.org/?DOI=c1sm06109g.

[17] S. A. Khan, "Effect of shear on the gelation of UV-curable polymers," *Journal of Rheology*, vol. 36, no. 4, pp. 573–587, May 1992, ISSN: 0148-6055. DOI: 10.1122/1.550364. [Online]. Available: http://sor.scitation.org/doi/10.1122/1.550364.

[18] S. M. Hashemnejad and S. Kundu, "Probing Gelation and Rheological Behavior of a Self-Assembled Molecular Gel," *Langmuir*, vol. 33, no. 31, pp. 7769–7779, Aug. 2017, ISSN: 15205827. DOI: 10.1021/acs.langmuir.7b01531. [Online]. Available: https://pubs.acs.org/doi/10.1021/acs.langmuir.7b01531.

[19] D. Dörr, U. Kuhn, and V. Altstädt, "Rheological study of gelation and crosslinking in chemical modified polyamide 12 using a multiwave technique," *Polymers*, vol. 12, no. 4, 2020, ISSN: 20734360. DOI: 10.3390/POLYM12040855. [Online]. Available: www.mdpi.com/journal/polymers.

[20] S.-Y. Kim, D.-G. Choi, and S.-M. Yang, "Rheological analysis of the gelation behavior of tetraethylorthosilane/ vinyltriethoxysilane hybrid solutions," *Korean Journal of Chemical Engineering*, vol. 19, no. 1, pp. 190–196, Jan. 2002, ISSN: 0256-1115. DOI: 10.1007/BF02706894. [Online]. Available: http://link.springer.com/10.1007/BF02706894.

[21] X. Hu, J. Fan, and C. Y. Yue, "Rheological study of crosslinking and gelation in bismaleimide/cyanate ester interpenetrating polymer network," *Journal of Applied Polymer Science*, vol. 80, no. 13, pp. 2437–2445, 2001, ISSN: 00218995. DOI: 10.1002/app.1350.

[22] S. R. Raghavan, L. A. Chen, C. McDowell, S. A. Khan, R. Hwang, and S. White, "Rheological study of crosslinking and gelation in chlorobutyl elastomer systems," *Polymer*, vol. 37, no. 26, pp. 5869–5875, 1996, ISSN: 00323861. DOI: 10.1016/S0032-3861(96)00446-6.

[23] M. Mours and H. H. Winter, "Time-resolved rheometry," *Rheologica Acta*, vol. 33, no. 5, pp. 385–397, Sep. 1994, ISSN: 00354511. DOI: 10.1007/BF00366581. [Online]. Available: https://link.springer.com/article/10.1007/BF00366581.

[24] S. A. Rogers, B. M. Erwin, D. Vlassopoulos, and M. Cloitre, "A sequence of physical processes determined and quantified in LAOS: Application to a yield stress fluid," *Journal of Rheology*, vol. 55, no. 2, pp. 435–458, Mar. 2011, ISSN: 0148-6055. DOI: 10.1122/1.3544591. [Online]. Available: https://doi.org/10.1122/1.3544591%20http://sor.scitation.org/doi/10.1122/1.3544591.

[25] S. A. Rogers, "A sequence of physical processes determined and quantified in LAOS: An instantaneous local 2D/3D approach," *Journal of Rheology*, vol. 56, no. 5, pp. 1129–1151, Sep. 2012, ISSN: 0148-6055. DOI: 10.1122/1.4726083. [Online]. Available: https://doi.org/10.1122/1.4726083%20http://sor.scitation.org/doi/10.1122/1.4726083.

[26] ——, "In search of physical meaning: defining transient parameters for nonlinear viscoelasticity," *Rheologica Acta*, vol. 56, no. 5, pp. 501–525, May 2017, ISSN: 00354511. DOI: 10.1007/s00397-017-1008-1. [Online]. Available: https://link.springer.com/article/10.1007/s00397-017-1008-1%20http://link.springer.com/10.1007/s00397-017-1008-1.

[27] J.-A. Serret, "Sur quelques formules relatives à la théorie des courbes à double courbure.," *Journal de Mathématiques Pures et Appliquées*, pp. 193–207, 1851, ISSN: 0021-7874.

[28] F. Frenet, "Sur les courbes à double courbure.," *Journal de Mathématiques Pures et Appliquées*, pp. 437–447, 1852, ISSN: 0021-7874.

[29] G. J. Donley, W. W. Hyde, S. A. Rogers, and F. Nettesheim, "Yielding and recovery of conductive pastes for screen printing," *Rheologica Acta*, vol. 58, no. 6-7, pp. 361–382, Jul. 2019, ISSN: 00354511. DOI: 10.1007/s00397-019-01148-w. [Online]. Available: https://doi.org/10.1007/s00397-019-01148-w.

[30] J. D. Park and S. A. Rogers, "The transient behavior of soft glassy materials far from equilibrium," *Journal of Rheology*, vol. 62, no. 4, p. 869, May 2018, ISSN: 0148-6055. DOI: 10.1122/1.5024701. [Online]. Available: https://sor.scitation.org/doi/abs/10.1122/1.5024701.

[31] H. H. Winter, "Evolution of rheology during chemical gelation," in *Permanent and Transient Networks*, Darmstadt: Steinkopff, Sep. 1987, pp. 104–110. DOI: 10.1007/BFb0109413. [Online]. Available: https://link.springer.com/chapter/10.1007/BFb0109413%20http://link.springer.com/10.1007/BFb0109413.

[32] H. H. Winter, P. Morganelli, and F. Chambon, "Stoichiometry effects on rheology of model polyurethanes at the gel point," *Macromolecules*, vol. 21, no. 2, pp. 532–535, 1988. DOI: 10.1021/MA00180A048. [Online]. Available: https://pubs.acs.org/doi/abs/10.1021/ma00180a048.

[33] S. Tagliaferri, A. Panagiotopoulos, and C. Mattevi, *Direct ink writing of energy materials*, 2021. DOI: 10.1039/d0ma00753f.

[34] M. Champeau, D. A. Heinze, T. N. Viana, E. R. de Souza, A. C. Chinellato, and S. Titotto, "4D Printing of Hydrogels: A Review," *Advanced Functional Materials*, vol. 30, no. 31, 2020, ISSN: 16163028. DOI: 10.1002/adfm.201910606. [Online]. Available: https://doi.org/10.1002/adfm.201910606..

[35] C. S. O'Bryan, T. Bhattacharjee, S. Hart, *et al.*, "Self-assembled micro-organogels for 3D printing silicone structures," *Science Advances*, vol. 3, no. 5, May 2017, ISSN: 23752548. DOI: 10.1126/sciadv.1602800. [Online]. Available: https://www.science.org/doi/10.1126/sciadv.1602800.

[36] J. C. Scanlan and H. H. Winter, "Composition Dependence of the Viscoelasticity of End-Linked Poly(dimethylsiloxane) at the Gel Point," *Macromolecules*, vol. 24, no. 1, pp. 47–54, 1991, ISSN: 15205835. DOI: 10.1021/ma00001a008. [Online]. Available: https://pubs.acs.org/sharingguidelines.

[37] M. Muthukumar and H. H. Winter, "Fractal Dimension of a Cross-Linking Polymer at the Gel Point," *Macromolecules*, vol. 19, no. 4, pp. 1284–1285, 1986, ISSN: 15205835. DOI: 10.1021/ma00158a064. [Online]. Available: https://pubs.acs.org/sharingguidelines.

[38] R. Sun Han Chang, J. C. W. Lee, S. Pedron, B. A. Harley, and S. A. Rogers, "Rheological Analysis of the Gelation Kinetics of an Enzyme Cross-linked PEG Hydrogel," *Biomacromolecules*, vol. 20, no. 6, pp. 2198–2206, 2019, ISSN: 15264602. DOI: 10.1021/acs.biomac.9b00116.

[39] R. D. Corder, S. C. Dudick, J. E. Bara, and S. A. Khan, "Photorheology and Gelation during Polymerization of Coordinated Ionic Liquids," *ACS Applied Polymer Materials*, vol. 2, no. 6, pp. 2397–2405, Jun. 2020, ISSN: 2637-6105. DOI: 10.1021/acsapm.0c00343. [Online]. Available: https://dx.doi.org/10.1021/acsapm.0c00343%20https://pubs.acs.org/doi/10.1021/acsapm.0c00343.

[40] H. H. Winter, "Can the gel point of a cross-linking polymer be detected by the G – G crossover?" *Polymer Engineering & Science*, vol. 27, no. 22, pp. 1698–1702, 1987, ISSN: 15482634. DOI: 10.1002/pen.760272209.

[41] K. Ghosh, X. Z. Shu, R. Mou, *et al.*, "Rheological Characterization of in Situ Cross-Linkable Hyaluronan Hydrogels," 2005. DOI: 10.1021/bm050361c. [Online]. Available: https://pubs.acs.org/sharingguidelines.

[42] J. C. Tilly, A. K. Pervaje, D. L. Inglefield, E. E. Santiso, R. J. Spontak, and S. A. Khan, "Spectroscopic and Rheological Cross-Analysis of Polyester Polyol Cure Behavior: Role of Polyester Secondary Hydroxyl Content," *ACS Omega*, vol. 4, no. 1, pp. 932–939, Jan. 2019, ISSN: 24701343. DOI: 10.1021/acsomega.8b02766. [Online]. Available: https://pubs.acs.org/sharingguidelines.

[43] B. A. Noskov, *Dilational surface rheology of polymer and polymer/surfactant solutions*, Aug. 2010. DOI: 10.1016/j.cocis.2010.01.006.

[44] R. Miller, J. K. Ferri, A. Javadi, J. Krägel, N. Mucic, and R. Wüstneck, *Rheology of interfacial layers*, 2010. DOI: 10.1007/s00396-010-2227-5.

Chapter 5

Locking in Microstructure via Physical Means

5.1 Chapter Overview

In this chapter, we explore the second of the two proposed mechanisms to increase the relaxation time of the bottlebrush solution. We achieve this effect by increasing the concentration of the polymer in solution. When testing the material at a concentration of 350 mg/ml, we observe features in the flow curve and amplitude sweep typically attributed to yield-like behavior. Specifically, the flow curve appears to asymptotically approach a constant stress at low shear rate and can be fit by the Herschel Bulkey model. The amplitude sweep exhibits a G" overshoot, a feature typically found in yield-stress fluids, as well as a G', G" crossover at high amplitudes which indicates a solid to liquid transition. Having identified yield-like behavior, proof of concept studies were carried out by applying steady shear pulses to the concentrated bottlebrush polymer followed by a zero rate or zero stress step. During these tests, the color of the sample was recorded using the rheo-microscope configuration. The resulting color relaxation times indicate that the material is not retaining its shear history and is rapidly reverting back to its quiescent state. This relaxation occurs on the order of a few seconds. We probe the yield-like behavior exhibited by the bottlebrush polymer using recovery rheology. By decomposing the strain into recoverable and unrecoverable components, we observe that the yielding process is not instantaneous, and thus will not effectively result in the retention of a shear-induced microstructure. Investigations into the processes that lead to yielding are also carried out by applying the Transient Deborah number,De_t and identifying the points within an oscillation where the material transitions between predominately elastic deformation and predominately plastic deformation. Structural studies were prepared to characterize the structural changes that occur during these plastic to elastic transitions and establish a structure-property relation between the microstructure and yielding behavior. This study has been delayed due to unforeseen circumstances limiting access to the NCNR neutron beamline. Iterative recovery rheology was carried out during shear startup to further study how the material behaves when undergoing yielding processes. The recoverable strain was found to increase linearly with time followed by a slight decrease and a plateau at longer times. These results suggest the bottlebrush is collapsing after initially stretching during steady shear. This collapse predominantly occurs at long times during high shear rate studies and appears to be negligible at lower shear rates. Additional studies are planned to further explore this phenomena and capture the long time behavior of the bottlebrush polymers in solution. Through these

studies, we begin the to understand how the structure of these materials develops during shear startup, not only providing insight into the behavior of the polymer at short times, but the longer term developments in the self-assembled microstructure.

5.2 Introduction

Having demonstrated that it is possible to effectively freeze the shear induced microstructure in a bottlebrush polymer solution in Chapter 4, we now turn towards a physical approach to increase the polymer solution's relaxation time and thus its memory of its shear history. In this chapter we explore the viability of increasing the concentration of the polymer in solution in an effort to increase the relaxation time and possibly obtain yield-like behavior. In the context of direct-ink-writing, controlling the relaxation time allows us to control how much of the shear induced microstructure is retained after the polymer solution is deposited onto a substrate. Yield-like behavior is particularly appealing as the liquid to solid transition should theoretically allow us to impose a microstructure during flow while the solution acts as a liquid, and then "lock-in" said structure by releasing the solution and allowing it to return to a solid state.

Increasing the concentration has been shown to increase the relaxation time of the polymer solution [1]–[4] and in certain cases result in a yield-stress fluid [5]. In the case of yield-stress fluids, Dinkgreve et al demonstrate how a jammed polymer system such as Carbopol 980 at low concentration exhibits viscoelastic properties. As concentration is increased, the resulting polymers being to interact with each other to a greater extend, forming a soft, jammed system that exhibits yield-like behavior [5]. Furthermore, these materials were found to exhibit yield-like behavior at concentrations below where jamming would be expected, instead forming attractive networks that span the sample and result in an observed yield stress [5]. Based on these results, we seek to achieve a yield-stress fluid with bottlebrush polymers, effectively increasing the material's relaxation time to infinity and allowing us to potentially lock in shear induced microstructures.

5.2.1 Yield-Stress Materials

Yielding has traditionally been characterized as a phenomenon where a material initially exhibits predominantly elastic behavior below a critical stress. Once this stress is exceeded, the material flows, undergoing plastic deformation and exhibiting fluid-like properties [6], [7]. This solid-to liquid transition has been extensively studied and identified in a wide range of materials, including foams, microgel suspensions, emulsions, polymer networks, colloidal gels, and magnetorheological fluids [8]–[20]. Through these studies, the yield stress has been characterized based on the stress bifurcation, minimum stress needed to achieve flow, initiation of non-linear behavior, G' and G" intersection, etc [6], [21]–[27].

Models developed for yield-stress fluids typically focus on spanning the liquid-to-solid transition by describing the elastic deformation as a rigid body that transitions to a fluid above a critical stress. These models capture this by defining a series of discrete piecewise functions that only describe the behavior immediately above or below the yield stress [6], [28]–[30]. In Saramito's model, the yield-stress fluid is represented as a Maxwell model with the viscous contributions locked using a binary component that only allows flow above a minimum stress [28]. Other works such as Herschel, Nordstrom et al., and Caggioni et al., explore the flow properties of yield stress fluids, describing the stress as a combination of the yield-stress and the stress due to the viscosity during flow [11], [16], [27], [31]–[33]. In general, these models treat yielding as a binary process where little to no plastic behavior is observed below the yield-stress. In the context

of bottlebrushes and printing processes, this allows us to design a material that can be frozen in place by releasing the stress and allowing it to return to a stress well below the measured yield stress.

It should also be noted that yield-stress behavior is often sought out when designing inks for direct-ink-writing processes. Though there exact requirements are still a point of discussion within the literature, most articles state that a 3-D printable ink must exhibit shear thinning behavior, be self-supporting once deposited on a substrate, and recover its elastic properties after being extruded [17], [34], [35]. These properties ensure that the ink can be easily extruded out of the print nozzle and can be used to build up layers of material, resulting in a three dimensional structure [34], [35]. Yield-stress materials have been shown to exhibit all of these characteristics, with the solid to liquid transition resulting in the material flowing when pressures above the yield stress are applied. Once the material has been deposited onto a substrate, the effective stress is zero, allowing the material to revert its solid-like state and thus retaining its shape and structure. Given that the bottlebrush polymer is being designed for applications in 3D printing, converting the material into a yield-stress fluid is particularly appealing as it ensures this material will be a suitable ink for direct-ink-writing processes.

5.2.2 Recovery Rheology

Recovery rheology explores the extent to which a material has been deformed elastically and plastically, defined as the recoverable and unrecoverable strain, respectively. This concept was explored back in 1958 by Reiner [36] and in 1978 by Weissenberg [37] in an effort to understand the energetic contributions to stress and strain and define a ground state for the material. In his 1958 work, Lodge, incorporated the idea of recovery mechanisms into his transient network theory of polymers in the form of constrained recovery [38]. By incorporating this component into his model, Lodge, was able to define relations between the recoverable strain and the first normal stress difference [38]. Laun et al., employed the concepts of recovery rheology into his elongational deformation studies to describe a materials strain dependant memory [39]. Recent studies carried out by the Rogers group have begun to explore the characterization and use of the recoverable strain to develop structure-property relations under oscillatory deformation, steady shear startup, creep, and step strain deformations [40]–[44]. These studies have identified the significance of recoverable components in explaining features observed during oscillatory shear such as the strain shift [41] and the G" overshoot exhibited by yield stress fluids [42].

These studies incorporate iterative recovery rheology techniques as described by Lee et al. [45], to understand how recoverable and unrecoverable strain is acquired during deformation [43], [46], [47]. These techniques involve applying a deformation to the material and then releasing the material with a zero stress step at a specific point along the deformation. By repeating this processes for select times throughout the deformation, a map of the recoverable and unrecoverable strains at each point in the deformation can be obtained. Recoverable and unrecoverable rates can then be calculated from these decomposed strains. A diagram depicting a single recovery test for steady shear startup and oscillatory shear can be seen in Figure 5.1. The recoverable component shown in Figure 5.1, γ_{rec}, is the difference between the total strain and the equilibrium strain after the stress has been set to zero. This strain is considered to have been acquired elastically [45]. Unrecoverable strain, γ_{unrec}, is the difference between the equilibrium strain during the zero stress step and the initial state of the material, which in this case corresponds to a strain of zero. This unrecoverable strain corresponds to plastic deformation and the rate at which it is acquired governs the viscous properties of the material [45]. To map out these values for a single shear startup test or oscillatory deformation, said deformation is first applied to the material followed by a zero stress step at time t. The

test is then repeated with the zero stress step started at $t + n*$ where n is the current iteration of the test.

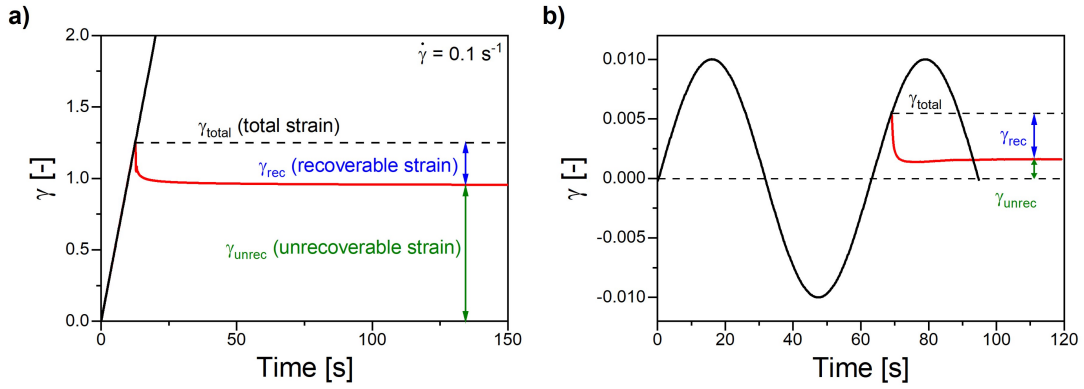

Figure 5.1: Diagrams depicting a single recovery rheology measurement or a) shear startup and b) oscillatory shear. These tests are repeated at regular intervals through the applied deformation to map out the recoverable and unrecoverable strain at each point.

Decomposing the strain into recoverable and unrecoverable components and then iteratively mapping them throughout a single deformation, allows for further insight into the fluid-like and solid-like contributions to individual rheological terms. In Donley et al., the storage and loss moduli are broken down into fluid and solid contributions based on the recoverable and unrecoverable strains. The resulting terms can be determined based on the following equations [42],

$$G'_{solid}(\omega) = \frac{2(\gamma_{rec}(t)\sigma(t))_{avg}}{\gamma_0^2}, \tag{5.1}$$

$$G'_{solid}(\omega) = \frac{2(\dot{\gamma}_{rec}(t)\sigma(t))_{avg}}{\omega\gamma_0^2}, \tag{5.2}$$

$$G'_{solid}(\omega) = \frac{2(\dot{\gamma}_{unrec}(t)\sigma(t))_{avg}}{\omega\gamma_0^2}. \tag{5.3}$$

From these equations Donley et al., are able to show how the solid and fluid contributions of the loss moduli provide insight into the point at which a soft, jammed polymer system begins to undergo a liquid-to-solid transition [42]. From this decomposition Donley et al., are able to show how fluid like contributions come into play at low stresses and strain, thus highlighting how yielding processes do not necessarily occur at a single stress [42].

Recovery rheology also allows for investigations into how elastic or plastic a given material is behaving at any given point during deformation. In their recent paper, Piyush Singh et al., proposed a definition for the a transient Deborah number, $De(t)$ based on the decomposition of a material strain response into elastic and viscous contributions [47]. This definition builds upon the traditional description of the The Deborah number, De, which is represented as the relaxation time of a material divided by the time of observation, effectively describing how liquid or solid-like a material is appearing to behave for a given experiment [36]. Instead of relying on experimentally averaged timescales, the proposed definition of $De(t)$ utilizes instantaneous values to capture the extent to which a material is behaving like a liquid or a solid and is defined as,

$$De(t) = \frac{\dot{\gamma}_{rec}(t)}{\dot{\gamma}_{unrec}(t)}. \tag{5.4}$$

This dimensionless number represents the extent to recoverable (elastic) deformation is acquired as compared to the extent to which unrecoverable (plastic) deformation is acquired. In the case of purely elastic deformation, $\dot{\gamma}_{unrec} \to 0$ which gives $De(t) \to \infty$. Under purely plastic deformation, $\dot{\gamma}_{rec} \to 0$, resulting in $De(t) \to 0$.

5.2.3 Transient Neutron Scattering

To capture the orientation and self-assembled structure of the bottlebrush polymers in solution during transient processes such as yielding, we turn to transient neutron scattering measurements. Introduced by Lettinga et al., in 2008 and revisited by Lopez-Barron et al., in 2014, these measurements involve performing neutron scattering while applying a repeatable deformation to the material [48], [49]. By recording the time each neutron is detected during the measurement, the neutrons can be placed into discrete bins based select time scales and points associated with the applied deformation. Significant statistics can thus be obtained by performing the deformation multiple times and adding the newly collected neutrons to their respetive time bin until sufficient statistics are collected [48], [49]. From this study, a comprehensive picture of the structure during the applied deformation can be assembled and used to develop structure-property relations. Calabrese et al., build upon this method by changing the bin to a sliding bin that is moved along the timeline of the applied deformation [50]. Through this technique, a finer time resolution can be obtained when compared to the discrete binning technique. A diagram depicting this method can be found in Figure 5.2.

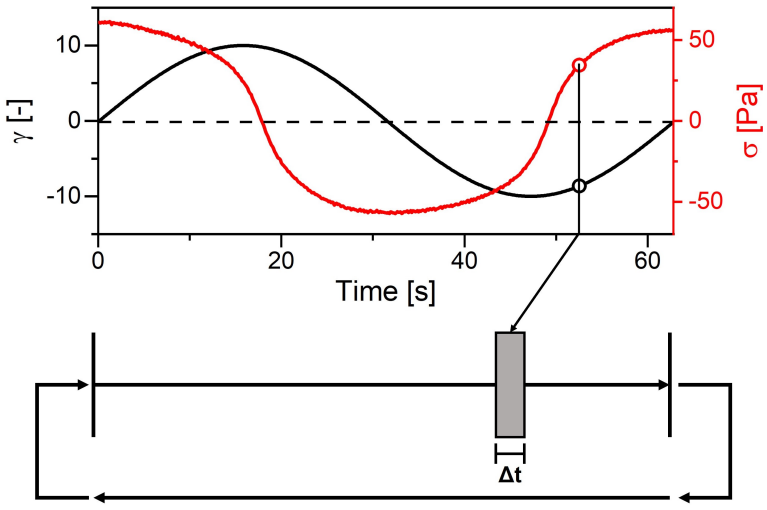

Figure 5.2: A diagram outlining the transient SANS method using the sliding bin technique. The applied deformation, in this case a large amplitude oscillatory strain is repeated until a suffient number of counts are measured over Δt.

5.3 Materials and Methods

5.3.1 Material Preparation

Well-defined poly(styrene)-b-poly(lactic acid) (PS-b-PLA) di-block bottlebrushes were synthesized by our collaborators in the Guironnet group through graft-through polymerization of macromonomers according to the methods and dimensions described in Section 3.3.1. Molecular weight distributions for these polymers can be found in Appendix B.

The PS-PLA diblock bottlebrush polymers were dissolved in toluene to form a solution with a concentration of 350 mg ml^{-1}. Solutions were gently mixed for 24 to 48 hours using a stir bar and a magnetic stirrer to uniformly distribute the polymer in the solution. Prior to pulling small portions of the sample to load onto the rheometer, the solution was stirred by hand to ensure the polymer sample had not settled. While we attempted to prepare solutions with concentrations greater than 350 mg ml^{-1}, these samples could not be used due to challenges uniformly distributing the polymer in solution without resorting to more aggressive mixing methods that might potentially damage the bottlebrush polymer. During tests, the samples were maintained at 5 °C to reduce evaporation. Further steps were taken to reduce evaporation by isolating the sample inside the MCR evaporation blocker. Excess toluene was added around the outer edge of the geometry to saturate the atmosphere within the evaporation blocker with toluene and thus further stabilize the sample.

5.3.2 Recovery Rheology during Shear Startup and Oscillatory Deformation

Iterative recovery studies were carried out under shear startup and oscillatory deformation. During the shear startup tests, shear rates from 0.1 to 31.6 s^{-1} were applied to the material and the stress response was measured as a function of time. At predetermined points in time throughout the test, a strain recovery test was carried out according to the methods discussed by Lee et al., [40], [41] by setting the stress to zero and allowing the sample to recover. The recoverable and unrecoverable strain components were calculated according to the discussion in Section 5.2.2 and shown in Figure 5.1. A short zero shear rate step was imposed prior to setting the stress to zero to prevent the inertia of the geometry and sample from affecting the measured recoverable strain. Tests were repeated with positive and negative shear rates to account for instrument drift under zero stress conditions.

Oscillatory shear studies were carried out in a similar fashion with a zero stress step iteratively applied after the material undergoes deformation. To ensure the measured recoverable strain, and in turn the recoverable and unrecoverable components of the moduli are representative of the material under steady oscillatory conditions, at least 10 oscillations are applied to the bottlebrush sample followed by a partial oscillation and the recovery step. Tests were repeated with positive and negative oscillations to account for instrument drift under zero stress conditions. To map the behavior of the acquisition of recoverable and unrecoverable strain, 16 evenly spaced points were captured over one half oscillation. Given that the material was undergoing steady alternates, these results could be mirrored to reasonably approximate the response of the bottlebrush polymer sample during the second half of the oscillation. 16 points per half period was found to reasonably capture the recoverable behavior of the bottlebrush under oscillatory shear while minimizing issues with evaporation and limited bulk sample.

Frequency sweeps were periodically carried out throughout the recovery tests under oscillatory shear and shear startup to ensure the material had not significantly changed over the course of the study. See Appendix D for these results.

5.3.3 Transient SANS Studies

Transient neutron scattering studies are to be carried out on the 30 meter SANS beamline at the NCNR with the detector positioned 19.4 m away from the sample. This allows us to capture a q range from 0.0027 $Å^{-1}$ to 0.027 $Å^{-1}$ which has been shown to encompass the length-scale of the self-assembled bottlebrush microstructure as described in Chapter 3. During the scattering measurements, oscillatory shear will be applied to the polymer with a frequency of 0.1 and amplitudes ranging from 5.62 to 1000%. Measurements will be carried out in the 1-3 and the 2-3 scattering plane in order to assemble a complete image of the bottlebrush polymer's microstructure under deformation. The oscillation will be split into 64 individual bins, 32 per half period, resulting in a time resolution of 1s/bin, to provide sufficient time resolution to resolve the solid to liquid transition and recovery step. The sliding bin analysis method discussed by Calabrese et al., will be used to improve this time resolution and allow us to more clearly see how the structure develops during yielding [50].

When planning these measurements, it is important to take into account the rate of neutrons scattered by the polymer sample, also known as the counts/s, as this rate dictates how quickly measurements can be carried out and thus how many tests can be run during a single trip to a beamline. Viability studies have been carried out at the NCNR on the 30 m SANS beam line, yielding a count rate of 240 counts/s. Given that at least 100,000 counts/bin is considered sufficient to make statistically significant [51] observations based on the scattering, and that we plan to capture a time resolution of at least 1 s/bin, a total of 6.2 10 ^{6} counts need to be recorded per measurement. As such, we expect each amplitude and sample orientation to take at least 9 hours to complete. A more detailed discussion of the sample environment and the experiment plan can be found in the submitted proposal shown in Appendix D.

5.4 Current Results and Future Work

5.4.1 Yield-Like Behavior in Concentrated Bottlebrush Solutions

To probe the typically measured viscoelastic behavior of concentrated bottlebrush polymer solutions, frequency sweeps, amplitude sweeps and flow curves were measured to characterize the modulus, linear regime, and viscosity respectively. From the amplitude and flow curves, we observe features that are typically associated with yield-like behavior. In Figure 5.3.a the flow curve was observed to taper off and approach a constant value of stress at low shear rate. We were able to fit the data to a Herschel Bulkley model, which is defined by the equation,

$$\sigma = \sigma_0 + k\dot{\gamma}^{\eta}, \tag{5.5}$$

where σ_0 is the stress offset, η is the flow index, and k is the proportionality constant. It is important to note that k has units of units of Pa s^{η} and is not a measure of the viscosity. From this model, we calculate the stress offset to be 44 Pa. Per the Herschel-Bulkley model, this value is the minimum amount of stress that must be applied to the polymer solution to achieve flow, also known as the yield-stress [27]. Interestingly enough, creep measurements, shown in Figure D.1 depict similar behavior in the form of flow bifurcation, where stresses below the yield-stress results in the material deforming short a short period of time followed by the shear rate eventually dropping to zero. Shear rates above the yield-stress result in constant flow. In the case of the results shown in Figure D.1, the yield stress appears to be in the ballpark of 1 to 3.16 Pa,

an order of magnitude lower than the measured highlights how the different methods for determining the yield-stress can result in vastly different values as discussed by Dinkgreve et al., [52].

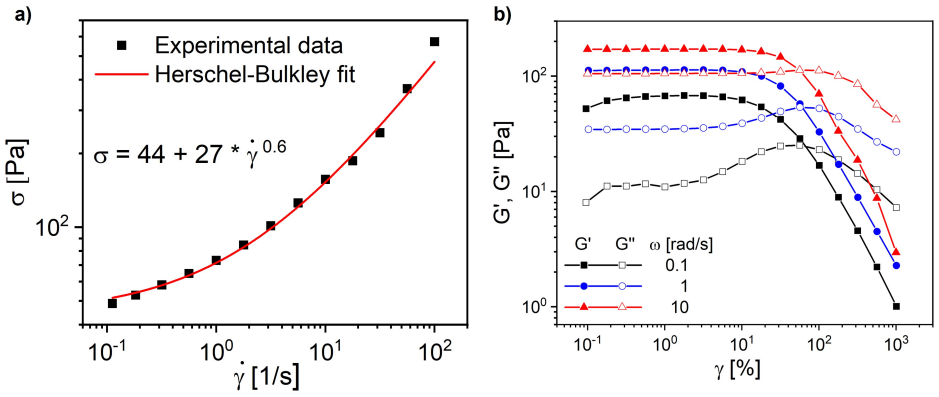

Figure 5.3: a) The stress measured at each shear rate during a flow sweep. The data are fit to a Herschel-Bulkley model (red) with the resulting equation being shown in the figure. b) Amplitude sweeps carried out at different frequencies, highlighting the G" overshoot and G', G" crossover at large amplitudes.

When considering the amplitude sweep shown in Figure 5.3, we observe features that are typically associated with yield-like behavior in the form of a G', G" crossover and a G" overshoot. The crossover between the moduli at moderately large amplitude indicates that the material is transitioning from behaving predominantly as a solid to predominantly as a liquid. The G" overshoot, known as the Payne effect [53], [54], has been typically associated with type III yield-stress materials and has been identified in a range of different polymer systems that exhibit yield-like behavior [55]–[60]. The presence of this feature in the bottlebrush polymer solution's amplitude sweep in the context with the other observed features supports the idea that the material is exhibiting yield-like behavior and undergoing a solid to liquid transition when sufficiently stressed. Based off of the fact that this material is acting as a yield-stress fluid and the idea that all flow stops the moment the applied stress is below the yield-stress for a yield-stress fluid, we predict that increasing the concentration to the point where the material is exhibiting yield-like properties should result in the self-assembled microstructure getting frozen in place once the applied stress is set to zero and the material reverts to behaving as a solid.

5.4.2 Color Retention in Concentrated Bottlebrush Solutions

To quantify the extent to which higher concentration and the resulting yield-like properties affect a diblock bottlebrush copolymer solution's relaxation time and in turn the samples's ability to retain shear-induced color, rheo-microscope studies were carried out under steady and pulse shear rates. Using the setup depicted in Figure 3.2, images of the concentrated bottlebrush polymer under steady shear conditions were captured at shear rates from 0.1 to 100 s^{-1}. The flow curve in Figure 5.4 depicts the viscosity of the concentrated bottlebrush solution with the corresponding colors shown in order of increasing shear rate below the plot. When compared to the data rheomicroscopy studies performed in Chapters 3 and 4, the observed range is significantly muted. We attribute this loss of intensity to an increased variation in lamellae orientation and characteristic length scale due to the higher concentration. That being said, we still observe distinct color changes at shear rates above 10 s^{-1}. Taking a closer look at the viscosity, we do not observe distinct

scaling regimes as was previously identified in Figure 3.6. This lack of scaling regimes suggests that the changes in microstructure with steady shear is not as significant as was previously measured for diblock bottlebrush samples with a concentration of 175 mg/ml. Neutron scattering studies will need to be carried out to characterize exactly how steady-shear impacts the self-assembled microstructure and how it differs from the lower concentration bottlebrush solutions.

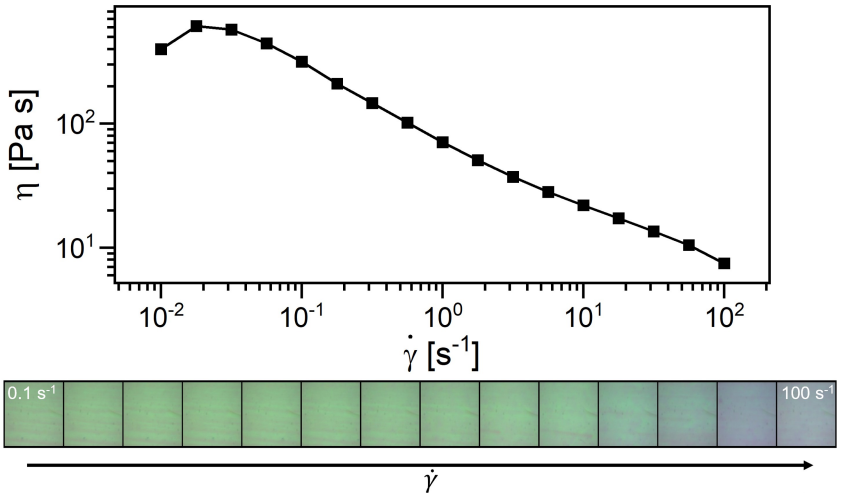

Figure 5.4: A flow curve depicting the viscosity of the bottlebrush polymer as a function of shear rate with corresponding images captured using the Rheo-microscope setup under steady shear conditions.

Based on this flow curve and the corresponding sample colors, steady shear pulses were applied to the bottlebrush polymer to characterize if the bottlebrush polymer reverts to its quiescent state and if so how quickly this relaxation from a sheared to quiescent state occurs. During these tests, 30 s of steady shear with shear rates from 0.1 to 31.6 s^{-1} were applied to the material followed by 30 s of 0 rate or 0 rate. Higher shear rates were not tested due to concerns with sample ejection and limited bulk bottlebrush polymer sample. During these pulse tests, videos were captured using the Rheo-microscope setup from Figure 3.2. Each frame from these videos was averaged and converted into Hue, Saturation, and Level values to provide a measure of the color as a function of time. An averaged result over multiple pulses with a shear rate of 31.6 s^{-1} followed by a zero shear rate step is shown in Figure 5.5.a. In this test, the color rapidly reverts from its sheared state shown in Figure 5.5.b to its quiescent state shown in Figure 5.5.b in approximately 5 s (indicated by the vertical red lines). Fitting this color relaxation to an exponential yields an exponential time constant, τ of 0.9 s. Pulse tests carried out a lower shear rates as well as pulse tests conducted with zero stress recovery step instead of a zero rate step are shown in Appendix D, Figure D.2 and show similar results and timescales to the data depicted in Figure 5.5.

From the data shown in Figures 5.5 and D.2, we can clearly see that increasing the concentration of the bottlebrush polymer solution to 350 mg/ml such that it exhibits yield-like behavior does not result in a long color relaxation time and thus a retention of shear-induced microstructure over long timescales. If this polymer solution had demonstrated instantaneous yielding, as has been previously described in the literature [6], [27]–[30] then we would have expected some of the color and thus shear induced microstructure to be retained after steady shear was stopped. The fact that the color reverted back to its quiescent state despite being held at a constant strain demonstrates how the material is not exclusively exhibiting solid-like behavior

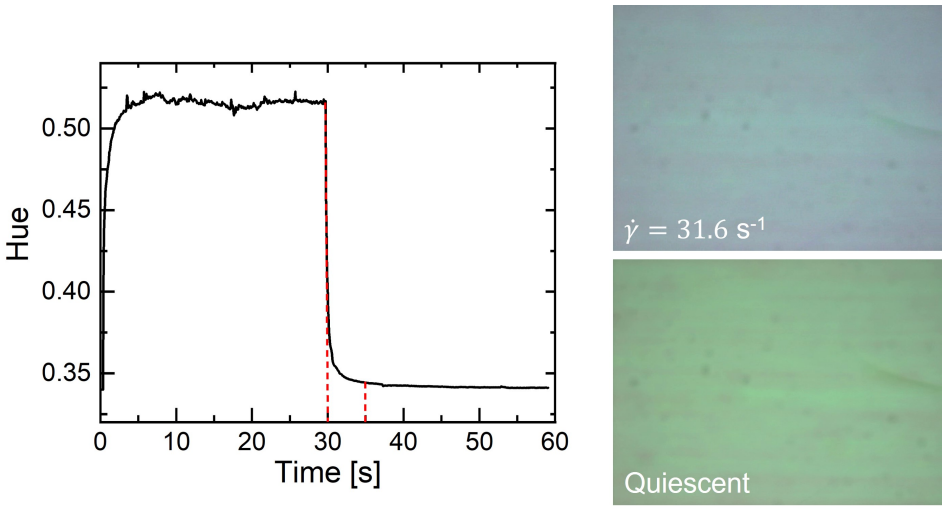

Figure 5.5: The color observed using a rheo-microscope during a single steady shear pulse followed by a zero rate step. The dashed red line at 30 s indicates where the rheometer was stopped and the second dashed red line indicates the time it takes for the material to revert to 99% of its original color (5 s). The two images on the right indicate the significant difference between the color under steady shear and the color under quiescence.

where some stress, and thus change in microstructure, is retained after the stress has dropped below the yield stress. Instead, the rapid return to the polymer's quiescent state suggests that there is some combination of viscous and elastic processes that govern the material's behavior during the solid to liquid transition and visa versa. To explore these transient processes and identify the changes in microstructure that lead to a solid to liquid transition typically associated with yield-stress fluids, we turn to iterative oscillatory and steady shear startup recovery rheology and time resolved neutron scattering measurements. These methods provide insight into the mechanisms that store and dissipate energy during transient deformation which can be related back to the microstructure of the polymer in solution.

5.4.3 Insight into Transient Yielding Through Recovery

In Figure 5.6, we show the decomposition of the loss moduli into recoverable and unrecoverable components, labeled $G"_{solid}$ and $G"_{fluid}$, respectively, as a function of oscillation amplitude. These calculated moduli are compared against the traditional measure for the loss moduli, demonstrating that the sum of $G"_{solid}$ and $G"_{fluid}$ is equal to the loss moduli. The decomposition of the storage moduli is not shown as the fluid component of the storage moduli is negligible, resulting in $G'_{solid} = G'$. Both of these results match up with previous studies into the moduli decomposition through recovery rheology as carried out by Gavin Donley, et al., [42]. At low amplitudes, we observe the $G"_{solid}$ to be the predominant contributor to $G"$. As oscillatory strain amplitude is increased, $G"_{solid}$ decreases while $G"_{fluid}$ until $G"_{fluid}$ becomes the primary contributor to $G"$. It is important to note that the transition from predominately solid-like contributions to predominantly fluid-like contributions is smooth as $G"_{fluid}$ gradually increases with increasing amplitude. Similar observations were made by Donley et al., noting how classical yield-stress models such as the Saramito model assume a rapid increase in the fluid-like contributions once a critical stress or strain has been exceeded [42]. Instead this behavior suggests that yielding is more of a gradual process, partially occurring at stresses

below the yield-stress.

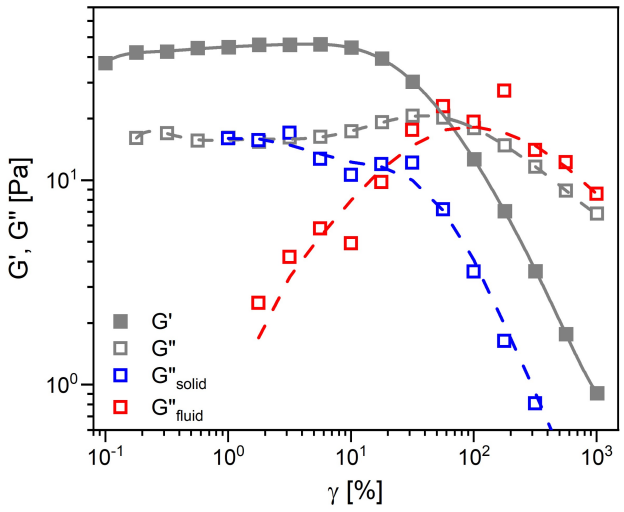

Figure 5.6: An amplitude sweep depicting the decomposed loss moduli compared traditional measure for the moduli. The amplitude sweep was carried out at a frequency of 0.1 rad/s.

Due to the inherently transient nature of iterative recovery rheology, we can use the data collected for Figure 5.6 to take a closer look at the behavior of the bottlebrush polymer solution within a single oscillation. This analysis allows us to identify the points at which the material undergoes a yielding transition and the extent to which yielding occurs based on $De(t)$ from Equation 5.7. In Figure 5.7, we show a representative set of stress-strain Lissajous curves under steady oscillatory shear conditions captured strain amplitudes that span from the linear regime to the non-linear regime. We map out the calculated transient Deborah number, $De(t)$, based on the recoverable and unrecoverable strain rates at each point in this oscillation. The resulting color maps allow us to identify the points within the oscillation where the material transitions from predominantly elastic deformation to predominantly plastic deformation and visa versa.

At a strain amplitude of 5.62%, the polymer solution exhibits predominantly elastic deformation and has a Lissajous curve that appears to approach a straight line. Such a feature matches with the traditional understanding of oscillatory shear rheology as purely elastic solids exhibit a linear relation between stress and strain, resulting in a Lisssajous curve that collapses into a straight line. It should be noted that at the highest stresses and strains experienced by the bottlebrush at a strain amplitude of 5.62% the polymer sample begins to exhibit an almost equal combination of elastic and plastic behavior as indicated by the gray color in that region. Higher strain amplitudes result in an opening of the Lissajous curve and the material exhibiting more plastic-like deformation. These regions of plastic deformation initially only appear at the highest strains and stresses experienced by the polymer solution (as seen at 17.7% and 56.2%). The highest strain amplitudes shown in Figure 5.7, exhibit almost exclusively plastic deformation with small regions of plastic deformation in regions where the stress is nearly equal to zero. From each of the amplitudes shown in Figure 5.7, we can clearly identify points in the oscillation where the material transitions from predominantly elastic deformation to predominantly liquid deformation and visa versa. These points correspond to moments where the bottlebrush polymer solution is undergoing yielding and recovery processes within the oscillation.

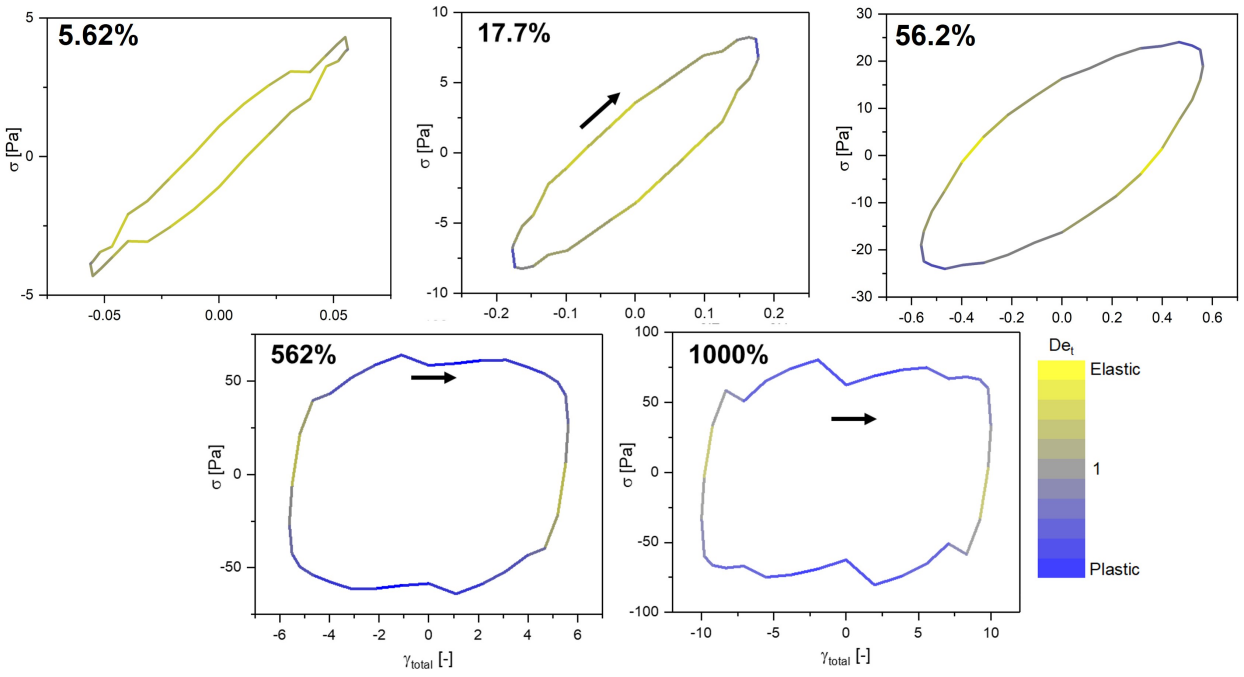

Figure 5.7: The stress-strain lissajous curves for oscillatory strain amplitudes of 5.62 to 1000%. The transient Deborah number calculated through recovery rheology is overlaid on top of the lissajous curves. The points where De_t is gray correspond to regions where De_t is equal to 1 and the material is undergoing either yielding or recovery processes.

From this analysis, we are able to map out how the material is behaving during deformation.

The next step in this study is understanding the structural changes that give rise to the solid to liquid transitions as described by De_t, thus giving us the opportunity to develop a structure-process relation between the microstructure and the yielding phenomena observed through rheological measurements. Transient neutron scattering measurements are currently planned for this study. A proposal detailing the experimental conditions and instrument settings was prepared and submitted approximately two years prior. Four days of beam time on the 30 m SANS beam line at the NIST Center for Neutron Research (NCNR) was awarded by the beam time allocation committee based on this proposal. During these 4 days and we plan to test a total of 5 different oscillation amplitudes from 5.62% to 1000% at a frequency of 0.1 rad/s, spanning a range of conditions where the polymer solution behaves exhibits almost exclusively plastic deformation to almost exclusively plastic deformation. Given the expectation that a single test will take approximately 9 hours and tests are to be repeated in the 1-3 and 2-3 scattering planes to ensure we have an understanding of the 3D structure, a total of 5 amplitudes will be tested resulting in a total experiment time of 3.9 days.

Unfortunately we have not yet had the opportunity to run these scattering studies. The nuclear reactor at the NCNR is undergoing a temporary shutdown and has yet to come back online. Once the reactor is back up an running, we will coordinate with our NCNR contact, Dr. Katie Weigandt, to schedule the time allocated for the beamtime proposal and carry out these studies. Once complete, these experiments will provide unprecedented insight into the transient structural and mechanical changes that occur during yielding processes. Our work will serve as one of the first to probe a yield-stress fluid, identifying the structural changes

that occur during yielding, and relate those microstructures back to the transient rheological properties.

5.4.4 Recovery Shear-Startup Studies

In an effort to further understand how the structure of the bottlebrush polymer develops as the material transitions from its quiescent state to its shear state, we turn to shear startup studies and recovery rheology. In the context of direct ink writing processes, this information is particularly useful as printing processes are not continuous. Instead flow out of the print nozzle is regularly stopped and restarted as the print head moves from one line to the next [34]. From a yield-stress perspective, such studies allow us to probe the structural and rheological changes that occur when a material transitions from a solid-like state at rest, to a liquid-like state under shear. Given the rapid fast color response observed during the steady shear pulse tests, shown in Figure 5.5 and Figure D.2, we expect the concentrated bottlebrush polymer to respond quite quickly during the steady shear startup tests. We carried out a rough sweep over the range of shear rates applied to identify the longest and shortest timescales that we would need to probe with iterative recovery tests. The results for a select set of rates are shown in Figure 5.8.

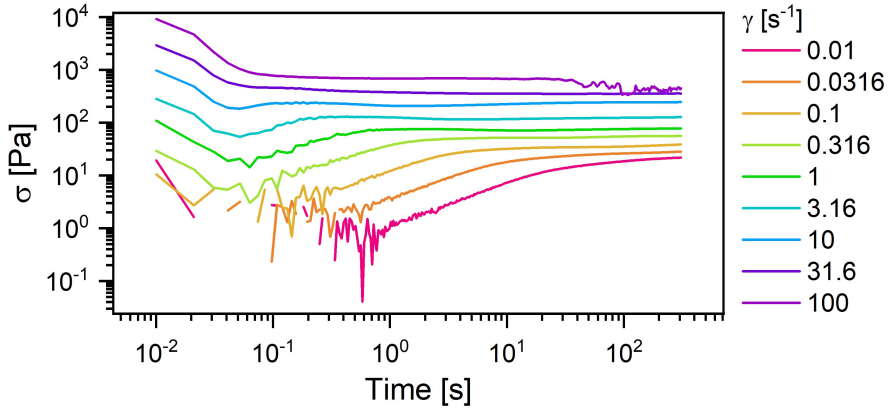

Figure 5.8: The results from a steady shear startup test for a select set of shear rates.

From this data, we see that at the lowest applied shear rates, the material appears to reach an equilibrium conditions within 1 to 10s. Higher shear rates result in the material reaching equilibrium at approximately 0.1 s. At very short times, we observe a stress overshoot followed by an undershoot around 0.03 s that can be attributed to the rheometer's PID controller.

Based on these results, we limit the time scales studied with recovery rheology during shear startup to a maximum of 100 s. The lowest time scale that could be accurately captured with recovery rheology was 0.1 s as this is the time it takes for the instrument to transition from applying steady shear to applying zero stress. The lowest shear rate tested was 0.1 s^{-1} due to challenges with material response and noise when attempting to capture the recovery rheology at a shear rate of 0.01 s^{-1}. The maximum rate tested was 31.6 s^{-1} due to concerns with sample ejection from repeatedly starting and stopping the rheometer at higher shear rates. The results from these recovery tests are shown in Figure 5.9.

The recoverable strain captured during shear startup is compared against the measured stress immediately before the strain recovery step. We would typically expect the stress and recoverable strain to follow similar trends as the material initially deforms elastically [40], [41], [47]. Once the molecule has been elongated completely, then the stress would be expected to continue increasing as the material flows while the recoverable

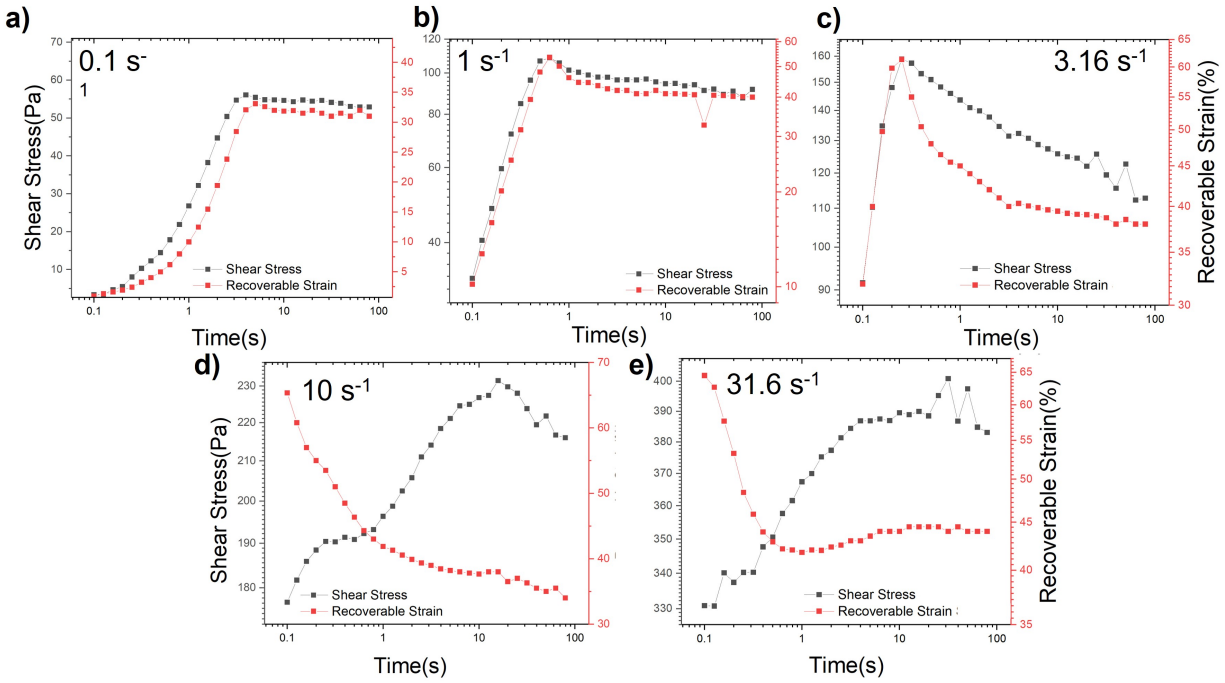

Figure 5.9: The measured stress during shear startup (left axis) compared to the recoverable strain (right axis) as calculated by recovery rheology for shear rates from 0.1 to 31.6 s^{-1}.

strain remains constant, or remain relatively constant if the material has not yielded. These trends are observed in Figures 5.9.a and b for shear rates of 0.1 to 1 s^{-1} where the recoverable strain reaches a equilibrium value of 30 to 40 % and the stress increases with the recoverable strain. For the test carried out at 0.1 s^{-1}, the measured stress at long times is 50 Pa, which is approximately equal to the yield stress calculated from the Herschel-Bulkley model (Figure 5.3). At higher shear rates of 10 and 31.6 s^{-1}, the recoverable strain appears to exceed the equilibrium value, reaching maximums on the order of 60 %. The recoverable strain then decreases to a similar value to that observed in the low shear rate tests. This behavior suggests that the material may have been fully at very low shear rates and may undergo some sort of rapid initial elongation followed by a collapse as the polymer begins to flow at higher shear rates. During these times, the stress is observed to gradually increase, indicating that the collapsing of the polymer over longer time scales results in shear thickening behavior. Surprisingly, at higher shear rates, the tests shown in Figure 5.9 do not capture the timescales over which the bottlebrush polymer reaches an equilibrium state during shear startup. Future recovery studies are planned or longer time scales from 100 to 1000 s. Despite not capturing the point where the material reaches equilibrium, these results shed some light into how this material is behaving as it transitions from quiescent to sheared stats. The gradual drop in recoverable strain and increase in stress for higher shear rates suggests that there are long term structural changes occurring within the material that merit further investigation. This work also serves as a starting point for future researchers who will be taking over this project, helping them identify the issues and key features to keep an eye out for when running these tests.

5.5 Outlook and Remaining Challenges

In this work, we investigate the effects of increasing the concentration of the bottlebrush polymer solution in order to increase the relaxation time. By doubling the concentration from 175 mg/ml to 350 mg/ml we observe several rheological features that are typically associated with yield stress fluids, such as a G" overshoot in the amplitude sweep as well as a G', G" crossover at high amplitudes. When examining the flow curve, we are able to fit the data to a Herschel-Bulkley model and calculate a minimum required stress for flow, a.k.a., a yield stress. Based on this and the traditional representation of yielding as an instantaneous process, we investigate the possibility of locking in the microstructure of the concentrated bottlebrush polymer by applying steady deformation or stress and then releasing the material, effectively setting the stress to zero, and allowing the material to return to a solid state. Through a series of steady shear rate pulse tests, we find that the material does not freeze when held at zero stress or zero rate. Instead the material quickly reverts back to its quiescent state with a relaxation time on the order of 1 s. Based on these results, we conclude that doubling the concentration to the point where yield-like behaviors are observed is not a viable mechanism for locking in the microstructure. Instead we find that these results highlight the transient nature of the yielding process.

To further explore this transient behavior, we employ recovery rheology to help us understand the plastic and elastic contributions to the behavior of the bottlebrush polymer under shear oscillation. By decomposing the loss moduli into solid and fluid components, we identify that there are fluid contributions to the loss moduli despite the material appearing in the linear regime. This result further lends credence to the idea that yielding is not a binary phenomena based on a single yield stress. We also utilize the transient Deborah number, defined by Singh et al. [47], to identify the points within an oscillation where the material undergoes a solid to liquid transition or visa versa. Specifically we seek to identify points where De_t crosses over 1 as this corresponds to the material transitioning from predominantly plastic deformation to predominantly elastic deformation or visa versa depending on whether the material is recovering or yielding. Transient neutron scattering measurements were planned in order to probe the structure under these oscillatory deformation conditions, however issues with the beamline undergoing an emergency shutdown have limited our access to neutrons and thus our ability to perform these measures. Once the beamline is up an running, we will carry out these tests asap and begin the process of analyzing the transient data. These measurements will serve as the first of their kind, providing insight into the yielding and recovery phenomena and allowing us to develop structure-property relations that relate any structural change we observe to the yielding behavior.

An additional set of iterative recovery rheology studies were carried out to investigate the development of structure during shear startup conditions. Motivated by the idea that printing is not a steady flow process, we identify how the recoverable strain changes as a function of time during shear startup. Surprisingly, the recoverable strain does not appear to increase linearly and then hold at a constant value. Instead higher shear rates result in a maximum at very short time scales followed by a slow decrease in recoverable strain at longer time scales. This result suggests that the polymer is collapsing at higher shear rates. Further tests are planned for these conditions at longer time scales in an attempt to capture the equilibrium value of the recoverable strain. Shorter timescales that might better capture the short time elastic behavior are unfortunately not accessible due to the limitations of the rheometer. Moving forward, these tests should allow us to map the self-assembled microstructure of the bottlebrush polymer as it is being extruded, thus allowing for further control over the properties of the material during on-the-fly printing processes. The results presented in this chapter serve as the groundwork for fully characterizing this behavior and are expected to lead to an eventual beamtime proposal for transient rheo-SANS measurements during steady shear startup.

5.6 References

[1] M. C. Williams, *Advances in Chemistry*. Wiley, 1967, vol. 111, p. 534.

[2] J. Klein, *Viscoelastic properties of polymers*, 5. Wiley, 1978, vol. 11, p. 852, ISBN: 9780471048947. DOI: 10.1149/1.2428174. [Online]. Available: https://pubs.acs.org/sharingguidelines.

[3] M. Baumgärtel and N. Willenbacher, "The relaxation of concentrated polymer solutions," *Rheologica Acta*, vol. 35, no. 2, pp. 168–185, 1996, ISSN: 00354511. DOI: 10.1007/bf00396044.

[4] Y. Liu, Y. Jun, and V. Steinberg, "Concentration dependence of the longest relaxation times of dilute and semi-dilute polymer solutions," *Journal of Rheology*, vol. 53, no. 5, pp. 1069–1085, 2009, ISSN: 0148-6055. DOI: 10.1122/1.3160734. [Online]. Available: https://doi.org/10.1122/1.3160734.

[5] M. Dinkgreve, J. Paredes, M. A. J. Michels, and D. Bonn, "Universal rescaling of flow curves for yield-stress fluids close to jamming," *Physical Review E*, vol. 92, no. 1, p. 12 305, Jul. 2015. DOI: 10.1103/PhysRevE.92.012305. [Online]. Available: https://link.aps.org/doi/10.1103/PhysRevE.92.012305.

[6] M. Dinkgreve, M. M. Denn, and D. Bonn, ""Everything flows?": elastic effects on startup flows of yield-stress fluids," *Rheologica Acta*, vol. 56, no. 3, pp. 189–194, Mar. 2017, ISSN: 00354511. DOI: 10.1007/s00397-017-0998-z. [Online]. Available: https://link.springer.com/article/10.1007/s00397-017-0998-z.

[7] K. Hyun, M. Wilhelm, C. O. Klein, *et al.*, "A review of nonlinear oscillatory shear tests: Analysis and application of large amplitude oscillatory shear (LAOS)," *Progress in Polymer Science (Oxford)*, vol. 36, no. 12, pp. 1697–1753, 2011, ISSN: 00796700. DOI: 10.1016/j.progpolymsci.2011.02.002. [Online]. Available: http://dx.doi.org/10.1016/j.progpolymsci.2011.02.002.

[8] D. Bonn, H. Tanaka, G. Wegdam, H. Kellay, and J. Meunier, "Aging of a colloidal "Wigner" glass," *Europhysics Letters*, vol. 45, no. 1, pp. 52–57, 1999, ISSN: 02955075. DOI: 10.1209/epl/i1999-00130-3.

[9] A. Burmistrova and R. Von Klitzing, "Control of number density and swelling/shrinking behavior of P(NIPAM-AAc) particles at solid surfaces," *Journal of Materials Chemistry*, vol. 20, no. 17, pp. 3502–3507, 2010, ISSN: 09599428. DOI: 10.1039/b923969c. [Online]. Available: www.rsc.org/materials.

[10] C. Clasen, B. P. Gearing, and G. H. McKinley, "The flexure-based microgap rheometer (FMR)," *Journal of Rheology*, vol. 50, no. 6, pp. 883–905, 2006, ISSN: 0148-6055. DOI: 10.1122/1.2357190. [Online]. Available: https://doi.org/10.1122/1.2357190.

[11] M. Cloitre, R. Borrega, F. Monti, and L. Leibler, "Glassy Dynamics and Flow Properties of Soft Colloidal Pastes," *Physical Review Letters*, vol. 90, no. 6, p. 4, Feb. 2003, ISSN: 10797114. DOI: 10.1103/PhysRevLett.90.068303. [Online]. Available: https://journals.aps.org/prl/abstract/10.1103/PhysRevLett.90.068303.

[12] M. Jalaal, G. Cottrell, N. Balmforth, and B. Stoeber, "On the rheology of Pluronic F127 aqueous solutions," *Journal of Rheology*, vol. 61, no. 1, pp. 139–146, 2017, ISSN: 0148-6055. DOI: 10.1122/1.4971992. [Online]. Available: https://sor.scitation.org/toc/jor/61/1https://doi.org/10.1122/1.5054598.

[13] T. Jiang and C. F. Zukoski, "Rheology of high density glass of binary colloidal mixtures in unentangled polymer melts," *Soft Matter*, vol. 9, no. 11, pp. 3117–3130, 2013, ISSN: 1744683X. DOI: 10.1039/c3sm27874c. [Online]. Available: www.rsc.org/softmatter.

[14] R. C. Kramb and C. F. Zukoski, "Nonlinear rheology and yielding in dense suspensions of hard anisotropic colloids," *Journal of Rheology*, vol. 55, no. 5, pp. 1069–1084, 2011, ISSN: 0148-6055. DOI: 10.1122/1.3613978. [Online]. Available: https://doi.org/10.1122/1.3613978.

[15] M. Le Merrer, R. Lespiat, R. Höhler, and S. Cohen-Addad, "Linear and non-linear wall friction of wet foams," *Soft Matter*, vol. 11, no. 2, pp. 368–381, 2015, ISSN: 17446848. DOI: 10.1039/c4sm01557f. [Online]. Available: www.rsc.org/softmatter.

[16] K. N. Nordstrom, E. Verneuil, P. E. Arratia, *et al.*, "Microfluidic rheology of soft colloids above and below jamming," *Physical Review Letters*, vol. 105, no. 17, p. 175 701, Oct. 2010, ISSN: 00319007. DOI: 10.1103/PhysRevLett.105.175701. [Online]. Available: https://journals.aps.org/prl/abstract/10.1103/PhysRevLett.105.175701.

[17] C. S. O'Bryan, T. Bhattacharjee, S. Hart, *et al.*, "Self-assembled micro-organogels for 3D printing silicone structures," *Science Advances*, vol. 3, no. 5, May 2017, ISSN: 23752548. DOI: 10.1126/sciadv.1602800. [Online]. Available: https://www.science.org/doi/10.1126/sciadv.1602800.

[18] J. M. Piau, "Carbopol gels: Elastoviscoplastic and slippery glasses made of individual swollen sponges. Meso- and macroscopic properties, constitutive equations and scaling laws," *Journal of Non-Newtonian Fluid Mechanics*, vol. 144, no. 1, pp. 1–29, Jun. 2007, ISSN: 03770257. DOI: 10.1016/j.jnnfm.2007.02.011.

[19] S. A. Rogers, B. M. Erwin, D. Vlassopoulos, and M. Cloitre, "Oscillatory yielding of a colloidal star glass," *Journal of Rheology*, vol. 55, no. 4, pp. 733–752, 2011, ISSN: 0148-6055. DOI: 10.1122/1.3579161. [Online]. Available: https://sor.scitation.org/toc/jor/55/4.

[20] H. Senff and W. Richtering, "Temperature sensitive microgel suspensions: Colloidal phase behavior and rheology of soft spheres," *Journal of Chemical Physics*, vol. 111, no. 4, pp. 1705–1711, 1999, ISSN: 00219606. DOI: 10.1063/1.479430. [Online]. Available: https://doi.org/10.1063/1.479430.

[21] D. Bonn and M. M. Denn, *Yield stress fluids slowly yield to analysis*, Jun. 2009. DOI: 10.1126/science.1174217. [Online]. Available: https://www.science.org/doi/10.1126/science.1174217.

[22] P. Coussot, Q. D. Nguyen, H. T. Huynh, and D. Bonn, "Avalanche behavior in yield stress fluids," *Physical Review Letters*, vol. 88, no. 17, pp. 1 755 011–1 755 014, Apr. 2002, ISSN: 00319007. DOI: 10.1103/PhysRevLett.88.175501. [Online]. Available: https://journals.aps.org/prl/abstract/10.1103/PhysRevLett.88.175501.

[23] T. Bauer, J. Oberdisse, and L. Ramos, "Collective rearrangement at the onset of flow of a polycrystalline hexagonal columnar phase," *Physical Review Letters*, vol. 97, no. 25, p. 258 303, Dec. 2006, ISSN: 00319007. DOI: 10.1103/PhysRevLett.97.258303. [Online]. Available: https://journals.aps.org/prl/abstract/10.1103/PhysRevLett.97.258303.

[24] T. Sentjabrskaja, P. Chaudhuri, M. Hermes, *et al.*, "Creep and flow of glasses: Strain response linked to the spatial distribution of dynamical heterogeneities," *Scientific Reports*, vol. 5, 2015, ISSN: 20452322. DOI: 10.1038/srep11884. [Online]. Available: www.nature.com/scientificreports.

[25] M. Siebenbürger, M. Ballauff, and T. Voigtmann, "Creep in colloidal glasses," *Physical Review Letters*, vol. 108, no. 25, p. 255 701, Jun. 2012, ISSN: 00319007. DOI: 10.1103/PhysRevLett.108.255701. [Online]. Available: https://journals.aps.org/prl/abstract/10.1103/PhysRevLett.108.255701.

[26] J. Sprakel, S. B. Lindström, T. E. Kodger, and D. A. Weitz, "Stress enhancement in the delayed yielding of colloidal gels," *Physical Review Letters*, vol. 106, no. 24, p. 248 303, Jun. 2011, ISSN: 00319007. DOI: 10.1103/PhysRevLett.106.248303. [Online]. Available: https://journals.aps.org/prl/abstract/10.1103/PhysRevLett.106.248303.

[27] V. W. H. Herschel and R. Bulkley, "Ronsistenzmessungen yon (ummi-BenzollGsungen)," *Colloid and Polymer Science*, vol. 39, p. 291, 1926.

[28] P. Saramito, "A new constitutive equation for elastoviscoplastic fluid flows," *Journal of Non-Newtonian Fluid Mechanics*, vol. 145, no. 1, pp. 1–14, Aug. 2007, ISSN: 03770257. DOI: 10.1016/j.jnnfm.2007.04.004.

[29] J. G. Oldroyd, "A rational formulation of the equations of plastic flow for a Bingham solid," *Mathematical Proceedings of the Cambridge Philosophical Society*, vol. 43, no. 1, pp. 100–105, 1947, ISSN: 14698064. DOI: 10.1017/S0305004100023239. [Online]. Available: https://www.cambridge.org/core/journals/mathematical-proceedings-of-the-cambridge-philosophical-society/article/rational-formulation-of-the-equations-of-plastic-flow-for-a-bingham-solid/5B69C6A5BD7BF69F4F92260AC4242E1C.

[30] P. Saramito, "A new elastoviscoplastic model based on the Herschel-Bulkley viscoplastic model," *Journal of Non-Newtonian Fluid Mechanics*, vol. 158, no. 1-3, pp. 154–161, May 2009, ISSN: 03770257. DOI: 10.1016/J.JNNFM.2008.12.001.

[31] M. Caggioni, V. Trappe, and P. T. Spicer, "Variations of the Herschel–Bulkley exponent reflecting contributions of the viscous continuous phase to the shear rate-dependent stress of soft glassy materials," *Journal of Rheology*, vol. 64, no. 2, pp. 413–422, Mar. 2020, ISSN: 0148-6055. DOI: 10.1122/1.5120633. [Online]. Available: http://sor.scitation.org/doi/10.1122/1.5120633.

[32] J. Paredes, M. A. Michels, and D. Bonn, "Rheology across the zero-temperature jamming transition," *Physical Review Letters*, vol. 111, no. 1, p. 015 701, Jul. 2013, ISSN: 00319007. DOI: 10.1103/PhysRevLett.111.015701. [Online]. Available: https://journals.aps.org/prl/abstract/10.1103/PhysRevLett.111.015701.

[33] A. Basu, Y. Xu, T. Still, *et al.*, "Rheology of soft colloids across the onset of rigidity: Scaling behavior, thermal, and non-thermal responses," *Soft Matter*, vol. 10, no. 17, pp. 3027–3035, 2014, ISSN: 1744683X. DOI: 10.1039/c3sm52454j. [Online]. Available: www.rsc.org/softmatter.

[34] S. Tagliaferri, A. Panagiotopoulos, and C. Mattevi, *Direct ink writing of energy materials*, 2021. DOI: 10.1039/d0ma00753f.

[35] M. Champeau, D. A. Heinze, T. N. Viana, E. R. de Souza, A. C. Chinellato, and S. Titotto, "4D Printing of Hydrogels: A Review," *Advanced Functional Materials*, vol. 30, no. 31, 2020, ISSN: 16163028. DOI: 10.1002/adfm.201910606. [Online]. Available: https://doi.org/10.1002/adfm.201910606..

[36] M. Reiner, *The Deborah Number*, 1964. DOI: 10.1063/1.3051374. [Online]. Available: https://doi.org/10.1063/1.3051374.

[37] D. K. Weissenberg, "A CONTINUUM THEORY OF RHEOLOGICAL PHENOMENA," Tech. Rep., 1947.

[38] A. S. Lodge, "A Network Theory of Constrained Elastic Recovery in Concentrated Polymer Solutions," Tech. Rep., 1958, pp. 2–2.

[39] H. M. Laun, "Prediction of Elastic Strains of Polymer Melts in Shear and Elongation," *Journal of Rheology*, vol. 30, no. 3, pp. 459–501, 1986, ISSN: 0148-6055. DOI: 10.1122/1.549855. [Online]. Available: https://doi.org/10.1122/1.549855.

[40] J. C.-W. Lee, L. Porcar, and S. A. Rogers, "Recovery rheology via rheo-SANS: Application to step strains under out-of-equilibrium conditions," *AIChE Journal*, vol. 65, no. 12, Dec. 2019, ISSN: 15475905. DOI: 10.1002/aic.16797. [Online]. Available: https://onlinelibrary.wiley.com/doi/abs/10.1002/aic.16797.

[41] J. C.-W. Lee, Y.-T. Hong, K. M. Weigandt, E. G. Kelley, H. Kong, and S. A. Rogers, "Strain shifts under stress-controlled oscillatory shearing in theoretical, experimental, and structural perspectives: Application to probing zero-shear viscosity," *Journal of Rheology*, vol. 63, no. 6, pp. 863–881, Nov. 2019, ISSN: 0148-6055. DOI: 10.1122/1.5111358. [Online]. Available: http://sor.scitation.org/doi/10.1122/1.5111358.

[42] G. J. Donley, P. K. Singh, A. Shetty, and S. A. Rogers, "Elucidating the G" overshoot in soft materials with a yield transition via a time-resolved experimental strain decomposition," *Proceedings of the National Academy of Sciences of the United States of America*, vol. 117, no. 36, pp. 21 945–21 952, 2020, ISSN: 10916490. DOI: 10.1073/pnas.2003869117.

[43] P. K. Singh, J. Ching-Wei Lee, K. A. Patankar, and S. A. Rogers, "Distinguishing thixotropy from viscoelasticity," *Citation: Journal of Rheology*, vol. 65, p. 663, 2021. DOI: 10.1122/8.0000154. [Online]. Available: https://sor.scitation.org/toc/jor/65/2.

[44] K. Kamani, G. J. Donley, and S. A. Rogers, "Unification of the Rheological Physics of Yield Stress Fluids," *Physical Review Letters*, vol. 126, no. 21, 2021, ISSN: 10797114. DOI: 10.1103/PhysRevLett.126.218002.

[45] J. C.-W. Lee, K. M. Weigandt, E. G. Kelley, and S. A. Rogers, "Structure-Property Relationships via Recovery Rheology in Viscoelastic Materials," *Physical Review Letters*, vol. 122, no. 24, p. 248 003, Jun. 2019, ISSN: 0031-9007. DOI: 10.1103/PhysRevLett.122.248003. [Online]. Available: https://link.aps.org/doi/10.1103/PhysRevLett.122.248003.

[46] G. J. Donley, W. W. Hyde, S. A. Rogers, and F. Nettesheim, "Yielding and recovery of conductive pastes for screen printing," *Rheologica Acta*, vol. 58, no. 6-7, pp. 361–382, Jul. 2019, ISSN: 00354511. DOI: 10.1007/s00397-019-01148-w. [Online]. Available: https://doi.org/10.1007/s00397-019-01148-w.

[47] P. K. Singh, J. C.-W. Lee, K. A. Patankar, and S. A. Rogers, "Revisiting the basis of transient rheological material functions: Insights from recoverable strain measurements," *Journal of Rheology*, vol. 65, no. 2, pp. 129–144, Mar. 2021, ISSN: 0148-6055. DOI: 10.1122/8.0000154. [Online]. Available: https://sor.scitation.org/toc/jor/65/2.

[48] B. Lonetti, J. Kohlbrecher, L. Willner, J. K. G. Dhont, and M. P. Lettinga, "Dynamic response of block copolymer wormlike micelles to shear flow," *Journal of Physics: Condensed Matter*, vol. 20, no. 40, p. 404 207, Oct. 2008, ISSN: 0953-8984. DOI: 10.1088/0953-8984/20/40/404207. [Online]. Available: https://iopscience.iop.org/article/10.1088/0953-8984/20/40/404207.

[49] C. R. López-Barrón, A. H. Tsou, J. R. Hagadorn, and J. A. Throckmorton, "Highly Entangled α-Olefin Molecular Bottlebrushes: Melt Structure, Linear Rheology, and Interchain Friction Mechanism," *Macromolecules*, vol. 51, no. 17, pp. 6958–6966, 2018, ISSN: 0024-9297. DOI: 10.1021/acs.macromol.8b01431. [Online]. Available: http://pubs.acs.org/doi/10.1021/acs.macromol.8b01431.

[50] M. A. Calabrese, N. J. Wagner, and S. A. Rogers, "An optimized protocol for the analysis of time-resolved elastic scattering experiments," *Soft Matter*, vol. 12, no. 8, pp. 2301–2308, 2016, ISSN: 17446848. DOI: 10.1039/c5sm03039k. [Online]. Available: www.rsc.org/softmatter.

[51] C. G. Lopez, T. Watanabe, A. Martel, L. Porcar, and J. T. Cabral, "Microfluidic-SANS: flow processing of complex fluids," *Scientific Reports*, vol. 5, no. 1, p. 7727, Jul. 2015, ISSN: 2045-2322. DOI: 10.1038/srep07727. [Online]. Available: http://www.nature.com/articles/srep07727.

[52] M. Dinkgreve, J. Paredes, M. M. Denn, and D. Bonn, "On different ways of measuring "the" yield stress," *Journal of Non-Newtonian Fluid Mechanics*, vol. 238, pp. 233–241, Dec. 2016, ISSN: 03770257. DOI: 10.1016/j.jnnfm.2016.11.001.

[53] X. Fan, H. Xu, Q. Zhang, D. Xiao, Y. Song, and Q. Zheng, "Insight into the weak strain overshoot of carbon black filled natural rubber," *Polymer*, vol. 167, pp. 109–117, Mar. 2019, ISSN: 0032-3861. DOI: 10.1016/J.POLYMER.2019.01.076.

[54] C. M. Roland, "Dynamic mechanical behavior of filled rubber at small strains," *Citation: Journal of Rheology*, vol. 34, p. 25, 2037. DOI: 10.1122/1.550111. [Online]. Available: https://sor.scitation.org/toc/jor/34/1.

[55] C. O. Klein, H. W. Spiess, A. Calin, C. Balan, and M. Wilhelm, "Separation of the nonlinear oscillatory response into a superposition of linear, strain hardening, strain softening, and wall slip response," *Macromolecules*, vol. 40, no. 12, pp. 4250–4259, Jun. 2007, ISSN: 00249297. DOI: 10.1021/MA062441U/ASSET/IMAGES/MEDIUM/MA062441UE00009.GIF. [Online]. Available: https://pubs.acs.org/doi/full/10.1021/ma062441u.

[56] C. Christopoulou, G. Petekidis, B. Erwin, M. Cloitre, Vlassopoulos, and D, "Ageing and yield behaviour in model soft colloidal glasses," *Trans. R. Soc. A*, vol. 367, pp. 5051–5071, 2009. DOI: 10.1098/rsta.2009.0166. [Online]. Available: https://royalsocietypublishing.org/.

[57] B. M. Erwin, M. Cloitre, M. Gauthier, and D. Vlassopoulos, "Dynamics and rheology of colloidal star polymers," *Soft Matter*, vol. 6, no. 12, pp. 2825–2833, 2010, ISSN: 17446848. DOI: 10.1039/b926526k. [Online]. Available: www.rsc.org/softmatter.

[58] A. Grand and G. Petekidis, "Effects of particle softness on the rheology and yielding of colloidal glasses," in *Rheologica Acta*, vol. 47, 2008, pp. 579–590. DOI: 10.1007/s00397-007-0254-z.

[59] K. C. Tam, L. Guo, R. D. Jenkins, and D. R. Bassett, "Viscoelastic properties of hydrophobically modified alkali-soluble emulsion in salt solutions," *Polymer*, vol. 40, no. 23, pp. 6369–6379, 1999, ISSN: 00323861. DOI: 10.1016/S0032-3861(98)00857-X.

[60] V. Tirtaatmadja, K. C. Ta, and R. D. Jenkins, "Rheological properties of model alkali-soluble associative (HASE) polymers: Effect of varying hydrophobe chain length," *Macromolecules*, vol. 30, no. 11, pp. 3271–3282, 1997, ISSN: 00249297. DOI: 10.1021/ma961202b. [Online]. Available: https://pubs.acs.org/sharingguidelines.

Chapter 6

Conclusions and Outlook

6.1 Conclusions and Summary

In this thesis, we explore the novel properties exhibited by diblock bottlebrush polymers under flow conditions by combining a range of rheological techniques, neutron scattering, and microscopy to characterize the structure-property-process relations exhibited by bottlebrush polymers. These relations allow us to identify the connections between the flow conditions experienced by the polymer, the microstructure, and the color of the sample. This work is carried out with intended applications in 3D and direct-ink-writing processes in which the color can be controlled simply by adjusting the printing conditions. As such, this work serves as a framework for exploring the properties of a responsive material and developing the structure-property-process relations necessary for on-the-fly property tuning.

We first review the development of highly branched polymers and bottlebrush polymers in the literature, noting the importance of polymer architecture and how slight changes can give rise to a broach range of macroscopic properties [1]–[11]. We also discuss how bottlebrushes have been distinguished from linear and comb polymers in the past due to their lack of entanglements, rapid dynamics, and hierarchical relaxation [12]–[24]. Due to their rapid dynamics, many groups have studied these materials for consideration in photonic applications. These studies predominantly focus on the color of these materials in kinetically trapped and equilibrium states [25]–[34]. We combine these ideas and the rapid dynamics associated with bottlebrush polymers with the understanding that shear and deformation can significantly impact the self-assembled microstructure of a bottlebrush polymer system and lead to new microstructures depending on the intensity of the deformation [35]–[44]. Based on this intersection between rapid dynamics, photonic properties, and shear-induced microstructures, we identify the possibility of developing bottlebrush polymers with microstructures and corresponding photonic properties that can be controlled through careful application of deformation.

Prior to investigating these structure-property-process relations we first worked to develop an understanding of the fundamental shape and size of the bottlebrush polymers as well as the sensitivity of the macroscopic properties of a bottlebrush polymer to changes in its architecture. This work serves as a basis for the structure-property-process relations we develop in this thesis, ensuring we understand the fundamental behavior of this complex molecule. Through intrinsic viscosity and dynamic light scattering measures, we identified how this material behaved under dilute conditions, noting that the molecule is often more collapsed than their linear counter parts in the same solvent. By combining these observations with simulations from our collaborators, we were able to identify that these molecules are reasonably flexible despite the steric

interactions between side chains stiffening the molecule. To probe the sensitivity of these molecules to changes in their architecture, we conducted time-temperature-superposition studies on a bottlebrush with mono-disperse side chain lengths and a bottle brush with bi-disperse side chains. Despite appearing to have a similar molecule weight when characterized via GPC, the two molecules exhibited different relaxation modes and with the uniform side chain bottlebrush having an increased susceptibility, suggesting that the uniform bottlebrush is a softer material than the bottlebrush with bi-disperse side chains. In addition to highlighting how sensitive the bottlebrush can be to changes in architecture, these studies also highlighted some of the limitations of SEC and its inability to distinguish between different architectures in complex molecules. The combination of these two works, establishes a fundamental understanding of how bottlebrush polymers behave and what conformations they might be able to access under flow conditions.

We proceed to explore the structure-property-process relations between the flow conditions applied to bottlebrush polymers, the polymer's microstructure, and photonic properties, through a combination of rheology, neutron scattering, and sample imaging techniques. By exploring all three of these techniques, we are able to identify how steady flow causes the self-assembled lamellae to distort, compress, and eventually develop incoherencies between the layers with increasing shear rates. The highest shear rates applied, were found to cause the incoherent layers to pinch off and rotate to form a lamellae microstructure oriented along the vorticity direction. We were able to relate these changes in microstructure back to changes in the color of the sample observed through Rheo-microscopy thus establishing a structure-property-process relation between the microstructure and sample color and how these can both be tune through flow. In the context of direct-ink-writing processes, this relation highlights how the complex flow environment experienced during printing can impact the self-assembled microstructure and in turn the macroscopic properties of this bottlebrush polymer system.

Having identified the relation between the self-assembled microstructure, bulk color, and flow conditions, we begin to explore the use of this material and this structural control for applications such as direct-ink-writing. As part of this study, we identify the rapid relaxation time exhibited by this material, returning to its quiescent state shortly after sample deformation is stopped. In order to extend the material's memory of its shear history and increase the time over which a shear-induced microstructure is retained, we propose two approaches to increasing the relaxation time. The first approach focuses on locking-in the microstructure through the formation of permanent bonds using a UV activated reaction between the molecules. The second approach considers the viability of using the solid-to-liquid transition observed in yield-stress fluids to impose an effectively infinite relaxation time on the material in its solid-state.

We first consider the UV-crosslinking approach, demonstrating proof of concept by curing the bottlebrush sample under steady stress conditions. By imaging these cured samples after they were removed from the rheometer and allow to sit a zero stress, we demonstrate that we are able to retain a broad range of sample colors and by extension successfully locked through the use of permanent bonds. After establishing proof of concept, we worked towards characterizing the critical gel point and the rate at which these bottlebrush polymers transition from a sol to a gel. Due to several key assumptions in the Winter-Chambon criterion breaking down for this polymer, we were unable to define an exact critical gel point. We were able to measure a rough approximation of the gelation time based on the G', G" crossover point, noting that the polymer cured on approximately the same timescale as the color relaxation time. With this curable bottlebrush polymer system, we also take a closer look at characterizing the gelation point and adjust the method so that the Mutation number, N_{Mu}, is no longer a factor when conducting gelation studies. This change in mentality is achieved through the use of the SPP framework and the transient measures of stress, strain, and strain

rate. By considering these transient values that are only limited by the time resolution of the rheometer, and not on the time it takes to complete an oscillation at a given frequency, this approach improves the range of gelation studies that can be carried out while also improving the accuracy of the reported gelation time.

The second approach of locking in the microstructure through physical means started with us increasing the concentration of the bottlebrush polymer solution in an effort to increase the relaxation time. After doubling the concentration to 350 mg/ml, we identified features in the amplitude sweep and flow curve typically associated with yield-stress fluids. Based on this, we investigated the viability of retaining the shear-induced microstructure through the application of steady shear pulse tests followed by zero stress or zero rate steps. The color relaxation of the material during these tests was on the order of a couple of approximately 1 s, indicating that this approach will not allow us to improve the polymer solution's shear memory and thus its ability to retain a shear-induced microstructure. At the same time, these results highlighted the transient nature of the yielding phenomena, prompting an investigation into the process through the application of recovery rheology. With this technique we were able to decompose the moduli measured in the amplitude sweep into fluid and solid contributions noting how fluid contributions contributed to the behavior of the material at very low strains despite being in the linear regime where solid-like contributions are traditionally thought to dominate. We further investigate the yielding process by calculating the transient Deborah number of the polymer solution as it undergoes oscillatory rheology at different amplitudes. From this analysis we are able to identify points within an oscillation where the material transitions from predominantly elastic behavior to predominantly plastic behavior. We plan to take advantage of the high count rates and well defined structure of the diblock bottlebrush solution when observed through neutron scattering studies to identify the structural changes that give rise to the liquid to solid transition observed during oscillatory shear. While we wait for beamtime for this study, experiments are on going, looking into the recovery rheology of the concentrated bottlebrush solution during shear startup. Through this work, we have observed the bottlebrush collapsing at long times during rapid flow. These results have prompted an investigation into the long term behavior of this material.

6.2 Outlook

In this thesis, we demonstrate the ability to characterize the structure-property-process relation of a diblock bottlebrush polymer solution. By taking advantage of the material's rapid dynamics at high molecular weights, we observe photonic properties that result from the self-assembled microstructure and are tunable through the application of flow and deformation. In the field of bottlebrush polymers, this work estalishes the the wide range of properties that can be achieved with a single bottlebrush polymer and the ability to tune the properties of said material through both processing conditions and changes to the molecular architecture. From a broader perspective, these studies serve as a road map for developing on-the-fly control mechanisms over the bulk properties of a polymer material for applications in direct-ink-writing other processes that involve complex flow conditions. Specifically, by establishing structure-property-process relations between the macroscopic properties, microstructure, and flow, it is possible to dial in specific microstructures and, in turn, bulk properties simply by changing how the material is processed.

Based on this work, a number of future studies are planned both as continuations of the research presented in this thesis and as further investigations into the physical properties of bottlebrush polymers. Ongoing studies using the sequence of physical processes framework to characterize the gelation of a UV curable bottlebrush polymer will allow for gelation studies to be carried out over a broader range of conditions

without being limited by a high N_{Mu}. Structural studies into the yield-stress stress behavior observed in the concentrated bottlebrush polymer solution will serve as the first of their kind, capturing the transient structural changes that occur as a material is undergoing yielding and recovery processes. In the context of direct-ink-writing, experiments are already being considered and carried out to adjust the formulation of the bottlebrush polymer solution in order to obtain an ink that is printable and can be layered to build three dimensional structures.

6.3 References

[1] F. W. Billmeyer, "The Molecular Structure of Polyethylene. III. Determination of Long Chain Branching 1," *Journal of the American Chemical Society*, vol. 75, no. 24, pp. 6118–6122, Dec. 1953, ISSN: 0002-7863. DOI: 10.1021/ja01120a007. [Online]. Available: https://pubs.acs.org/doi/abs/10.1021/ja01120a007.

[2] C. A. Sperati, W. A. Franta, and H. W. Starkweather, "The Molecular Structure of Polyethylene. V. The Effect of Chain Branching and Molecular Weight on Physical Properties," *Journal of the American Chemical Society*, vol. 75, no. 24, pp. 6127–6133, Dec. 1953, ISSN: 0002-7863. DOI: 10.1021/ja01120a009. [Online]. Available: https://pubs.acs.org/doi/abs/10.1021/ja01120a009.

[3] E. van Ruymbeke, H. Lee, T. Chang, *et al.*, "Molecular rheology of branched polymers: decoding and exploring the role of architectural dispersity through a synergy of anionic synthesis, interaction chromatography, rheometry and modeling," *Soft Matter*, vol. 10, no. 27, p. 4762, 2014, ISSN: 1744-683X. DOI: 10.1039/c4sm00105b. [Online]. Available: http://xlink.rsc.org/?DOI=c4sm00105b.

[4] J. Meissner, "Basic Parameters, Melt Rheology, Processing and End-use Properties of Three Similar Low density Polyethylene Samples," *Pure and Applied Chemistry*, vol. 4, pp. 551–574, 1975.

[5] J. Tian, W. Yu, and C. Zhou, "The preparation and rheology characterization of long chain branching polypropylene," *Polymer*, vol. 47, no. 23, pp. 7962–7969, Oct. 2006, ISSN: 00323861. DOI: 10.1016/j.polymer.2006.09.042. [Online]. Available: https://linkinghub.elsevier.com/retrieve/pii/S0032386106011074.

[6] M. H. Wagner, S. Kheirandish, and M. Yamaguchi, "Quantitative analysis of melt elongational behavior of LLDPE/LDPE blends," *Rheologica Acta*, vol. 44, no. 2, pp. 198–218, Dec. 2004, ISSN: 00354511. DOI: 10.1007/s00397-004-0400-9. [Online]. Available: https://link.springer.com/article/10.1007/s00397-004-0400-9.

[7] F. La Mantia, A. Valenza, and D. Acierno, "Influence of the structure of linear density polyethylene on the rheological and mechanical properties of blends with low density polyethylene," *European Polymer Journal*, vol. 22, no. 8, pp. 647–652, Jan. 1986, ISSN: 00143057. DOI: 10.1016/0014-3057(86)90163-1. [Online]. Available: https://linkinghub.elsevier.com/retrieve/pii/0014305786901631.

[8] T. C. B. McLeish, "Molecular rheology of H-polymers," *Macromolecules*, vol. 21, no. 4, pp. 1062–1070, Apr. 1988, ISSN: 0024-9297. DOI: 10.1021/ma00182a037. [Online]. Available: https://pubs.acs.org/doi/abs/10.1021/ma00182a037.

[9] T. C. McLeish, "Polymer architecture influence on rheology," *Current Opinion in Solid State and Materials Science*, vol. 2, no. 6, pp. 678–682, Dec. 1997, ISSN: 13590286. DOI: 10.1016/S1359-0286(97)80009-5. [Online]. Available: https://linkinghub.elsevier.com/retrieve/pii/S1359028697800095.

[10] L. J. Fetters, A. D. Kiss, D. S. Pearson, M. Ag, D. Frankfurt, and F. J. Vitus, "Rheological Behavior of Star-Shaped Polymers," pp. 647–654, 1993.

[11] M. Doi and N. Y. Kuzuu, "Rheology of star polymers in concentrated solutions and melts," *Journal of Polymer Science: Polymer Letters Edition*, vol. 18, no. 12, pp. 775–780, Dec. 1980, ISSN: 03606384. DOI: 10.1002/pol.1980.130181205. [Online]. Available: https://onlinelibrary.wiley.com/doi/full/10.1002/pol.1980.130181205%20https://onlinelibrary.wiley.com/doi/abs/10.1002/pol.1980.130181205%20https://onlinelibrary.wiley.com/doi/10.1002/pol.1980.130181205.

[12] S. Rathgeber, T. Pakula, A. Wilk, K. Matyjaszewski, H. i. Lee, and K. L. Beers, "Bottle-brush macromolecules in solution: Comparison between results obtained from scattering experiments and computer simulations," *Polymer*, vol. 47, no. 20, pp. 7318–7327, Sep. 2006, ISSN: 00323861. DOI: 10.1016/j.polymer.2006.06.010. [Online]. Available: https://www.sciencedirect.com/science/article/pii/S0032386106006872.

[13] S. Dutta, M. A. Wade, D. J. Walsh, D. Guironnet, S. A. Rogers, and C. E. Sing, "Dilute solution structure of bottlebrush polymers," *Soft Matter*, vol. 15, no. 14, pp. 2928–2941, 2019, ISSN: 17446848. DOI: 10.1039/c9sm00033j.

[14] H. Liang, Z. Wang, S. S. Sheiko, and A. V. Dobrynin, "Comb and Bottlebrush Graft Copolymers in a Melt," *Macromolecules*, vol. 52, no. 10, pp. 3942–3950, 2019, ISSN: 15205835. DOI: 10.1021/acs.macromol.9b00611. [Online]. Available: https://pubs.acs.org/sharingguidelines.

[15] H. Liang, G. S. Grest, and A. V. Dobrynin, "Brush-Like Polymers and Entanglements: From Linear Chains to Filaments," *ACS Macro Letters*, vol. 8, no. 10, pp. 1328–1333, 2019, ISSN: 2161-1653. DOI: 10.1021/acsmacrolett.9b00519.

[16] S. J. Dalsin, M. A. Hillmyer, and F. S. Bates, "Molecular weight dependence of zero-shear viscosity in atactic polypropylene bottlebrush polymers," *ACS Macro Letters*, vol. 3, no. 5, pp. 423–427, 2014, ISSN: 21611653. DOI: 10.1021/mz500082h. [Online]. Available: https://pubs.acs.org/sharingguidelines.

[17] S. L. Pesek, Q. Xiang, B. Hammouda, and R. Verduzco, "Small-angle neutron scattering analysis of bottlebrush backbone and side chain flexibility," *Journal of Polymer Science, Part B: Polymer Physics*, vol. 55, no. 1, pp. 104–111, 2017, ISSN: 10990488. DOI: 10.1002/polb.24251.

[18] S. J. Dalsin, M. A. Hillmyer, and F. S. Bates, "Linear Rheology of Polyolefin-Based Bottlebrush Polymers," *Macromolecules*, vol. 48, no. 13, pp. 4680–4691, 2015, ISSN: 15205835. DOI: 10.1021/acs.macromol.5b01153. [Online]. Available: https://pubs.acs.org/sharingguidelines%20http://pubs.acs.org/doi/pdf/10.1021/acs.macromol.5b01153.

[19] M. Hu, Y. Xia, G. B. McKenna, J. A. Kornfield, and R. H. Grubbs, "Linear Rheological Response of a Series of Densely Branched Brush Polymers," *Macromolecules*, vol. 44, no. 17, pp. 6935–6943, Sep. 2011, ISSN: 0024-9297. DOI: 10.1021/ma2009673. [Online]. Available: https://pubs.acs.org/sharingguidelines%20https://pubs.acs.org/doi/10.1021/ma2009673.

[20] C. R. López-Barrón, A. H. Tsou, J. R. Hagadorn, and J. A. Throckmorton, "Highly Entangled α-Olefin Molecular Bottlebrushes: Melt Structure, Linear Rheology, and Interchain Friction Mechanism," *Macromolecules*, vol. 51, no. 17, pp. 6958–6966, 2018, ISSN: 0024-9297. DOI: 10.1021/acs.macromol.8b01431. [Online]. Available: http://pubs.acs.org/doi/10.1021/acs.macromol.8b01431.

[21] I. N. Haugan, M. J. Maher, A. B. Chang, *et al.*, "Consequences of Grafting Density on the Linear Viscoelastic Behavior of Graft Polymers," *ACS Macro Letters*, vol. 7, no. 5, pp. 525–530, 2018, ISSN: 21611653. DOI: 10.1021/acsmacrolett.8b00116. [Online]. Available: http://pubs.acs.org/doi/10.1021/acsmacrolett.8b00116%20https://pubs.acs.org/sharingguidelines.

[22] C. R. López-Barrón, M. E. Shivokhin, and J. R. Hagadorn, "Extensional rheology of highly-entangled α-olefin molecular bottlebrushes," *Journal of Rheology*, vol. 63, no. 6, pp. 917–926, 2019, ISSN: 0148-6055. DOI: 10.1122/1.5110557.

[23] M. Abbasi, L. Faust, and M. Wilhelm, "Comb and Bottlebrush Polymers with Superior Rheological and Mechanical Properties," *Advanced Materials*, vol. 31, no. 26, p. 1 806 484, Feb. 2019, ISSN: 15214095. DOI: 10.1002/adma.201806484. [Online]. Available: http://doi.wiley.com/10.1002/adma.201806484.

[24] H. Liang, B. J. Morgan, G. Xie, *et al.*, "Universality of the Entanglement Plateau Modulus of Comb and Bottlebrush Polymer Melts," *Macromolecules*, vol. 51, no. 23, pp. 10 028–10 039, Dec. 2018, ISSN: 0024-9297. DOI: 10.1021/acs.macromol.8b01761. [Online]. Available: https://pubs.acs.org/sharingguidelines%20https://pubs.acs.org/doi/10.1021/acs.macromol.8b01761.

[25] A. L. Liberman-Martin, C. K. Chu, and R. H. Grubbs, "Application of Bottlebrush Block Copolymers as Photonic Crystals," *Macromolecular Rapid Communications*, vol. 38, no. 13, p. 1 700 058, Jul. 2017, ISSN: 10221336. DOI: 10.1002/marc.201700058. [Online]. Available: http://doi.wiley.com/10.1002/marc.201700058%20www.advancedsciencenews.com.

[26] C. M. Bates and F. S. Bates, "50th Anniversary Perspective : Block Polymers—Pure Potential," *Macromolecules*, vol. 50, no. 1, pp. 3–22, Jan. 2017, ISSN: 0024-9297. DOI: 10.1021/acs.macromol.6b02355. [Online]. Available: https://pubs.acs.org/doi/10.1021/acs.macromol.6b02355.

[27] B. M. Boyle, T. A. French, R. M. Pearson, B. G. McCarthy, and G. M. Miyake, "Structural Color for Additive Manufacturing: 3D-Printed Photonic Crystals from Block Copolymers," *ACS Nano*, vol. 11, no. 3, pp. 3052–3058, Mar. 2017, ISSN: 1936-0851. DOI: 10.1021/acsnano.7b00032. [Online]. Available: http://pubs.acs.org/doi/10.1021/acsnano.7b00032.

[28] G. M. Miyake, R. A. Weitekamp, V. A. Piunova, and R. H. Grubbs, "Synthesis of isocyanate-based brush block copolymers and their rapid self-assembly to infrared-reflecting photonic crystals," *Journal of the American Chemical Society*, vol. 134, no. 34, pp. 14 249–14 254, 2012, ISSN: 00027863. DOI: 10.1021/ja306430k. [Online]. Available: https://pubs.acs.org/sharingguidelines.

[29] G. M. Miyake, V. A. Piunova, R. A. Weitekamp, and R. H. Grubbs, "Precisely tunable photonic crystals from rapidly self-assembling brush block copolymer blends," *Angewandte Chemie - International Edition*, vol. 51, no. 45, pp. 11 246–11 248, Nov. 2012, ISSN: 14337851. DOI: 10.1002/anie.201205743. [Online]. Available: http://doi.wiley.com/10.1002/anie.201205743.

[30] R. J. Macfarlane, B. Kim, B. Lee, *et al.*, "Improving brush polymer infrared one-dimensional photonic crystals via linear polymer additives," *Journal of the American Chemical Society*, vol. 136, no. 50, pp. 17 374–17 377, Dec. 2014, ISSN: 15205126. DOI: 10.1021/ja5093562. [Online]. Available: https://pubs.acs.org/sharingguidelines%20https://pubs.acs.org/doi/10.1021/ja5093562.

[31] C. G. Chae, Y. G. Yu, H. B. Seo, M. J. Kim, R. H. Grubbs, and J. S. Lee, "Experimental Formulation of Photonic Crystal Properties for Hierarchically Self-Assembled POSS-Bottlebrush Block Copolymers," *Macromolecules*, vol. 51, no. 9, pp. 3458–3466, 2018, ISSN: 15205835. DOI: 10.1021/acs.macromol.8b00298.

[32] M. B. Runge and N. B. Bowden, "Synthesis of High Molecular Weight Comb Block Copolymers and Their Assembly into Ordered Morphologies in the Solid State," 2007. DOI: 10.1021/ja072929q. [Online]. Available: https://pubs.acs.org/sharingguidelines.

[33] B. R. Sveinbjörnsson, R. A. Weitekamp, G. M. Miyake, *et al.*, "Rapid self-assembly of brush block copolymers to photonic crystals," *Proceedings of the National Academy of Sciences of the United States of America*, vol. 109, no. 36, pp. 14 332–14 336, 2012, ISSN: 00278424. DOI: 10.1073/pnas.1213055109. [Online]. Available: www.pnas.org/lookup/suppl/.

[34] B. B. Patel, D. J. Walsh, D. H. Kim, *et al.*, "Tunable structural color of bottlebrush block copolymers through direct-write 3D printing from solution," *Science Advances*, vol. 6, no. 24, In Press, Jun. 2020, ISSN: 2375-2548. DOI: 10.1126/sciadv.aaz7202. [Online]. Available: http://advances.sciencemag.org/%20https://www.science.org/doi/10.1126/sciadv.aaz7202.

[35] D. E. Angelescu, J. H. Waller, R. A. Register, and P. M. Chaikin, "Shear-Induced Alignment in Thin Films of Spherical Nanodomains," *Advanced Materials*, vol. 17, no. 15, pp. 1878–1881, Aug. 2005, ISSN: 1521-4095. DOI: 10.1002/ADMA.200401994. [Online]. Available: https://onlinelibrary.wiley.com/doi/full/10.1002/adma.200401994%20https://onlinelibrary.wiley.com/doi/abs/10.1002/adma.200401994%20https://onlinelibrary.wiley.com/doi/10.1002/adma.200401994.

[36] K. I. Winey, S. S. Patel, R. G. Larson, and H. Watanabe, "Interdependence of Shear Deformations and Block Copolymer Morphology," *Macromolecules*, vol. 26, no. 10, pp. 2542–2549, 1993, ISSN: 15205835. DOI: 10.1021/ma00062a024.

[37] A. Nikoubashman, R. A. Register, and A. Z. Panagiotopoulos, "Sequential Domain Realignment Driven by Conformational Asymmetry in Block Copolymer Thin Films," *Macromolecules*, vol. 47, no. 3, pp. 1193–1198, Feb. 2014, ISSN: 0024-9297. DOI: 10.1021/ma402526q. [Online]. Available: https://pubs.acs.org/doi/10.1021/ma402526q.

[38] A. P. Marencic and R. A. Register, "Controlling Order in Block Copolymer Thin Films for Nanopatterning Applications," *Annual Review of Chemical and Biomolecular Engineering*, vol. 1, no. 1, pp. 277–297, Jun. 2010, ISSN: 1947-5438. DOI: 10.1146/annurev-chembioeng-073009-101007. [Online]. Available: https://www.annualreviews.org/doi/10.1146/annurev-chembioeng-073009-101007.

[39] A. S. Wunenburger, A. Colin, T. Colin, and D. Roux, "Undulation instability under shear: A model to explain the different orientations of a lamellar phase under shear?" *European Physical Journal E*, vol. 2, no. 3, pp. 277–283, 2000, ISSN: 12928941. DOI: 10.1007/PL00013669. [Online]. Available: https://link.springer.com/content/pdf/10.1007%2FPL00013669.pdf.

[40] O. Diat, D. Roux, and F. Nallet, "Effect of shear on a lyotropic lamellar phase," *Journal de Physique II*, vol. 3, no. 9, pp. 1427–1452, 1993, ISSN: 1427-1452. DOI: 10.1051/jp2:1993211{\"{i}}. [Online]. Available: https://hal.archives-ouvertes.fr/jpa-00247917.

[41] J. Raeburn, A. Z. Cardoso, and D. J. Adams, "The importance of the self-assembly process to control mechanical properties of low molecular weight hydrogels," *Chemical Society Reviews*, vol. 42, no. 12, pp. 5143–5156, 2013, ISSN: 14604744. DOI: 10.1039/c3cs60030k.

[42] G. Qu, J. J. Kwok, and Y. Diao, "Flow-Directed Crystallization for Printed Electronics," *Accounts of Chemical Research*, vol. 49, no. 12, pp. 2756–2764, 2016, ISSN: 15204898. DOI: 10.1021/acs.accounts.6b00445.

[43] Y. Diao, L. Shaw, Z. Bao, and S. C. B. Mannsfeld, "Morphology control strategies for solution-processed organic semiconductor thin films," *Energy and Environmental Science*, vol. 7, no. 7, pp. 2145–2159, 2014, ISSN: 17545706. DOI: 10.1039/c4ee00688g.

[44] R. C. Hayward and D. J. Pochan, "Tailored assemblies of block copolymers in solution: It is all about the process," *Macromolecules*, vol. 43, no. 8, pp. 3577–3584, 2010, ISSN: 00249297. DOI: 10.1021/ma9026806.

Appendix A

Supplementary Materials for Chapter 2 [1]

A.1 Material Synthesis and Characterization

Synthesis and characterization of the diblock bottlebrush polymer used in Chapter 2 was carried out by Dr. Dylan Walsh from the Guironnet group. Further details regarding the synthesis, NMR spectra, and impurity concentrations were carried out by Dylan and can be found in more detail in the supporting information of Wade et al. [1], [2].

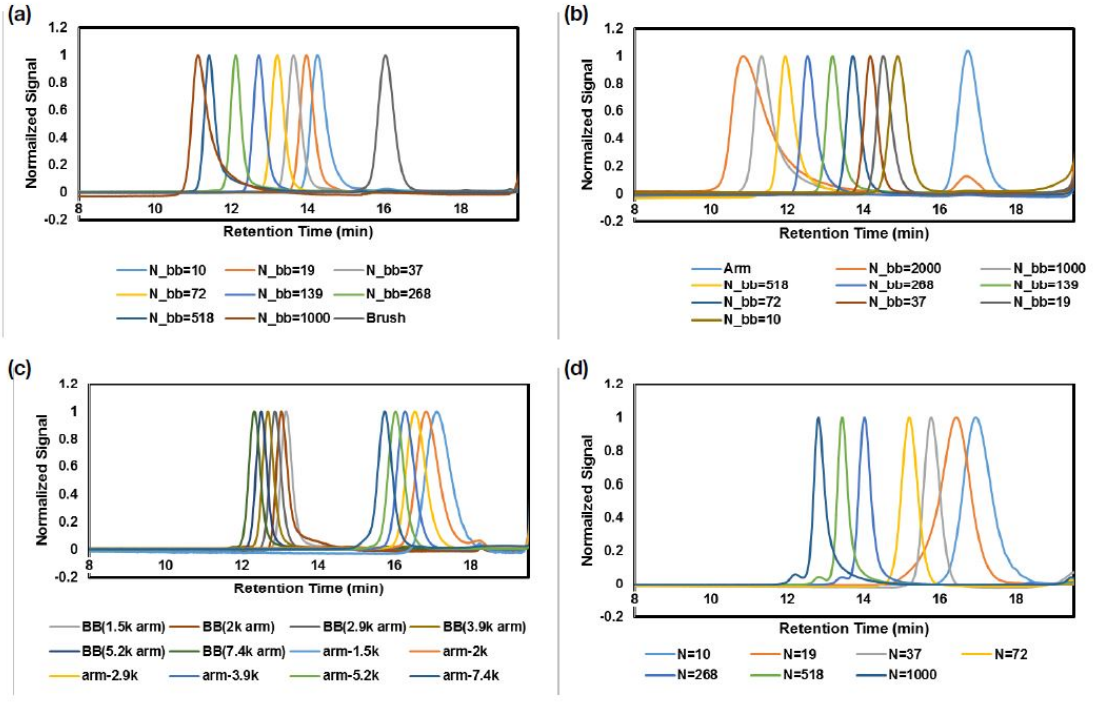

Figure A.1: GPC chromatograms: a) backbone length sweep for long sidechains; b) backbone length sweeps for short side chains; c) side chain sweep with constant n_{bb}; d) sweep for 5-norbornene-2(methylbenzoate).

[1] This appendix has been adapted from the following publication with permission: [1], [2]

A.2 Huggins and Kraemer Fits to Calculate Intrinsic Viscosity

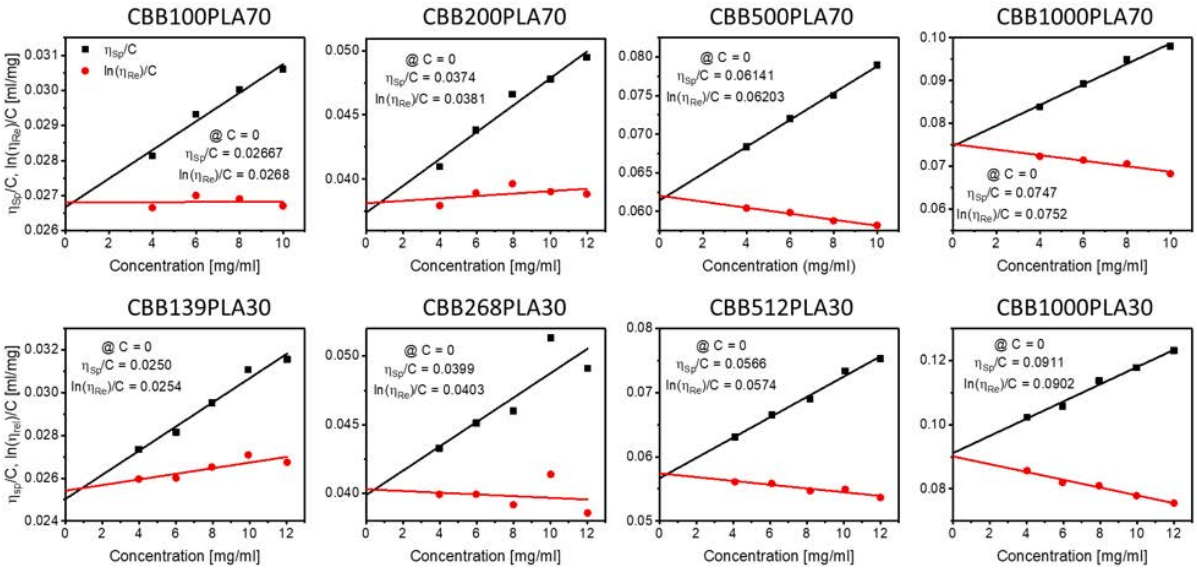

Figure A.2: Viscosity measurements for an select set of bottlebrush polymers fitted using the Huggins (black) and Kraemer (red) equations. Labels above each plot correspond to the bottlebrush sample used to collect the data in each plot. The value of both fits extrapolated to zero is included in each plot.

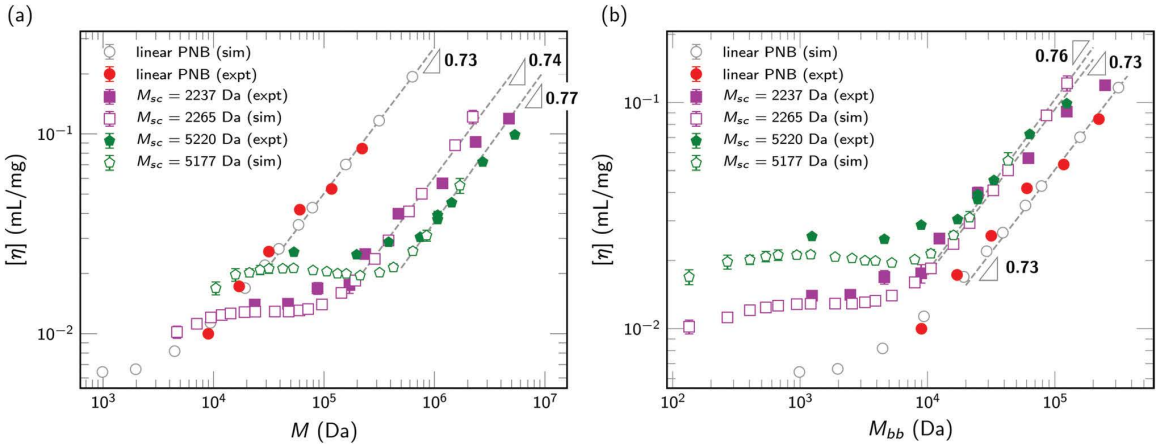

Figure A.3: Intrinsic viscosity $[\eta]$ as a function of bottlebrush molecular weight. Filled symbols denote experimental measurements at 30 °C and unfilled symbols denote simulation results. The dashed lines are fits to the simulation data. (a) $[\eta]$ vs. M for both experimental and simulation data; (b) $[\eta]$ vs. M_{bb} for both experimental and simulation data. Figure assembled by Dr. Dutta for [1]. Reprinted with permission.

A.3 Calculation of Hydrodynamic Radius

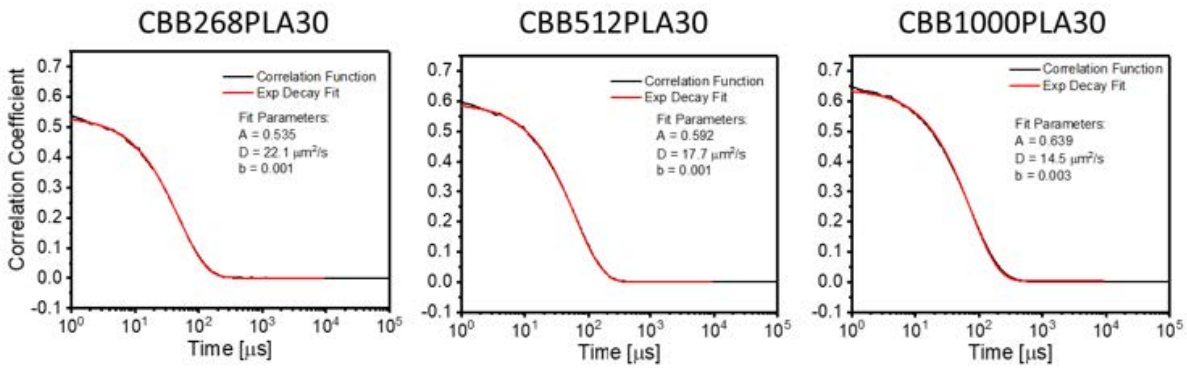

Figure A.4: Autocorrelation data extracted from the Zetasizer software package for a sample set of data (black). Data were fitted according to a modified version of equation 2.4. All samples presented were at concentrations of 12 mg/mL.

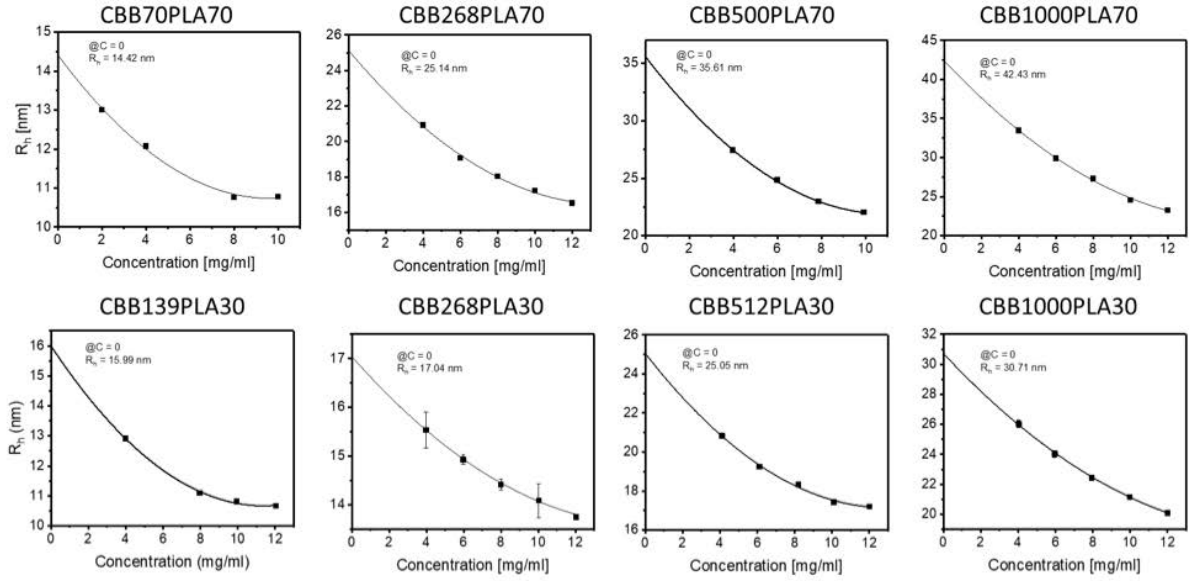

Figure A.5: SEC Traces for graft-through polymerization with different arm dispersities. (SEC data is from conventional calibration with respect to PS standards).

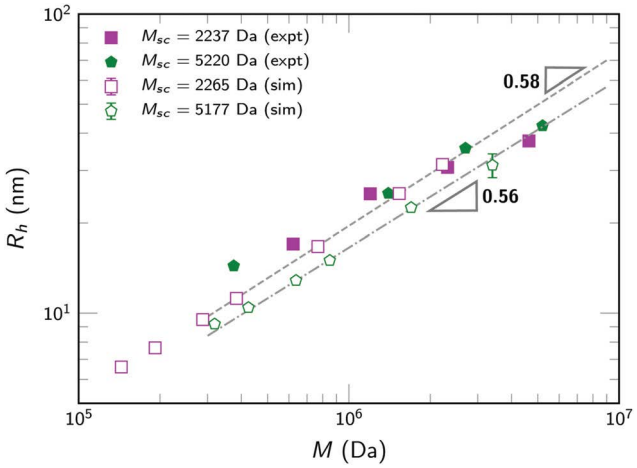

Figure A.6: Hydrodynamic radius as a function of bottlebrush molecular weight. Filled symbols denote experimental measurements and unfilled symbols denote simulation results. The dashed lines are fits to the simulation data. Figure assembled by Dr. Dutta for [1]. Reprinted with permission.

Appendix B

Supplementary Materials for Chapter 3 [1]

B.1 Polymer Characterization and Synthesis

Synthesis and characterization of the diblock bottlebrush polymer used in Chapter 3 was carried out by Dr. Dylan Walsh and Yash Kamble from the Guironnet group. We include a short description of the characterization and synthesis of these polymers. Further details regarding the arm synthesis, NMR spectra, and impurity concentrations were carried out by Dylan and Yash and can be found in more detail in the supporting information of Wade et al. [1].

B.1.1 Polymer Characterization Methods

All reactions were performed in an argon-filled glovebox ($O^2 < 2$ ppm, $H_2O < 0.5$ ppm) at room temperature using oven-dried glassware. THF, toluene, and DCM was dried using a commercial solvent purification system. rac-Lactide Aldrich, sec-butyllithium solution 1.3 mol/L in cyclohexane/hexane (92/8),ACROS Organics and ethylene oxide solution (2.5-3.3 mol/L in THF, Aldrich) was used as received. 1,8-diazabicyclo[5.4.0]undec-7-ene (DBU) Aldrich was distilled over CaH_2 and storage under argon at -20 °C. Styrene was pass through neutral alumina plug and stored under argon at -20 °C. [(H2IMes)(3-Brpy) 2(Cl)2Ru=CHPh], G3 was synthesized according to literature [2]. Exo-5-Norbornene-2-carboxylic acid and exo-5-Norbornene-2-methanol was synthesized according to literature [3].

Conventional Gel Permeation Chromatography (GPC) was performed using a Tosoh Ecosec HLC- 8320GPC at 40 °C fitted with a guard column (6.0 mm ID x 4.0 cm), and two analytical columns (TSKgel GMHHR-H, 7.8 mm ID x 30 cm x 5 µm). A flow rate of 1.0 mL/min was used. THF (HPLC grade) was used as the eluent, and polystyrene standards (15 points ranging from 500 Mw to 8.42 million Mw) were used as the general calibration. An additional calibration was created for specifically for linear polylactic acid and only used for linear polylactic acid (10 points ranging from 500 Mw to 10,000 Mw). UV detector was recorded at 266 nm.

Absolute molecular weight was obtained with a Tosoh Ecosec HLC-8320GPC and LenS3 Multi-Angle Light Scattering Detector at 40 °C fitted with a guard column (6.0 mm ID x 4.0 cm x 5 µm), and two analytical columns (TSKgel Alpha-M, 7.8 mm ID x 30 cm). THF (HPLC grade) was used as the eluent and a flow rate of 0.6 mL·min-1 was used. The detectors were calibrated with a narrow polystyrene standard (Mw= 99,000 Da). Polymer solutions were prepared at a known concentration (ca. 3 mg/mL) and an injection

[1] This appendix has been adapted from the following publication with permission: [3]

volume of 20 μL was used. dn/dc values for the bottlebrush polymers were obtained for each injection by assuming 100% mass elution from the columns.

B.1.2 Representative Synthesis of PS-b-PLA Bottlebrush Polymers

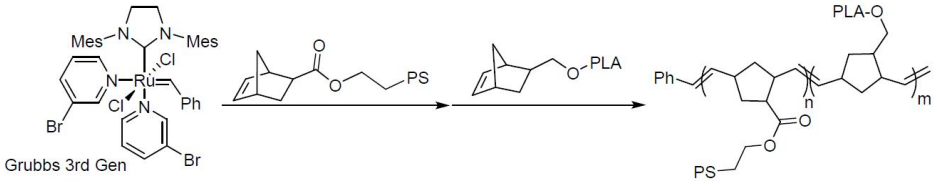

Figure B.1: A summary of the reaction used to manufacture PS-b-PLA bottlebrush polymers.

The synthesis of PLA macromonomers was performed just prior to the diblock bottlebrush synthesis so that the quenched ROP reaction mixture could be added directly into the graft-through ROMP polymerizations to form the second block. This method was used instead of isolated PLA macromonomers because low molecular weights ($<$ 5,000 g/mol) do not precipitate well, making it challenging to recover pure PLA macromonomers.

B.1.2.1 Procedure for the Synthesis of PLA Macromonomers

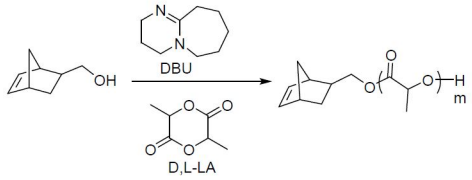

Figure B.2: Synthesis of PLA macromonomers.

The procedure for the ring opening polymerization (ROP) of lactide has been adapted from the previous work of the Guironnet group [4], [5].

To an oven-dried 20 mL glass vial, lactide (1.4g, 9.71 mmol) and exo-5-Norbornene-2-methanol (30.2 mg, 0.243 mmol) dissolved in 8.7 mL of THF. The polymerization was initiated by adding DBU (7.38 mg, 0.0485 mmol) dissolved in 1 mL of THF. This reaction mix for 60 min at which time B(OH)3 (60.0 mg, 0.969 mmol) in 4 ml of THF was added to the reaction mixture. An aliquot was removed for GPC and NMR analysis. (This crude reaction mixture will contain 1 g of PLA macromonomers and will be added directly into the graft-through ROMP.) $M_{n,GPC}$ = 4,200 g/mol; Đ=1.05. Note: In order to get $B(OH)_3$ to dissolve into THF, the solution was heated to 80-90 °C till all the $B(OH)_3$ dissolved and allowed to cool back to room temperature before use. Avoid rapid cooling of the solution, as it will cause $B(OH)_3$ to drop out of solution.

B.1.2.2 Procedure for the Graft-Through ROMP

In an oven-dried 20 mL glass vial, PS macromonomer (1000 mg, 0.22) was dissolved into THF (6 ml). The polymerization is initiated by adding G3 via a stock solution (0.5 ml add of: 5 mg G3 in 2.55 ml THF stock solution; 0.98 mg, 0.0011 mmol resulting in a total backbone length 400). After 10 mins, an aliquot was taken

and injected into 1 ml of THF with a large excess of ethyl vinyl ether for GPC analysis of the first block. Then, the crude PLA macromonomer from above was added and allow to react for 30 min before a large excess of vinyl ether was added. The polymer was obtained by precipitating into methanol twice and dried under vacuum.

Table B.1: Characterization data for PS-PLA diblock bottlebrush (PS: 4.5 kg/mol; PLA: 4.2 kg/mol, 50 wt% PS).

n_{bb}	M_n (kg/mol)	M_w/M_n	Monomer Conversion	Block Length PS:PLA
400	610	1.03	>98%	196:210

Table B.2: Composition of synthesized PS-PLA bottlebrush sample by Wt %

Diblock Bottlebrush	PLA Bottlebrush	PLA Brush	PS Brush
94	4	>1	2

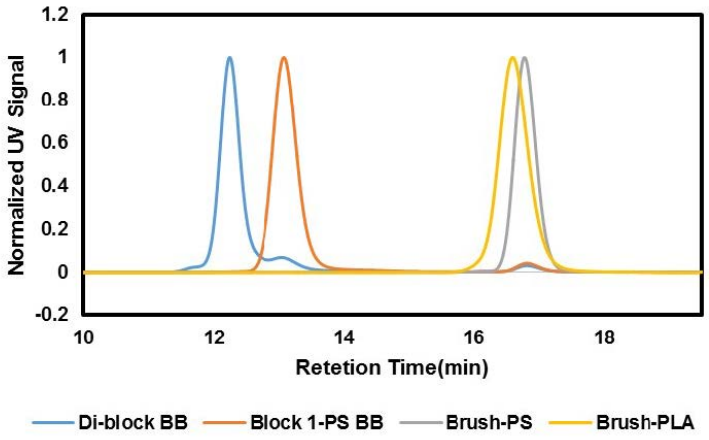

Figure B.3: UV-GPC traces for the synthesis of PS-b-PLA diblock bottlebrush.

B.2 Impact of Deutrerated Solvents on Rheology

Lopez-Barron, et al demonstrated the differences between protonated and deuterated solvents can have a significant impact on the assembly of worm-like micelles [6]. We characterized the linear rheology and steady shear response of PS-PLA diblock bottlebrush dispersed in both solvents to confirm that the differences between protonated and deuterated toluene did not have any significant impact on the reported observations. Measurements for the protonated toluene sample were carried out on an Anton-Paar MCR 702 with a 43 mm parallel plate, while measurements for the deuterated toluene sample were conducted on an Anton-Paar MCR 501 in a Couette cell with a 50 mm cup and a 48 mm bob. As can be seen in Figure B.4, both the frequency and flow sweeps were found to be comparable with similar trends across the tested range of shear rates and frequencies. Data are observed to be offset by approximately 30%, which is comparable to observations made by Lopez-Barron, et al and Mukerjee, et al [6], [7].

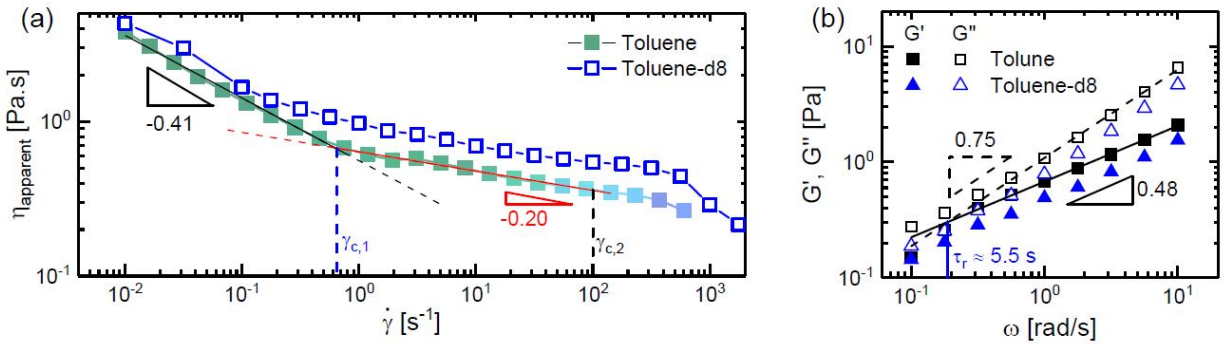

Figure B.4: (a) Flow sweeps for polymer dispersed in toluene and toluene-d8. (b) Frequency sweeps for polymer dispersed in toluene and toluene-d8.

B.3 Analyzing 2D Small Angle Scattering Data

Azimuthal and sector averages were performed to quantify the exact location, width, and azimuthal smearing of the peaks observed in the 2D scattering data. Diagrams depicting how these averages were performed are shown in Figures 3.8, 3.10, and 3.12. Azimuthal averages were centered at the peaks located at q^* and q_p to quantify the alignment of the bottlebrushes and the alignment of the self-assembled lamellae, respectively. The width of the average was set to 0.01 Å^{-1} when centered at q^* and 0.001 Å^{-1} when centered at q_p such that the majority of the peak was captured when performing the average. Sector averages were carried out across the entire q range, encompassing data located on both the front and back set of detectors. The width of the sector averages was set to 15 ° to the center of the peak while simultaneously limiting the effects of azimuthal smearing on the average. Sector averages were conducted along the gradient direction in the 2-3 scattering plane and along the vorticity direction in the 1-3 scattering plane. Sector averages were also taken along the vorticity direction in the 2-3 scattering plane but were found to match the sector averages taken in the 1-3 plane. As such these sector averages are not reported. All averages and data reduction were conducted SANS reduction software protocols provided by NIST [8].

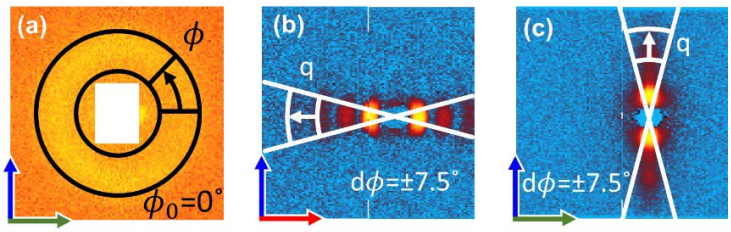

Figure B.5: Blown up inset images from figures Figures 3.8, 3.10, and 3.12 highlighting the region on the 2D scattering data characterized by (a) azimuthal sweeps, (b) sector averages at 0°, and (c) sector averages at 90°.

To quantify how shear rate affected the exact location of the primary lamellae peak and relative dispersity of the lamellae spacing, 5 gaussian peaks were fit to the sector averages taken along the gradient and vorticity directions as shown in Figure B.6. A constant baseline was used during this fitting to simplify the fitting process. The value of this baseline was selected such that the 5th peak, q^*, corresponding to the interaction

distance between bottlebrush backbones was isolated from the other peaks. Characterization of the lamellae spacing and dispersity was done carried out with the primary lamellae peak q_p due to the calculated standard error reported by OriginPro being significantly higher for the higher order peaks.

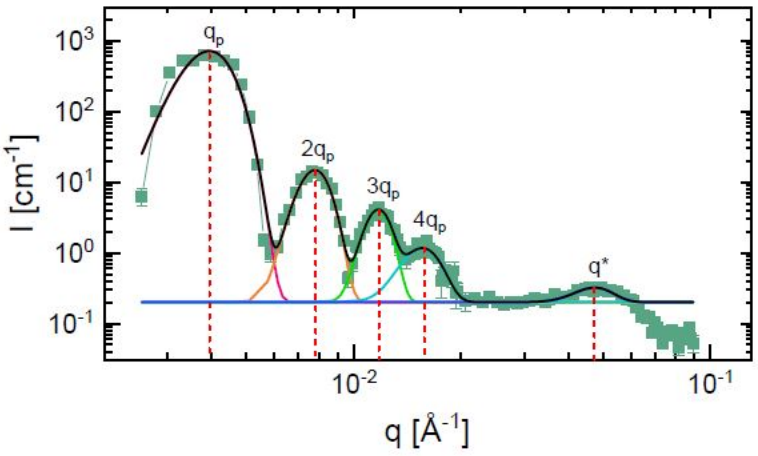

Figure B.6: 5 gaussian peaks fit to the sector average taken during quiescence in the 2-3 originally plotted in Figure 3.10.a. The term q_p represents the primary lamellar peak with subsequent peaks labeled according to the integer multiple. The peak labeled q^* corresponds to the intramolecular interaction peak observed at high q. Red dashed lines serve as guides to the eye, highlighting the location of the peak center.

B.4 Disclaimer for Chapter 3

Any mention of commercial products in this manuscript are for information only and does not imply endorsement by NIST.

B.5 References

[1] M. A. Wade, D. Walsh, J. C. W. Lee, *et al.*, "Color, Structure, and Rheology of a Diblock Bottlebrush Copolymer Solution," *Soft Matter*, vol. 16, no. 21, pp. 4919–4931, Jun. 2020, ISSN: 17446848. DOI: 10.1039/d0sm00397b. [Online]. Available: https://pubs.rsc.org/en/content/articlehtml/2020/sm/d0sm00397b%20https://pubs.rsc.org/en/content/articlelanding/2020/sm/d0sm00397b.

[2] J. A. Love, J. P. Morgan, T. M. Trnka, and R. H. Grubbs, "A Practical and Highly Active Ruthenium-Based Catalyst that Effects the Cross Metathesis of Acrylonitrile," *Angewandte Chemie International Edition*, vol. 41, no. 21, pp. 4035–4037, Nov. 2002, ISSN: 1433-7851. DOI: https://doi.org/10.1002/1521-3773(20021104)41:21<4035::AID-ANIE4035>3.0.CO;2-I. [Online]. Available: https://doi.org/10.1002/1521-3773(20021104)41:21%3C4035::AID-ANIE4035%3E3.0.CO%202-I.

[3] S. C. Radzinski, J. C. Foster, R. C. Chapleski, D. Troya, and J. B. Matson, "Bottlebrush Polymer Synthesis by Ring-Opening Metathesis Polymerization: The Significance of the Anchor Group," *Journal of the American Chemical Society*, vol. 138, no. 22, pp. 6998–7004, Jun. 2016, ISSN: 15205126. DOI: 10.1021/jacs.5b13317. [Online]. Available: https://pubs.acs.org/doi/10.1021/jacs.5b13317%20https://pubs.acs.org/sharingguidelines.

[4] D. J. Walsh and D. Guironnet, "Macromolecules with programmable shape, size, and chemistry," *Proceedings of the National Academy of Sciences of the United States of America*, vol. 116, no. 5, pp. 1538–1542, Jan. 2019, ISSN: 10916490. DOI: 10.1073/pnas.1817745116.

[5] S. Dutta, M. A. Wade, D. J. Walsh, D. Guironnet, S. A. Rogers, and C. E. Sing, "Dilute solution structure of bottlebrush polymers," *Soft Matter*, vol. 15, no. 14, pp. 2928–2941, 2019, ISSN: 17446848. DOI: 10.1039/c9sm00033j.

[6] C. R. López-Barrón and N. J. Wagner, "Solvent isotope effect on the microstructure and rheology of cationic worm-like micelles near the isotropic-nematic transition," *Soft Matter*, vol. 7, no. 22, pp. 10 856–10 863, 2011, ISSN: 1744-683X. DOI: 10.1039/c1sm05878a. [Online]. Available: http://xlink.rsc.org/?DOI=c1sm05878a.

[7] P. Mukerjee, P. Kapauan, and H. G. Meyer, "Micelle formation and hydrophobic bonding in deuterium oxide," *Journal of Physical Chemistry*, vol. 70, no. 3, pp. 783–786, 1966, ISSN: 00223654. DOI: 10.1021/j100875a029.

[8] S. R. Kline, "Reduction and analysis of SANS and USANS data using IGOR Pro," *Journal of Applied Crystallography*, vol. 39, no. 6, pp. 895–900, Dec. 2006, ISSN: 00218898. DOI: 10.1107/S0021889806035059.

Appendix C

Supplementary Materials for Chapter 5

C.1 Preparation of Functionalized Bottlebrush Polymers

For the materials studied in this chapter, Yash Kamble, from the Guironnet group, synthesized functionalized diblock bottlebrush polymers with a thiol-ene click chemistry for the purposes of UV-crosslinking studies. The choice to use this reaction scheme was motivated by the high yield of this reaction and the ability to trigger the reaction by UV light (in presence of a photo initiator). Kamble et al., developed a post-polymerization modification technique to introduce crosslinking groups (allyl) at the tips of the PLA brushes of PS-b-PLA BB copolymers, shown in Figure C.3. The molecular weight distribution of the polymer remained unchanged through the post-polymerization reaction (as evident from the Gel Permeation Chromatography in Figure C.2) and the integration of the allyl protons in the 1H NMR spectrum suggested that >95% of the PLA brushes were allyl terminated. A diagram outlining the reaction of these polymers to form a networked gel can be seen in Figure C.1

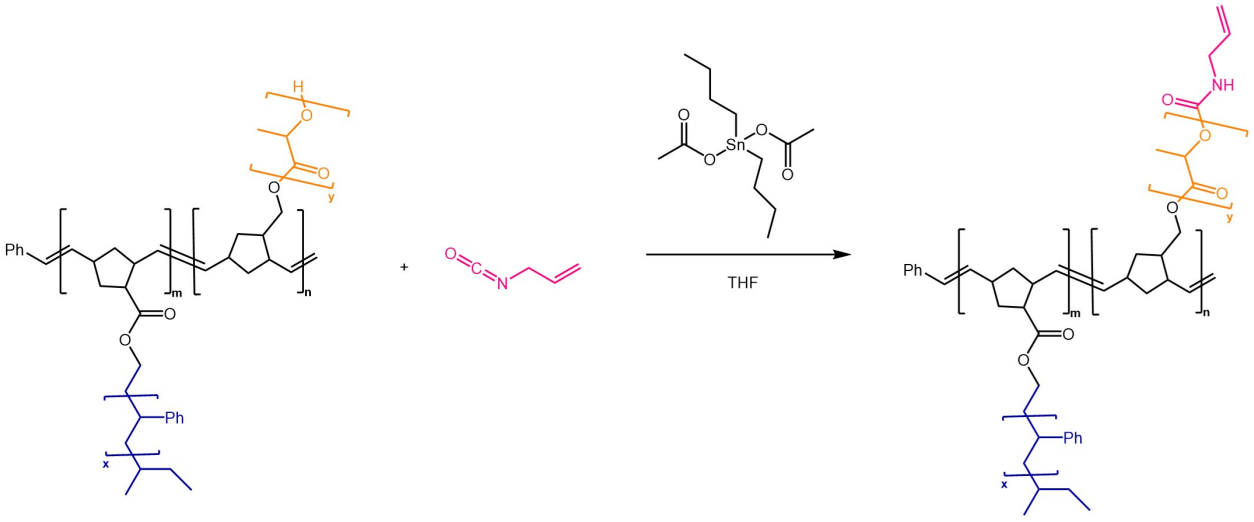

Figure C.1: Reaction scheme for the functionalization of PS-b-PLA bottlebrush with alcohol-isocyanate coupling.

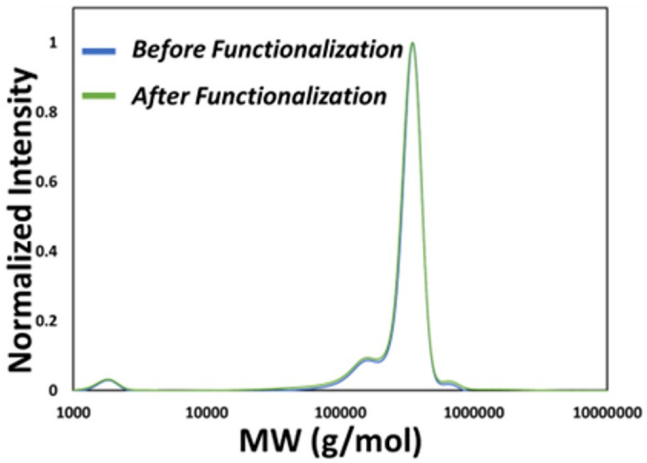

Figure C.2: Gel Permeation Chromatography results for functionalized and unfunctionalized diblock bottlebrush polymers. The addition of the functional group had little to no impact on the measured molecular weight as higlighted by the similarities between the two curves.

Table C.1: Characterization data for functionalized PS-PLA diblock bottlebrush (PS: 4.5 kg/mol; PLA: 3.6 kg/mol, 55 wt% PS).

n_{bb}	M_n (kg/mol)	M_w/M_n	Monomer Conversion	Block Length PS:PLA
436	522	1.14	97%	200:236

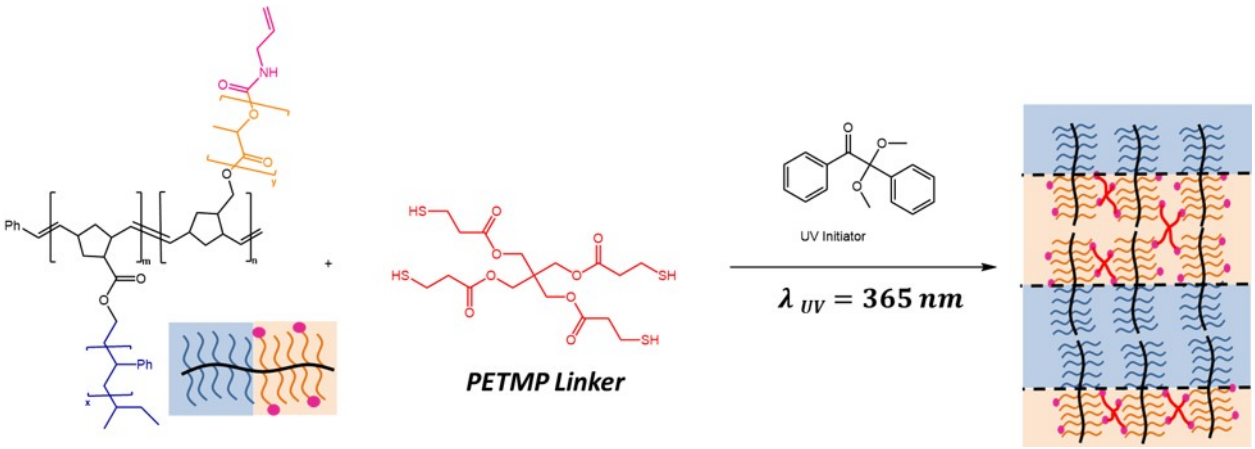

Figure C.3: Crosslinking of allyl functionalized PS-b-PLA diblock bottlebrush polymer in presence of PETMP linker and DMPA UV initiator.

Table C.2: Composition of synthesized PS-PLA bottlebrush sample by Wt %

PS-PLA Diblock Bottlebrush	PS-PLA-PS Triblock Bottlebrush	PLA Bottlebrush	PS Brushes
84	7	8	1

C.2 Color Relaxation at Additional Shear Rates

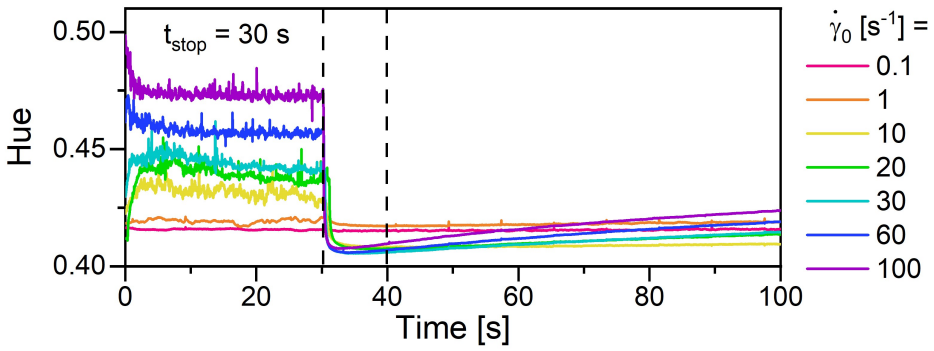

Figure C.4: The color recovery observed after shearing the bottlebrush polymer for 30 s. Rates from 0.1 to 100 s^{-1} were tested with more emphasis placed on the higher shear rates as this resulted in the most significant color change. Dashed lines are shown to serve as guides to the eye, indicating where the shear rate was stopped and the time after which the material had recovered 99% of its original color.

Videos depicting the bottlebrush polymer solution during shear cessation as shown in Figure C.4 have been included with this thesis as supplemental files. The video files are labled according to the applied shear rate prior to cessation. A list of all files, and their corresponding file names is as follows:

- $\dot{\gamma} = 0.1$ s^{-1} ColorCessation_ShearRate_0.1s-1.wmv
- $\dot{\gamma} = 1$ s^{-1} ColorCessation_ShearRate_1s-1.wmv
- $\dot{\gamma} = 10$ s^{-1} ColorCessation_ShearRate_10s-1.wmv
- $\dot{\gamma} = 20$ s^{-1} ColorCessation_ShearRate_20s-1.wmv
- $\dot{\gamma} = 30$ s^{-1} ColorCessation_ShearRate_30s-1.wmv
- $\dot{\gamma} = 60$ s^{-1} ColorCessation_ShearRate_60s-1.wmv
- $\dot{\gamma} = 100$ s^{-1} ColorCessation_ShearRate_100s-1.wmv

C.3 Supplemental Data for Gelation Studies

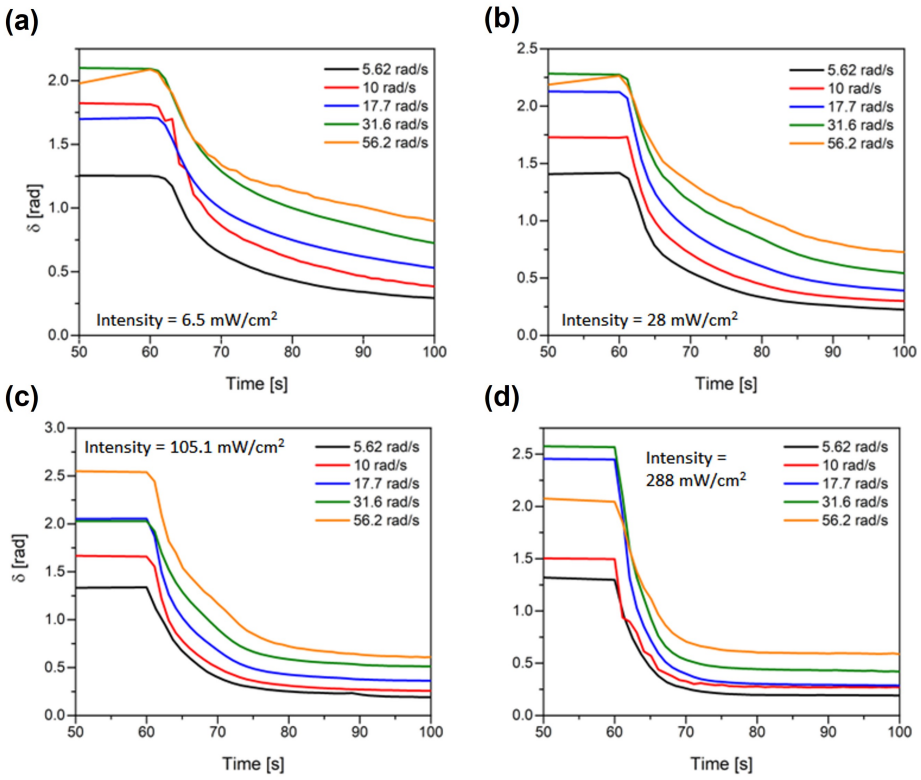

Figure C.5: Calculated phase angles during gelation for frequencies from 5.62 to 56.2 rad/s. Gelation studies were carried out at UV light intensities of a) 6.5, b) 28, c) 105.1, and d) 288 mW/cm^2. Corresponding G' and G" can be found in Figure 4.5.

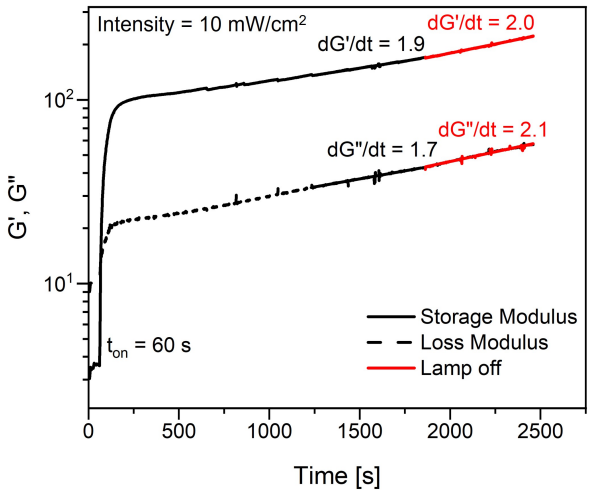

Figure C.6: The full gelation of the a bottlebrush polymer at 10 mW/cm^2 at a frequency of 10 rad/s. Steady oscillatory shear was applied to the sample for 60 s followed by 1800 s, during which the material was exposed to UV light. At 1860 s, the UV lamp was turned off (highlighted in red). Steady oscillatory shear was continued for an additional 300 s (final time 2160 s). At long times, the moduli were fit to linear equations to determine the average slope of the moduli. The slopes while the material was exposed to UV light and shortly after the lamps were turned off were found to be similar, suggesting that the change in storage and loss modulus at long times were due to factors such as evaporation.

C.4 Data Used for SPP Analysis of Gelation

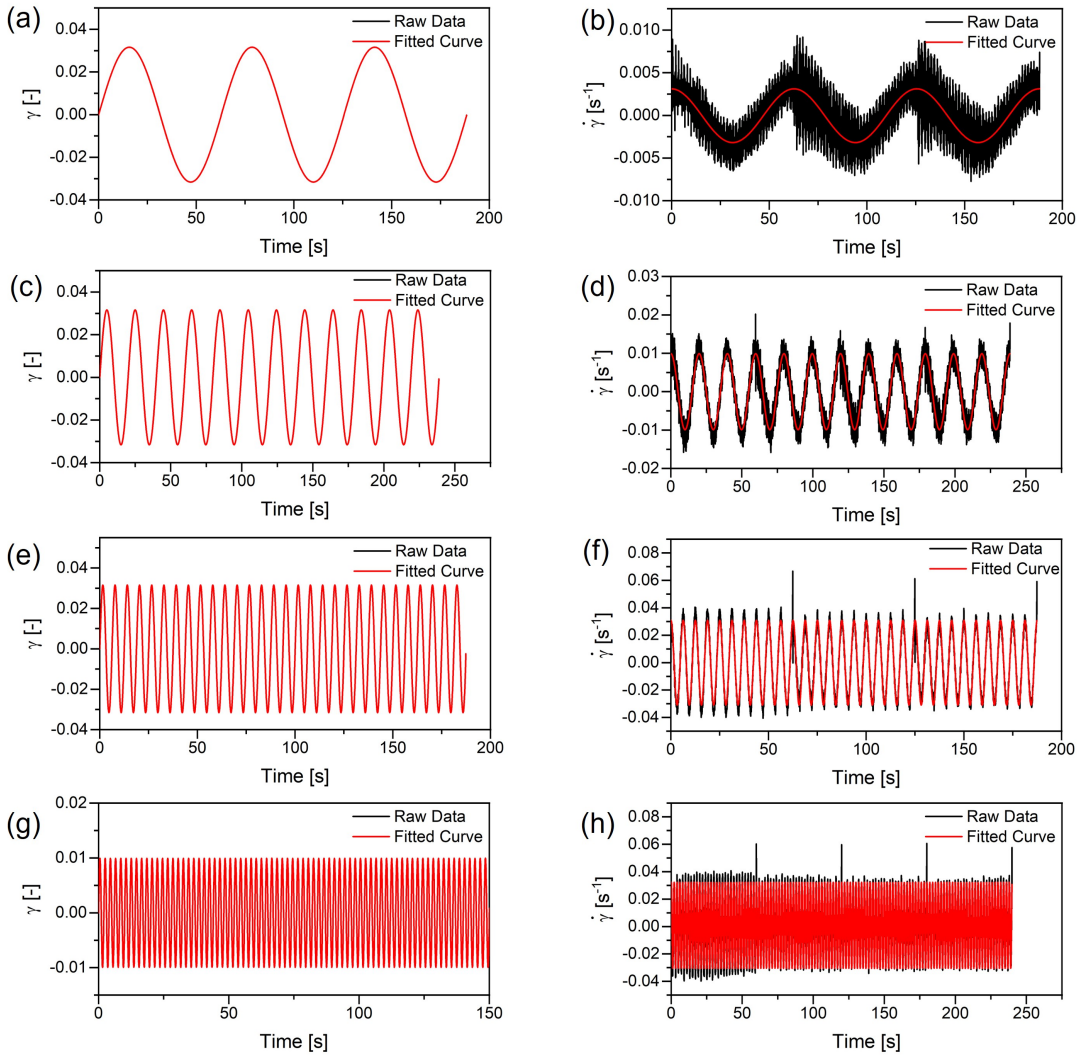

Figure C.7: Raw strain and strain rate data measured by the MCR 702 rheometer during a gelation experiment. Note that t = 0 corresponds to the moment that the UV lamp was turned on. Data are shown for frequencies from 0.1 to 3.16 rad/s with a strain amplitude of 0.01. Spikes in the measured shear rate were found to the slight delay that occurs between intervals on the MCR 702.

Appendix D

Supplementary Materials for Chapter 6

D.1 Stress Bifurcation Demonstrating Yield-Stress Behavior

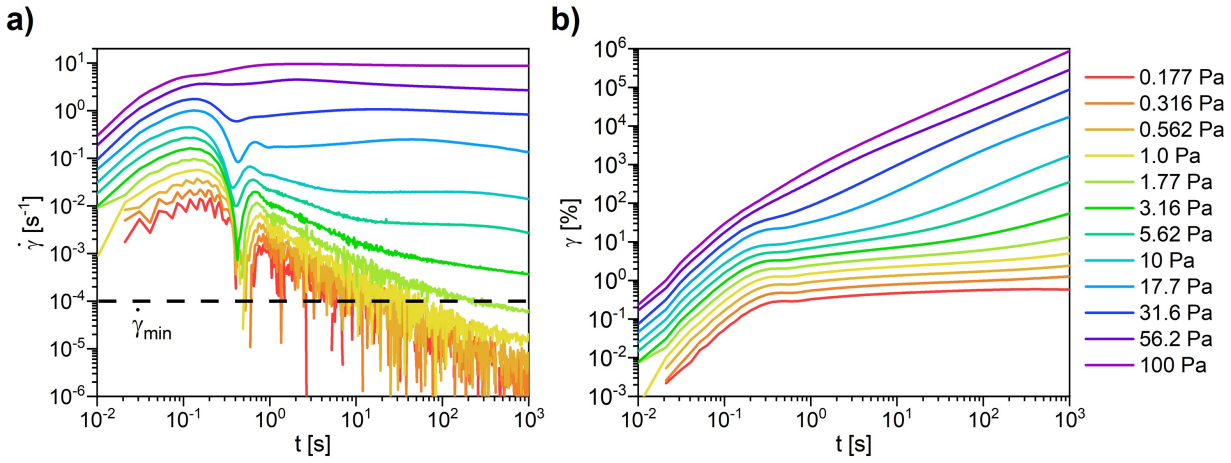

Figure D.1: The a) strain rate and b) strain as a function of time during creep tests, demonstrating stress bifurcation. A minimum reliably measureable shear rate of $4*10^{-4}$ is indicated in a) with a dashed line to serve as a guide to the eye.

D.2 Color Retention During Pulse Tests

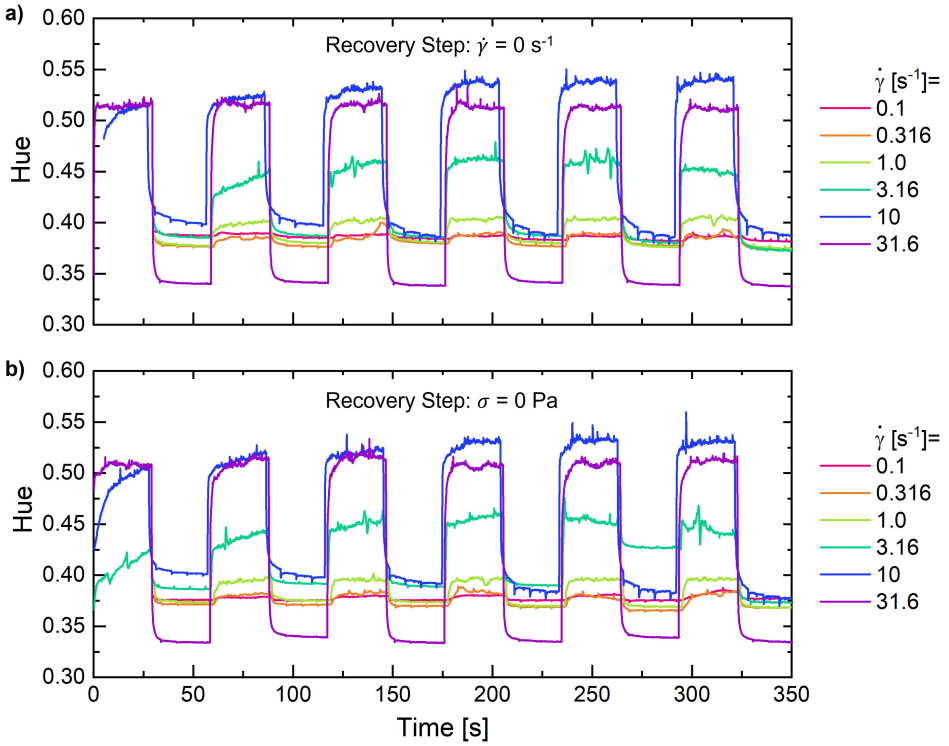

Figure D.2: The hue captured during steady shear pulse tests at shear rates from 0.1 to 31.6 s^{-1} with each step of steady shear followed by an a) zero shear rate step or b) zero stress step. Due to the similarities between the two, we only focus on one set of pulse tests in the main body of the thesis.

D.3 Supplemental Data and Figures for Iterative Recovery Rheology Measurements

Due to the repeated nature of iterative recovery measurements, it is common for these tests to take upwards of 3 or more hours, depending on the time resolution of the iterative study as well as the inclusion of preshear protocols. As such, it is necessary to monitor the sample throughout testing in order to ensure that the material does not significantly change due to effects such as solvent evaporation, aging, phase separation, etc that might occur on the order of 3+ hours. This monitoring is achieved by conducting frequency sweeps periodically throughout the recovery test and comparing the results to a frequency sweep conducted at the start of the test. An representative depiction of this comparison can be seen in Figure D.3 in which the complete frequency sweep captured at the start of a test is compared to a frequency sweep carried out after a full sweep of 16 recovery tests had been completed (~3.5 hrs of instrument run time). If the frequency sweep was found to differ from the original sweep by more than 20 to 30%, then the test was stopped, the material either redissolved or removed and replaced with fresh material, and the test resumed. This ensured that the measured recoverable and unrecoverable components are representative of a well defined sample. It is important to note that a threshold of 20 to 30% was selected due to limitations in sample volume and

accessibility that resulted in lower thresholds being impractical.

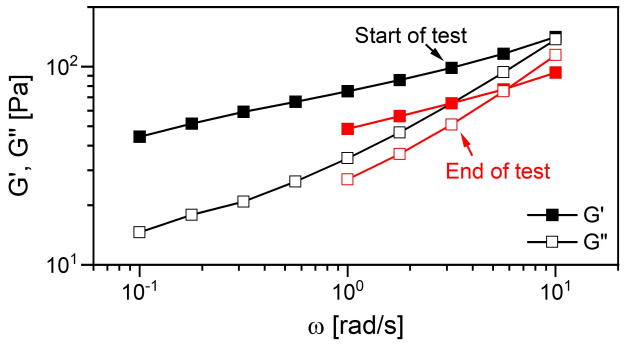

Figure D.3: A comparision of frequency sweeps carried out at the start of a set of iterative recovery tests and at the end of said tests. Note that the resulting frequency sweep at the end of the test is only 25% different from the original conditions and is thus considered valid.

Oscillatory recovery tests were carried out on amplitudes from 1% up to 1000%. The corresponding Lissasjous curves for all of these oscillations can be seen in Figure D.4. In this thesis we chose to focus on 5 amplitudes from this subset due to limited time available to run experiments at the NCNR SANS beamline. Strain amplitudes of 5.62, 17.7, 31.6, 562 and 1000% effectively spanning the behavior exhibited by the material in small and large amplitude oscillatory shear regimesl.

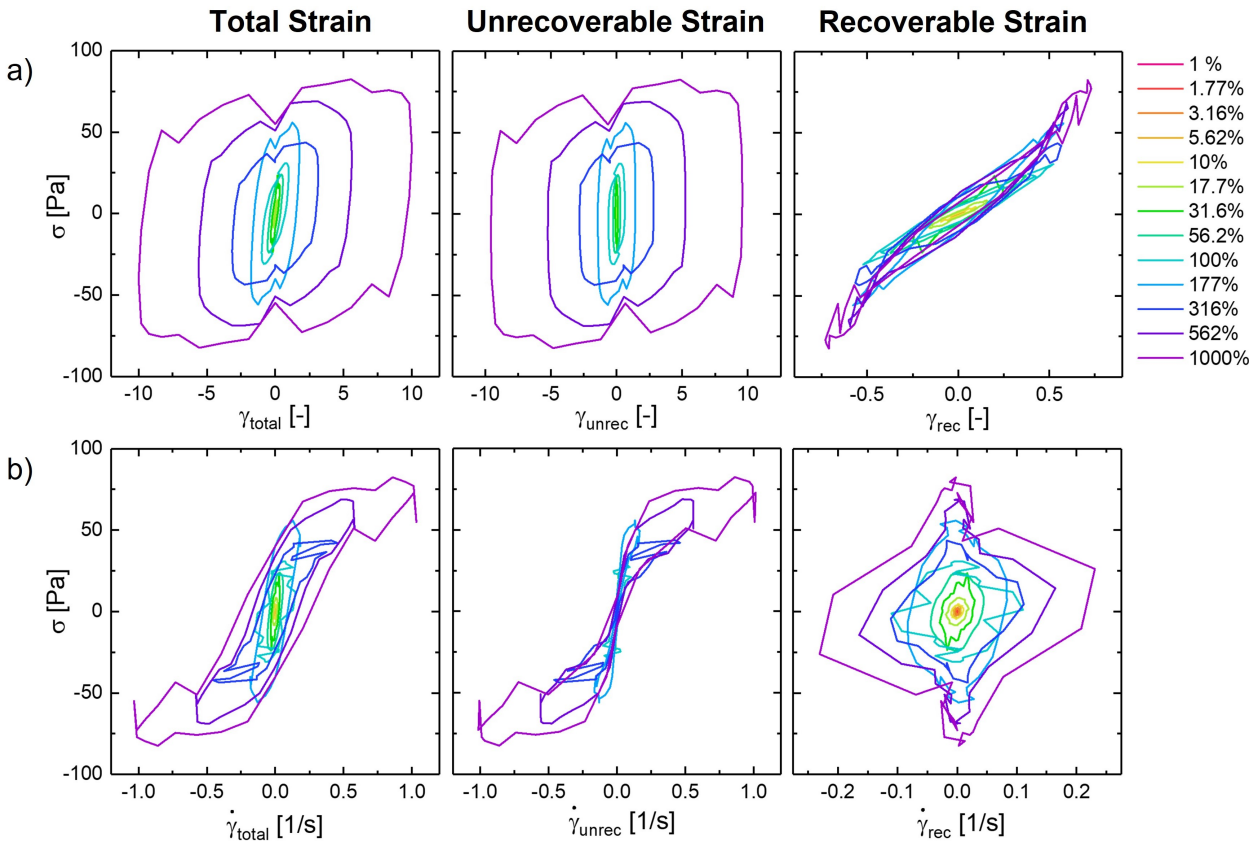

Figure D.4: Lissajous Curves for a) the strain and its recoverable and unrecoverable components and b) the strain rate and its recoverable and unrecoverable components for strain amplitudes from 1% to 1000%.

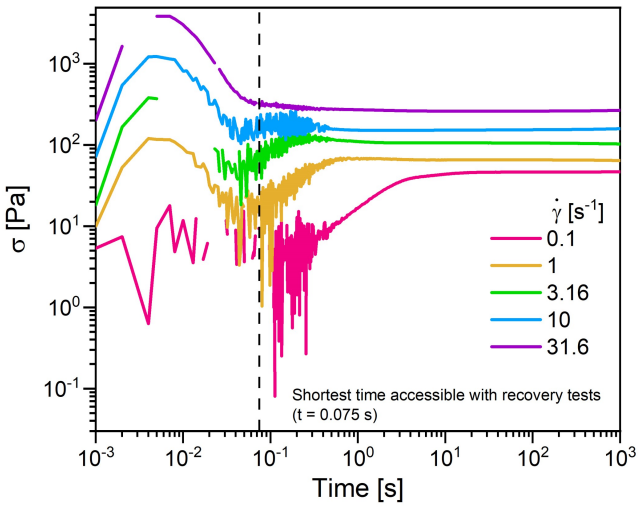

Figure D.5: Steady shear startup for select shear rates from 0.1 to 31.6 s^{-1} from the lowest accessible time scale on the MCR 702 to 1000 s. The lowest accessible with recovery tests is highlighted with a dashed line at t = 0.075 s. Note how all curves appear to reach steady state a long times.

D.4 Proposal Submitted to the NCNR for Four Days of Beamtime on 30m SANS

A transient rheo-SANS study of the yielding of a concentrated diblock bottlebrush solution
Matthew Wade and Simon Rogers

Background and Problem Statement

This proposal aims to investigate the link between the recoverable component of the strain in oscillatory tests in which yielding is observed, and the hierarchical structure formed by the concentrated suspensions of diblock bottlebrush polymers. The reversible transition between solid-like and fluid-like behavior found in yield stress fluids is desirable in a wide range of processes [1]. In industrial applications such as additive manufacturing, the existence of a yield-stress ensures that the material can be easily extruded out of a narrow nozzle while simultaneously retaining its shape once it is deposited on a substrate [2]–[4]. Understanding the physics that governs the yielding transition is an outstanding challenge due to the inherent nonequilibrium conditions associated with solid to liquid transitions. Recent rheological techniques developed by the Rogers group have shown that signatures of yielding seen in amplitude sweeps can be understood in terms of recoverable and unrecoverable strains [4], [5]. These techniques can also help elucidate the transient nature of yielding. Despite this progress on understanding the bulk-scale rheology, our understanding of the microstructural changes before and during yielding is still incomplete.

Concentrated suspensions of diblock bottlebrush polymers form yield stress fluids, as shown by their response to an oscillatory amplitude sweep, as shown in fig. 1 a. At small amplitudes, the storage modulus is larger than the loss modulus, indicating a solid-like behavior. As the amplitude is increased, an overshoot in the loss modulus is observed, followed by a crossing of the dynamic modulus at larger amplitudes, indicating a transition to liquid-like behavior. Following the experimental and analysis methods laid out by Lee et al. and Donley et al., we can decompose the total strain acquired (γ_{total}) into its recoverable and unrecoverable components (γ_{rec} and γ_{unrec} , respectively) and understand the rheology of the amplitude sweep, as shown in Figure D.6 [4], [5].

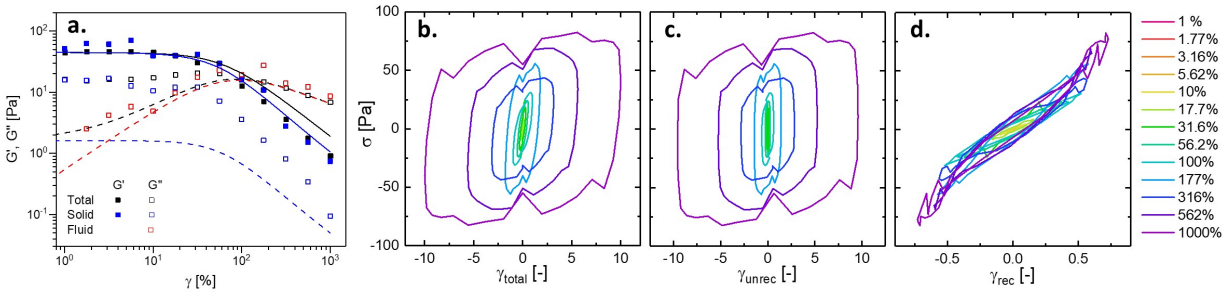

Figure D.6: a. An amplitude sweep for a concentrated diblock bottlebrush solution measured at a frequency of 0.1 rad/s decomposed into its solid and fluid components (blue and red symbols, respectively). The experimental data are compared to an unpublished model (shown as lines). Lissajous curves plotted with the b. total, c. unrecoverable, and d. recoverable strain of the material as measured using recovery rheology.

Prior studies have already been carried out on the diblock bottlebrush polymer solution, where the impact of steady shear on the self-assembled microstructure was investigated [6]. Using a combination

of rheo-VSANS and rheo-microscopy, we developed a structure-property-process relationship linking the self-assembled microstructure of the diblock bottlebrush in solution to the material's photonic properties over a wide range of steady shear conditions, as shown in Figure D.7

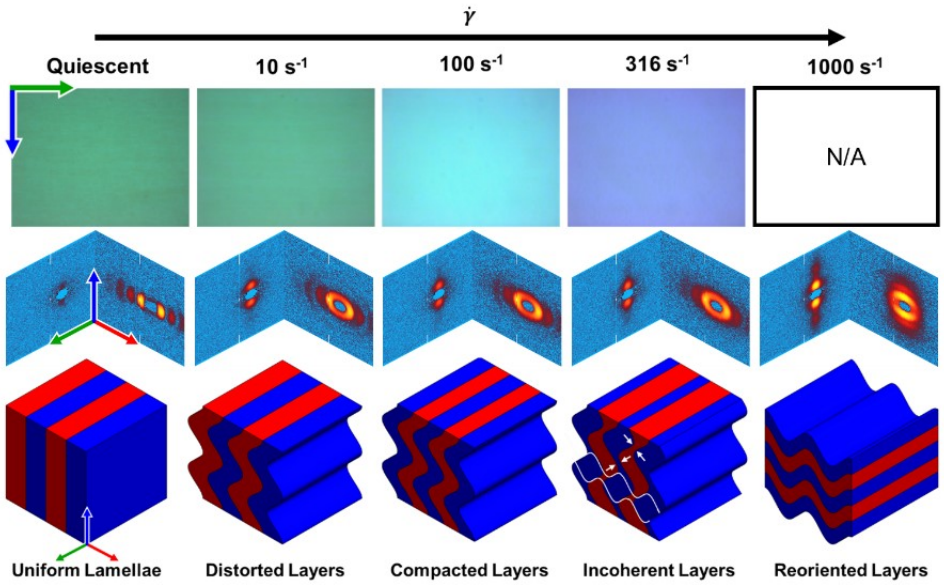

Figure D.7: Images of a diblock bottlebrush taken in the 1-3 shear plane (top row), 2D scattering patterns in the 1-3 and 2-3 shear planes (middle row), and the corresponding interpretation of the self-assembled microstructure (bottom row) for a diblock bottlebrush block copolymer during steady shear.

Work carried out by Patel et al. further explores the impact of flow conditions on the microstructure and resulting photonic properties on diblock bottlebrush polymers in solution by focusing on the impact of printing conditions on reflected color of the deposited, dried polymer film [7]. Patel et al. identify the kinetic trapping of metastable microstructures as being the cause of dried polymer films retaining some memory of their shear history when deposited onto a print substrate. While both of these recent studies provide insight into the polymer's properties after it has been allowed to reach equilibrium, the impact of dynamic shearing on the self-assembled microstructure and the resulting photonic properties remain unknown.

The photonic properties found in diblock bottlebrush polymer solutions, in addition to the yielding behavior observed in our preliminary results, put us in a unique position to simultaneously explore the transient development of microstructures that give rise to the wide range of photonic properties of diblock bottlebrush polymers in solution and the microstructural changes that occur during the yielding process. We propose a series of measurements to address the transient structural features of a concentrated diblock bottlebrush polymer suspension during yielding. These time-resolved rheo-SANS measurements will be combined with already-measured microscopy and rheology, as well as rheological predictions from a new model (predictions shown in Figure D.6.a to develop a transient structure-property-process relation between the microstructure, photonic properties, and bulk rheology.

Propose Study

We will measure the time-resolved structures exhibited by a concentrated DBB solution in the radial and tangential configurations to capture projections of the fully 3-D structure during oscillatory shearing in which yielding is observed. The sample used during this study will be

poly(norbornene-g-poly(lactic acid)$_{60}$)$_{200}$-b-poly(norbornene-g-poly(styrene)$_{45}$)$_{200}$ dissolved in deuterated toluene to form a solution with a concentration of 350 mg/ml. This sample is the same material previously characterized under steady shear conditions [6], but at a higher concentration. The microstructure will first be characterized under quiescence, followed by a series of transient measurements made during oscillatory shearing across a range of amplitudes. A total of 5 strain amplitudes, ranging from 10 to 1000 % strain will be measured, allowing us to form links between the complex yielding rheology including the acquisition of recoverable strain and changes in the hierarchical self-assembled microstructure. The frequency of the oscillation will be held constant at 0.1 rad/s, reflecting the data shown in Figure D.6.

Quiescent and oscillatory shear tests will be carried out using the Anton-Paar 501 Rheometer currently available at NIST with the 28 mm titanium cup and 27 mm titanium bob. Using the liquid nitrogen cooling setup for the rheometer, the sample will be held at a constant temperature of 5 °C to limit the effects of evaporation on solution concentration. The sample volume will be checked periodically. Deuterated toluene will be added to the sample as needed to ensure the concentration of the sample remains constant throughout testing.

Time-resolved oscillatory shear studies will be carried out according to the procedure described by Lopez-Barron et al. [8], where the oscillation is repeated until sufficient scattering events are recorded over an interval of time. We will have measured the recoverable components separately, so we can use the well-established procedures for measuring oscillatory rheo-SANS. The oscillation will be split into 64 individual bins, 32 per half period, to provide enough resolution to resolve the structural changes that occur during yielding. The experiment will be repeated until there are approximately 100,000 scattering events per bin. Based on prior experiments using the 30 m SANS beamline at NIST, we expect scattering count rates of approximately 240 counts/s and 200 counts/s in the 1-3 and 2-3 scattering configurations. We therefore expect each testing amplitude in the two configurations to take approximately 9 hours to complete. Including setup of the rheometer, alignment, and sample loading, we propose using 4 days of beamtime (5 tests in the 1-3 configuration and 5 tests in the 2-3 configuration) on one of the 30 m SANS beamlines.

Broader Impact

The proposed study addresses questions associated with the transient self-assembly of a polymeric system, the energetic contributions associated with yielding, and the development of transient photonic materials. We therefore anticipate this work to be publishable in a high impact journal. This work will also serve as an integral part of the thesis work of graduate student Matthew Wade.

D.5 References

[1] P. Coussot, "Yield stress fluid flows: A review of experimental data," *Journal of Non-Newtonian Fluid Mechanics*, vol. 211, pp. 31–49, Sep. 2014, ISSN: 03770257. DOI: 10.1016/j.jnnfm.2014.05.006. [Online]. Available: http://dx.doi.org/10.1016/j.jnnfm.2014.05.006.

[2] A. Z. Nelson, K. S. Schweizer, B. M. Rauzan, R. G. Nuzzo, J. Vermant, and R. H. Ewoldt, "Designing and transforming yield-stress fluids," *Current Opinion in Solid State and Materials Science*, vol. 23, no. 5, p. 100 758, Oct. 2019, ISSN: 13590286. DOI: 10.1016/j.cossms.2019.06.002.

[3] G. J. Donley, W. W. Hyde, S. A. Rogers, and F. Nettesheim, "Yielding and recovery of conductive pastes for screen printing," *Rheologica Acta*, vol. 58, no. 6-7, pp. 361–382, Jul. 2019, ISSN: 00354511. DOI: 10.1007/s00397-019-01148-w. [Online]. Available: https://doi.org/10.1007/s00397-019-01148-w.

[4] G. J. Donley, P. K. Singh, A. Shetty, and S. A. Rogers, "Elucidating the G" overshoot in soft materials with a yield transition via a time-resolved experimental strain decomposition," *Proceedings of the National Academy of Sciences of the United States of America*, vol. 117, no. 36, pp. 21 945–21 952, 2020, ISSN: 10916490. DOI: 10.1073/pnas.2003869117.

[5] J. C.-W. Lee, K. M. Weigandt, E. G. Kelley, and S. A. Rogers, "Structure-Property Relationships via Recovery Rheology in Viscoelastic Materials," *Physical Review Letters*, vol. 122, no. 24, p. 248 003, Jun. 2019, ISSN: 0031-9007. DOI: 10.1103/PhysRevLett.122.248003. [Online]. Available: https://link.aps.org/doi/10.1103/PhysRevLett.122.248003.

[6] M. A. Wade, D. Walsh, J. C. W. Lee, *et al.*, "Color, Structure, and Rheology of a Diblock Bottlebrush Copolymer Solution," *Soft Matter*, vol. 16, no. 21, pp. 4919–4931, Jun. 2020, ISSN: 17446848. DOI: 10.1039/d0sm00397b. [Online]. Available: https://pubs.rsc.org/en/content/articlehtml/2020/sm/d0sm00397b%20https://pubs.rsc.org/en/content/articlelanding/2020/sm/d0sm00397b.

[7] B. B. Patel, D. J. Walsh, D. H. Kim, *et al.*, "Tunable structural color of bottlebrush block copolymers through direct-write 3D printing from solution," *Science Advances*, vol. 6, no. 24, In Press, Jun. 2020, ISSN: 2375-2548. DOI: 10.1126/sciadv.aaz7202. [Online]. Available: http://advances.sciencemag.org/%20https://www.science.org/doi/10.1126/sciadv.aaz7202.

[8] C. R. López-Barrón, A. K. Gurnon, A. P. Eberle, L. Porcar, and N. J. Wagner, "Microstructural evolution of a model, shear-banding micellar solution during shear startup and cessation," *Physical Review E - Statistical, Nonlinear, and Soft Matter Physics*, vol. 89, no. 4, p. 42 301, 2014, ISSN: 15502376. DOI: 10.1103/PhysRevE.89.042301. [Online]. Available: https://journals.aps.org/pre/pdf/10.1103/PhysRevE.89.042301.